ANALYSIS OF BROADBAND AND DUAL BAND MICROSTRIP PATCH ANTENNAS

By:

Ritu Bhalla

A Thesis

Submitted to the Faculty of Graduate Studies

in Partial Fulfillment of the requirements

for the Degree of

Master of Science in Electrical Engineering

Department of Electrical and Computer Engineering

University of Manitoba

Winnipeg, Manitoba, Canada

THE UNIVERSITY OF MANITOBA

FACULTY OF GRADUATE STUDIES

*****

COPYRIGHT PERMISSION

ANALYSIS OF BROADBAND AND DUAL BAND MICROSTRIP PATCH ANTENNAS

BY

RITU BHALLA

A Thesis/Practicum submitted to the Faculty of Graduate Studies of The University of Manitoba in partial fulfillment of the requirement of the degree

of

MASTER OF SCIENCE

Acknowledgments

I would like to express my appreciation and gratitude to my advisor Prof. L. Shafai for his advice, support, insight and continuous encouragement throughout the development of this thesis project. I would not have been able to complete this thesis project without his guidance and patience. I would like to thank Prof. J. LoVetri and Prof. A. Shah for serving in my committee.

I am thankful to Ms. S. Girardian for her help whenever it was needed. I would like to thank all the technicians in the Department of Electrical and Computer Engineering for their technical help. Special thanks to Dr. Satish Sharma for his assistance and advice in this study.

Financial support during this study was provided by a grant and a scholarship from the Natural Science and Engineering Council of Canada (NSERC), their contribution is greatly appreciated.

I would like to dedicate this thesis to my parents and my family members. Their love, support and understanding have helped me to realize all my dreams.

I would like to thank my friend Mehran and his family members; Dr. Amir Fallah–Rad, Dr. Shahnaz Danesh and Nazanin. Their continuous moral support and affection helped me achieving my goals at school. Finally, I would like to thank my friend Jeeva Raj for his friendship.

Abstract

In this thesis a parametric study of various broadband microstrip patch antennas and a dual band patch antenna is investigated. The broadband patch antennas studied in this thesis are: a rectangular microstrip patch antenna with a U–shaped slot, a rectangular microstrip patch antenna with a circular arc slot, a circular patch antenna with a circular arc slot and a circular patch antenna with a circular arc slot and L–shaped probe. The feed for these antennas is a coaxial probe feed. Different parameters such as probe radius, probe location, substrate height, width of the slot and location of the slot are considered in the parametric study. The resonance behavior of a rectangular patch antenna with a U–slot and a rectangular patch antenna with a circular arc slot is also investigated. The radiation patterns, gain patterns and the return loss of the broadband antennas are also discussed.

For dual band operation, a new coaxially–fed microstrip patch antenna with two asymmetric U–shaped slots is discussed in this thesis. Two approximate equations for the resonant frequencies based on the surface current distribution are presented. The simulation results of the radiation patterns, gain patterns and the return loss of the antenna are presented.

In addition, a single U–slot patch antenna, a rectangular microstrip patch antenna with a circular arc slot, and dual U–slots patch antenna are fabricated and tested in the Antenna Laboratory at the University of Manitoba. The simulation and experimental results are then compared.

Table of contents

List of Figures

List of Tables

Chapter 1

Introduction

1.1 Preface

The concept of microstrip antennas was first introduced by Deschamps as early as 1953 [1]. However, the first practical microstrip antenna was designed by Howell and Munson in the early 1970's [2–3]. Since then, extensive research has been devoted to the study and further development of the concept of microstrip antennas. Microstrip antennas have many advantages such as light weight, low volume, low profile, low cost and compatibility with integrated circuits. The advantages of microstrip antennas make them popular in many applications that require a low profile and light weight antenna. Some of these applications are in mobile radio, satellite communications, radars, biomedical radiators and reflector feeds. They can be made very thin and easily mounted on missiles, rockets and satellites. However, microstrip antennas also have some disadvantages compared to conventional microwave antennas such as narrow bandwidth, high loss, limitations on the maximum gain and lower power handling capability [4].

Microstrip patch antennas come in many different shapes such as rectangular, square, circular and ring configuration. The rectangular patch is the most commonly used microstrip antenna. It is characterized by its length and width. The far field radiation pattern, resonance frequency, input impedance and bandwidth of rectangular microstrip patch antennas are well documented and reported in [5, 6]. The other configuration that is widely used is the circular microstrip patch antenna. The geometry of the circular patch is

characterized by the radius of the patch. The expression for the far field radiation pattern, resonance frequency, input impedance and bandwidth of the circular patch antenna have also been documented and reported by Bahl and Bhartia [4] and Shafai and Antoskiewicz [7]. The annular ring patch antenna was first studied by Bergman and Schultz [8]. It has been shown that the annular ring patch antenna can be used in medical applications [9].

For many practical designs, the advantages of microstrip antennas far outweigh their disadvantages. Due to the increasing demand for these antennas, many efforts have been made to reduce their disadvantages. The narrow bandwidth of the microstrip antenna is a major obstacle for using it in today's communication systems. During the last decade, an extensive amount of research has been devoted to bandwidth–widening techniques of microstrip antennas. The use of parasitic patches either in another layer of a stacked geometry [10] or in the same layer of a coplanar geometry [11] has been suggested to increase the bandwidth of microstrip antenna. However, the stacked geometry has the disadvantage of increasing the thickness of the antenna while the coplanar geometry has the disadvantage of increasing the lateral size of the antenna. Therefore, it would be very beneficial if a single–layer single–patch broadband microstrip patch antenna could be developed.

Recently, Huynh and Lee presented an experimental study of a new kind of broadband microstrip patch antenna with a U–shaped slot, in which two different but close resonant frequencies in a single patch are combined to give a wideband operation [12]. The first resonance is assumed to be generated by the microstrip patch, while the second one by the U–shaped slot. This single–layer single–patch wideband microstrip antenna maintains the thin profile and small size characteristics. Bandwidths in the range of 30% are

obtained using the single layer probe fed patch antenna with a U–shaped slot. Even though the wideband characteristics of a microstrip patch antenna with a single U–shaped slot has been confirmed by many published results [12–22], no information is provided on the resonance behavior of this antenna, which is the essential point in obtaining the wideband operation of this antenna.

In this study, the resonance behavior of the microstrip patch antenna with a single U–shaped slot is studied. Two approximate equations for the resonance frequencies are derived based on the surface current distribution analysis. Along with the microstrip patch antenna with a single U–shaped slot, the design of microstrip patch with dual U slots is also given which provides dual band operation.

1.2 Objective of the thesis

The purpose of this research is to study various types of broadband patch antennas and a dual band microstrip patch antenna. The resonance behavior of the microstrip patch antenna with a single U–shaped slot is studied. Two approximate equations for the operating frequencies are derived based upon the analyses of the surface current distribution on the patch. These equations are used to compute the resonance frequencies of the microstrip patch antenna with a single U–shaped slot. The computed results are compared with the simulated results of moment method solution using the Ansoft ENSEMBLE software and they are found to be accurate within 5%.

A new type of broadband rectangular microstrip patch antenna with a circular arc shaped slot is also studied in this thesis. A parametric study is performed on this rectangular microstrip patch with a circular arc slot. This thesis also investigates the

properties of another new type of circular microstrip patch antenna with a circular arc shaped slot. Through the parametric study, it is found that the rectangular microstrip patch with a circular arc shaped slot has wideband characteristics, while the bandwidth of the circular microstrip patch with a circular arc shaped slot is slightly lower. The resonance properties of the rectangular microstrip patch with a circular arc slot are also investigated. Based upon the surface current distribution analyses, two equations are proposed for the resonance frequencies of this antenna. The accuracy of the proposed equations is justified by small percentage errors.

Another new type of broadband circular microstrip patch antenna with a circular arc shaped slot and L–shaped probe is studied. Earlier it has been shown that a circular microstrip patch antenna with a L–shaped probe has a bandwidth of 24% [23]. By cutting a U–shaped slot on the circular patch with L–probe feeding, the bandwidth increases to 38% with a gain value of 6.8 dBi [24]. In this thesis, it is demonstrated that this new broadband circular microstrip patch antenna with a circular arc shaped slot and L–probe feeding provides a bandwidth of 40% and a higher gain value of 9.0 dBi. Therefore, the new broadband circular patch antenna with a circular arc slot and L–probe feeding gives better results from both the high bandwidth and high gain standpoint.

For dual band operation, a new coaxially–fed microstrip patch antenna with two asymmetric U–shaped slots is discussed in this thesis. The optimum ratio of the two frequencies is found to be $f_2 / f_1 = 1.57$. Two approximate equations for the resonant frequencies based on the surface current distribution are presented. The computed results of the resonance frequencies using the proposed equations are compared with the simulated results of the Ansoft ENSEMBLE software. The two proposed equations are

accurate within 2.3%.

1.3 Thesis Outline

This thesis is organized into different sections in order to give the reader a better understanding of the work done. Chapter 1 gives an introduction to microstrip antennas, the objective of the thesis and an outline of the thesis. In Chapter 2, the background theory of rectangular microstrip patch antenna and circular microstrip patch antenna is discussed. This chapter also covers the different types of broadband patch antennas. Chapter 3 discusses the simulation results of the different applications of the broadband patch antennas such as a rectangular microstrip patch with a single U–shaped slot, a rectangular microstrip patch antenna with a circular arc shaped slot, a circular microstrip patch antenna with a circular arc shaped slot and a circular microstrip patch antenna with a circular arc shaped slot and L–shaped probe. The parametric study of these antennas is also presented in Chapter 3. In Chapter 4, the simulation results of the rectangular microstrip patch antenna with dual U–shaped slots are discussed. Chapter 5 covers the experimental results of the fabricated antennas measured in the Anechoic Chamber Antenna Laboratory at the University of Manitoba. Finally, a conclusion of the thesis is given in Chapter 6.

Chapter 2

Background Theory

2.1 Introduction

Microstrip patch antenna is a type of open wave guiding structure, which consists of a radiating patch on one side of a dielectric substrate and a ground plane on the other side [4]. The radiating patch may be rectangular, square, circular, ring, elliptical, triangular or any other shape. Rectangular, square and circular shapes are the most common because of their radiation characteristics with low cross–polarization and ease of analysis and fabrication. Linear and circular polarizations can be achieved with either single elements or arrays of microstrip antennas [4]. This chapter covers the background theory of both rectangular and circular microstrip patch antennas.

2.2 Rectangular microstrip patch antenna

The geometry of a rectangular microstrip patch antenna is shown in Figure 2.1. A rectangular patch of dimensions L x W is separated from the ground plane with a dielectric substrate with dielectric constant ε_r and height h. A rectangular patch antenna can be considered to be an open–ended section of transmission line of length L and width W. A rectangular patch antenna behaves as a one–dimensional resonator, and its width W at resonance is equal to one half wavelength, $1/2\lambda_{eff}$. A coaxial probe is used to feed the rectangular patch, as shown in Figure 1. In this feeding method, the center conductor of a

coaxial probe is connected to the patch [25].

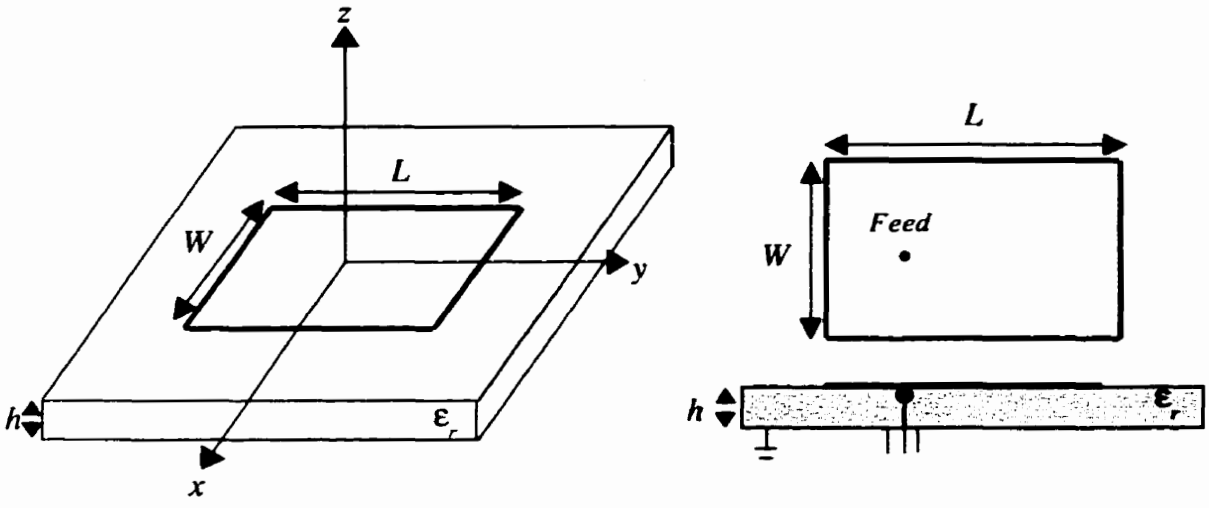

Figure 2.1: Geometry of a rectangular microstrip patch antenna.

For small h, the electric field under the patch is normal to the patch (vertical E), as shown in Figure 2.2. The fringing fields at the two open ends are accounted for by adding equivalent lengths ΔL at both ends. The expression for ΔL is given in equation 2.1 [25].

$$\Delta L = 0.412\,h\frac{(\epsilon_e+0.3)\cdot(\frac{W}{h}+0.264)}{((\epsilon_e-0.258)\cdot(\frac{W}{h}+0.8))} \tag{2.1}$$

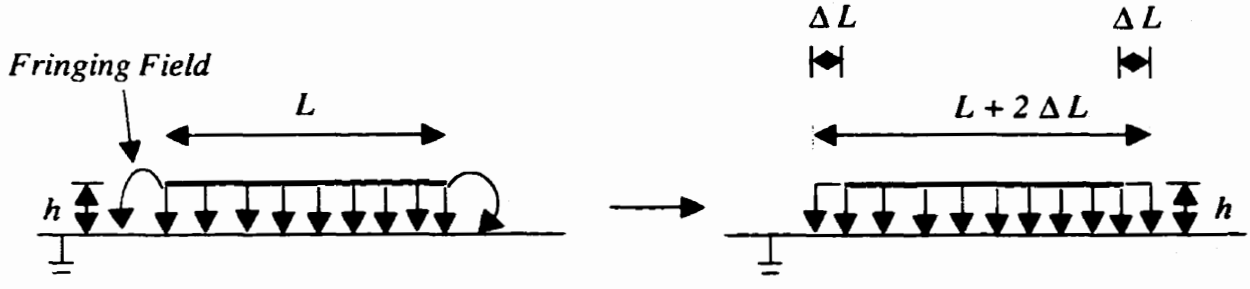

Figure 2.2: Patch enlargement due to Fringing Fields.

The parameter ε_e in equation 2.1 is the effective dielectric constant of the dielectric substrate, which is given by equation 2.2 [25].

$$\epsilon_e = \frac{(\epsilon_r+1)}{2} + \frac{(\epsilon_r-1)}{2}\left(1+\frac{10\cdot h}{W}\right)^{\frac{-1}{2}} \tag{2.2}$$

For a rectangular patch, the first resonance occurs when the effective length of the patch L_e shown in Figure 2.3 is equal to $L_e = \lambda_d/2$. The effective length of the patch is obtained from the patch enlargement due to fringing fields and is equal to $L_e = L + 2\,\Delta L$. As a result, $\lambda_d = 2\,(L + 2\,\Delta L)$, where $\lambda_d = \lambda_0 / \sqrt{\varepsilon_e}$ and $\lambda_0 = c / f$ [25]. Consequently, an equation for the resonance frequency can be written and is shown in equation 2.3 [25].

$$f_r = \frac{c}{(\lambda_d\sqrt{\epsilon_e})} = \frac{c}{(2(L+2\Delta L)\sqrt{\epsilon_e})} \quad c = \textit{velocity of light} \tag{2.3}$$

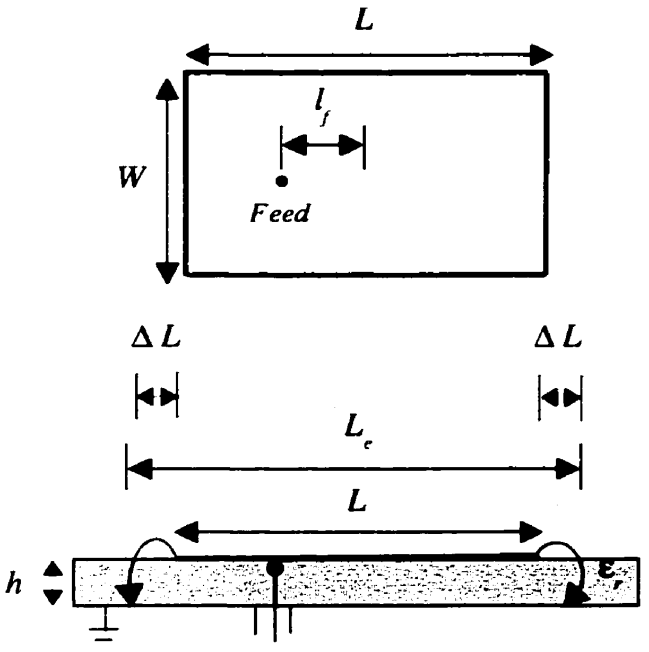

Figure 2.3: Rectangular patch effective length.

The bandwidth of a microstrip patch antenna is the range of frequencies within which the performance of the antenna conforms to a specific standard [26]. In the case of the microstrip patch antenna, the bandwidth is usually the variation of impedance, which limits the standard of performance. If the antenna impedance is matched to the transmission line at resonance, the mismatch off resonance is related to the VSWR. The specified value of the VSWR then defines the bandwidth of the microstrip patch antenna. For VSWR < S, the usable bandwidth of a microstrip patch antenna is given by equation 2.4 [26].

$$Bandwidth = 100\frac{(S-1)}{(Q_t\sqrt{S})} \tag{2.4}$$

The quality factor Q_t in equation 2.4 is defined as the ratio of the resonance frequency f_r of the antenna and the frequency band Δf over which the reflected power is not more than one ninth (VSWR < 2) of that absorbed at resonance. An expression for quality factor Q_t is given in equation 2.5 [26].

$$Q_t = \frac{f_r}{(\Delta f)} \tag{2.5}$$

The total radiated fields of a rectangular microstrip patch antenna, shown in Figure 2.3, can be found by treating the patch, ground plane and the dielectric substrate as a cavity. The field equations of a rectangular microstrip patch antenna are given by equations (2.6) and (2.7). These far field equations are obtained using the cavity model [26].

$$E_\vartheta = [\frac{jkWV_o}{\pi}\frac{e^{-jkr}}{r}e^{j(X+Y+Z)}]\cos(\phi)[\cos(X)\frac{(\sin(Y))}{Y}] \tag{2.6}$$

$$E_{\phi} = [\frac{jkWV_o}{\pi}\frac{e^{-jkr}}{r}e^{j(X+Y+Z)}]\cos(\vartheta)\sin(\phi)[\cos(X)\frac{(\sin(Y))}{Y}] \quad (2.7)$$

The variable V_o in equations 2.6 and 2.7 is the applied voltage at the feed and the expressions for variables X, Y, Z are given by the following equations [26]

$$X = k\frac{L_e}{2}\sin(\vartheta)\cos(\phi) \quad (2.8)$$

$$Y = k\frac{W}{2}\sin(\vartheta)\sin(\phi) \quad (2.9)$$

$$Z = k\frac{h}{2}\cos(\vartheta) \quad (2.10)$$

2.3 Circular microstrip patch antenna

Other than the rectangular patch, the next popular configuration that is most commonly used is the circular microstrip patch antenna. It has received much attention not only as a single element, but also in arrays. The geometry of the circular microstrip patch antenna is shown in Figure 2.4. The circular patch is characterized by its radius R [26].

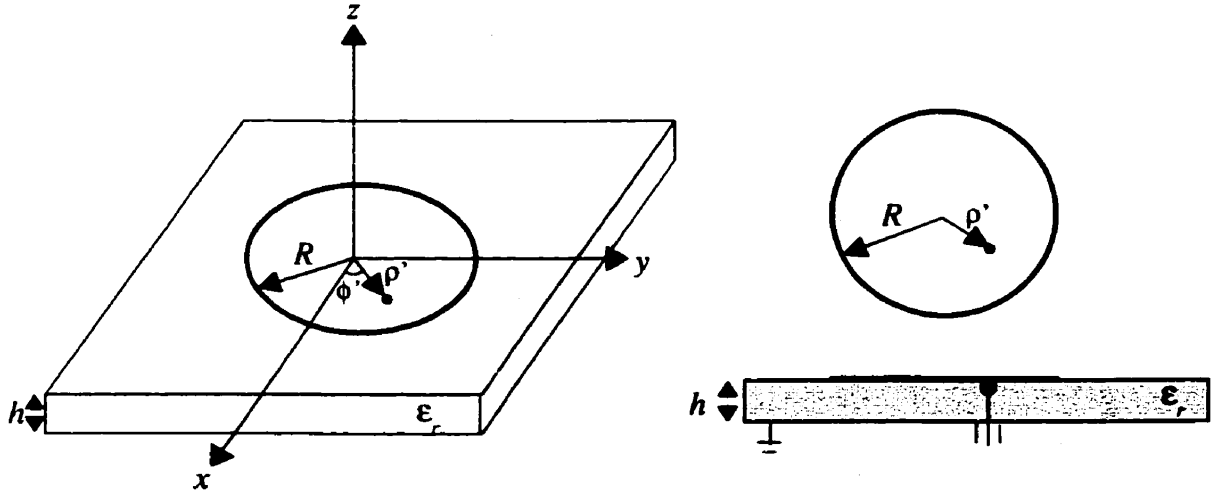

Figure 2.4: Geometry of a circular microstrip patch antenna.

As with a rectangular patch, the modes that are supported by a circular patch with small substrate height ($h << \lambda$) are TM^z modes with z being perpendicular to the circular patch. The resonant frequencies of a circular microstrip patch antenna for the TM^z_{mn0} modes can be written as follows [26]:

$$(f_r)_{mn0} = \frac{1}{(2\pi\sqrt{\mu\epsilon})}\left(\frac{\chi_{mn}}{R}\right) \tag{2.11}$$

In equation 2.11, χ'_{mn} represents the zeros of the derivative of the Bessel function $J_m(x)$ and they determine the order of the resonant frequencies. The first four values of χ'_{mn} are [26]

$$\begin{aligned} \chi_{11} &= 1.8412 \\ \chi'_{21} &= 3.0542 \\ \chi'_{01} &= 3.8318 \\ \chi'_{31} &= 4.2012 \end{aligned} \tag{2.12}$$

Based on the values of χ'_{mn}, the first four modes are TM^z_{110}, TM^z_{210}, TM^z_{010}, and TM^z_{310} [26]. The dominant mode of the circular microstrip patch antenna is the TM^z_{110} whose resonant frequency can be written as [26]

$$(f_r)_{110} = \frac{1.8412}{(2\pi R\sqrt{\mu\epsilon})} = \frac{1.8412 \cdot c}{(2\pi R\sqrt{\epsilon_r})}, \quad c = \textit{velocity of light} \tag{2.13}$$

The resonant frequency of equation 2.13 does not take the fringing fields into account. As was shown for a rectangular patch, the fringing fields make the patch look slightly larger and a length correction factor was used to take the fringing fields into account. Similarly, for the circular microstrip patch a correction factor is introduced for the effective radius R_e to replace the actual radius R in equation 2.13. The expression for R_e in terms of the antenna parameters is given equation 2.14 [26].

$$R_e = R\left[1+\frac{2\cdot h}{(\pi R\epsilon_r)}\left[\ln\left(\frac{\pi\cdot R}{(2\cdot h)}\right)+1.7726\right]\right]^{1/2} \tag{2.14}$$

Hence, the resonant frequency in equation 2.13 of the circular microstrip patch antenna for the dominant mode TM^z_{110} becomes [26]

$$(f_r)_{110} = \frac{1.8412\cdot c}{(2\pi R_e\sqrt{\epsilon_r})},\ c = velocity\ of\ light \tag{2.15}$$

As discussed earlier, the bandwidth of a microstrip patch antenna is considered to be the range of frequencies within which the performance of the antenna conforms to a specific standard. For a circular microstrip patch antenna, the bandwidth of the antenna is limited by its impedance. If the antenna impedance is matched to the transmission line at resonance, the mismatch off resonance is related to the VSWR. The bandwidth of the microstrip patch antenna is then defined by the acceptable value of the VSWR [26]. The bandwidth of a circular microstrip patch antenna for VSWR < S is given by equation 2.16

$$Bandwidth = 100\frac{(S-1)}{(Q_t\sqrt{S})},\ Q_t = \frac{f_r}{(\Delta f)} \tag{2.16}$$

where Q_t is the quality factor [26].

As with the rectangular patch, the total radiated fields of a circular microstrip patch antenna can be found by treating the patch, ground plane and the dielectric substrate as a cavity [26]. Using the cavity model, the radiated far field equations for a circular microstrip patch antenna operating in the dominant mode TM^z_{110} can be written as follows

$$E_r = 0 \tag{2.17}$$

$$E_{\vartheta} = -j\frac{(k_0 R_e V_0 e^{-j k_0 r})}{2r}\{\cos(\phi) J_{02}^{'}\} \tag{2.18}$$

$$E_{\phi} = j\frac{(k_0 R_e V_0 e^{-j k_0 r})}{2r}\{\cos(\vartheta)\sin(\phi) J_{02}\} \tag{2.19}$$

$$J_{02}^{'} = J_0(k_0 R_e \sin(\vartheta)) - J_2(k_0 R_e \sin(\vartheta)) \tag{2.20}$$

$$J_{02} = J_0(k_0 R_e \sin(\vartheta)) + J_2(k_0 R_e \sin(\vartheta)) \tag{2.21}$$

where R_e is the effective radius of the circular patch and $V_0 = hE_0J_1(kR_e)$ is the edge voltage at $\phi = 0°$ [26].

The fields in the principle planes are reduced to

E–plane ($\phi = 0°, 180°, 0° \le \theta \le 90°$) [26]

$$E_{\vartheta} = -j\frac{(k_0 R_e V_0 e^{-j k_0 r})}{2r}\{J_{02}^{'}\} \tag{2.35}$$

$$E_{\phi} = 0 \tag{2.36}$$

H–plane ($\phi = 90°, 270°, 0° \le \theta \le 90°$) [26]

$$E_{\vartheta} = 0 \tag{2.37}$$

$$E_{\phi} = j\frac{(k_0 R_e V_0 e^{-j k_0 r})}{2r}\{\cos(\vartheta) J_{02}\} \tag{2.38}$$

2.4 Broadband and dual band microstrip patch antennas

The major drawback of the conventional microstrip patch antennas (rectangular and circular patch antennas) is their narrow bandwidth. A technique used to widen the bandwidth of resonant circuits is to couple several resonators with very close resonance

frequencies. In order to understand the role of coupled resonators to enhance the bandwidth, an equivalent circuit can be used, as shown in Figure 2.5. This circuit consists of two coupled parallel resonant circuits, standing for two patches or one patch and a slot. Each resonant circuit has its own resonance frequencies and bandwidth. If these two resonance frequencies are close enough to each other, the total circuit seems to have a bandwidth equal to the sum of the two individual ones. However, if these two resonance frequencies are far apart from each other, then a dual band operation can be obtained [27].

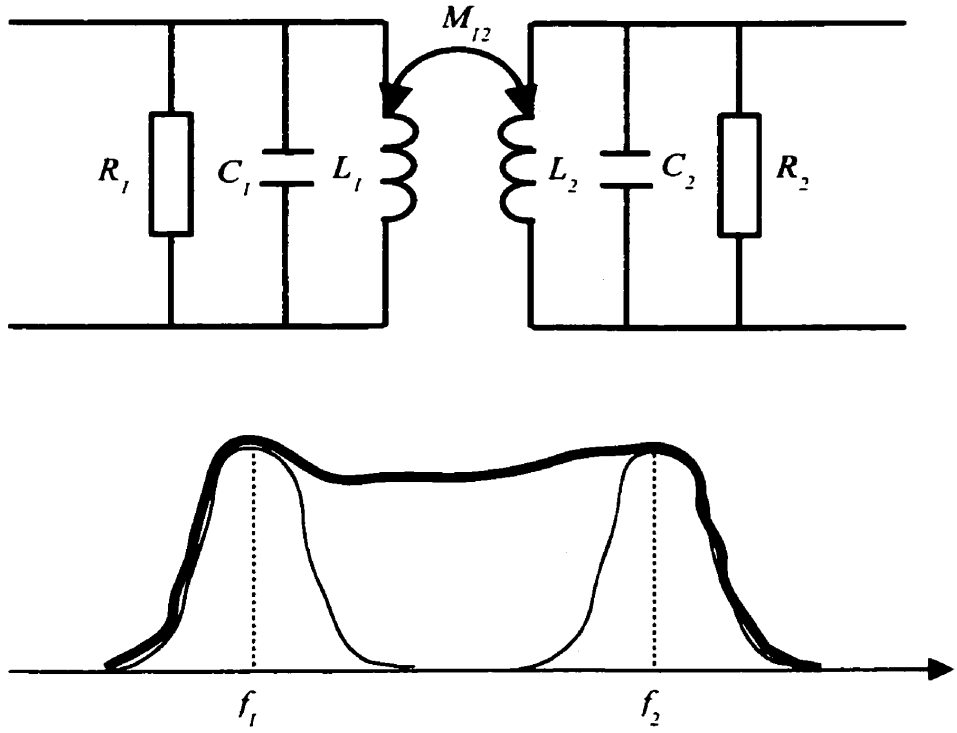

Figure 2.5: Equivalent circuit to model two coupled resonators.

One way of improving the bandwidth of a microstrip patch antenna to 10 – 20% is to use parasitic elements in the same layer [11]. In this coplanar geometry, the parasitic elements (dipoles) are placed next to the main radiating patch with slightly different

lengths, as shown in Figure 2.6. The side parasitic elements are excited by coupling from the main radiating patch. The parasitic elements must be placed symmetrical on both sides of the central patch so that the radiation maximum is normal to the antenna plane and the crosspolarization level is low [27]. The parasitic elements and the main radiating patch resonate at different frequencies that are very close to each other and they merge together to increase the bandwidth of the antenna.

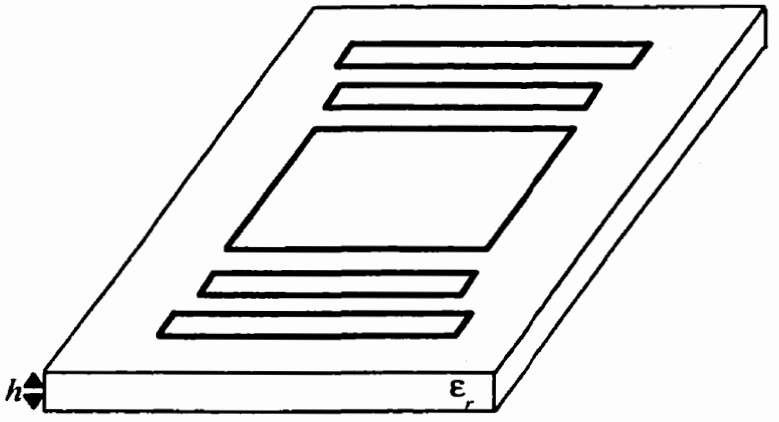

Figure 2.6: Geometry of a patch antenna with parasitic elements.

Even if bandwidth enhancement of a microstrip patch antenna can be achieved with the coplanar geometry, this geometry has many disadvantages. The coplanar geometry increases the lateral size of the antenna, hence increasing the cost of the antenna and making the fabrication process more difficult.

Another way of increasing the bandwidth of the microstrip patch antenna is to use two or more electromagnetically coupled patches that are placed on top of one another or stacked [10]. Figure 2.7 shows the geometry of stacked microstrip patches used to

increase the bandwidth. Because the surroundings of the two microstrip patches in a stacked geometry are slightly different, the resonant frequencies of the two patches are also slightly different, and they merge together to increase the frequency bandwidth. One can select different sizes of the two patches to increase the frequency bandwidth or to obtain dual band operation of the antenna [27]. In the stacked configuration, the lower patch is fed using one of the feeding methods, while the upper patch is electromagnetically coupled. The bandwidth of a microstrip patch antenna can also be increased by increasing the thickness of the double–layer structure or the single–layer geometry. However, the use of the thicker substrate leads to the excitation of the surface waves, which in not desired [27].

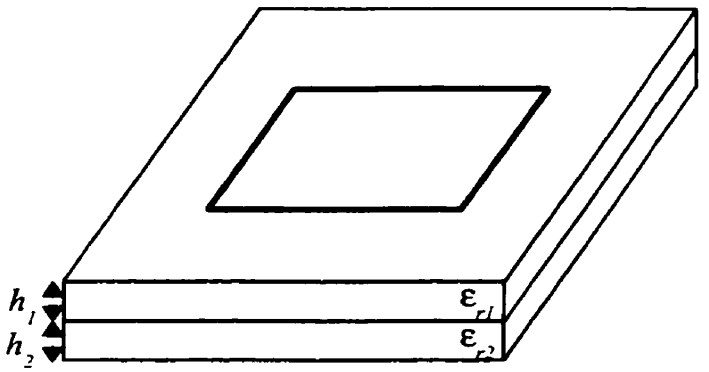

Figure 2.7 : Geometry of a stacked microstrip patch antenna.

Nevertheless, the stacked geometry has the disadvantage of increasing the thickness of the antenna and the coplanar geometry has the disadvantage of increasing the size of the antenna. Therefore, it would be of considerable interest if a single–layer single–patch wideband microstrip antenna could be designed. Such a microstrip antenna would still have its thin profile characteristics.

Lately, an experimental study was done on a new kind of broadband microstrip patch antenna with a U–shaped slot by Huynh and Lee [12]. In this single–layer single–patch microstrip antenna two different but close resonant frequencies are combined to a give a wideband operation [12]. Based on an assumption, it is presumed that the first resonance is generated by the microstrip patch, while the second resonance is excited by the U–shaped slot. This single–layer single–patch wideband microstrip antenna maintains its thin profile and small size characteristics. It has been confirmed by many published results that the bandwidths in the range of 30% can be obtained with the microstrip patch antenna with a U–shaped slot [12–22]. Even if the wideband characteristics of a microstrip patch antenna with a single U–shaped slot has been confirmed by many published results, no information is given on the resonance behavior of this antenna, which is the key point in obtaining the wideband operation of this antenna.

In the present work, the resonance behavior of the microstrip patch antenna with a single U–shaped slot is studied extensively. Two approximate equations for the resonance frequencies of the microstrip patch antenna with a single U–shaped slot are derived based on the surface current distribution analysis, which will be discussed in the next chapter along with other applications of broadband patch antennas and a dual band patch antenna.

2.5 Summary

In this chapter the background theory of a rectangular microstrip patch and a circular microstrip patch antenna was given. The formulas for the resonant frequency, input impedance, impedance bandwidth, quality factor and far field radiation were discussed for

both the rectangular patch and the circular patch microstrip antennas.

The background theory behind the broadband patch antennas was also discussed. Different ways of increasing the bandwidth of a conventional microstrip patch antenna were described; these are the use of coplanar geometry or stacked geometry. It was shown that the coplanar geometry has the disadvantage of increasing the size of the antenna while the stacked geometry increases the volume of the antenna. As opposed to the coplanar and stacked geometry, a single–layer single–patch microstrip antenna with a single U–shaped slot was introduced. As earlier mentioned, many published papers have confirmed the wideband characteristics of the microstrip patch antenna with a single U–shaped slot. However, no information has been provided on how the wideband operation of this antenna is achieved. This thesis project studies the resonance phenomena of the rectangular microstrip patch antenna with a U–shaped slot. As well as, some other broadband microstrip patch antennas and a dual band microstrip patch antennas are studied.

Chapter 3

Analysis of different Broadband Microstrip Patch Antennas

3.1 Introduction

In this thesis four different single–layer single–patch broadband microstrip antennas are studied. Since it has already been shown by many published results that the rectangular microstrip patch with a single–U shaped slot exhibits broadband characteristics [12–22], it is the first broadband patch antennas which is studied extensively in this thesis. The simulation results of this antenna for the resonance frequencies, impedance bandwidth, radiation patterns and surface current components are discussed in the first section. A bandwidth in the range of 30% can be achieved with this antenna. Even though many published papers have confirmed the broadband characteristics of this antenna, no study has been done on its resonance properties. This is investigated here. Two approximate equations are derived, which are based on the surface current distribution analysis on the microstrip patch.

A new type of broadband patch antenna is designed by making a significant change to the rectangular patch with a U–shaped slot. The U–shaped slot is replaced with a circular arc slot. The resonance frequencies, impedance bandwidth, radiation patterns and surface current components are presented for the rectangular patch with a circular arc shaped slot. This broadband patch antenna also provides a bandwidth in the range of 30%. Approximate equations for its two resonance frequencies are also developed, based on the

surface current distribution analyses.

The third configuration is obtained by changing the rectangular patch antenna with a circular arc slot to a circular patch. However, this new antenna does not have very broadband characteristics, and its bandwidth is limited to about 18%. Its simulation results are shown and discussed. As a fourth configuration, this chapter discusses the simulation results of another new type of broadband circular patch antenna with a circular arc shaped slot and L–shaped probe. Earlier, it has been shown by Guo, Luk and Lee that the circular patch antenna with a U–shaped slot and L–shaped probe demonstrate broadband properties with a bandwidth of 38% and gain of 6.8 dBi [24]. The new broadband circular patch antenna with a circular arc slot and L–shaped probe has a higher bandwidth and gain of 40% and 9.0 dBi, respectively.

3.2 Analysis of Antenna 1

Figure 3.1 shows the geometry of Antenna 1, which is the rectangular microstrip patch antenna with a single U–shaped slot. The rectangular patch of dimensions L x W is separated from the ground plane with a foam substrate of ε_r = 1.0006, and the U slot is located in its center. The location of the U–slot on the patch can be specified by parameters a and b. The width and the length of the two arms of the slot are denoted by W_s and L_s, while the thickness of the U slot is indicated by the parameter t. The rectangular patch is fed using a 50Ω coaxial probe with the inner diameter of 1.27 mm. The coaxial probe is located slightly below the center of the patch along the y–direction.

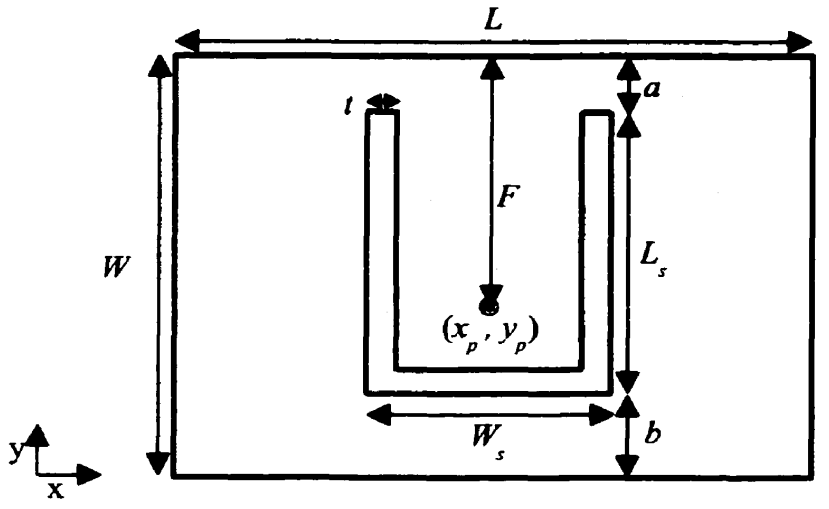

Figure 3.1: Geometry of the microstrip antenna with a single U–shaped slot.

3.2.1 Resonance frequencies and impedance bandwidth

Recently Lee et al. presented an extensive study on the U–slot rectangular patch antenna [13]. In order to study the characteristics of this antenna, the same dimensions as given in reference [13] are considered and will be referred to as Antenna 1. A rectangular patch with dimensions L x W = 35.5 mm x 26 mm is considered, which is separated from the ground plane with a foam substrate with ε_r = 1.0006 and thickness of h = 5.0 mm. The U–shaped slot with dimensions L_s x W_s = 19.5 mm x 12 mm is placed in the middle of the patch such that a = 3.2 mm and b = 3.3 mm. The ground plane is assumed to be infinite and the patch is fed using a coaxial probe at (x_p, y_p) = (0 mm, −2 mm) with the inner probe diameter of 1.27 mm, where (0, 0) is the center of the patch. Extensive computations are carried out to obtain the characteristics of this antenna.

The two resonance frequencies of Antenna 1 occur at f_1 = 4.16 GHz and f_2 = 5.28 GHz;

thus, the antenna is dual band, as shown in Figure 3.2. By lowering the location of the U–shaped slot so that $a = 4.2$ mm and $b = 2.3$ mm, the first resonance frequency increases from $f_1 = 4.16$ GHz to $f_1 = 4.24$ GHz and the second resonance frequency decreases from $f_2 = 5.28$ GHz to $f_2 = 5.0$ GHz. The simulation results from software Ansoft ENSEMBLE of this antenna for different locations of the U–shaped slot are shown in Figure 3.2.

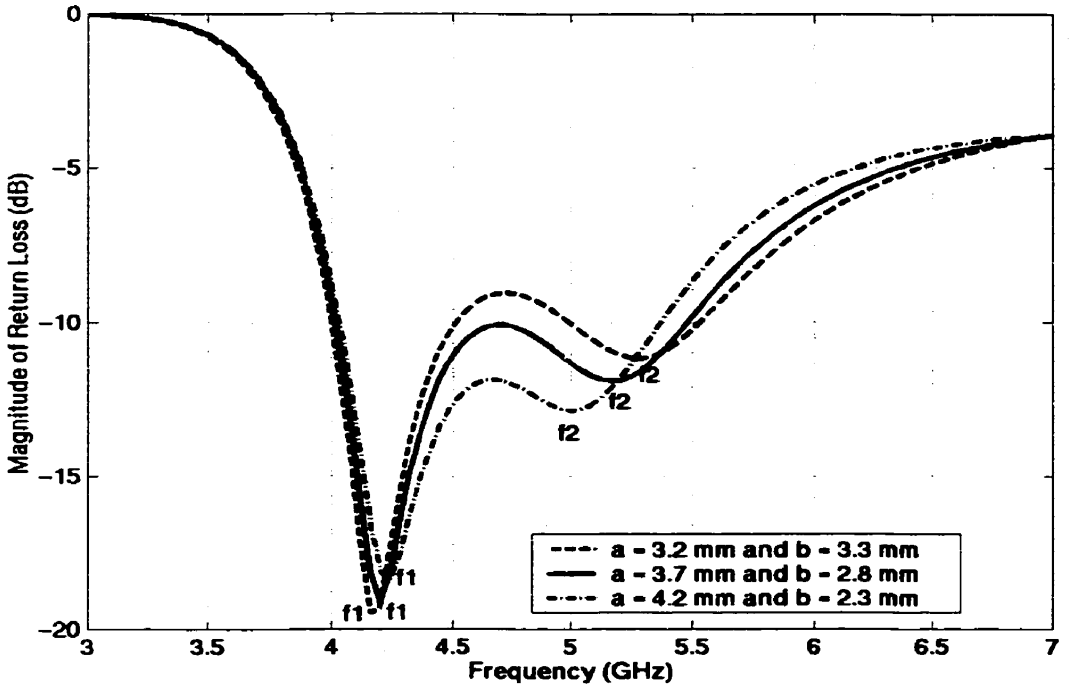

Figure 3.2: Return Loss of Antenna 1 for different a and b values with dimensions L = 35.5, W = 26, L_s = 19.5, W_s = 12, t = 2.1, F = 15, h = 5.0. All dimensions in mm.

As the U slot is lowered on the patch, the antenna becomes broadband and the −10 dB bandwidth of the antenna increases to 30.98% and then drops down to 28.33%. Therefore, the best result for the −10 dB bandwidth is obtained with $a = 3.7$ mm and $b = 2.8$ mm, where $f_1 = 4.2$ GHz and $f_2 = 5.16$ GHz.

The effect of various values of W_s (horizontal arm of the U–shaped slot) on the

resonance frequencies is investigated next. Figure 3.3 shows that by decreasing the value of W_s from 12 mm to 11.8 mm, the frequency f_1 stays the same at f_1 = 4.2 GHz and f_2 increases from f_2 = 5.16 GHz to f_2 = 5.2 GHz. With W_s = 12.2 mm, the frequency f_1 still occurs at f_1 = 4.2 GHz, however f_2 decreases from f_2 = 5.16 GHz to f_2 = 5.12 GHz. According to the results in Figure 3.3, the antenna becomes dual band with the decrease in W_s from 12 mm to 11.8 mm, while the bandwidth is slightly decreased with the increase in W_s from 12 mm to 12.2 mm. Hence, the best value of W_s is equal to 12 mm, where f_1 = 4.2 GHz and f_2 = 5.16 GHz.

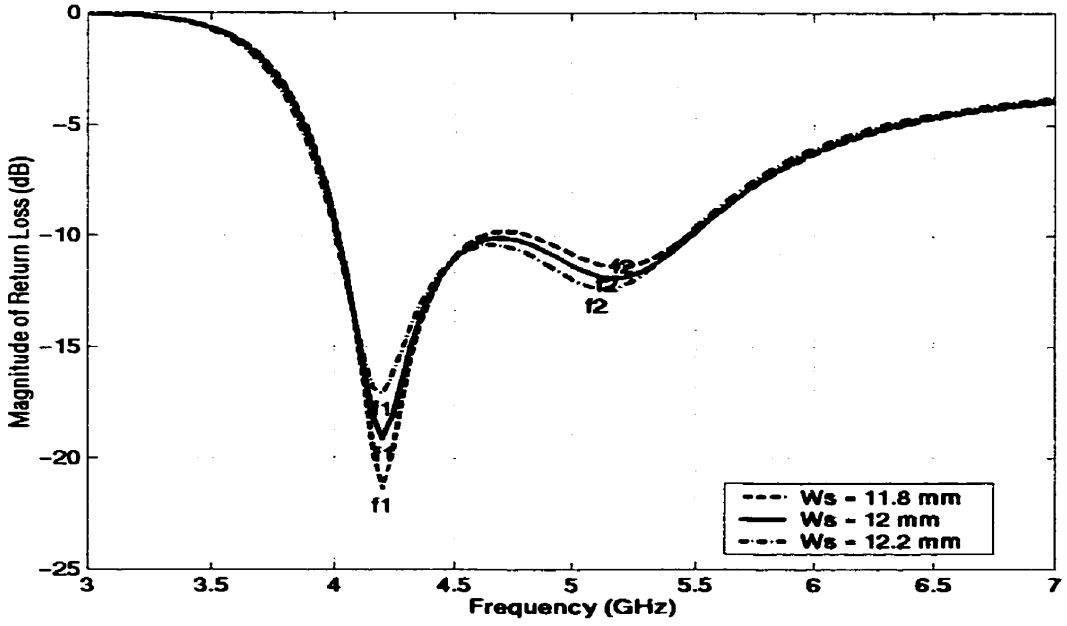

Figure 3.3: Return Loss of Antenna 1 for different values of W_s with dimensions L = 35.5, W = 26, L_s = 19.5, a = 3.7, b = 2.8, t = 2.1, F = 15, h = 5.0. All dimensions in mm.

It is observed that by changing the value of L_s (length of the two vertical arms of the U−slot) from 19.5 mm to 19.0 mm, f_1 stays the same and f_2 increases, while the −10 dB bandwidth decreases. By changing L_s from 19.5 mm to 20 mm, f_1 stays fixed and both f_2

and −10 dB bandwidth decrease. From this observation, it can be seen that L_s = 19.5 mm gives better results than the other two values of L_s.

Next, some observations are made when the width of the U−shaped slot t is varied. When the width of the U−shaped slot t is decreased from 2.1 mm to 2.0 mm, f_1 stays the same and f_2 is decreased. As t is increased from 2.1 mm to 2.2 mm, f_1 does not change and f_2 increases. From the high bandwidth standpoint, t = 2.1 mm gives the best results.

The effect of different values of W on the resonance frequencies is also studied. The results are shown in Figure 3.4. As the width of the patch W is decreased from W = 26 mm to 25 mm, f_1 increases from 4.2 GHz to 4.36 GHz, however f_2 does not change. The −10 dB bandwidth seems to decrease from 30.98% to 29.98% as the width of the patch is decreased. On the other hand, when the width of the patch W is increased from 26 mm to 27 mm, the frequency f_1 decreases from 4.2GHz to 4.04 GHz and f_2 is increased from 5.16 GHz to 5.2 GHz, while the −10 dB bandwidth decreases from 30.98% to 10.22%. Therefore, with the increase in the width of the patch W the frequency f_1 decreases and the frequency f_2 increases slightly. Consequently, the width of the patch W = 26 mm is near the optimal value since it gives the highest value of impedance bandwidth of 30.98%.

Next, the effect of different values of L is considered on the bandwidth of the antenna. Figure 3.5 shows that when L is changed from 35.5 mm to 37.5 mm, f_1 stays fixed and f_2 decreases slightly. However, the bandwidth decreases slightly and the matching gets better. From the high bandwidth and good matching standpoint, L = 37.5 mm is chosen as the best value, where f_1 = 4.2 GHz and f_2 = 5.12 GHz.

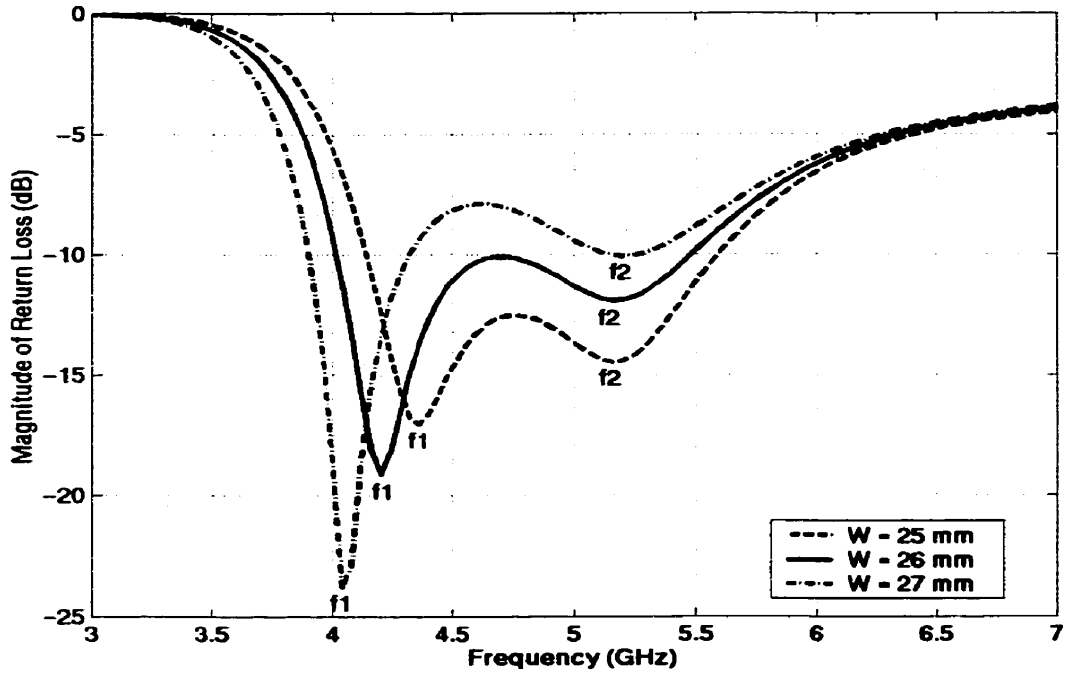

Figure 3.4:Return Loss of Antenna 1 for different values of W with dimensions L = 35.5, L_s = 19.5, W_s = 12, a = 3.7, b = 2.8, t = 2.1, F = 15, h = 5.0. All dimensions in mm.

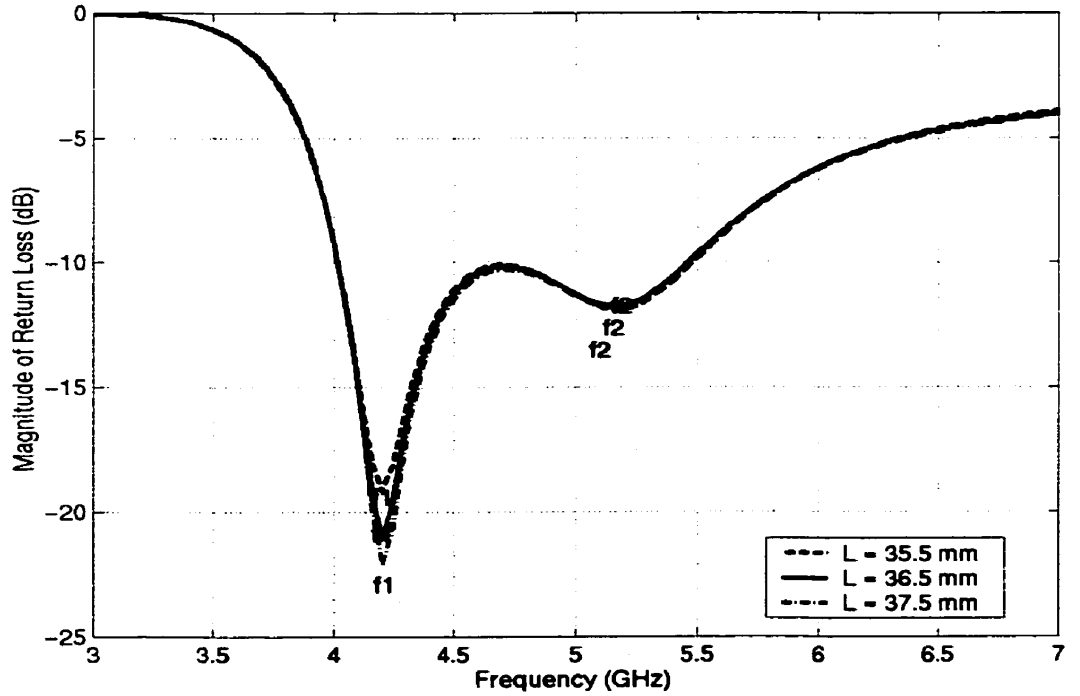

Figure 3.5:Return Loss of Antenna 1 for different values of L with dimensions W = 26, L_s = 19.5, W_s = 12, a = 3.7, b = 2.8, t = 2.1, F = 15, h = 5.0. All dimensions in mm.

It is observed that by increasing the height of the foam substrate from h = 5.0 mm to 5.5 mm and 6.0 mm, both frequencies f_1 and f_2 decrease, but the best result of −10 dB bandwidth of 32.7% is obtained with h = 5.5 mm, where f_1 = 4.12 GHz and f_2 = 5.08 GHz. This is demonstrated in Figure 3.6.

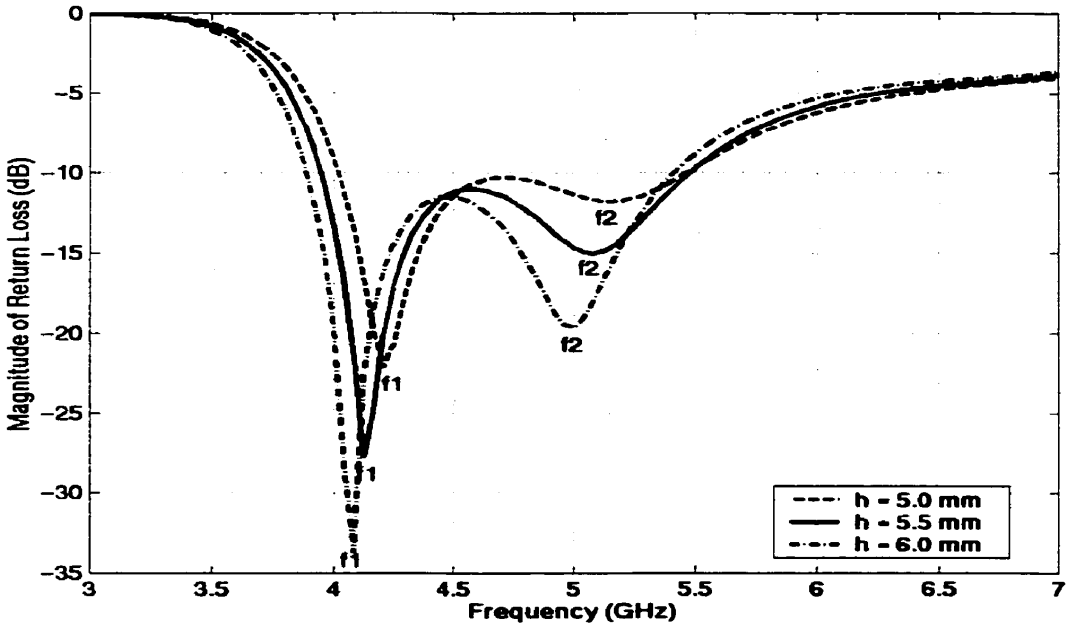

Figure 3.6: Return Loss of Antenna 1 for different values of h with dimensions L = 37.5, W = 26, L_s = 19.5, W_s = 12, a = 3.7, b = 2.8, t = 2.1, F = 15. All dimensions in mm.

3.2.2 Radiation patterns and gain patterns

The E and H plane radiation patterns of Antenna 1 with the optimal dimensions are shown in Figure 3.7. Like a simple rectangular patch, the rectangular patch with a single U−shaped slot also has a broad radiation pattern. Figure 3.7 shows the computed results of E_θ and E_ϕ in $\phi = 0$ plane and $\phi = 90$ plane at f_1 = 4.12 GHz. The copolarization results shown in Figure 3.7 in $\phi = 0$ plane and $\phi = 90$ plane appear to come from the TM_{01} mode since they have a maximum in the broadside direction. The crosspolarization level in ϕ =

0 plane seems to come from another mode due to the null at $\theta = 0$ and it is below −13 dB.

On the other hand, it is below −35 dB in $\phi = 90$ plane for f_1, which is very low.

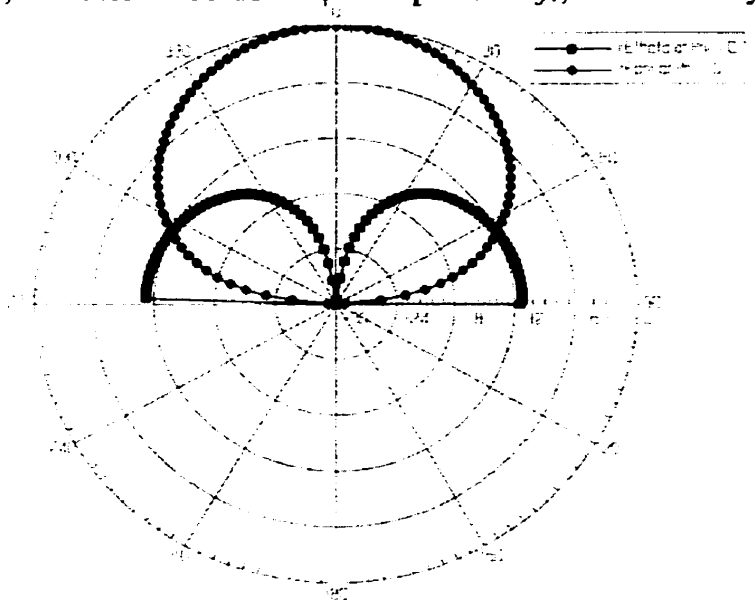

(*a*)

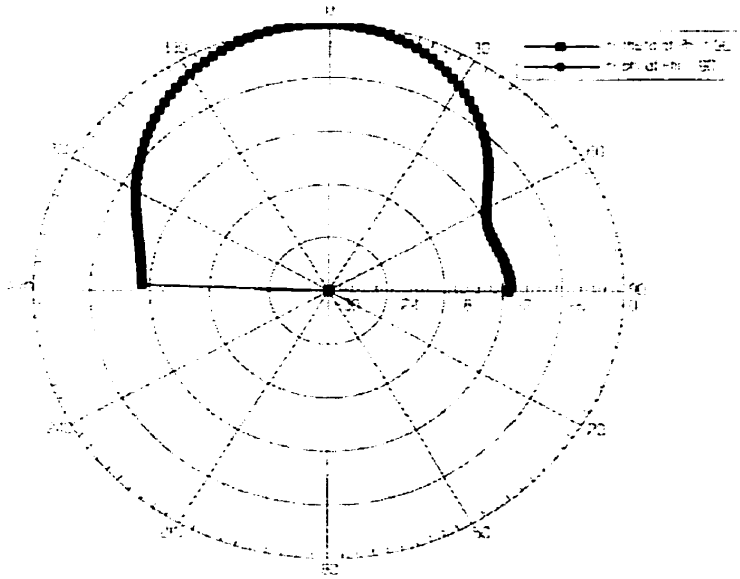

(*b*)

Figure 3.7:(a) Radiation patterns in ϕ = 0 plane of Antenna 1 with optimized dimensions at f_1 = 4.12 GHz. (b) Radiation patterns in ϕ = 90 plane of the Antenna 1 with optimized dimensions at f_1 = 4.12 GHz.

The computed results of E_θ and E_ϕ in $\phi = 0$ plane and $\phi = 90$ plane at $f_2 = 5.08$ GHz are shown in Figure 3.8. Figure 3.8 shows that the crosspolarization level in $\phi = 0$ plane for $f_2 = 5.08$ GHz is slightly higher than the crosspolarization level at $f_1 = 4.12$ GHz. In contrast, it is still below −35 dB in $\phi = 90$ plane for $f_2 = 5.08$ GHz.

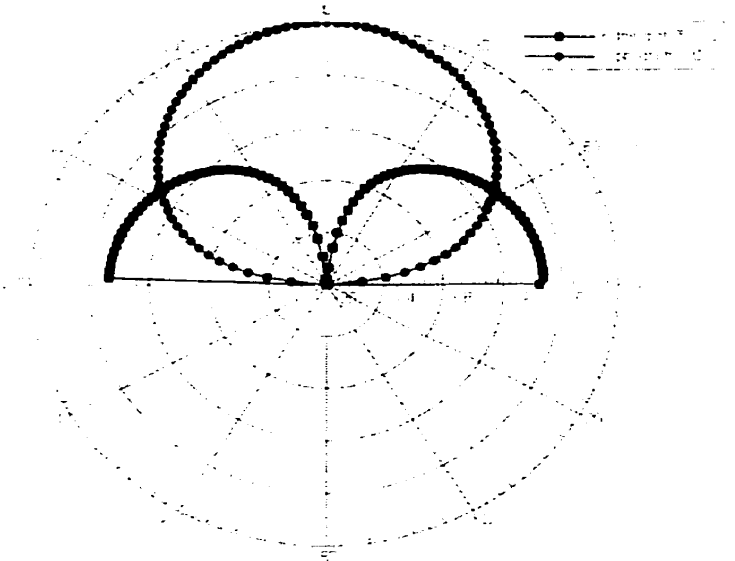

(*a*)

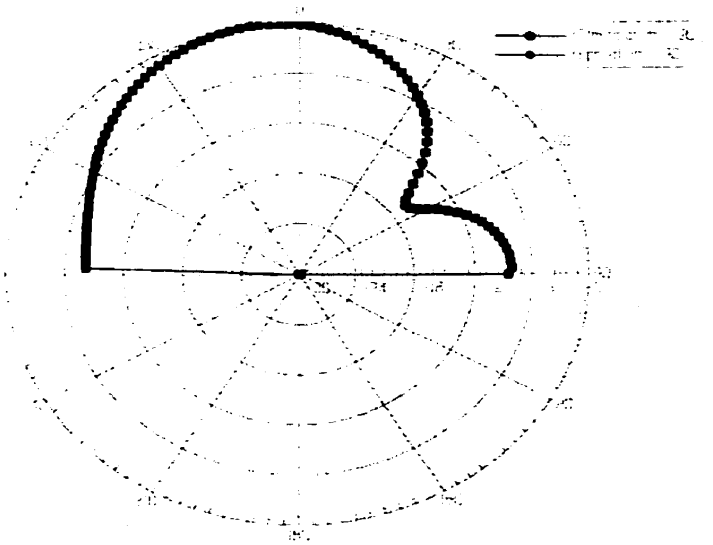

(*b*)

Figure 3.8:(a) Radiation patterns in $\phi = 0$ plane of Antenna 1 with optimized dimensions at $f_2 = 5.08$ GHz. (b) Radiation patterns in $\phi = 90$ plane of Antenna 1 with optimized dimensions at $f_2 = 5.08$ GHz.

The computed gain patterns of the antenna by Ansoft Ensemble software at f_1 = 4.12 GHz in ϕ = 0 plane and ϕ = 90 plane are shown plotted in Figure 3.9. Figure 3.10 shows the computed gain patterns in ϕ = 0 plane and ϕ = 90 plane at f_2 = 5.08 GHz. It can be seen that both resonance frequencies have similar gain patterns and the same polarization. The broadside gain of the antenna at f_1 = 4.12 GHz in ϕ = 0 plane and ϕ = 90 plane is 8.78 dBi. By observing the gain patterns in Figure 3.10 at f_2 = 5.08 GHz in ϕ = 0 plane and ϕ = 90 plane, it can be seen that the broadside gain of 8.19 dBi is achievable with this antenna. The crosspolarization level in ϕ = 0 plane for f_1 = 4.12 GHz is below −13 dB. However, the crosspolarization level in ϕ = 0 plane for f_2 = 5.08 GHz is slightly higher. In ϕ = 90 plane, the crosspolarization level for both f_1 and f_2 is below −35 dB, which is very low.

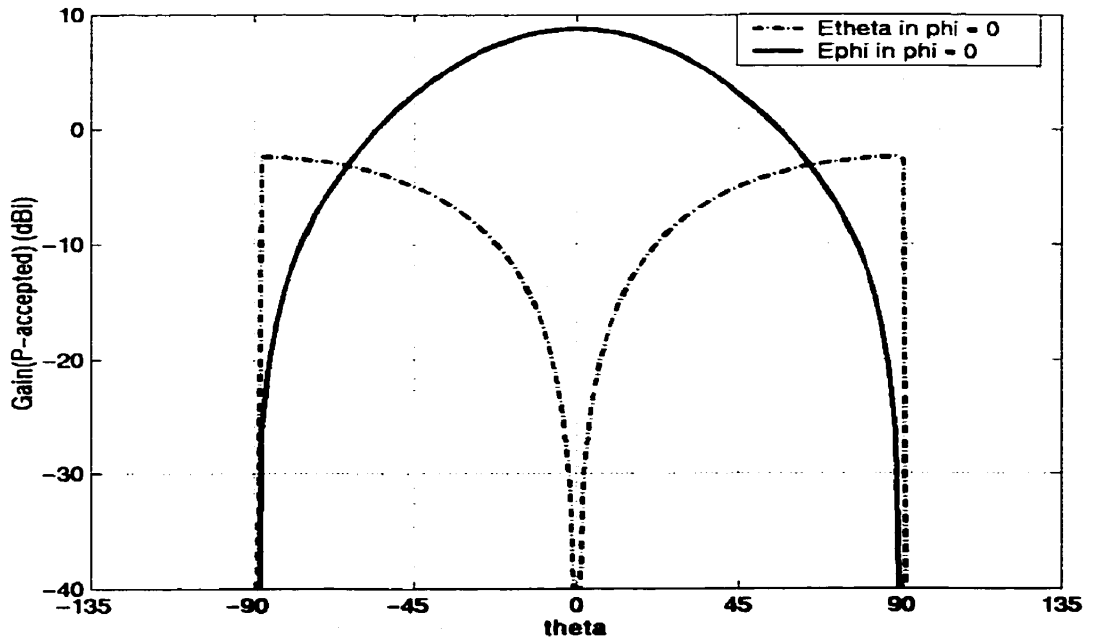

(a)

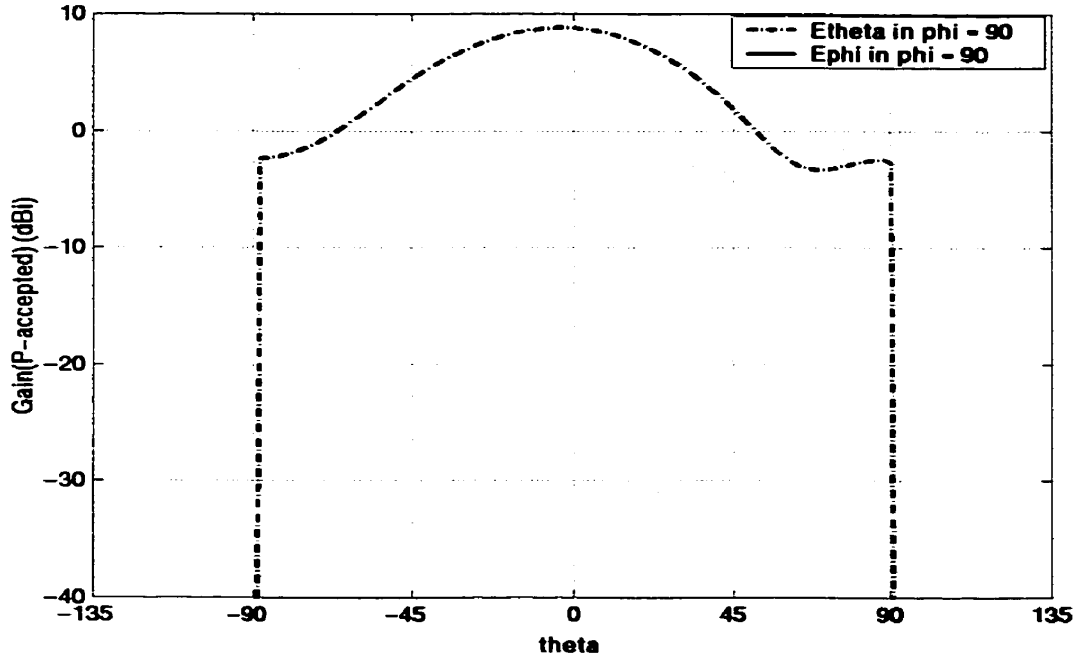

(*b*)

Figure 3.9: (a) Gain patterns in ϕ = 0 plane of Antenna 1 with optimized dimensions at f_1 = 4.12 GHz. (b) Gain patterns in ϕ = 90 plane of Antenna 1 with optimized dimensions at f_1 = 4.12 GHz.

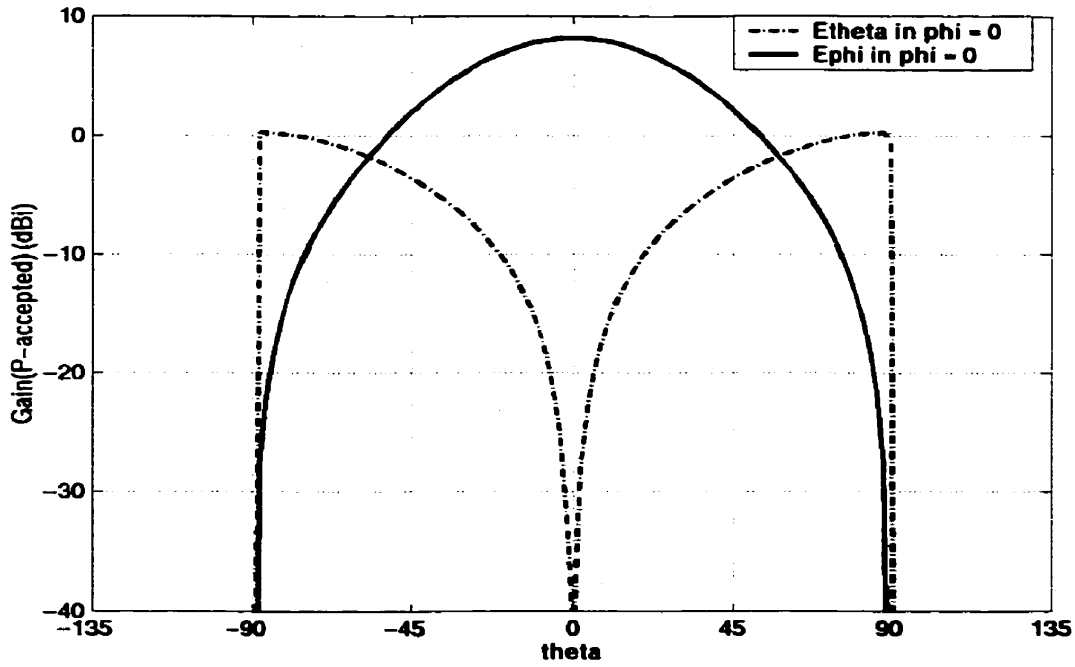

(*a*)

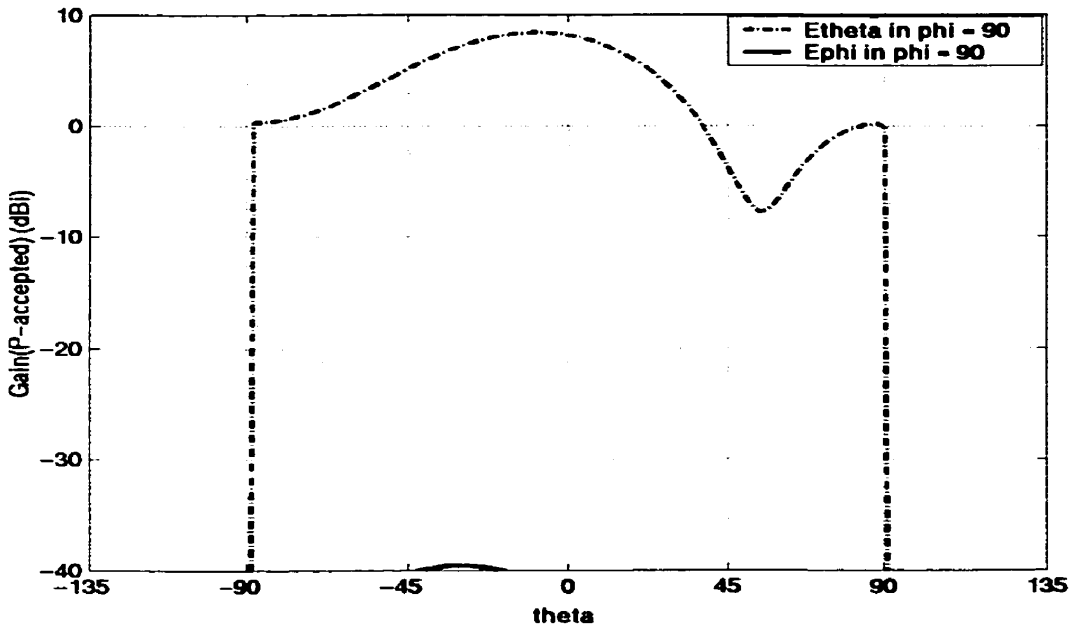

(*b*)

Figure 3.10:(a) Gain patterns in $\phi = 0$ *plane of Antenna 1 with optimized dimensions at* $f_2 = 5.08$ *GHz. (b) Gain patterns in* $\phi = 90$ *plane of Antenna 1 with optimized dimensions at* $f_2 = 5.08$ *GHz.*

3.2.3 Surface current components and current distribution analysis

In this section, the resonance behavior of the rectangular patch antenna with a single U-shaped slot is discussed. Approximate equations for the operating frequencies of this antenna are presented based on the surface current distribution analysis on the microstrip patch. They are found to be accurate within 2.36%.

Figure 3.11 (a) shows the surface current distribution of Antenna 1 with the optimum dimensions at the frequency $f_1 = 4.12$ GHz. This current distribution is that of the TM_{01} mode, but is strongly affected by the U slot. The surface currents originate behind the U slot and are strong on the patch outside the slot. Due to the presence of the U slot, the surface currents of the TM_{01} mode at $f_1 = 4.12$ GHz are forced to travel around it. Noting

that for this mode the resonance occurs when the current path length is equal to one half wavelength an approximate equation for f_1 can be derived. This condition is enforced on the average current path–length, which from Figure 3.11 (b) is the sum of two components A and B. Note that this average current path length includes the effect of fringing fields. Recall that the fringing fields at the two open ends are accounted for by adding equivalent lengths ΔW at both ends. The components of the current path length can be found from Figure 3.1, in terms of the antenna parameters as $A = W_s/2$ and $B = W + 2\Delta W - (b + \Delta W)/2$. The sum of these two components is equal to $\lambda_1/2 = A + B = W_s/2 + W + 3/2\Delta W - b/2$. An approximate equation for f_1 can then be written as

$$f_1 = \frac{c}{(2(\frac{W_s}{2} + W + \frac{3}{2}\Delta W - \frac{b}{2})\sqrt{\epsilon_e})}, \quad c = Velocity\ of\ light \tag{3.1}$$

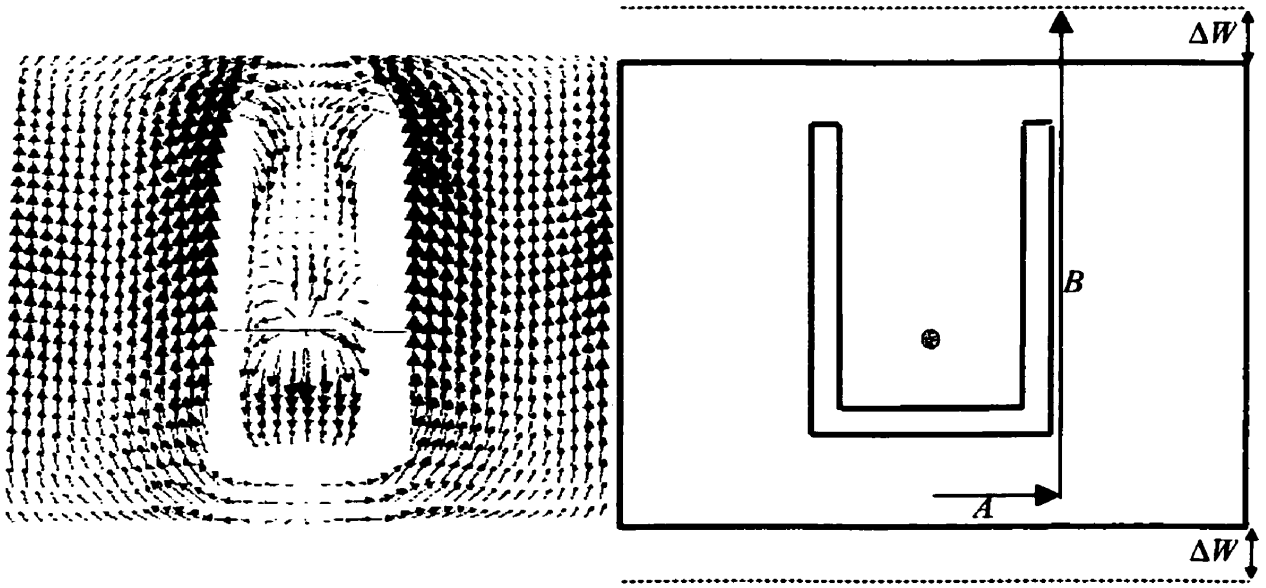

Figure 3.11: (a) Surface current distribution on microstrip patch at f_1 = 4.12 GHz. (b) Surface current–line path on the patch at f_1 = 4.12 GHz.

As it was shown in Chapter 2, the expression for ΔW in equation 3.1 can be written as

$$\Delta W = 0.412\,h\frac{(\epsilon_e+0.3)\cdot(\frac{L}{h}+0.264)}{((\epsilon_e-0.258)\cdot(\frac{L}{h}+0.8))} \tag{3.2}$$

where ε_e is the effective dielectric constant and is given by equation 2.2.

The situation is somewhat different at the second resonance f_2 = 5.08 GHz. The surface current distribution is strong at the patch center and immediate vicinity outside slot as shown in Figure 3.12 (a). It originates at the same level as probe location *P*, circulates around the arms of the U slot, and eventually terminates at the center point behind the slot. By inspection, one distinct path length in terms of the wavelength can be identified, which is shown in Figure 3.12 (b). It is the average distance between the probe and mid–point *P'* behind the slot. This current path length which is the sum of components *M*, *N*, *O* and *Q* appears to be equal to one wavelength. Noting that these components can be written in terms of the antenna parameters as $M = L/4$, $N = (W+2\Delta W) - (a + \Delta W)/2 - (b + \Delta W)/2$, $O = L/4 - (W_s - 2t)/4$ and $Q = (F + \Delta W) - (a + \Delta W)/2$. The sum of these components is equal to $\lambda_2 = M + N + O + Q = L/2 + W + 3/2\,\Delta W - W_s/4 + F - a - b/2 + t/2$. An approximate equation for f_2 can be written as

$$f_2 = \frac{c}{((\frac{L}{2}+W+\frac{3}{2}\Delta W-\frac{W_s}{4}+F-a-\frac{b}{2}+\frac{t}{2})\sqrt{\epsilon_e})} \tag{3.3}$$

where ΔW is the effective path length and is given by equation 3.2.

These two equations are used to compute the resonance frequencies of Antenna 1 for various antenna parameters that were considered in this section. Table 3.1 compares the

single U–slot microstrip patch resonance frequencies computed by Ansoft ENSEMBLE software and Equations (3.1) to (3.3) for different values of antenna parameters *a* and *b* in Figure 3.2.

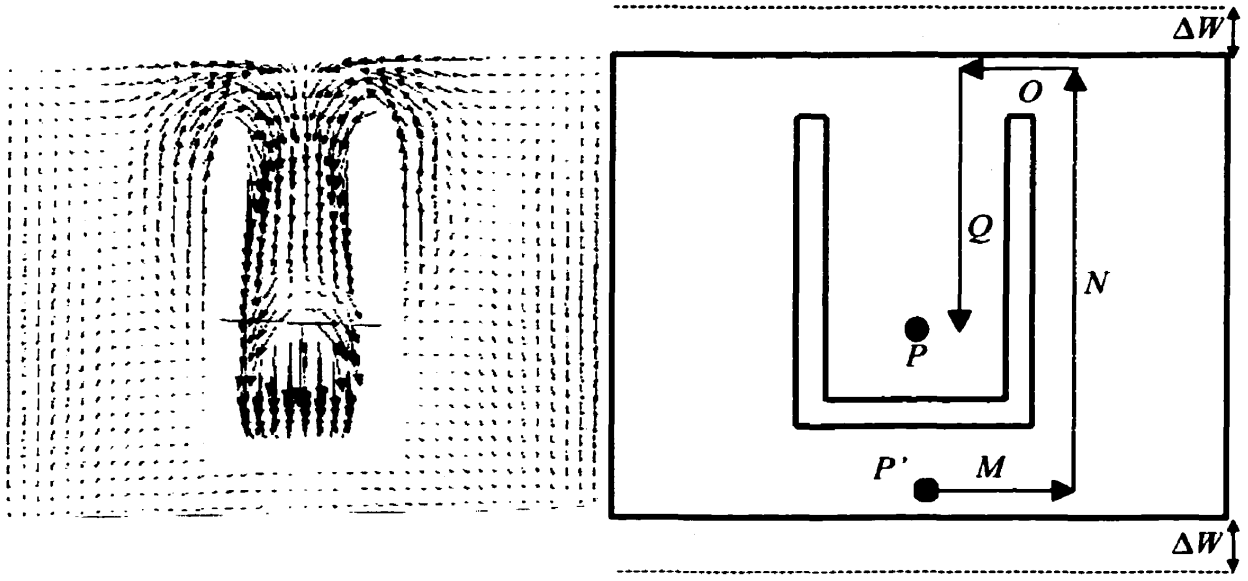

(*a*) (*b*)

Figure 3.12: (a) Surface current distribution on microstrip patch at f_1 = 5.08 GHz. (b) Surface current–line path on the patch at f_1 = 5.08 GHz.

Table 3.1: Comparison of Antenna 1 resonance frequencies computed by ENSEMBLE software and Equations (3.1) to (3.3) for *a* and *b* values in Figure 3.2.

U–slot Location (mm)	Computed using ENSEMBLE		Calculated by Equations (3.1) to (3.3)		Error between computed and calculated values	
	f_1 (GHz)	f_2 (GHz)	f_1 (GHz)	f_2 (GHz)	Δf_1 (%)	Δf_2 (%)
a=3.2, *b*=3.3	4.16	5.28	4.19	5.23	0.72	0.95
a=3.7, *b*=2.8	4.2	5.16	4.17	5.25	0.71	1.74
a=4.2, *b*=2.3	4.24	5	4.17	5.28	2.36	5.6

Table 3.1 shows that the computed results of the resonance frequencies using Ansoft

ENSEMBLE and equations 3.1 and 3.3 are very close to each other. Next, the computed results of the patch resonance frequencies by Ansoft ENSEMBLE and Equations (3.1) to (3.3) are compared for different values of W_s in Figure 3.3 and similar observations are made. The results are shown in Table 3.2.

Table 3.2: Comparison of Antenna 1 resonance frequencies computed by ENSEMBLE software and Equations (3.1) to (3.3) for values of W_s in Figure 3.3.

Horizontal arm of U−slot (mm)	Computed using ENSEMBLE		Calculated by Equations (3.1) to (3.3)		Error between computed and calculated values	
	f_1 (GHz)	f_2 (GHz)	f_1 (GHz)	f_2 (GHz)	Δf_1 (%)	Δf_2 (%)
W_s=11.8	4.2	5.2	4.18	5.25	0.48	0.96
W_s=12	4.2	5.16	4.17	5.25	0.71	1.74
W_s=12.2	4.2	5.12	4.15	5.26	1.19	2.73

Similarly, Table 3.3 and Table 3.4 compare the simulated values of the patch resonance frequencies with the calculated values for different W values in Figure 3.4 and different L values in Figure 3.5, respectively.

Table 3.3: Comparison of Antenna 1 resonance frequencies computed by ENSEMBLE software and Equations (3.1) to (3.3) for values of W in Figure 3.4.

Width of the patch (mm)	Computed using ENSEMBLE		Calculated by Equations (3.1) to (3.3)		Error between computed and calculated values	
	f_1 (GHz)	f_2 (GHz)	f_1 (GHz)	f_2 (GHz)	Δf_1 (%)	Δf_2 (%)
W=25	4.36	5.2	4.28	5.35	1.83	2.88

Width of the patch (mm)	Computed using ENSEMBLE		Calculated by Equations (3.1) to (3.3)		Error between computed and calculated values	
	f_1 (GHz)	f_2 (GHz)	f_1 (GHz)	f_2 (GHz)	Δf_1 (%)	Δf_2 (%)
W=26	4.2	5.16	4.17	5.25	0.71	1.74
W=27	4.04	5.16	4.05	5.16	0.25	0

Table 3.4: Comparison of Antenna 1 resonance frequencies computed by ENSEMBLE software and Equations (3.1) to (3.3) for values of L in Figure 3.5.

Length of the patch (mm)	Computed using ENSEMBLE		Calculated by Equations (3.1) to (3.3)		Error between computed and calculated values	
	f_1 (GHz)	f_2 (GHz)	f_1 (GHz)	f_2 (GHz)	Δf_1 (%)	Δf_2 (%)
L =35.5	4.2	5.16	4.17	5.25	0.71	1.74
L =36.5	4.2	5.12	4.17	5.21	0.71	1.76
L =37.5	4.2	5.12	4.17	5.16	0.71	0.78

Table 3.5 compares the computed results of the resonance frequencies of Antenna 1 by the equations 3.1 and 3.3 and Ansoft ENSEMBLE for various values of substrate height h, as shown in Figure 3.6. As the substrate height h is increased, both f_1 and f_2 decrease, this is due to the fringing fields on the microstrip patch. Equations 3.1 and 3.3 are function of ΔW, which is due to the fringing fields. Equation 3.2 shows that the parameter ΔW is a function of substrate height h. Therefore, as the substrate height h is varied, the frequencies f_1 and f_2 also vary. The results shown in Table 3.5 demonstrate that the simulated values of the resonance frequencies are in good agreement with the

calculated values. Small percentage errors of the calculations shown in Table 3.1 to Table 3.5 confirm the accuracy of the selected equations and the selected resonant length of currents on the patch.

Table 3.5: Comparison of Antenna 1 resonance frequencies computed by ENSEMBLE software and Equations (3.1) to (3.3) for values of h in Figure 3.6.

Substrate height (mm)	Computed using ENSEMBLE		Calculated by Equations (3.1) to (3.2)		Error between computed and calculated values	
	f_1 (GHz)	f_2 (GHz)	f_1 (GHz)	f_2 (GHz)	Δf_1 (%)	Δf_2 (%)
h =5.0	4.2	5.12	4.17	5.16	0.71	0.78
h =5.5	4.12	5.08	4.1	5.11	0.49	0.59
h =6.0	4.04	5	4.04	5.07	0	1.4

3.2.4 Antenna synthesis and parametric study of Antenna 1

In this section, the antenna synthesis of the single U slot patch antenna is studied. By doubling the dimensions of the antenna, the resonant frequency of the antenna is reduced by half, however the operation bandwidth remains the same. This is applied to Antenna 1 with dimensions L = 40 mm, W = 26 mm, L_s = 19.5 mm, W_s = 12 mm, a = 3.7 mm, b = 2.8 mm, t = 2.1 mm, F = 15 mm, h = 5.5 mm, ε_r = 1.03 and R_p = 0.635 mm (radius of probe), as shown in Figure 3.1. The ε_r = 1.03 is used to do this study because that is the only foam substrate material available to fabricate the antenna. With these dimensions, the operating frequencies of Antenna 1 occur at f_1 = 4.12 GHz, f_2 = 5.0 GHz, f_3 = 3.92 GHz and f_4 = 5.4 GHz, as shown in Figure 3.13, where the −10 dB bandwidth is 31.76%.

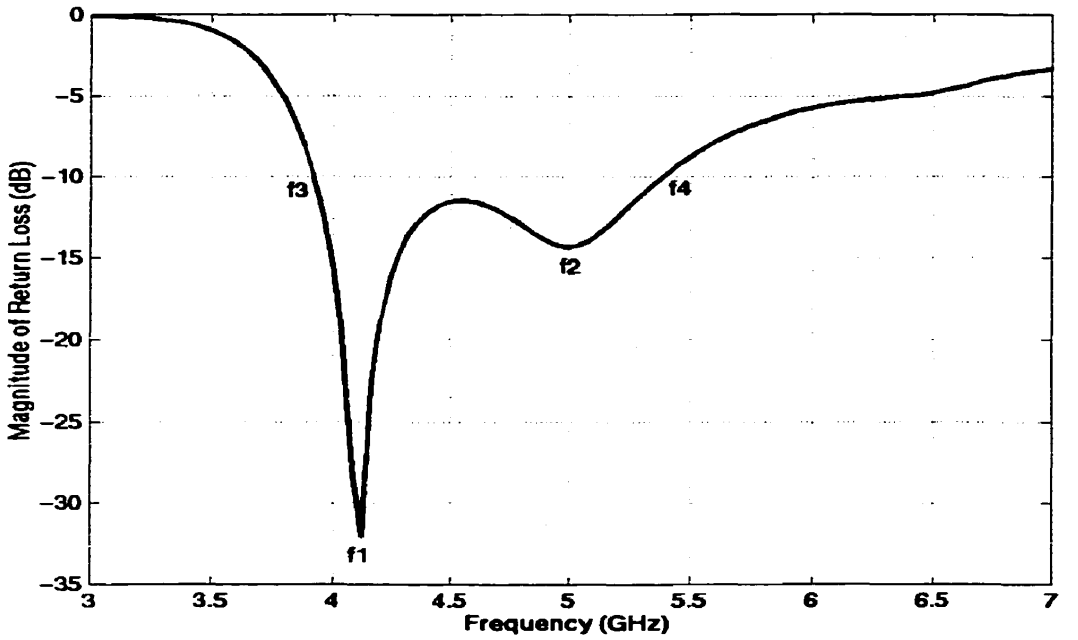

Figure 3.13: Return Loss of Antenna 1 with dimensions L = 40, W = 26, Ls = 19.5, Ws = 12, a = 3.7, b = 2.8, t = 2.1, F = 15, h = 5.5, R_p = 0.635. All dimensions in mm.

The same operation bandwidth of 31.76% can be obtained at the lower frequencies by adjusting the dimensions of the antenna. For example, if the antenna dimensions in Figure 3.13 are doubled, such that L = 80 mm, W = 52 mm, L_s = 39 mm, W_s = 24 mm, a = 7.4 mm, b = 5.6 mm, t = 4.2 mm, F = 30 mm, h = 11 mm, ε_r = 1.03 and R_p = 1.27 mm then the operating frequencies are reduced by half. This is demonstrated in Figure 3.14 where the operating frequencies of Antenna 1 occur at f_1 = 2.06 GHz, f_2 = 2.5 GHz, f_3 = 1.96 GHz and f_4 = 2.7 GHz and the −10 dB bandwidth is equal to 31.76%. Note that the frequencies f_1 to f_4 shown in Figure 3.14 are exactly half of the frequencies f_1 to f_4 in Figure 3.13, while the −10 dB bandwidth of 31.76% remains the same.

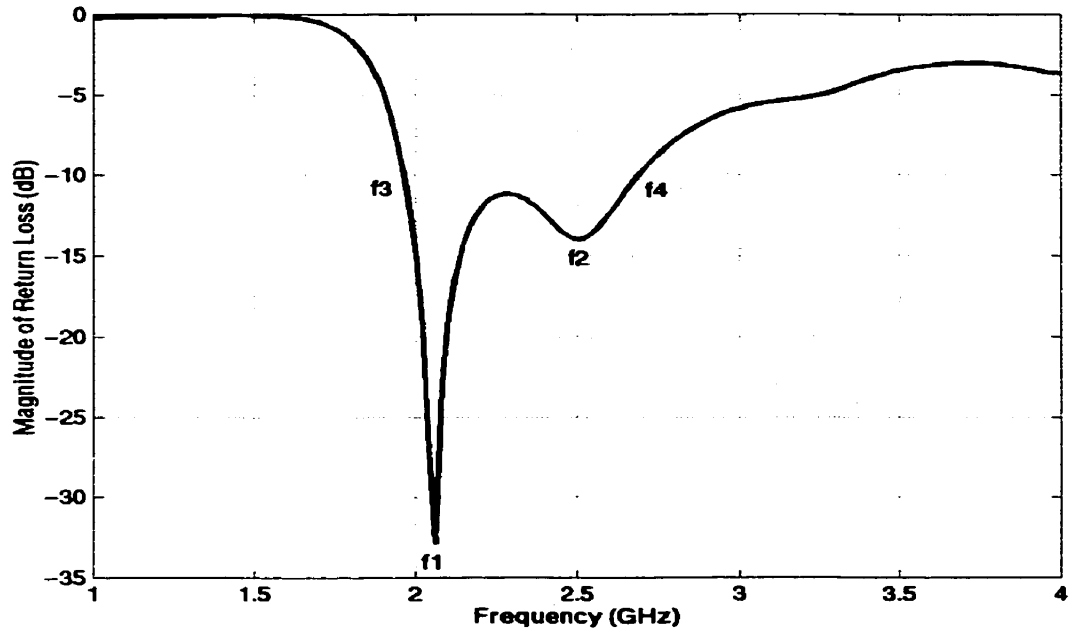

Figure 3.14: Return Loss of Antenna 1 with dimensions L = 80, W = 52, L_s = 39, W_s = 24, a = 7.4, b = 5.6, t = 4.2, F = 30, h = 11, R_P = 1.27. All dimensions in mm.

Next the parametric study of the synthesized single U slot microstrip patch antenna is presented which has the dimensions as in Figure 3.14. Figure 3.15 shows the effect of different probe radii on the impedance bandwidth, for various substrate heights while the rest of the antenna dimensions are the same as in Figure 3.14. The probe radius R_p = 1.27 mm gives the best impedance bandwidth of 31.76% at h = 11 mm. On the other hand, R_p = 0.635 mm gives slightly lower −10 dB bandwidth in the upper range of substrate heights, while it gives higher bandwidth values in the lower range. The bandwidth values around 5% to 12% are achieved with R_p = 2.0 mm, which are extremely low, which is due to antenna becoming dual band. Similarly, the effect of changing the probe location on the antenna bandwidth for various values of substrate heights is shown plotted in Figure 3.16.

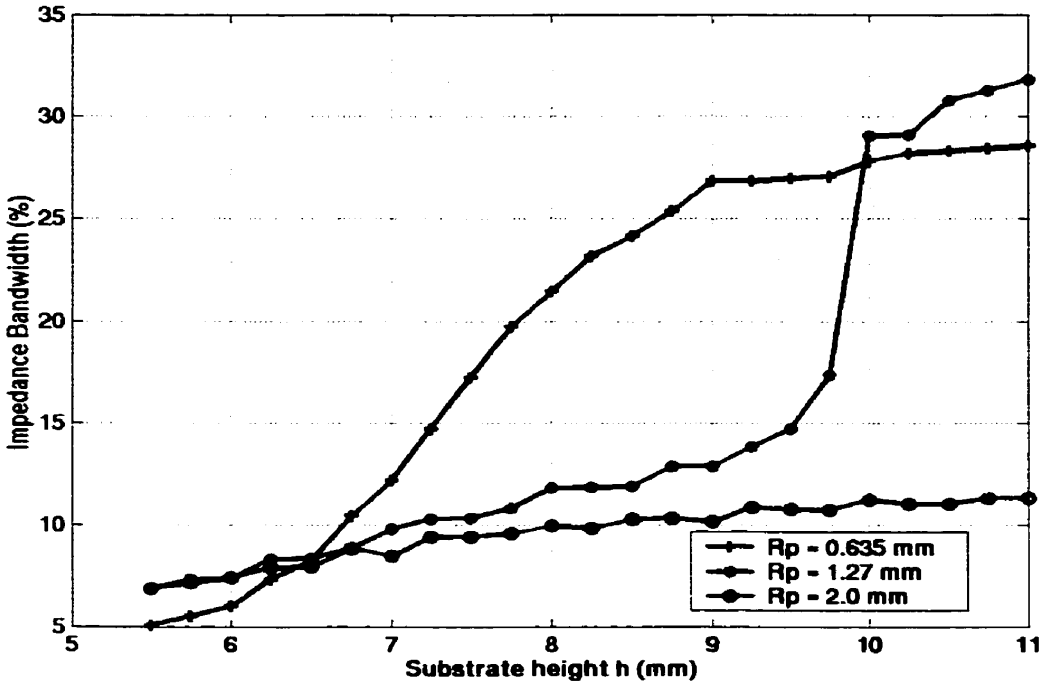

Figure 3.15: Effect of different values of R_p on the impedance bandwidth with L = 80, W = 52, L_s = 39, W_s = 24, a = 7.4, b = 5.6, t = 4.2, F = 30. All dimensions in mm.

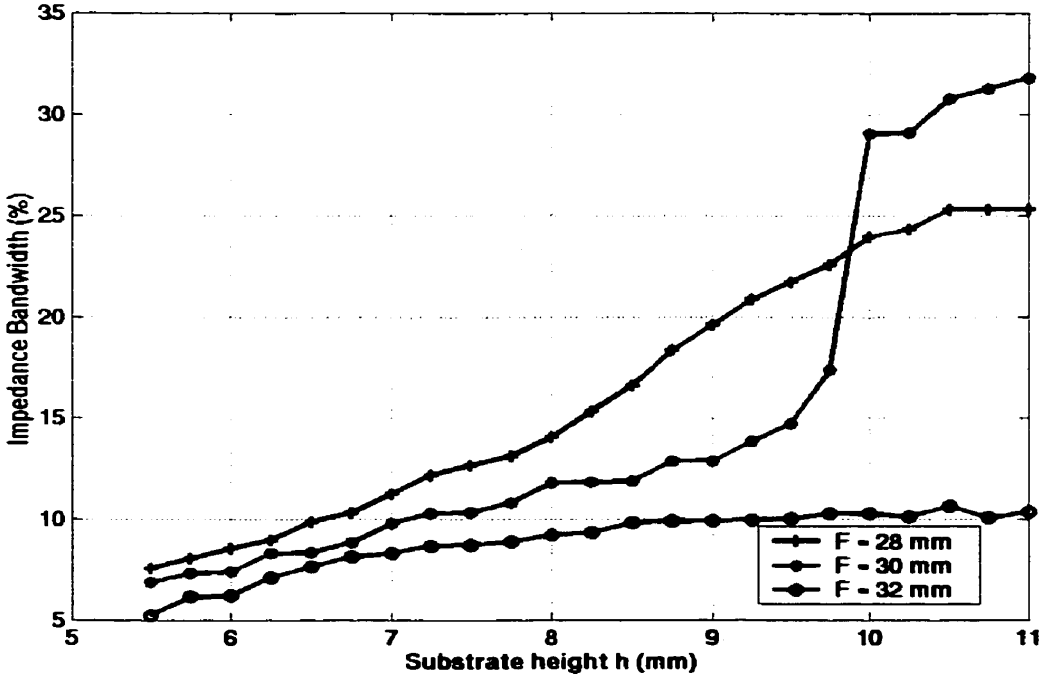

Figure 3.16: Effect of different values of F on the impedance bandwidth with L = 80, W = 52, L_s = 39, W_s = 24, a = 7.4, b = 5.6, t = 4.2, R_p = 1.27. All dimensions in mm.

Figure 3.16 shows that the highest bandwidth is obtained with $F = 30$ mm. In contrast, $F = 28$ mm produces a bit lower bandwidth in upper substrate height range and slightly higher bandwidth in the lower substrate height range. The probe location $F = 32$ mm gives the lowest impedance bandwidths for all values of substrate heights, again due to antenna becoming dual band.

Next the vertical arm length L_s and the horizontal arm W_s of the U slot is varied to observe the effect on the impedance bandwidth of the antenna. From Figure 3.17, it can be seen that the bandwidth increases as the substrate height is increased. The best bandwidth is achieved with $L_s = 39.0$ mm at $h = 11$ mm. The bandwidth results obtained with $L_s = 41.0$ mm are also good.

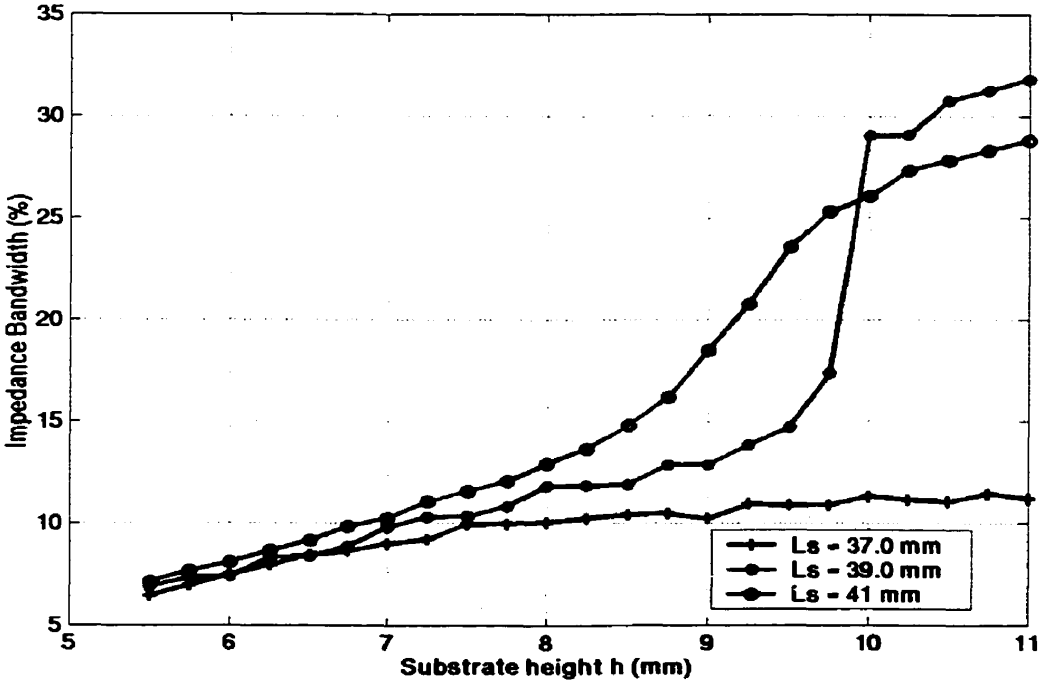

Figure 3.17: Effect of different values of L_s on the impedance bandwidth with $L = 80$, $W = 52$, $W_s = 24$, $a = 7.4$, $b = 5.6$, $t = 4.2$, $F = 30$, $R_p = 1.27$. All dimensions in mm.

It can be seen from the results shown in Figure 3.18 that the similar impedance bandwidths are obtained for three different values of W_s. The bandwidth increases as the substrate height increases. Three different values of W_s give good bandwidth results in the higher range of the substrate heights.

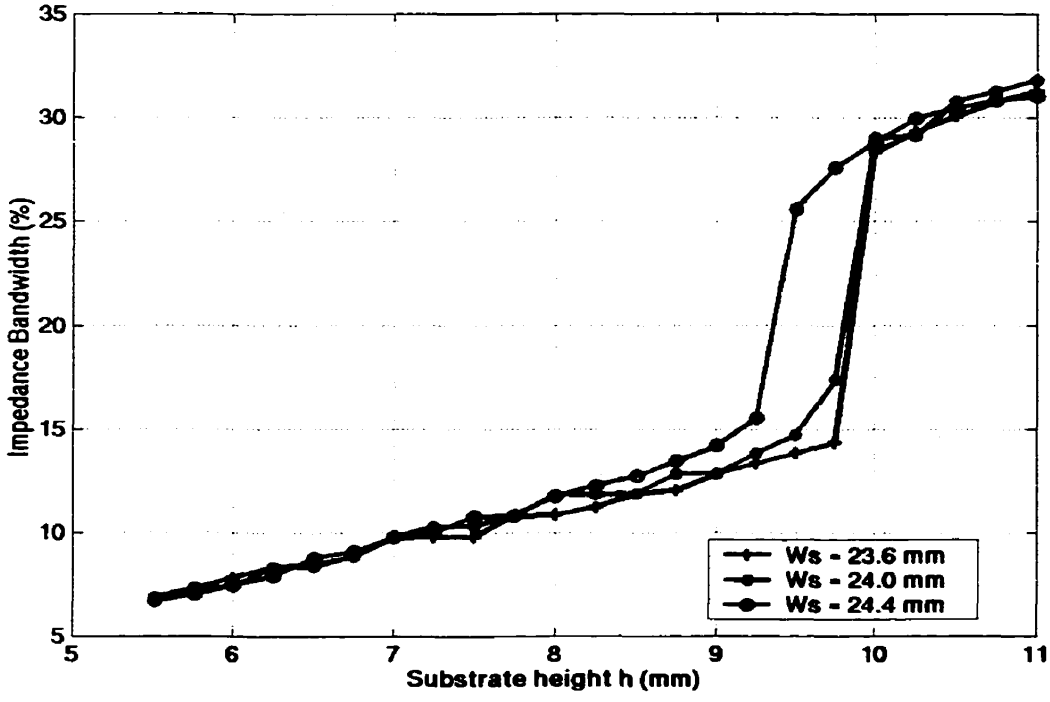

Figure 3.18: Effect of different values of W_s on the impedance bandwidth with L = 80, W = 52, L_s = 39, a = 7.4, b = 5.6, t = 4.2, F = 30, R_p = 1.27. All dimensions in mm.

In a similar manner, the plots of impedance bandwidth vs. substrate height h are produced for different values of a and b. Figure 3.19 shows the bandwidth curves for three different values of a and b. They give similar bandwidth results in the lower range of substrate height, but in the higher range, a = 7.4 mm and b = 5.6 mm give the best bandwidth results. Figure 3.20 displays the plots of bandwidth vs. h for various t (width of the U slot) values.

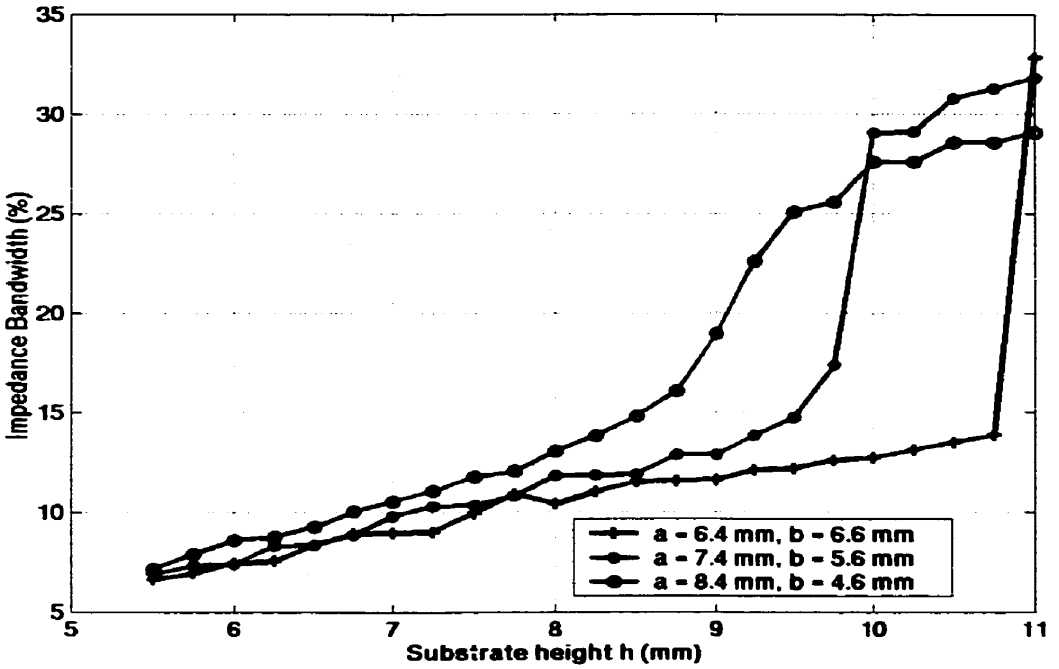

Figure 3.19: Effect of different values of a and b on the impedance bandwidth with L = 80, W = 52, L_s = 39, W_s = 24, t = 4.2, F = 30, R_p = 1.27. All dimensions in mm.

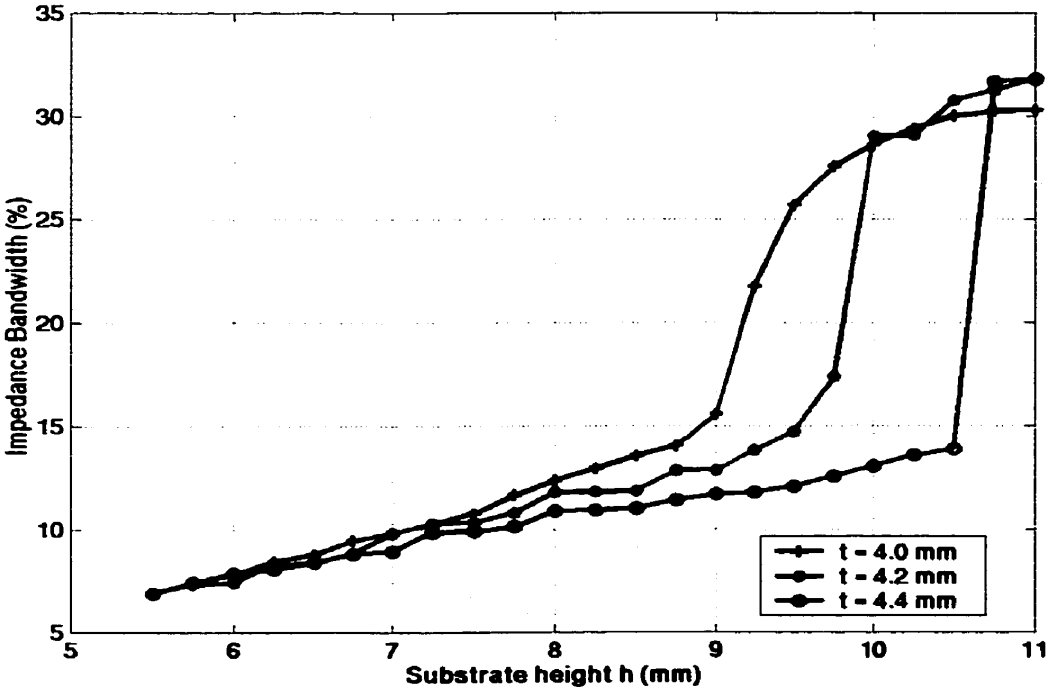

Figure 3.20: Effect of different values of t on the impedance bandwidth with L = 80, W = 52, L_s = 39, W_s = 24, a = 7.4, b = 5.6, F = 30, R_p = 1.27. All dimensions in mm.

Similar observations can be made from the results shown in Figure 3.20. In the lower range of h, the bandwidth results are very similar for three different t values. As the substrate height increases more than 9 mm, the bandwidth increases smoothly with $t = 4.0$ mm. On the other hand, there is a sharp change in the impedance bandwidth with $t = 4.2$ mm and 4.4 mm.

3.3 Analysis of Antenna 2

In the previous section, the broadband characteristics of the single U–slot patch antenna were verified. The bandwidths in the range of 30% to 32% were achieved. In this section, a new type of broadband patch antenna is studied. In this new configuration, the U–slot is replaced with a circular arc slot. This new antenna also demonstrates broadband characteristics. The obtainable bandwidth with this antenna is also in the range of 30%. The parametric study of this new broadband antenna is presented in the following sections.

The geometry of the rectangular microstrip patch antenna with a circular arc shaped slot is shown in Figure 3.21. The rectangular patch of dimensions L x W is separated from the ground plane with a foam substrate of height h and $\varepsilon_r = 1.0006$, and a circular arc shaped slot is located in its center. The center point of the two circular arcs is given by (x_c, y_c), as shown in Figure 3.21. The end points of the first and second arcs are given by (a_1, b_1) and (a_2, b_2), respectively. The position of the circular arc slot on the rectangular patch can be specified by the parameter d, while the width of the circular arc slot is indicated by the variable t. The patch is fed using a 50Ω coaxial probe at (x_p, y_p) with the inner diameter of 1.27 mm. The coaxial probe is located slightly below the center of the

patch along the y–direction. To study the characteristics of this antenna, extensive computations are performed, and discussed below.

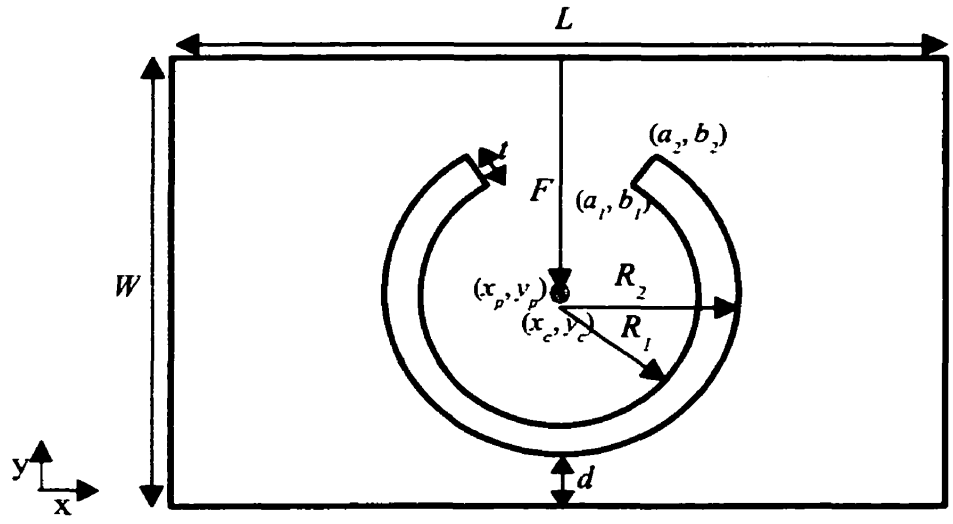

Figure 3.21: Geometry of the microstrip patch antenna with a circular arc shaped slot.

3.3.1 Resonance frequencies and impedance bandwidth

To begin with, the optimized dimensions of the rectangular patch antenna with a U–shaped slot are applied to the rectangular patch with a circular arc slot. The two resonance frequencies of the circular arc slot antenna with the dimensions, L x W = 37.5 mm x 26 mm, (x_c, y_c) = (0, 1 mm), (a_1, b_1) = (5.5 mm, 7.5 mm), (a_2, b_2) = (7 mm, 9 mm), t = 2.12 mm, (x_p, y_p) = (0, −2 mm) such that F = 15 mm and h = 5.5 mm, occur at f_1 = 3.56 GHz and f_2 = 5.16 GHz. The −10 dB bandwidth of the patch antenna with these dimensions is calculated to be 12.4%. This means that the dimensions of the rectangular patch antenna with a circular shaped slot needs to be optimized to obtain wide impedance bandwidth. By changing the thickness of the circular arc slot to t = 2.83 mm, the −10 dB

bandwidth increases to 15.2% but then drops back to 13.0% with t = 3.18 mm. As the thickness of the circular arc slot is increased, both frequencies f_1 and f_2 increase. The computed results are shown in Figure 3.22. Since t = 2.83 mm gives the highest bandwidth in Figure 3.22, it seems to be near the optimal value.

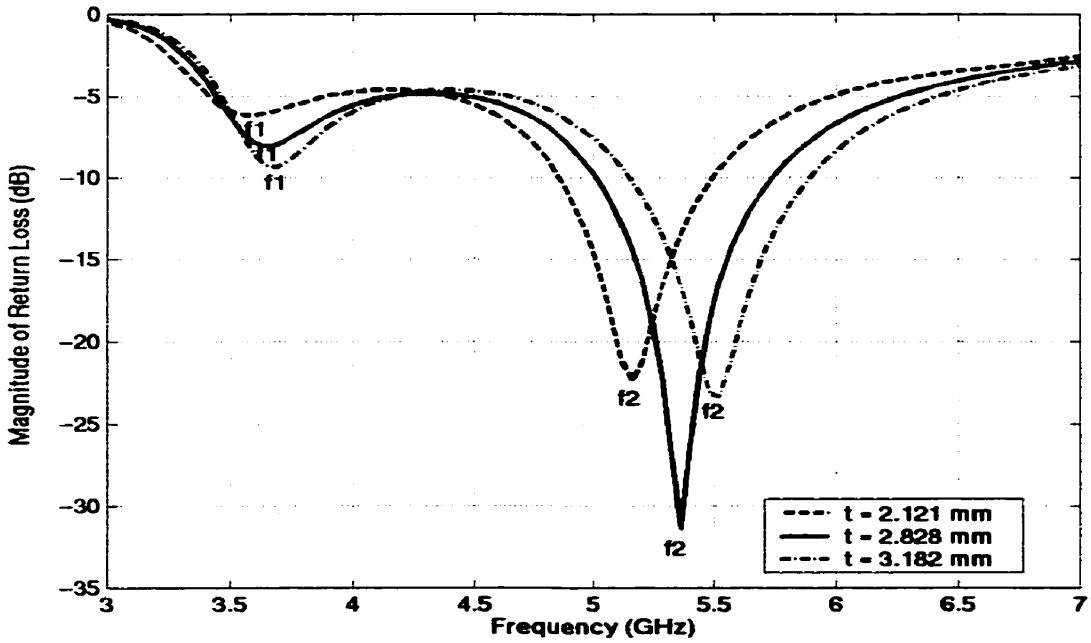

Figure 3.22: Return Loss of Antenna 2 for different values of t with antenna dimensions of L = 37.5, W = 26, (x_c, y_c) = (0, 1), (a_1, b_1) = (5.5, 7.5), (a_2, b_2) = (7, 9), d = 3.37, (x_p, y_p) = (0, −2), F = 15, h = 5.5. All dimensions in mm.

By carrying out several computations, it is observed that in order to obtain wide bandwidths with this antenna, the size of the patch must be increased and the location of the arc slot must be lowered. Accordingly, the new dimensions of the antenna are computed with the Ansoft ENSEMBLE, where L x W = 54 mm x 27 mm, (x_c, y_c) = (0, −1.5 mm), (a_1, b_1) = (5.0 mm, 4.5 mm), (a_2, b_2) = (7 mm, 6.5 mm), t = 2.83 mm, (x_p, y_p) = (0, −1.5 mm) such that F = 15 mm and h = 5.5 mm. With these dimensions, the two resonances occur at f_1 = 3.76 GHz and f_2 = 4.68 GHz, as shown in Figure 3.23. However,

the −10 dB bandwidth is still not very broad with 6.32% in the first band and 15.5% in the second band. Figure 3.23 also shows the effect of changing the width of patch W on the two resonance frequencies and −10 dB bandwidth. It can be seen from Figure 3.23 that as the width of the patch is increased, both f_1 and f_2 decrease. The −10 dB bandwidth in the first band increases and thus the probability of obtaining a wide bandwidth increases.

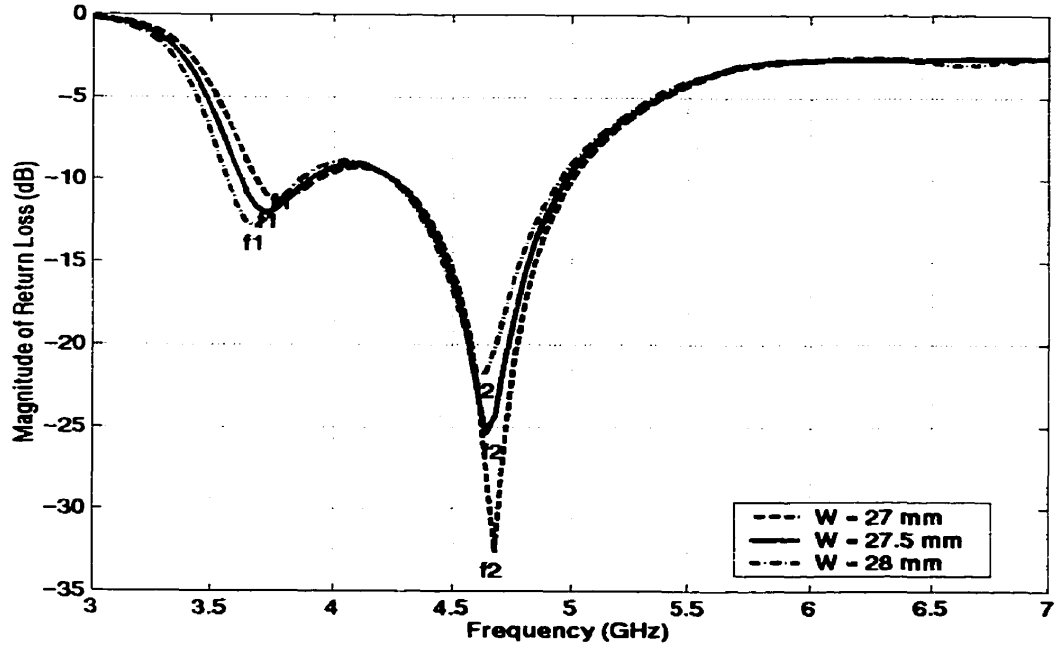

Figure 3.23: Return Loss of Antenna 2 for different values of W with antenna dimensions of L = 54, (x_c, y_c) = (0, −1.5), (a_1, b_1) = (5, 4.5), (a_2, b_2) = (7, 6.5), t = 2.83, (x_p, y_p) = (0, −2), h = 5.5. All dimensions in mm.

Next, the size of the patch is increased further and the location of the circular arc slot in lowered more to observe the effect on the bandwidth. The −10 dB bandwidth of 30.1% is achieved with the following dimensions of the antenna: L x W = 55.5 mm x 29 mm, (x_c, y_c) = (0, −2.5 mm), (a_1, b_1) = (5.0 mm, 3.5 mm), (a_2, b_2) = (7 mm, 5.5 mm), t = 2.83 mm, d = 1.37 mm, (x_p , y_p) = (0, −1.5 mm) such that F = 16 mm and the foam substrate height h = 5.5 mm. With this configuration, the first resonance f_1 appears at f_1 = 3.64 GHz

and the second one at f_2 = 4.44 GHz, as shown in Figure 3.24. The simulation results obtained from the software Ansoft Ensemble for the return loss, and different probe feed locations, are shown in Figure 3.24. According to these results, as the probe position is lowered (i.e. as F increases) the frequency f_1 does not change, while the second resonance f_2 increases with the −10 dB bandwidth. However, if the probe position is lowered any further so that the value of F increases more than 16 mm, the antenna looses its broad bandwidth characteristics.

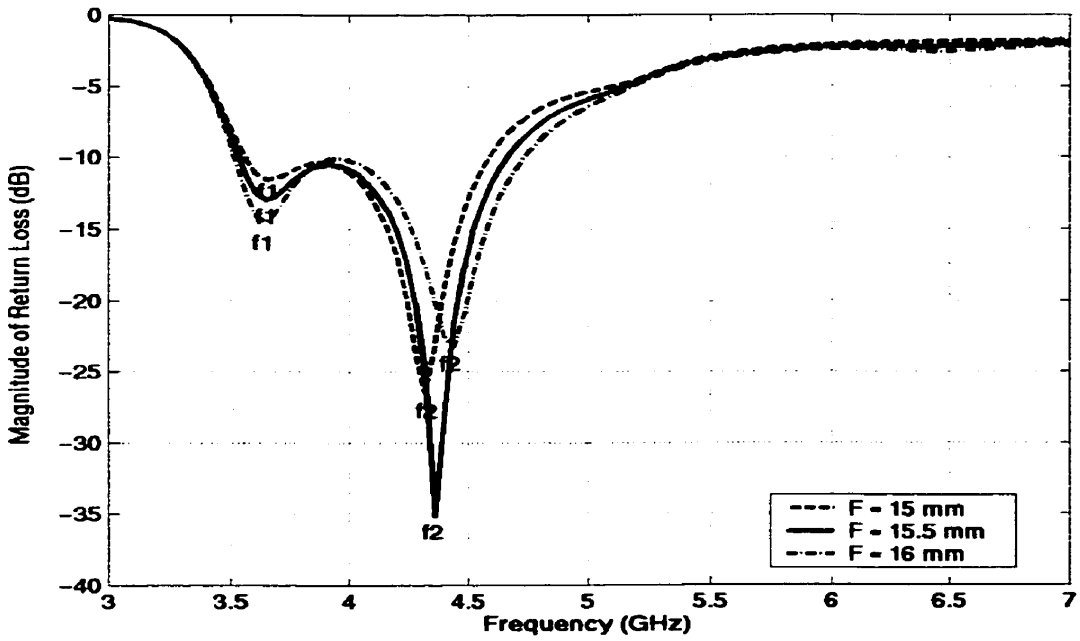

Figure 3.24: Return Loss of Antenna 2 for different values of F with antenna dimensions of L = 55.5, W = 29, (x_c, y_c) = (0, −2.5), (a_1, b_1) = (5, 3.5), (a_2, b_2) = (7, 5.5), t = 2.83, d = 1.37, h = 5.5. All dimensions in mm.

3.3.2 Radiation patterns and gain patterns

According to the results in Figure 3.24, the dimensions of Antenna 2 near optimum values give 30.1% impedance bandwidth and the two resonances occur at f_1 = 3.64 GHz and f_2 = 4.44 GHz. The E and H plane radiation patterns obtained from Ansoft Ensemble

at f_1 = 3.64 GHz are shown in Figure 3.25. The rectangular patch with a circular arc slot also has a broad radiation pattern. Figure 3.25 shows the computed results of E_θ and E_ϕ in $\phi = 0$ plane and $\phi = 90$ plane at f_1 = 3.64 GHz.

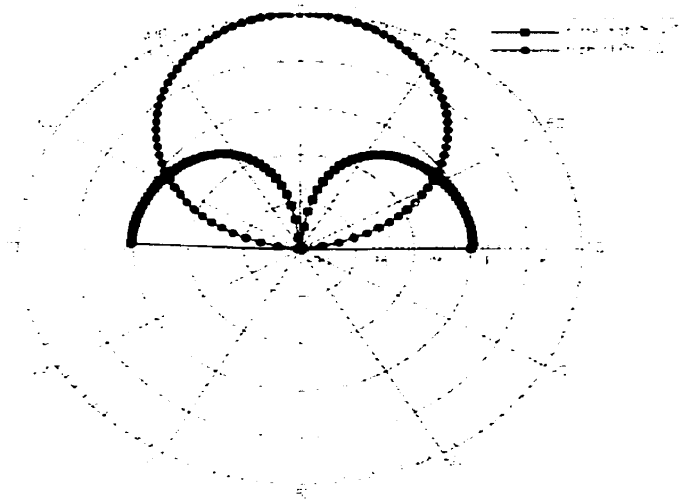

(*a*)

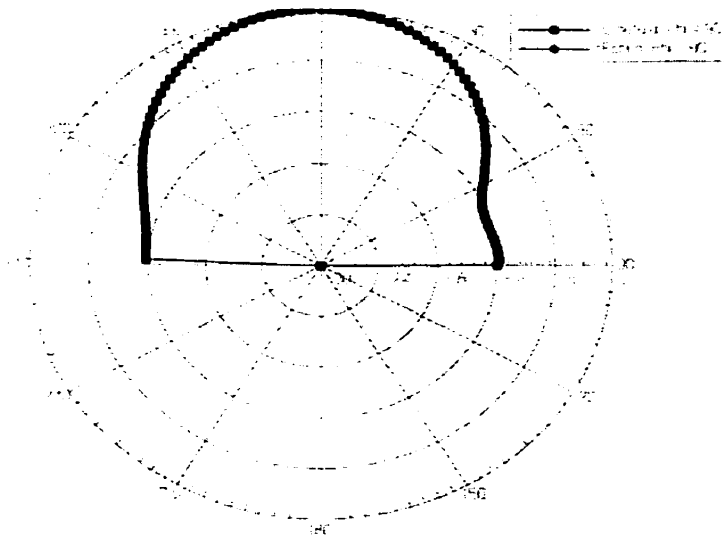

(*b*)

Figure 3.25:(a) Radiation patterns in ϕ = 0 plane of Antenna 2 with optimized dimensions at f_1 = 3.64 GHz. (b) Radiation patterns in ϕ = 90 plane of Antenna 2 with optimized dimensions at f_1 = 3.64 GHz.

In Figure 3.25, the copolarization patterns in $\phi = 0$ and $\phi = 90$ planes seem to come from the TM_{01} radiating mode, while the crosspolarization in $\phi = 0$ plane is due to another radiating mode. Figure 3.25 shows that the crosspolarization level in $\phi = 0$ plane for f_1 = 3.64 GHz is below −13 dB, while in $\phi = 90$ plane its level for f_1 is extremely low.

Figure 3.26 displays the computed results of E_θ and E_ϕ in $\phi = 0$ plane and $\phi = 90$ plane at f_2 = 4.44 GHz. When comparing Figure 3.25 with Figure 3.26, at f_2 = 4.44 GHz the crosspolarization level in $\phi = 0$ plane is a little higher than the crosspolarization level at f_1 = 3.64 GHz. Nevertheless, it is below −35 dB in $\phi = 90$ for f_2 as well.

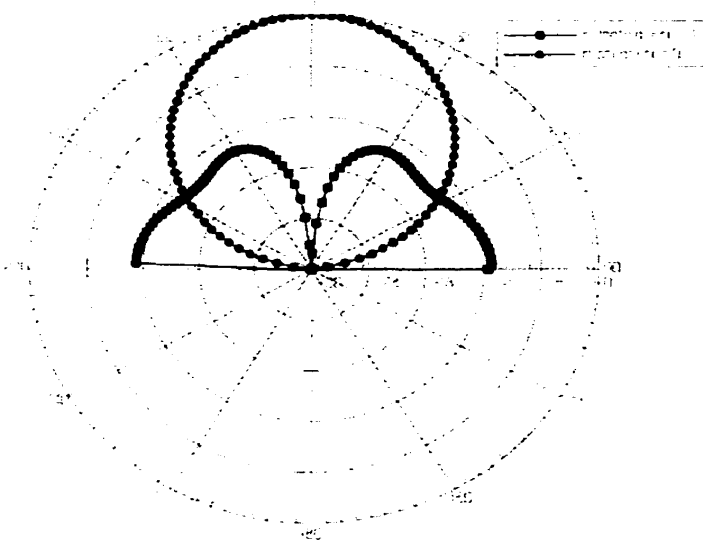

(*a*)

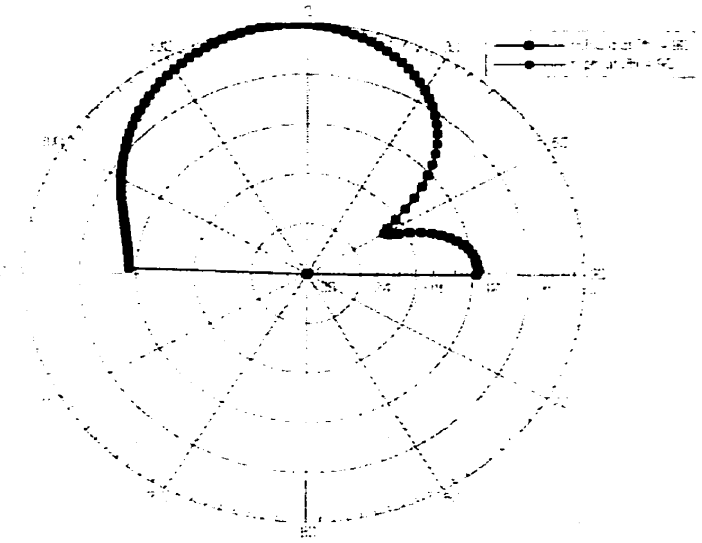

(*b*)

Figure 3.26: (a) Radiation patterns in ϕ *= 0 plane of Antenna 2 with optimized dimensions at* f_2 *= 4.44 GHz. (b) Radiation patterns in* ϕ *= 90 plane of Antenna 2 with optimized dimensions at* f_2 *= 4.44 GHz.*

The gain patterns of the antenna at f_1 = 3.64 GHz in ϕ = 0 plane and ϕ = 90 plane are plotted in Figure 3.27. Figure 3.28 shows the computed gain patterns at f_2 = 4.44 GHz in ϕ = 0 plane and ϕ = 90 plane. While comparing the gain patterns of both f_1 = 3.64 GHz and f_2 = 4.44 GHz, it can be seen that both resonance frequencies have similar gain patterns and the polarization is also similar. The broadside gain of the antenna at f_1 = 3.64 GHz in ϕ = 0 plane and ϕ = 90 plane is 9.45 dBi, while at f_2 = 4.44 GHz the broadside gain of 9.53 dBi can be achieved. The crosspolarization level in ϕ = 0 plane at f_1 = 3.64 GHz is below −13 dB, however it is slightly higher at f_2 = 4.44 GHz in the same plane. In ϕ = 90 plane, the crosspolarization level for both f_1 and f_2 is extremely low.

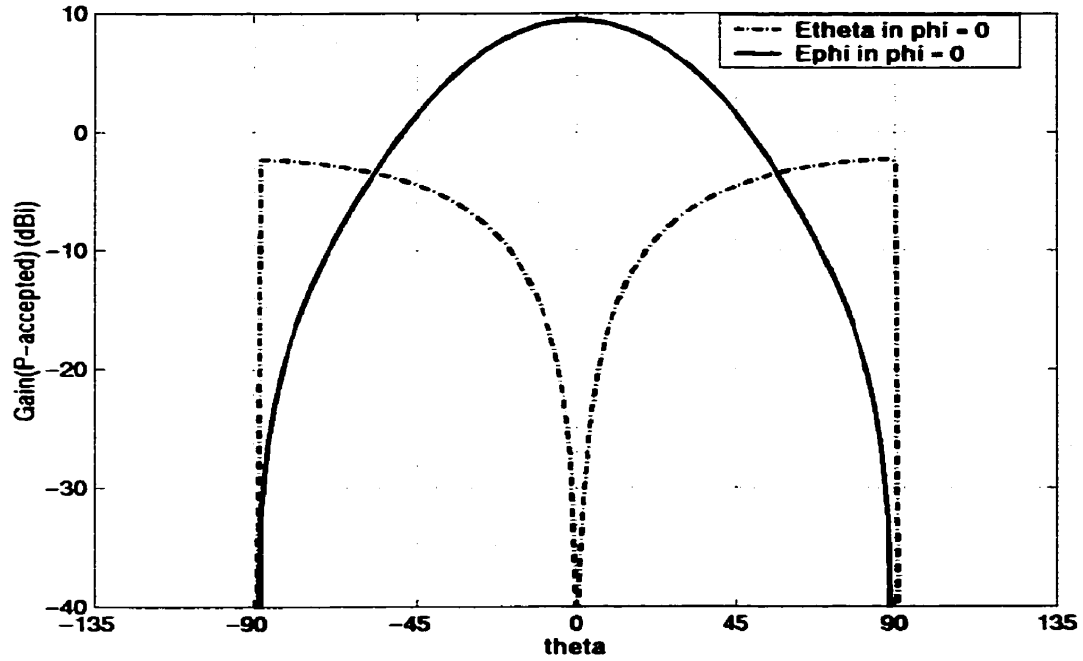

(*a*)

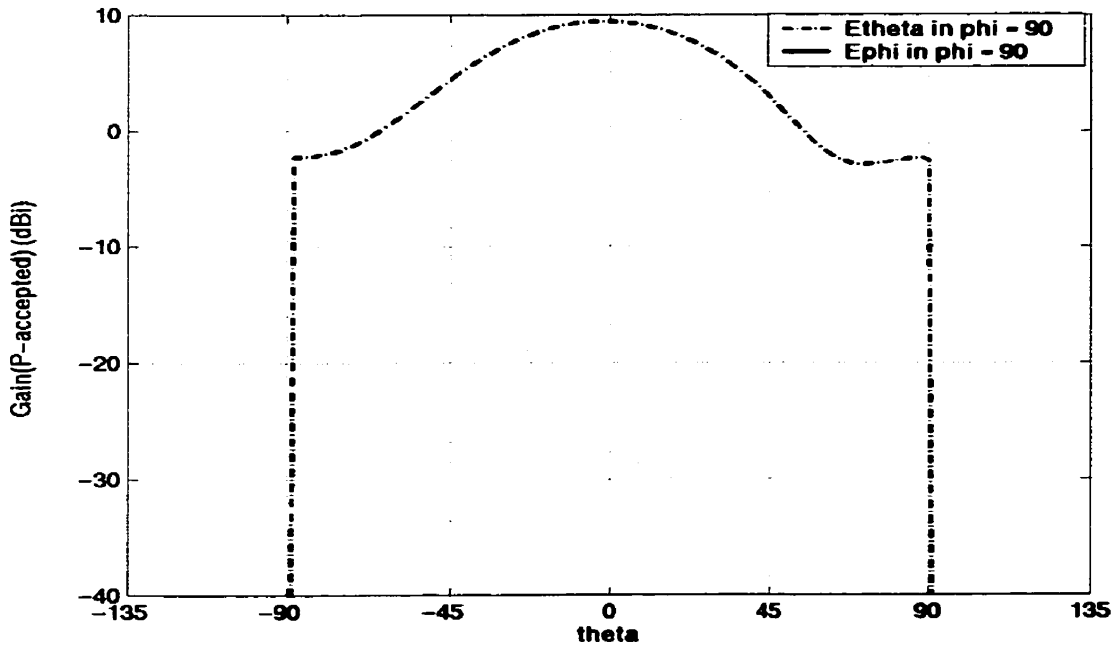

(*b*)

Figure 3.27:(a) Gain patterns in ϕ = 0 plane of Antenna 2 with optimized dimensions at f_l = 3.64 GHz. (b) Gain patterns in ϕ = 90 plane of Antenna 2 with optimized dimensions at f_l = 3.64 GHz.

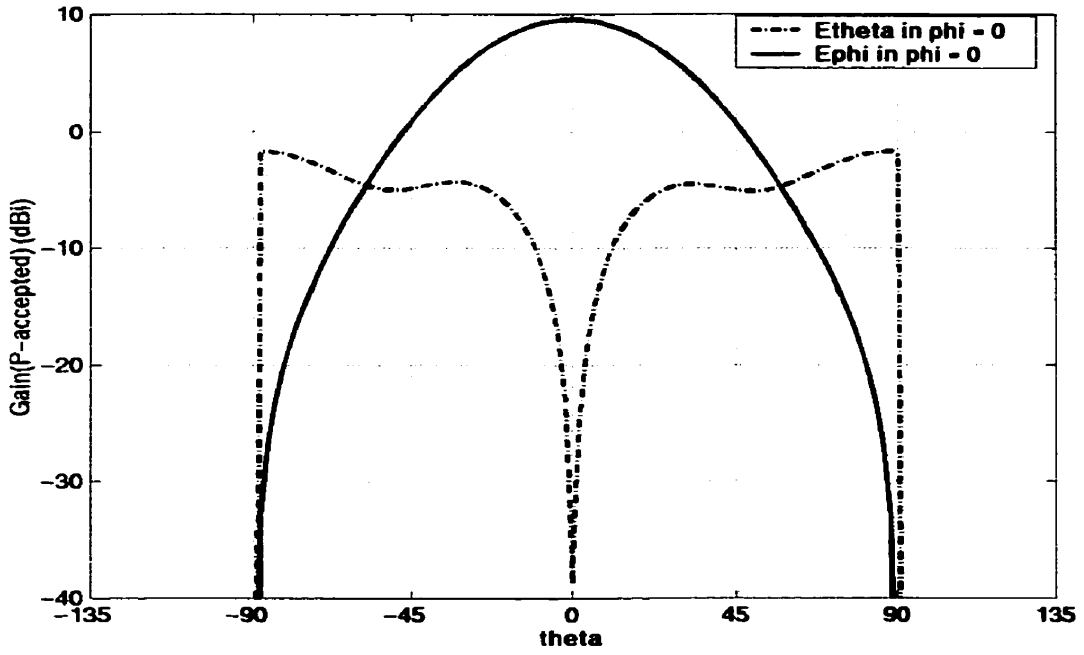

(*a*)

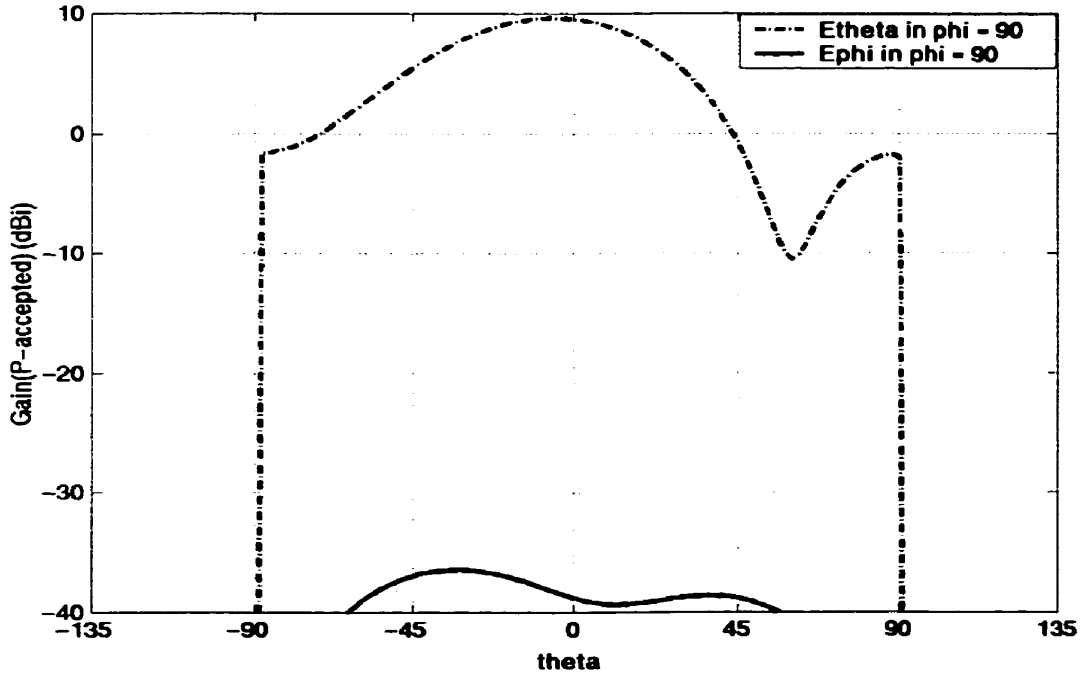

(*b*)

Figure 3.28:(a) Gain patterns in ϕ = 0 plane of Antenna 2 with optimized dimensions at f_2 = 4.44 GHz. (b) Gain patterns in ϕ = 90 plane of Antenna 2 with optimized dimensions at f_2 = 4.44 GHz.

3.3.3 Surface current components and current distribution analysis

As was done with the rectangular patch with a U–shaped slot, the resonance behavior of the rectangular patch antenna with a circular arc slot is also studied. The surface current distribution at the frequency f_1 = 3.64 GHz is shown in Figure 3.29 (a). The surface currents originate behind the circular arc slot and are strong on the patch outside the slot. Due to the presence of the circular arc slot on the microstrip patch, the surface currents of the TM_{01} mode are forced to travel around it. Recall that for the TM_{01} mode, the resonance occurs when the current path length is equal to one half wavelength an approximate equation for f_1 can be derived. This condition is implemented on the current path–length, which is the sum of two components A and B as shown in Figure 3.29 (b). Note that this average current path length includes the effect of the fringing fields on the microstrip patch, and the fringing fields at the two open ends are accounted for by adding equivalent lengths ΔW at both ends. The current path length components can be found from Figure 3.21, in terms of the antenna parameters as $A = R_1$ and $B = (W + 2\,\Delta W) - (\Delta W + d)/2$, where R_1 is the radius of the first arc and is given by $R_1 = \sqrt{(a_1 - x_c)^2 + (b_1 - y_c)^2}$. The component ΔW is the equivalent length due to fringing fields and its expression is shown in equation 3.2. An approximate equation for f_1 can then be written as

$$f_1 = \frac{c}{\left(2\left(R_1 + (W + 2\Delta W) - \frac{(\Delta W + d)}{2}\right)\sqrt{\epsilon_e}\right)}, \quad c = Velocity\ of\ light \tag{3.4}$$

The expression for the effective dielectric constant ε_e is given by equation 2.2.

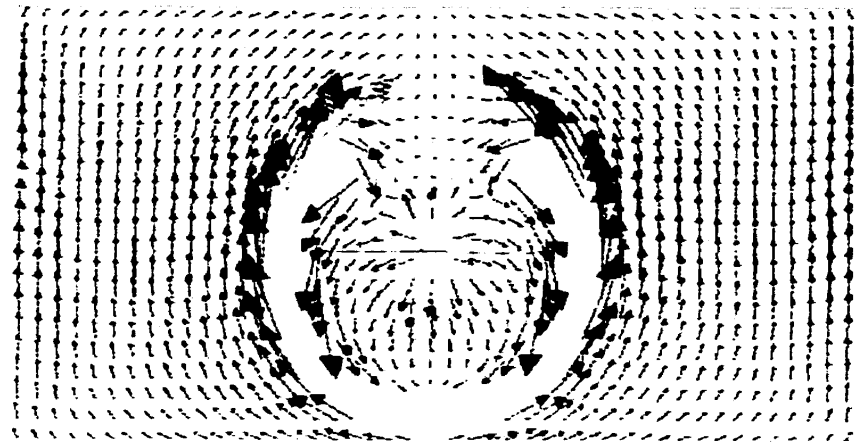

(*a*)

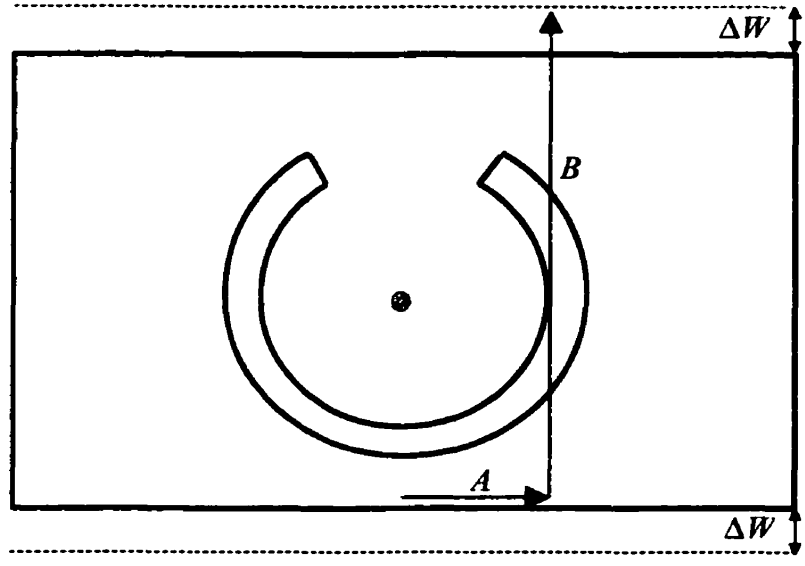

(*b*)

Figure 3.29:(a) Surface current distribution on microstrip patch at f_1 = 3.64 GHz. (b) Surface current−line path on the patch at f_1 = 3.64 GHz.

The surface current distribution is very different at the second resonance f_2 = 4.44 GHz. It is very strong at the patch center and proximate surroundings outside slot as shown in Figure 3.30 (a). The surface currents begin at a point just behind the slot and circulate around the arc slot, and finally stop at the center point P' behind the slot. One

distinct path length in terms of the wavelength is identified by examination of the current distribution, it is shown in Figure 3.30 (b). It is the average distance between the probe and mid–point *P'* behind the slot. This current path length is the sum of components *M*, *N*, *O* and *Q* and it is about one wavelength. Note that the parameter *M* is equal to one fourth of the patch length and *N* is the average distance between the two non–radiating edges of the patch. The expressions for the components *M*, *N*, *O* and *Q* can be written as $M = L/4$, $N = (W + 2\,\Delta W) - (\Delta W + F - R_2)/2 - (\Delta W + d)/2$, $O = L/4 - R_2/2$ and $Q = (F + \Delta W) - (\Delta W + F - R_2)/2$, where R_2 is the radius of the second arc and is given by $R_2 = \sqrt{(a_2 - x_c)^2 + (b_2 - y_c)^2}$. The sum of these components is equal to $\lambda_2 = M + N + O + Q = L/2 + W/2 + 3/2\,\Delta W + R_2/2 + F - d/2$. An approximate equation for f_2 can be given by

$$f_2 = \frac{c}{\left(\left(\frac{L}{2} + \frac{W}{2} + \frac{3}{2}\Delta W + \frac{R_2}{2} + F - \frac{d}{2}\right)\cdot\sqrt{\epsilon_e}\right)} \tag{3.5}$$

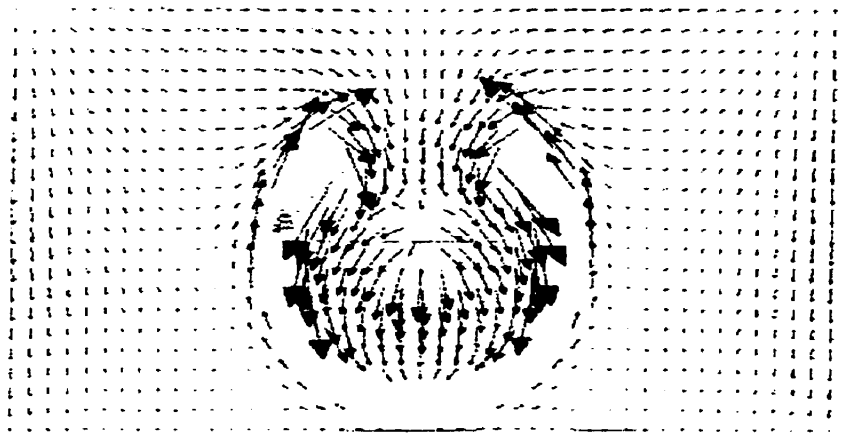

(*a*)

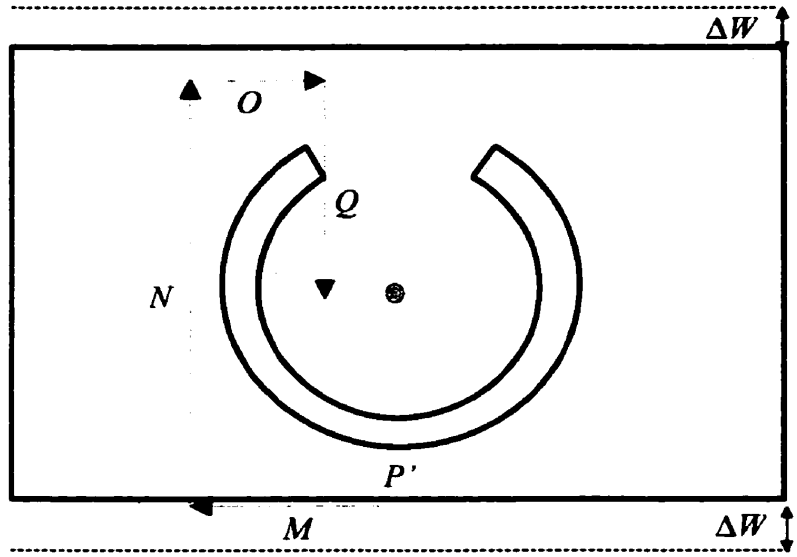

(*b*)

Figure 3.30:(a) Surface current distribution on microstrip patch at f_2 = 4.44 GHz. (b) Surface current−line path on the patch at f_2 = 4.44 GHz.

These derived equations are used to calculate the resonance frequencies of the microstrip patch antenna with a circular arc slot for different values of W shown in Figure 3.23. Table 3.6 compares the calculated results of the resonance frequencies from equations 3.4 and 3.5 with the simulated results of moment method solution using the Ansoft ENSEMBLE for various values of W in Figure 3.23.

Table 3.6: Comparison of Antenna 2 resonance frequencies computed by ENSEMBLE software and Equations (3.4) to (3.5) for various values of W in Figure 3.23.

Width of the patch (mm)	Computed using ENSEMBLE		Calculated by Equations (3.4) to (3.5)		Error between computed and calculated values	
	f_1 (GHz)	f_2 (GHz)	f_1 (GHz)	f_2 (GHz)	Δf_1 (%)	Δf_2 (%)
W = 27.0	3.76	4.68	3.74	4.51	0.53	3.63

Width of the patch (mm)	Computed using ENSEMBLE		Calculated by Equations (3.4) to (3.5)		Error between computed and calculated values	
	f_1 (GHz)	f_2 (GHz)	f_1 (GHz)	f_2 (GHz)	Δf_1 (%)	Δf_2 (%)
W = 27.5	3.72	4.64	3.71	4.49	0.27	3.23
W = 28.0	3.68	4.6	3.67	4.47	0.27	2.83

By utilizing the equations 3.4 and 3.5, the resonance frequencies of Antenna 2 are also calculated for the three different probe locations shown in Figure 3.24. Table 3.7 shows the calculated results of the resonance frequencies from these equations, simultaneously with the computed results of moment method solution using the Ansoft ENSEMBLE. The accuracy of the derived equations and the selected resonant length of the currents on the rectangular patch with a circular arc slot are confirmed by small percentage errors of the calculations, as shown in Table 3.6 and 3.7.

Table 3.7: Comparison of Antenna 2 resonance frequencies computed by ENSEMBLE software and Equations (3.4) to (3.5) for various values of F in Figure 3.24.

Probe Feed Location (mm)	Computed using ENSEMBLE		Calculated by Equations (3.4) to (3.5)		Error between computed and calculated values	
	f_1 (GHz)	f_2 (GHz)	f_1 (GHz)	f_2 (GHz)	Δf_1 (%)	Δf_2 (%)
F = 15.0	3.64	4.32	3.56	4.42	2.2	2.31
F = 15.5	3.64	4.36	3.56	4.39	2.2	0.69
F = 16.0	3.64	4.44	3.56	4.36	2.2	1.8

3.3.4 Parametric study of Antenna 2

In this section, the effect of different parameters of the circular arc slot antenna on the impedance bandwidth is studied. It is shown in Chapter 5 that to fabricate the antennas, the available foam substrate material has εr = 1.03. The antenna dimensions used to perform the parametric study of the circular arc slot antenna are taken to be the same as the fabricated antenna dimensions. These dimensions are: L = 62 mm, W = 29 mm, (x_c, y_c) = (0, −2.5 mm), (a_1, b_1) = (5 mm, 3.5 mm), (a_2, b_2) = (7 mm, 5.5 mm), t = 2.83 mm, d = 1.37 mm, F = 16 mm and ε_r = 1.03. Figure 3.31 shows the effect of different values of the R_p on the −10 dB bandwidth for various substrate heights. R_p = 1.27 mm seems to give the best −10 dB bandwidth for the higher end of h, whereas R_p = 0.635 mm gives higher bandwidth values in the middle range. The lower bandwidth values around 5% to 10% are achieved with R_p = 0.3 mm, due to the antenna becoming dual band.

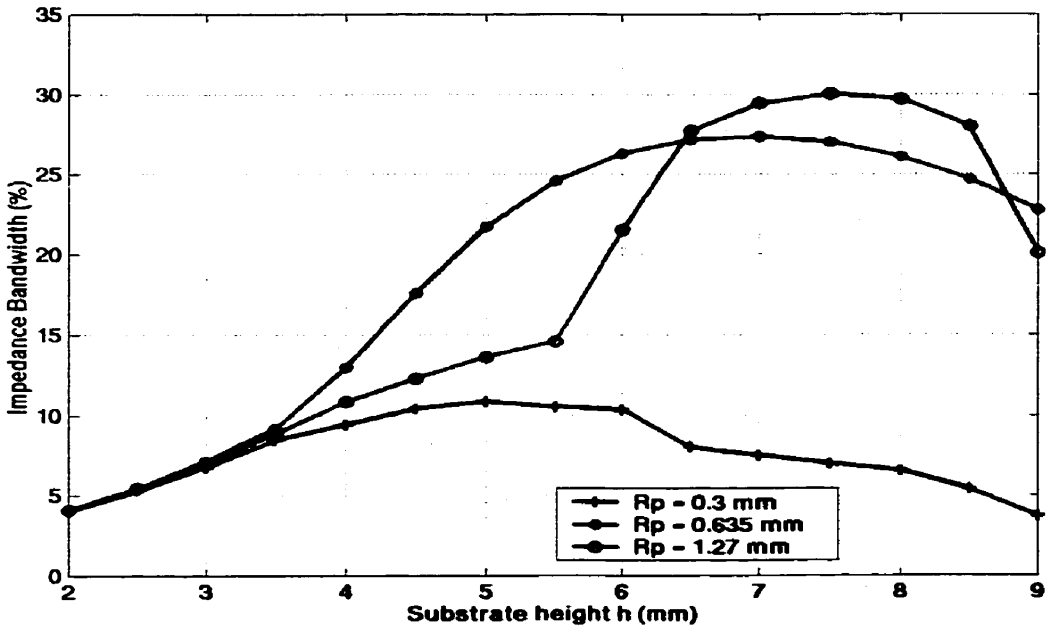

Figure 3.31: Effect of different values of R_p (probe radius) on the impedance bandwidth with L = 62, W = 29, (x_c, y_c) = (0, −2.5), (a_1, b_1) = (5, 3.5), (a_2, b_2) = (7, 5.5), t = 2.83, d = 1.37 and F = 16. All dimensions in mm.

Similarly, the effect of changing the probe location on the antenna bandwidth for various values of substrate heights is shown plotted in Figure 3.32. In the lower end of substrate heights, all three values of F give similar bandwidths, as shown in Figure 3.32. F = 15 mm seems to dominate in the middle range of substrate heights. As the substrate height h increases more than 6.5 mm, the best bandwidths are achieved with F = 16 mm.

Next the slot location, which is identified by the parameter d, is varied to observe the effect on the bandwidth. The plot of impedance bandwidth vs. substrate height h is shown in Figure 3.33 for three different values of d.

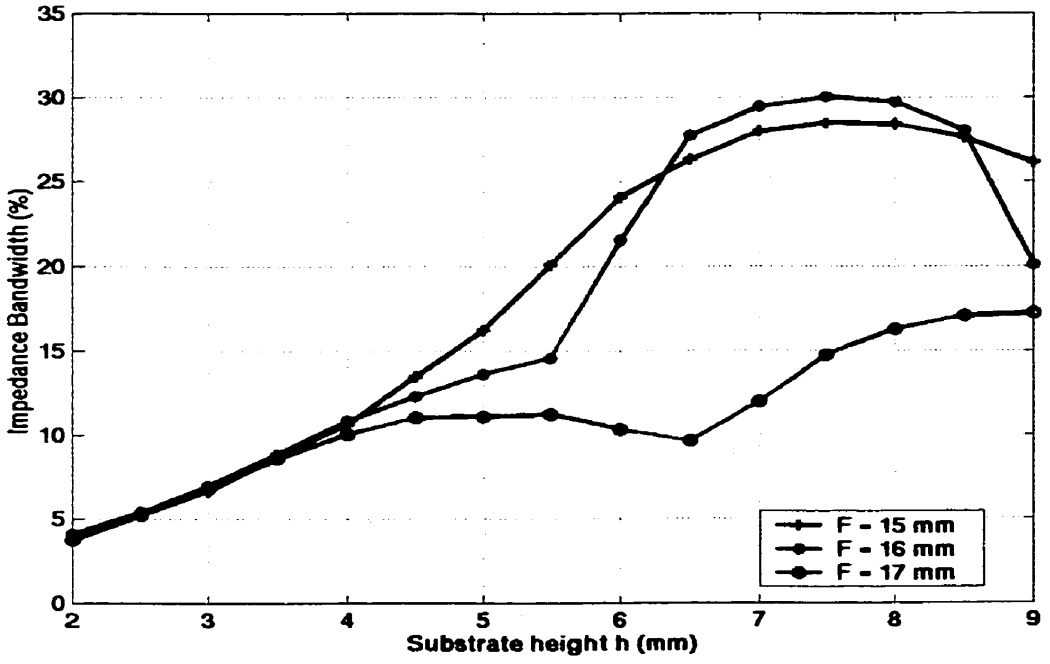

Figure 3.32: Effect of different values of F (probe location) on the impedance bandwidth with L = 62, W = 29, (x_c, y_c) = (0, −2.5), (a_1, b_1) = (5, 3.5), (a_2, b_2) = (7, 5.5), t = 2.83, d = 1.37 and R_p = 1.27. All dimensions in mm.

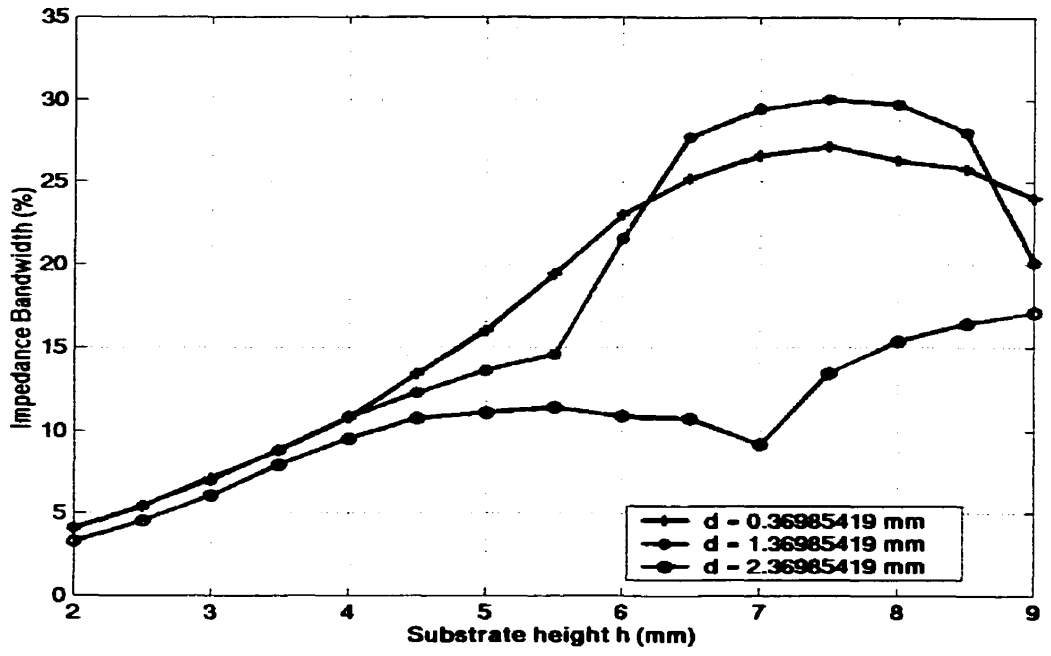

Figure 3.33: Effect of different values of d (slot location) on the impedance bandwidth with L = 62, W = 29, (x_c, y_c) = (0, −2.5), (a_1, b_1) = (5, 3.5), (a_2, b_2) = (7, 5.5), t = 2.83, F = 16, and R_p = 1.27. All dimensions in mm.

Three different values of *d* give fairly small bandwidths with substrate heights lower than 4.0 mm. For the substrate heights between 4.0 mm to 6.0 mm, the value of *d* = 0.37 mm gives higher bandwidths than the other two slot locations. The best bandwidth results are achieved with *d* = 1.37 mm as *h* increases more than 6.0 mm. The similar study is done on the antenna bandwidth by varying the width of the circular arc slot, which is given by the parameter *t*. Figure 3.34 shows the plot of impedance bandwidth vs. substrate height *h* for three different values of *t*.

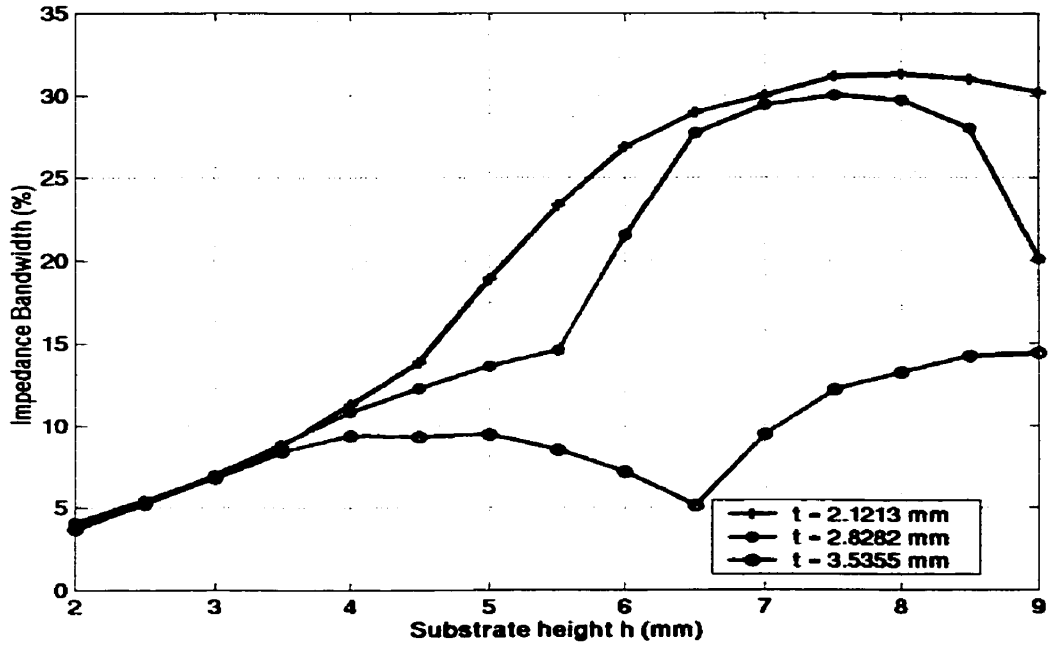

Figure 3.34: Effect of different values of t (slot width) on the impedance bandwidth with $L = 62$, $W = 29$, $(x_c, y_c) = (0, -2.5)$, $(a_1, b_1) = (5, 3.5)$, $(a_2, b_2) = (7, 5.5)$, $d = 1.37$, $F = 16$ and $R_p = 1.27$. All dimensions in mm.

From Figure 3.34 it can be seen that t = 2.12 mm provides the highest bandwidth values for substrate heights more than 4.0 mm. The highest bandwidth value of 31.31% is obtained at h = 8.0 mm with t = 2.12 mm. On the other hand, the bandwidth results are very similar for all three t values for the heights lower than 4.0 mm.

The results shown in Figure 3.31 to Figure 3.34 present the parametric study of the circular arc slot antenna. Figure 3.31 shows the highest bandwidth value of 30.03% is achieved with the probe radius R_p = 1.27 mm at h = 7.5 mm. From Figure 3.32 and Figure 3.33, it can be deduced that F = 16.0 mm and d = 1.37 mm give the best result of 30.03% bandwidth at h = 7.5 mm. While Figure 3.34 gives even better bandwidth value of 31.31% with t = 2.12 mm at h = 8.0 mm. In order to confirm that, R_p = 1.27 mm, F =

16.0 mm, d = 1.37 mm and t = 2.12 mm, are the optimized antenna dimensions, the −10 dB antenna bandwidth is calculated at a fixed substrate height of h = 8.0 mm for various values of R_p, F, d and t. Figure 3.35 shows the plot of bandwidth vs. probe radius. Other antenna dimensions are shown in Figure 3.35. It can be seen from Figure 3.35 that the maximum occurs when R_p = 1.27 mm and therefore it is taken to be near the optimum probe radius value. In Figure 3.35, the sharp change in the bandwidth occurs due to the antenna being dual band.

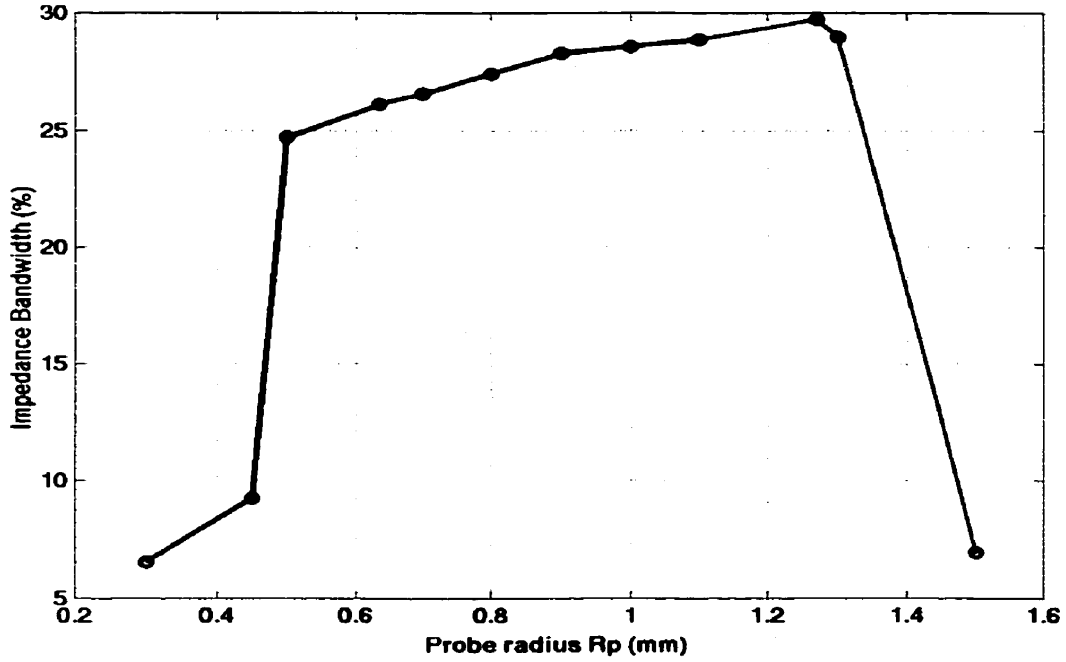

Figure 3.35: Effect of different values of R_p (probe radius) on the impedance bandwidth with L = 62, W = 29, (x_c, y_c) = (0, −2.5), (a_1, b_1) = (5, 3.5), (a_2, b_2) = (7, 5.5), d = 1.37, F = 16, t = 2.83 and h = 8.0. All dimensions in mm.

Likewise, Figure 3.36 shows the plot of bandwidth vs. probe location at h = 8.0 mm with the other antenna dimensions as listed in Figure 3.36. From Figure 3.36, it is obvious that the maximum bandwidth occurs with F = 16.0 mm. As F is increased from 16.0 mm to 16.5 mm, the major drop in the bandwidth occurs due to the split in the return

loss curve at the −10 dB line.

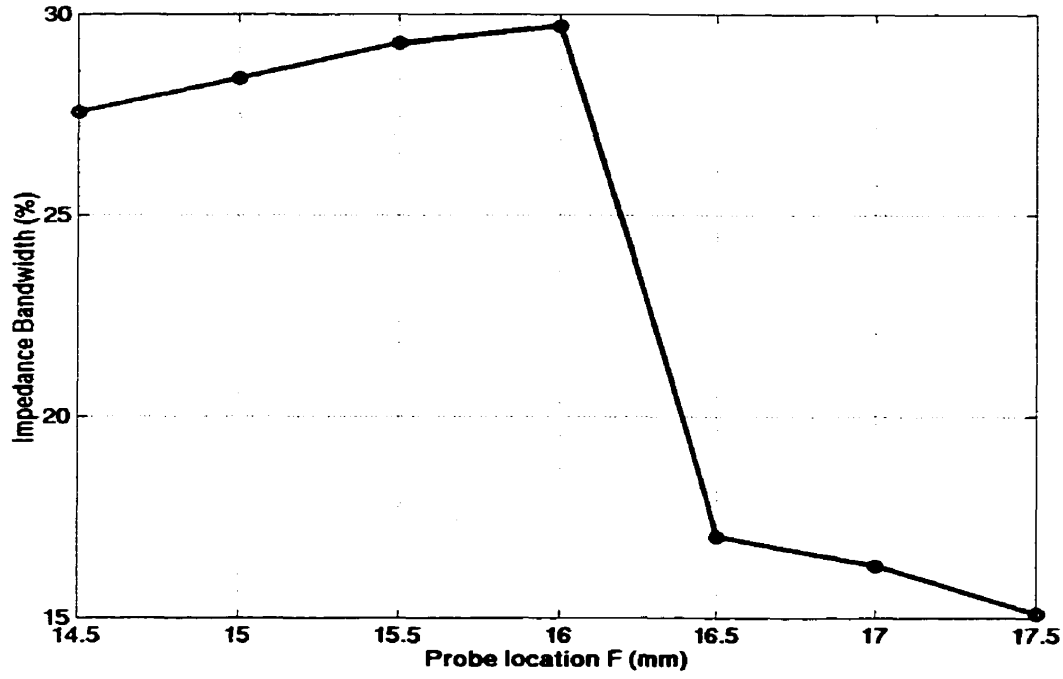

Figure 3.36: Effect of different values of F (probe location) on the impedance bandwidth with L = 62, W = 29, (x_c, y_c) = (0, −2.5), (a_1, b_1) = (5, 3.5), (a_2, b_2) = (7, 5.5), d = 1.37, R_p = 1.27, t = 2.83, and h = 8.0. All dimensions in mm.

Similarly, the bandwidth results shown in Figure 3.37 are used to observe whether or not d = 1.37 mm is the optimized value. The antenna dimensions used to obtain this curve are shown in Figure 3.37. It shows that the highest bandwidth value occurs when d = 1.37 mm and remains high when the slot location is below d = 1.37 mm. However, the major drop in the bandwidth occurs when d increases 1.37 mm due to the split in the s11 curve. Therefore, the optimized location of the circular arc slot is achieved with d = 1.37 mm.

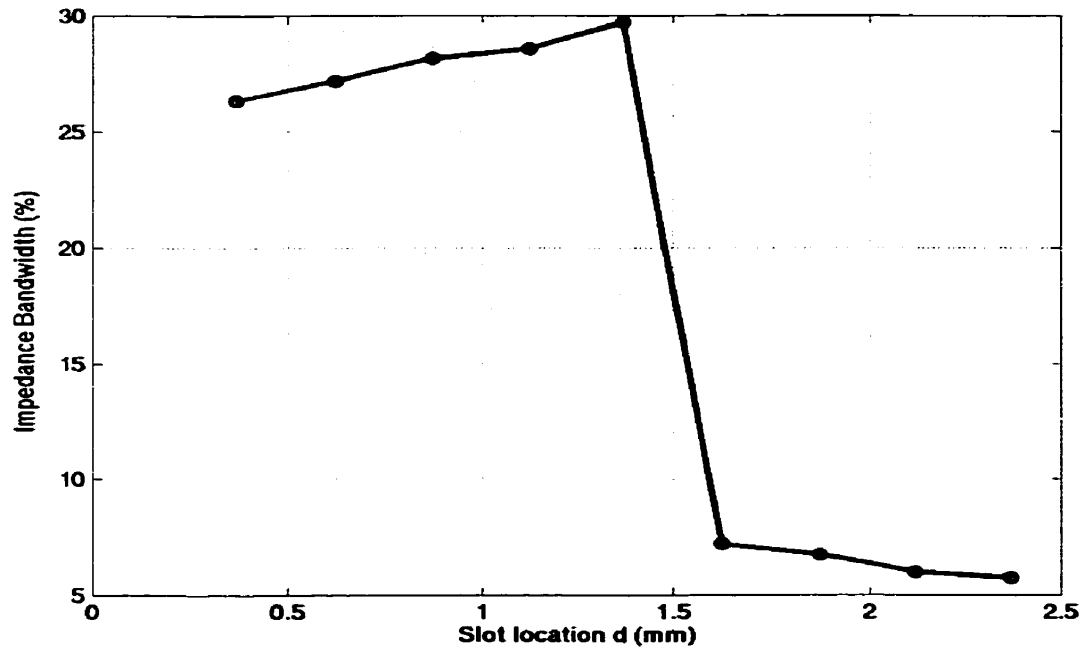

Figure 3.37: Effect of different values of d (slot location) on the impedance bandwidth with L = 62, W = 29, (x_c, y_c) = (0, −2.5), (a_1, b_1) = (5, 3.5), (a_2, b_2) = (7, 5.5), F = 16, R_p = 1.27, t = 2.83 and h = 8.0. All dimensions in mm.

In a similar manner, the results shown in Figure 3.38 are used to obtain the optimized width of the circular arc slot. Figure 3.38 shows the plot of bandwidth vs. slot width at the substrate height of h = 8.0 mm. It was shown earlier that the bandwidth of 31.31% can be obtained with t = 2.12 mm and the antenna dimensions as in Figure 3.38. However, the results in Figure 3.38 show that t = 2.12 mm is not the optimized value since the maximum bandwidth of 32.6% is obtained when t = 1.41 mm. Because of the split in the s11 curve, the sharp decline in the bandwidth happens when t is changed from 1.41 mm to 1.06 mm and from 2.83 mm to 3.18 mm. Hence, the optimized slot width is equal to 1.41 mm.

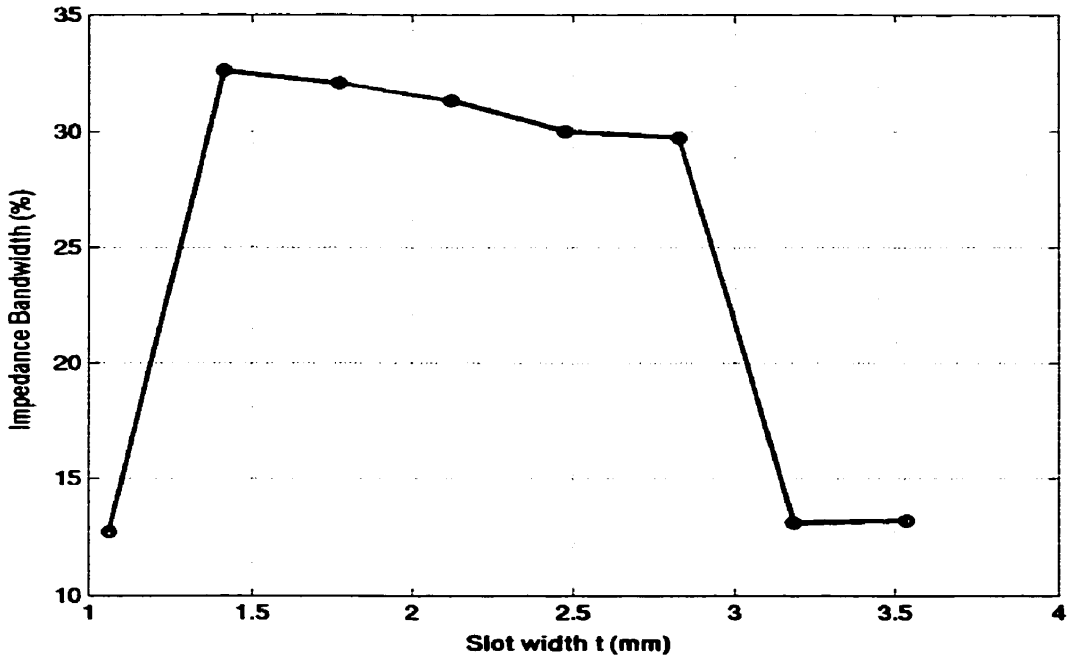

Figure 3.38: Effect of different values of t (slot width) on the impedance bandwidth with $L = 62$, $W = 29$, $(x_c, y_c) = (0, -2.5)$, $(a_1, b_1) = (5, 3.5)$, $(a_2, b_2) = (7, 5.5)$, $F = 16$, $R_p = 1.27$, $d = 1.37$ and $h = 8.0$. All dimensions in mm.

3.3.5 Simulation results of Antenna 2 matched with a tuning stub

Initially the optimized dimensions of the rectangular patch antenna with a U slot were applied to the rectangular patch antenna with a circular arc slot to observe its bandwidth is achievable with this configuration or not. It was observed that it was not possible to achieve broad bandwidth with those dimensions. Therefore the rectangular patch dimensions with a circular arc slot were optimized to obtain its wide impedance bandwidth. Here, a stub tuning matching technique is used instead of optimizing the dimensions of the patch. According to the stub tuning matching method, any impedance which has resistive component can be matched at any frequency to a 50Ω transmission

line [25]. In this section, the simulation results of the rectangular patch antenna with a circular arc slot, which is matched using a tuning stub are presented.

Figure 3.39 shows the return loss of the rectangular patch with a circular arc slot without the stub tuning matching. The antenna dimensions used to obtain this result are L x W = 37.5 mm x 26 mm, (x_c, y_c) = (0, 1 mm), (a_1, b_1) = (5 mm, 7 mm), (a_2, b_2) = (7 mm, 9 mm), t = 2.83 mm, (x_p, y_p) = (0, −2 mm) such that F = 15 mm and h = 5.5 mm. The two resonance frequencies with these dimensions occur at f_1 = 3.64 GHz and f_2 = 5.36 GHz where the −10 dB bandwidth value is equal to 15.2%.

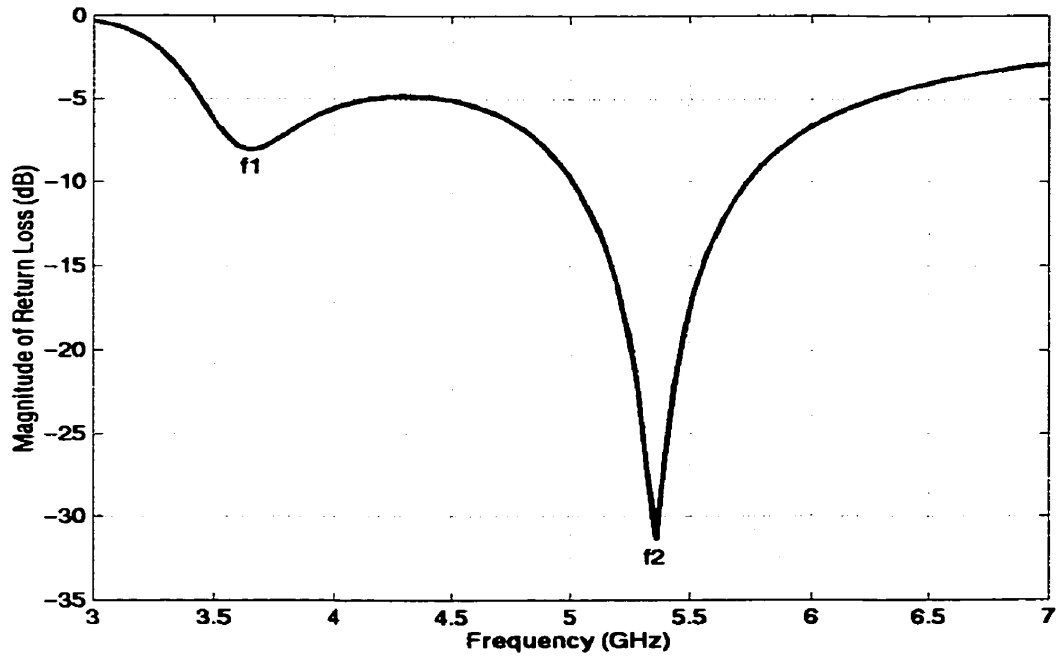

Figure 3.39: Return Loss of Antenna 2 with antenna dimensions of L = 37.5, W = 26, (x_c, y_c) = (0, 1), (a_1, b_1) = (5, 7), (a_2, b_2) = (7, 9), t = 2.83, d = 3.37, (x_p, y_p) = (0, −2), F = 15, h = 5.5. All dimensions in mm.

The corresponding impedance locus on the Smith chart is shown in Figure 3.40. The potential bandwidth of the antenna calculated using the loop on the Smith chart is 43.8%.

In order to obtain this broad bandwidth, the loop on the Smith chart must be moved, so that it comes closer to the circle 1 on the Smith chart. One can match the impedance locus loop using a 50Ω transmission lines with a stub of length L_1, which is located a distance L_2 from a 50Ω via position. Since the tuning stub is fed with a microstrip transmission line, a 50Ω coaxial probe is replaced with a 50Ω via. Its geometry is shown in Figure 3.41.

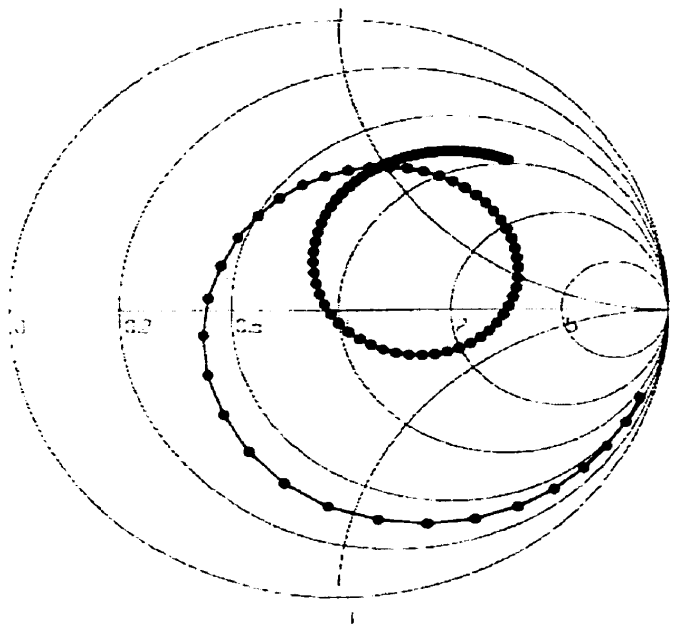

Figure 3.40: Smith chart plot of Antenna 2 with antenna dimensions of L = 37.5, W = 26, $(x_c, y_c) = (0, 1)$, $(a_1, b_1) = (5, 7)$, $(a_2, b_2) = (7, 9)$, t = 2.83, d = 3.37, $(x_p, y_p) = (0, -2)$, F = 15, h = 5.5. All dimensions in mm.

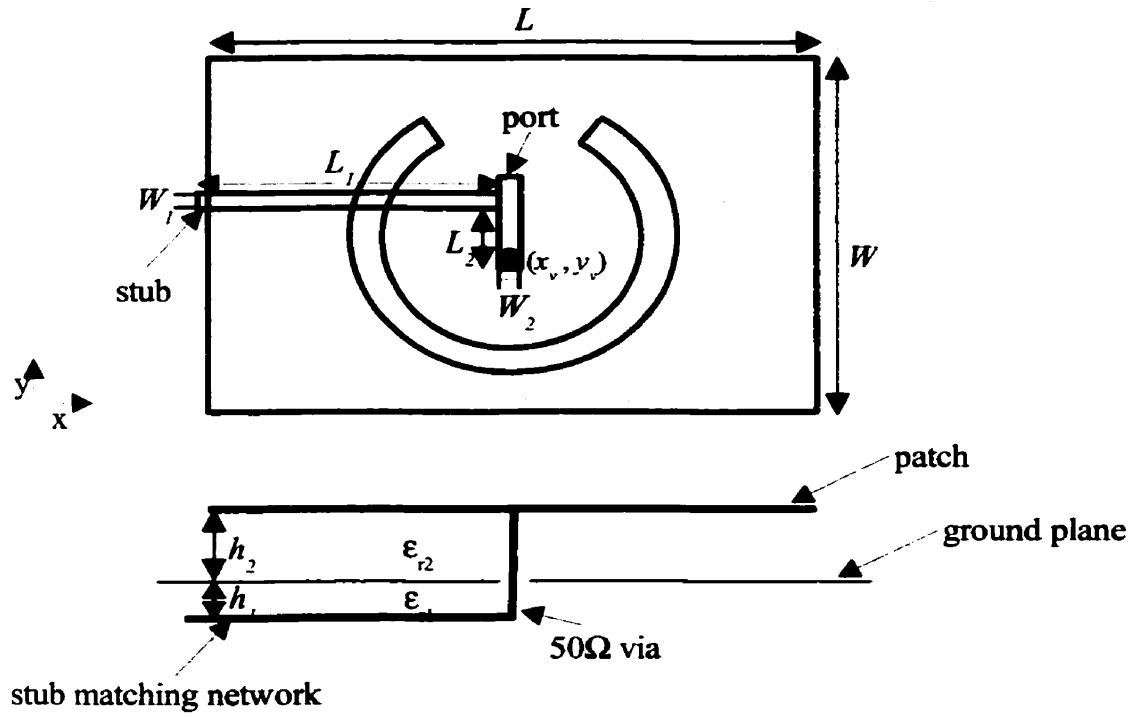

Figure 3.41: Geometry of Antenna 2 matched using the stub tuning matching method.

Simulation studies were conducted on the antenna with dimensions shown in Figure 3.39. The rectangular patch with an arc slot is placed on top of a foam substrate with height h_2 = 5.5 mm over the ground plane. On the other side of the ground plane, the single stub matching network is situated on a substrate with ε_{r1} = 2.5 and h_1 = 0.46 mm. The single stub matching network is fed at the port, as shown in Figure 3.41, with a 50Ω transmission line. The signal is sent to the patch through the single stub matching network using a 50Ω via. The widths of the 50Ω transmission lines used in the stub matching network are $W_1 = W_2 = 1.31$ mm. The utilized length of the stub is $L_1 = 18.25$ mm and it is located a distance of $L_2 = 4.83$ mm from the 50Ω via. Figure 3.42 shows the computed results for the return loss of Antenna 2 matched with the stub tuning method.

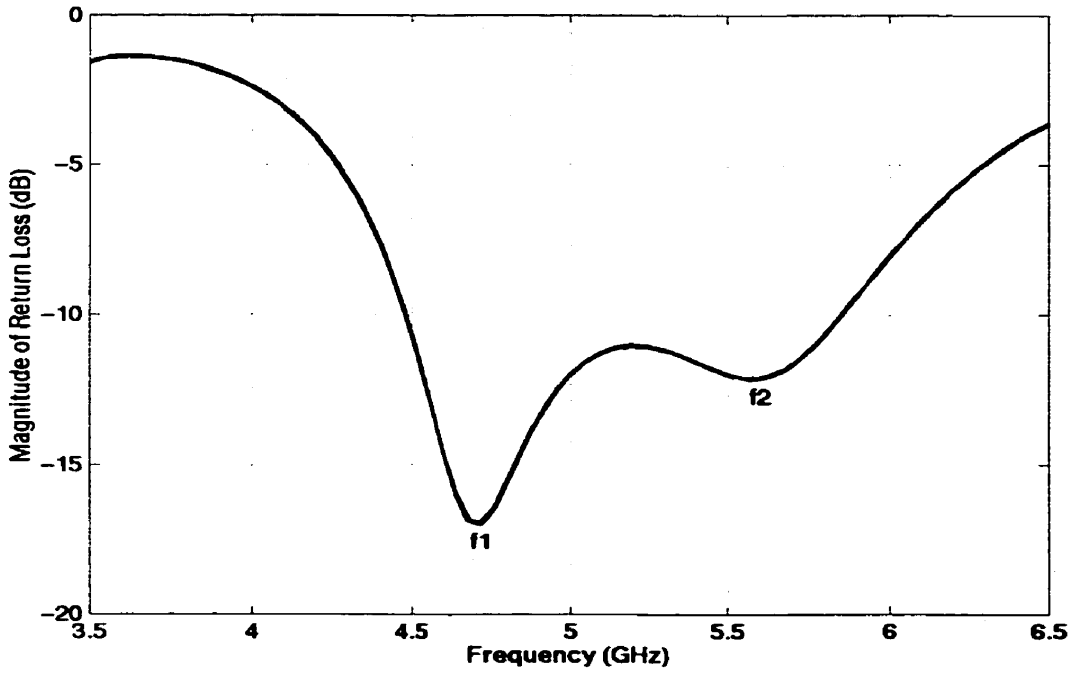

Figure 3.42: Return Loss of Antenna 2 matched using the tuning stub with antenna dimensions: $L = 37.5$, $W = 26$, $(x_c, y_c) = (0, 1)$, $(a_1, b_1) = (5, 7)$, $(a_2, b_2) = (7, 9)$, $t = 2.83$, $d = 3.37$, $(x_v, y_v) = (0, -2)$, $h_1 = 5.5$, $h_2 = 0.46$, $W_1 = W_2 = 1.31$, $L_1 = 18.25$ and $L_2 = 4.83$. All dimensions in mm.

By comparing the results shown in Figure 3.39 and Figure 3.42, it can be seen that the impedance bandwidth of Antenna 2 increases from 14.13% to 26.64% with the utilization of the stub tuning matching method. Figure 3.42 shows that the first resonance occurs at f_1 = 4.7 GHz and the second resonance at f_2 = 5.57 GHz. The impedance locus on the Smith chart of the rectangular patch antenna with a circular arc slot with the stub matching network is shown in Figure 3.43. While comparing the smith chart plots shown in Figure 3.40 and Figure 3.43, it can be seen that the antenna is matched well to the 50Ω transmission line using the stub tuning matching method.

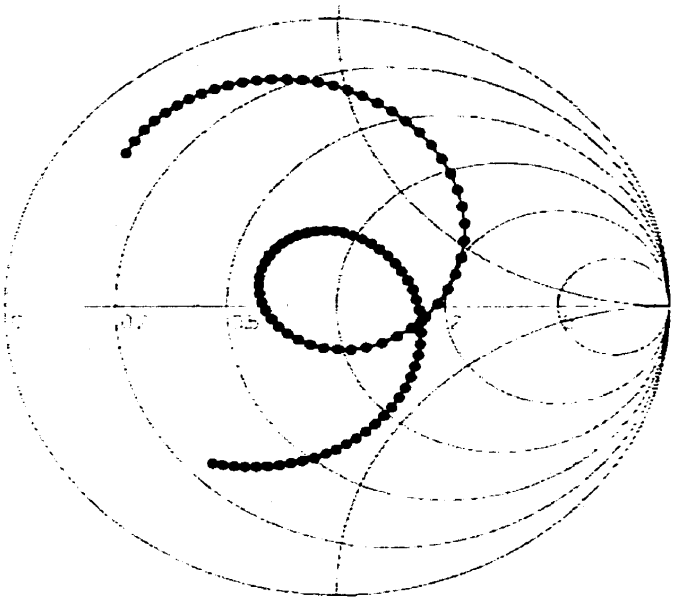

Figure 3.43: Smith chart plot of Antenna 2 matched using the tuning stub with antenna dimensions: $L = 37.5$, $W = 26$, $(x_c, y_c) = (0, 1)$, $(a_1, b_1) = (5, 7)$, $(a_2, b_2) = (7, 9)$, $t = 2.83$, $d = 3.37$, $(x_v, y_v) = (0, -2)$, $h_1 = 5.5$, $h_2 = 0.46$, $W_1 = W_2 = 1.31$, $L_1 = 18.25$ and $L_2 = 4.83$. All dimensions in mm.

Figure 3.44 shows the computed results of E_θ and E_ϕ in $\phi = 0$ plane and $\phi = 90$ plane at $f_1 = 4.7$ GHz. The radiation pattern plots in the $\phi = 0$ plane and $\phi = 90$ plane at $f_1 = 4.7$ GHz exhibit good broadside radiation and crosspolarization levels. Similarly, for $f_2 = 5.57$ GHz the results of E_θ and E_ϕ in $\phi = 0$ plane and $\phi = 90$ plane are shown plotted in Figure 3.45. These results of the radiation patterns also demonstrate good broadside radiation characteristics with a slightly higher crosspolarization level in $\phi = 0$ plane.

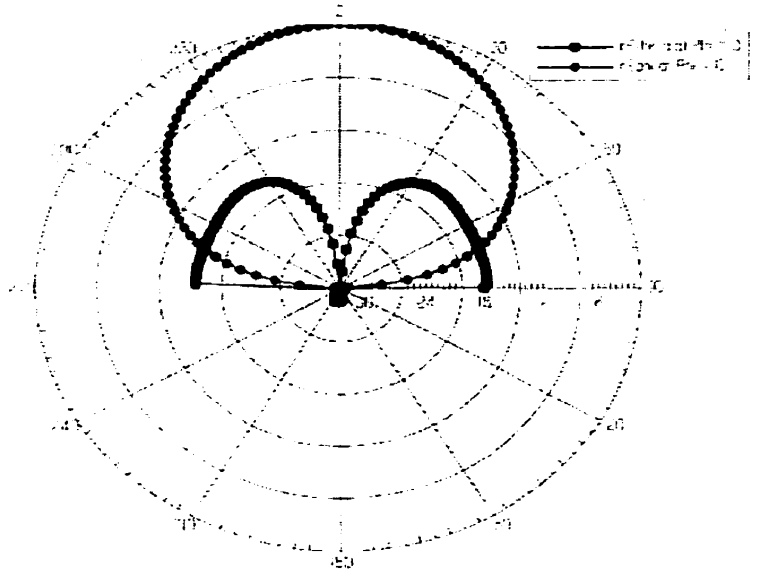

(*a*)

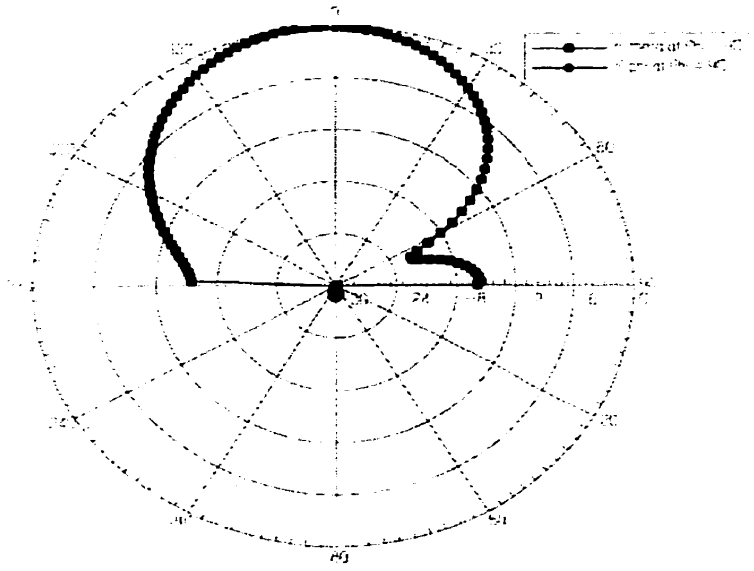

(*b*)

Figure 3.44: (a) Radiation patterns in ϕ = 0 plane of Antenna 2 matched using the tuning stub at f_1 = 4.7 GHz. (b) Radiation patterns in ϕ = 90 plane of t Antenna 2 matched using the tuning stub at f_1 = 4.7 GHz.

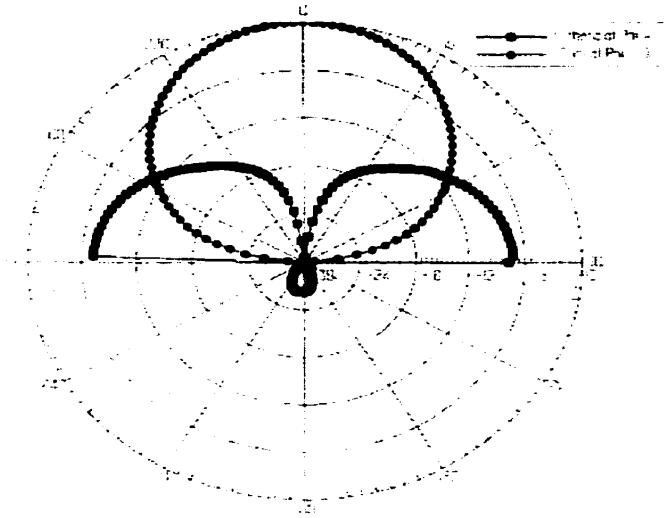

(*a*)

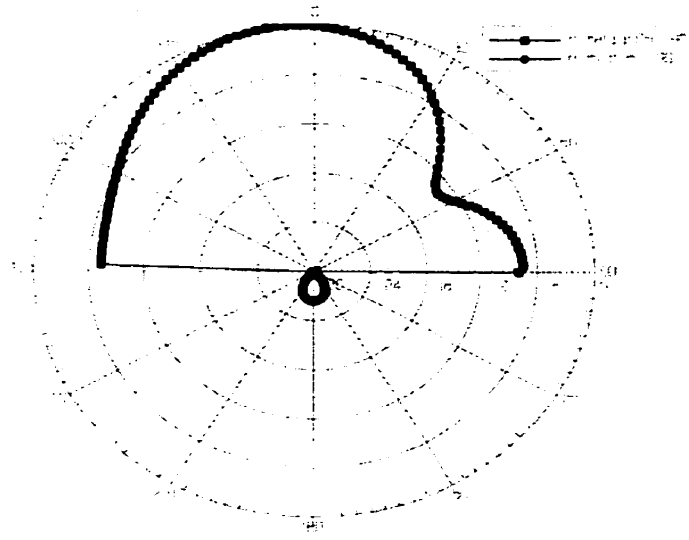

(*b*)

Figure 3.45: (a) Radiation patterns in ϕ = 0 plane of Antenna 2 matched using the tuning stub at f_2 = 5.57 GHz. (b) Radiation patterns in ϕ = 90 plane of Antenna 2 matched using the tuning stub at f_2 = 5.57 GHz.

Figure 3.46 and Figure 3.47 display the gain patterns of Antenna 2 matched with the

stub tuning matching technique at f_1 = 4.70 GHz and f_2 = 5.57 GHz. The antenna has the broadside gain of 9.62 dBi at f_1 = 4.70 GHz in the ϕ = 0 plane and ϕ = 90 plane. The gain patterns show that the antenna has good crosspolarization level in ϕ = 0 plane and ϕ = 90 plane, but it is a little higher in the ϕ = 0 plane. The antenna also has backward radiation due to the stub matching network, which is shown in the gain pattern plots in Figure 3.46. Similarly, it can be seen from Figure 3.47 that the broadside gain of the rectangular patch antenna with a circular arc slot matched with the stub tuning at f_2 = 5.57 GHz is equal to 8.48 dBi. The crosspolarization level in the ϕ = 0 plane for f_2 = 5.57 GHz is higher than f_1 = 4.70 GHz, while it is comparable in the ϕ = 90 plane for both f_1 = 4.70 GHz and f_2 = 5.57 GHz. The backward radiation is also similar in the ϕ = 0 plane and ϕ = 90 plane for both f_1 and f_2.

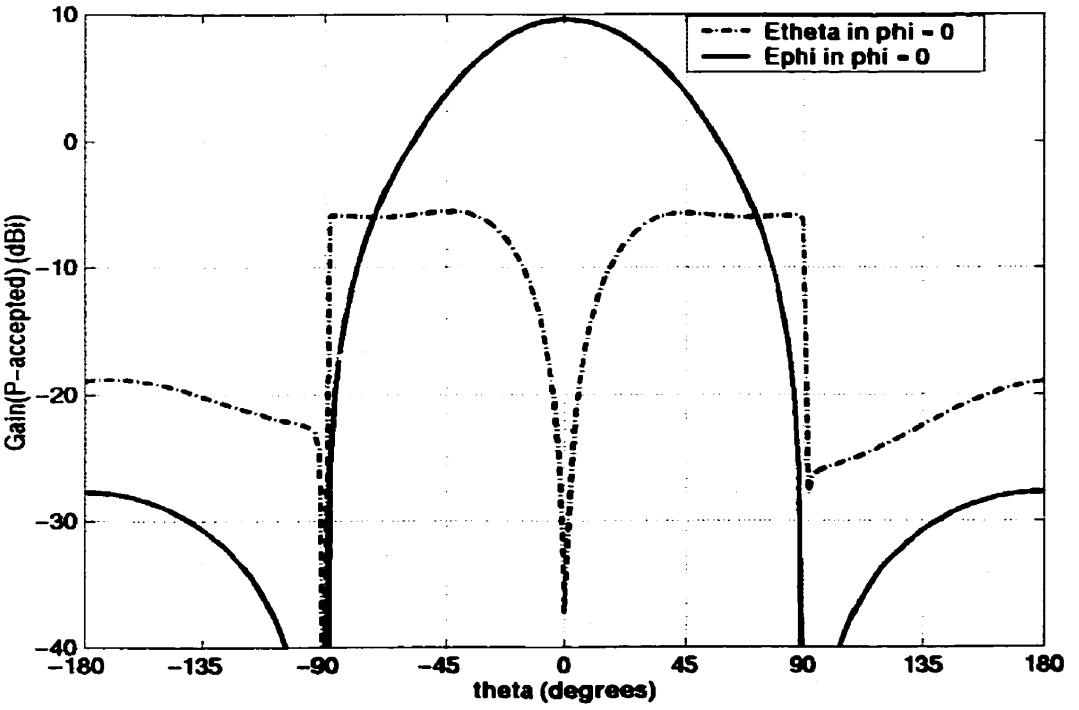

(*a*)

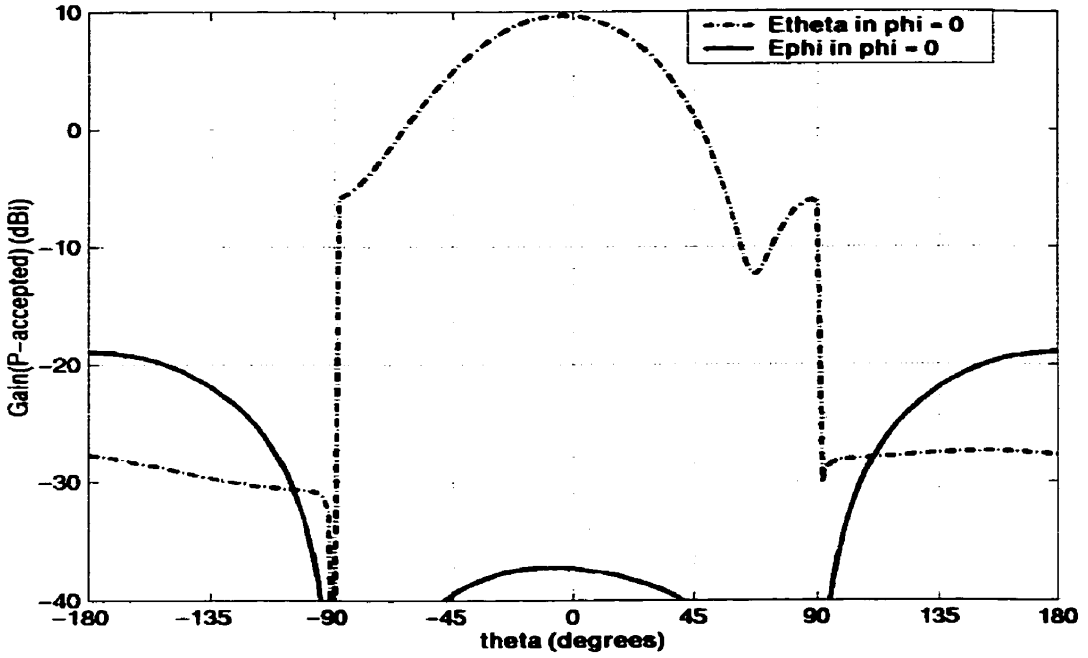

(*b*)

Figure 3.46: (a) Gain patterns in ϕ = 0 plane of Antenna 2 matched using the tuning stub at f_1 = 4.7 GHz. (b) Gain patterns in ϕ = 90 plane of Antenna 2 matched using the tuning stub at f_1 = 4.7 GHz.

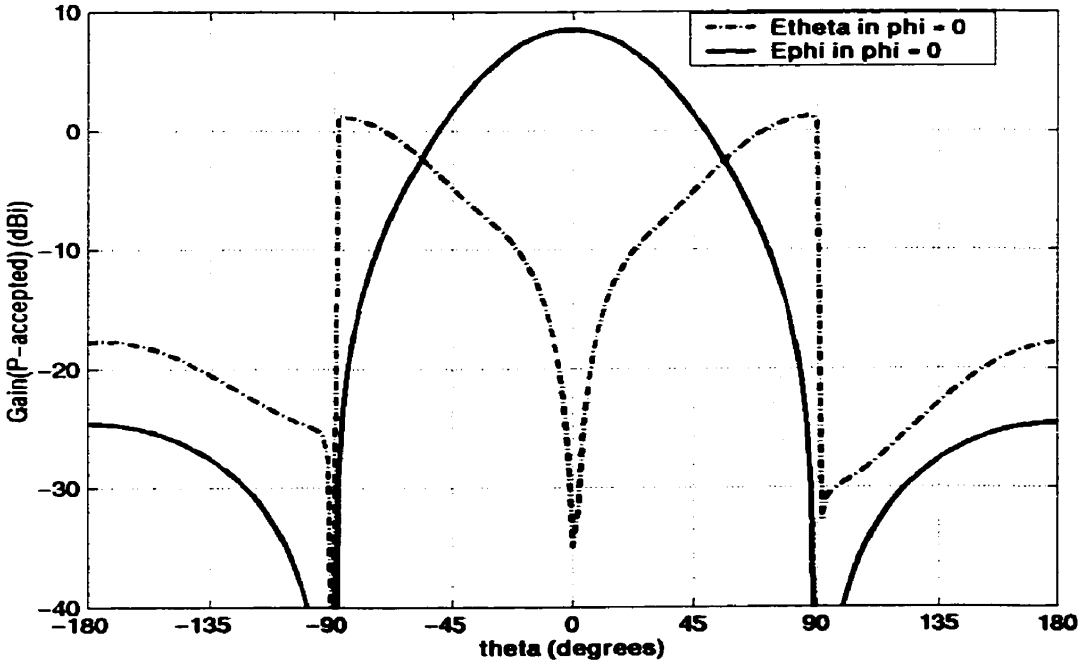

(*a*)

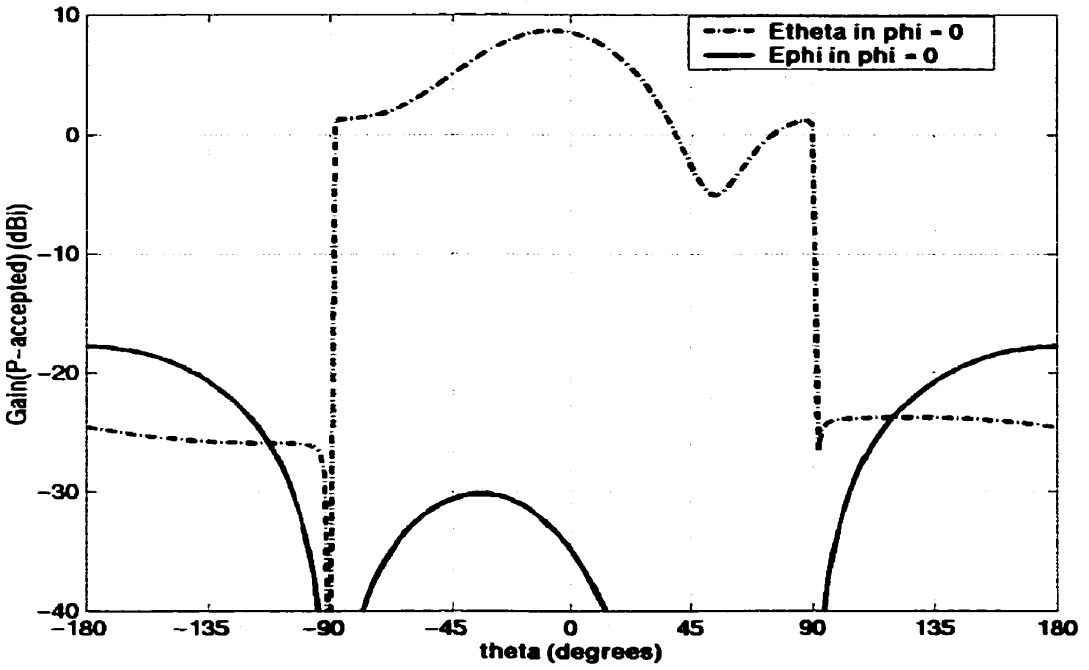

(*b*)

Figure 3.47: (a) Gain patterns in ϕ = 0 plane of Antenna 2 matched using the tuning stub at f_2 = 5.57 GHz. (b) Gain patterns in ϕ = 90 plane of Antenna 2 matched using the tuning stub at f_2 = 5.57 GHz.

3.4 Analysis of Antenna 3

As shown in the previous section, the bandwidth of 30% can be achieved with the rectangular patch antenna with a circular arc shaped slot. One can observe the effect on the bandwidth of the rectangular patch antenna with circular arc slot if a rectangular patch is replaced with a circular patch, which is the third configuration studied in this thesis. By replacing the rectangular patch with the circular patch, it is found that the impedance bandwidth of the antenna decreases. This section presents the design simulation results of the circular microstrip patch antenna with a circular arc shaped slot.

The geometry of Antenna 3 is shown in Figure 3.48. The circular patch with diameter

C_d is separated from the ground plane with a foam substrate of height h, and a circular arc shaped slot is located in its center. The parameters (x_c, y_c) denote the center point of the two circular arcs, as shown in Figure 3.48. The end points of the first and second arcs are given by (a_1, b_1) and (a_2, b_2), respectively. The parameter d is used to indicate the position of the circular arc slot on the circular patch and the thickness of the arc slot is given by the variable t. The patch is fed using a 50Ω coaxial probe at (x_p, y_p) with the inner diameter of 1.27 mm, which is located slightly below the center of the patch along the y–direction.

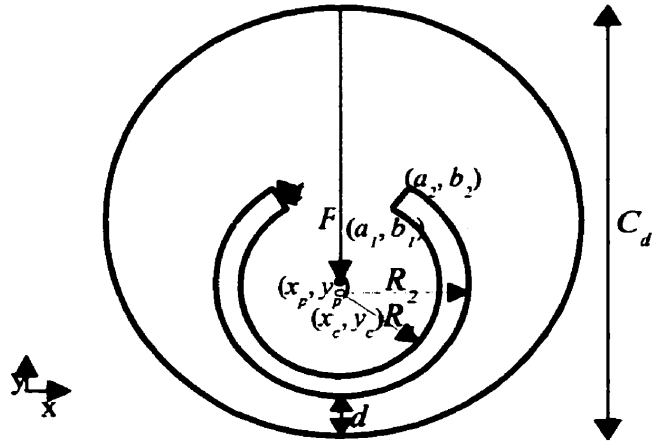

Figure 3.48: Geometry of a circular patch antenna with a circular arc shaped slot.

An extensive amount of computations are performed to study the characteristics of Antenna 3. Through these computations it is observed that the circular patch antenna with a circular arc slot does not have as broadband characteristics as compared to the rectangular patch antenna with a circular arc slot. The circular patch antenna with a circular arc slot give −10 dB bandwidth values only in the range of 18% − 20%, which is not as high as 30.1%, obtained by the rectangular patch with a circular arc slot. The next

section presents its simulation results for the return loss, radiation patterns and gain patterns.

3.4.1 Design simulation results

The dimensions of Antenna 3 are: $C_d = 41$ mm, $(x_c, y_c) = (0, -7.5$ mm), $(a_1, b_1) = (3.78$ mm, -1.28 mm), $(a_2, b_2) = (5.9$ mm, 0.85 mm), $t = 3.01$ mm, $(x_p, y_p) = (0, -3.25$ mm), $F =$ 23.75 mm, $\varepsilon_r = 1.0006$ and $h = 5.5$ mm. Figure 3.49 shows the computed results of the return loss by Ansoft ENSEMBLE. With these dimensions, the two resonance frequencies occur at $f_1 = 3.25$ GHz and $f_2 = 3.65$ GHz. The -10 dB bandwidth of the circular patch antenna with a circular arc slot with the above mentioned dimensions is 18.3%, which is not very broad.

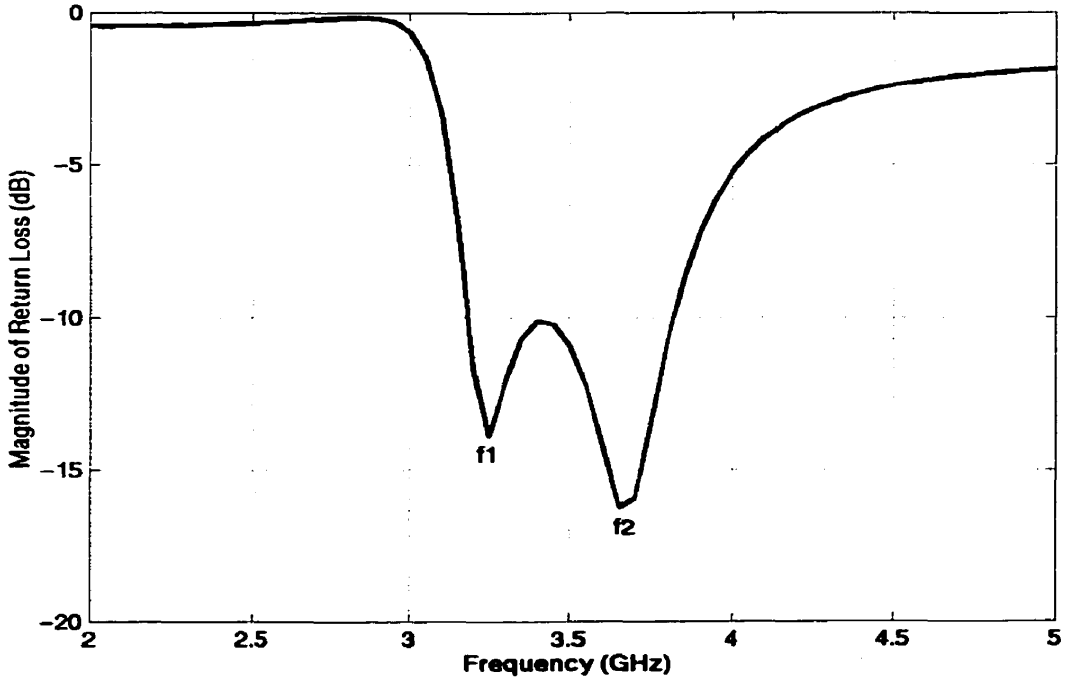

Figure 3.49: Return Loss of Antenna 3 with dimensions $C_d = 41$, $(x_c, y_c) = (0, -7.5)$, $(a_1, b_1) = (3.78, -1.28)$, $(a_2, b_2) = (5.9, 0.85)$, $t = 3.01$, $(x_p, y_p) = (0, -3.25)$, $d = 1.40$, $F = 23.75$, $R_p = 0.635$ and $h = 5.5$. All dimensions in mm.

It is apparent from the radiation pattern plots shown in Figure 3.50 that the acceptable crosspolarization level is obtained in both $\phi = 0$ plane and $\phi = 90$ plane at $f_1 = 3.25$ GHz. This also applies for the second resonance $f_2 = 3.65$ GHz, which can be observed from the radiation pattern plots shown in Figure 3.51 in $\phi = 0$ plane and $\phi = 90$ plane. The two resonance frequencies have similar radiation characteristics and similar polarization.

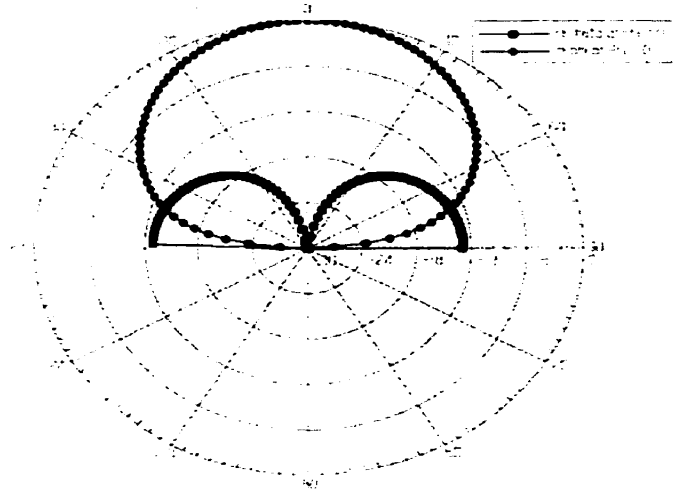

(*a*)

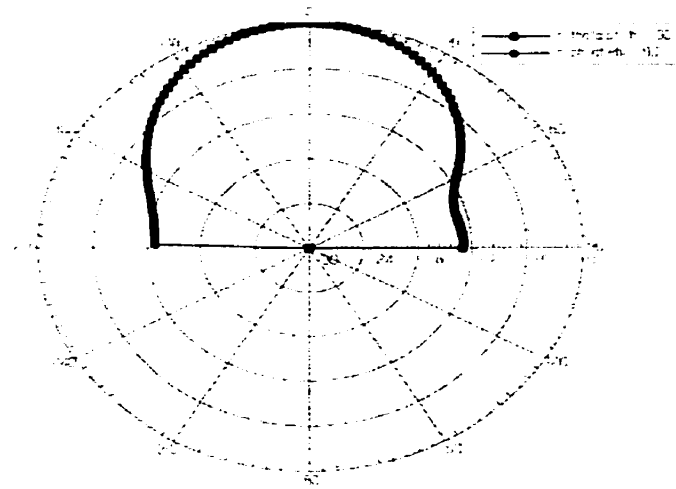

(*b*)

Figure 3.50: (a) Radiation patterns in $\phi = 0$ plane of Antenna 3 with optimized dimensions at $f_1 = 3.25$ GHz. (b) Radiation patterns in $\phi = 90$ plane of Antenna 3 with optimized dimensions at $f_1 = 3.25$ GHz.

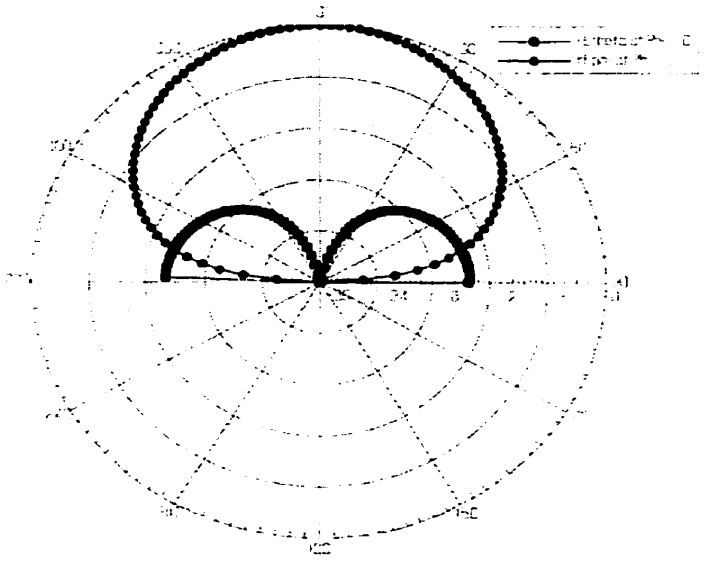

(*a*)

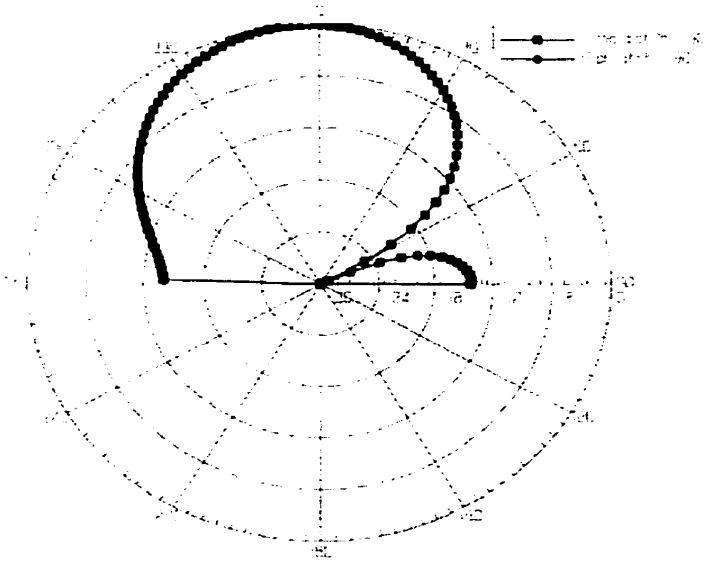

(*b*)

Figure 3.51: (a) Radiation patterns in $\phi = 0$ *plane of Antenna 3 with optimized dimensions at* $f_2 = 3.65$ *GHz. (b) Radiation patterns in* $\phi = 90$ *plane of Antenna 3 with optimized dimensions at* $f_2 = 3.65$ *GHz.*

Similarly, the gain patterns plots of Antenna 3 in Figure 3.52 show that the crosspolarization level of −13 dB is achieved in $\phi = 0$ plane at $f_1 = 3.25$ GHz. Whereas it is very low in $\phi = 90$ plane at $f_1 = 3.25$ GHz. The antenna has a broadside gain of 8.98 dBi at the first resonance frequency $f_1 = 3.25$ GHz. The gain patterns of the antenna at the second resonance $f_2 = 3.65$ GHz are very similar to the patterns at $f_1 = 3.25$ GHz, as can be seen from Figure 3.53. The circular patch antenna with a circular arc slot has the crosspolarization level below −13 dB in $\phi = 0$ plane at $f_2 = 3.65$ GHz. It is extremely low in $\phi = 90$ plane at $f_2 = 3.65$ GHz. Both resonance frequencies exhibit similar radiation characteristics and similar polarization.

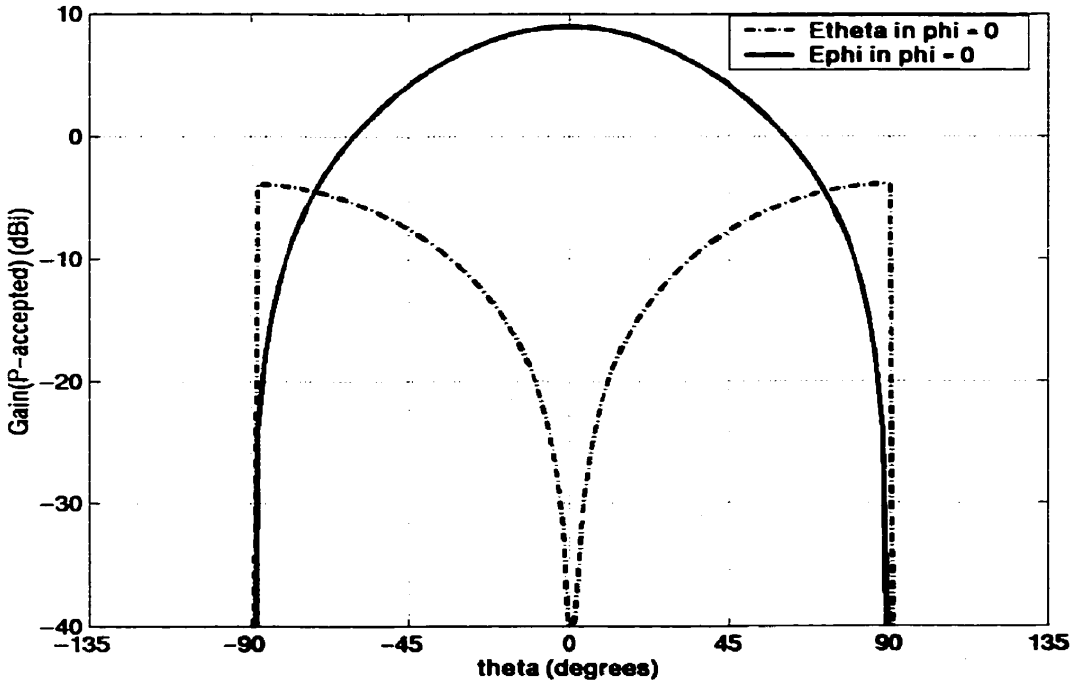

(*a*)

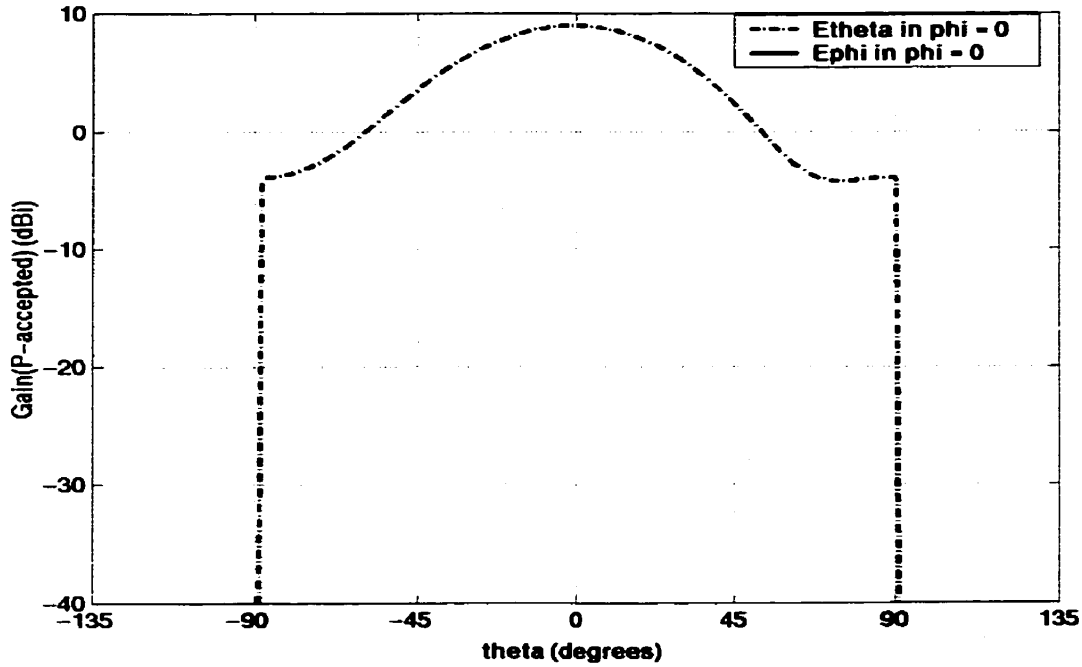

(*b*)

Figure 3.52: (a) Gain patterns in $\phi = 0$ *plane of Antenna 3 with optimized dimensions at* $f_l = 3.25$ *GHz. (b) Gain patterns in* $\phi = 90$ *plane of Antenna 3 with optimized dimensions at* $f_l = 3.25$ *GHz.*

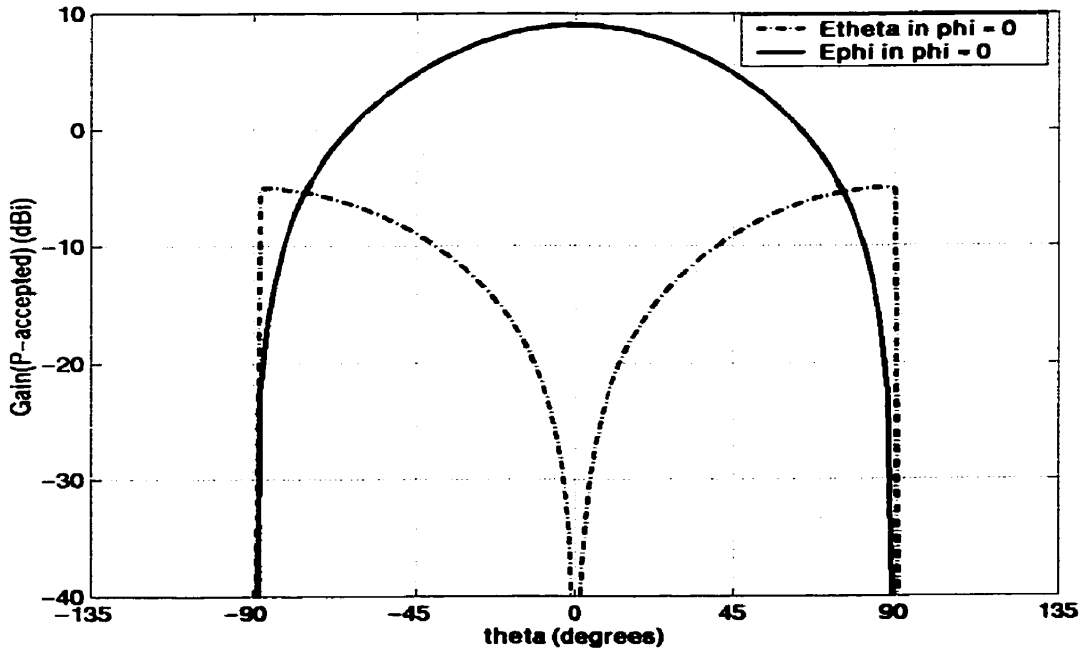

(*a*)

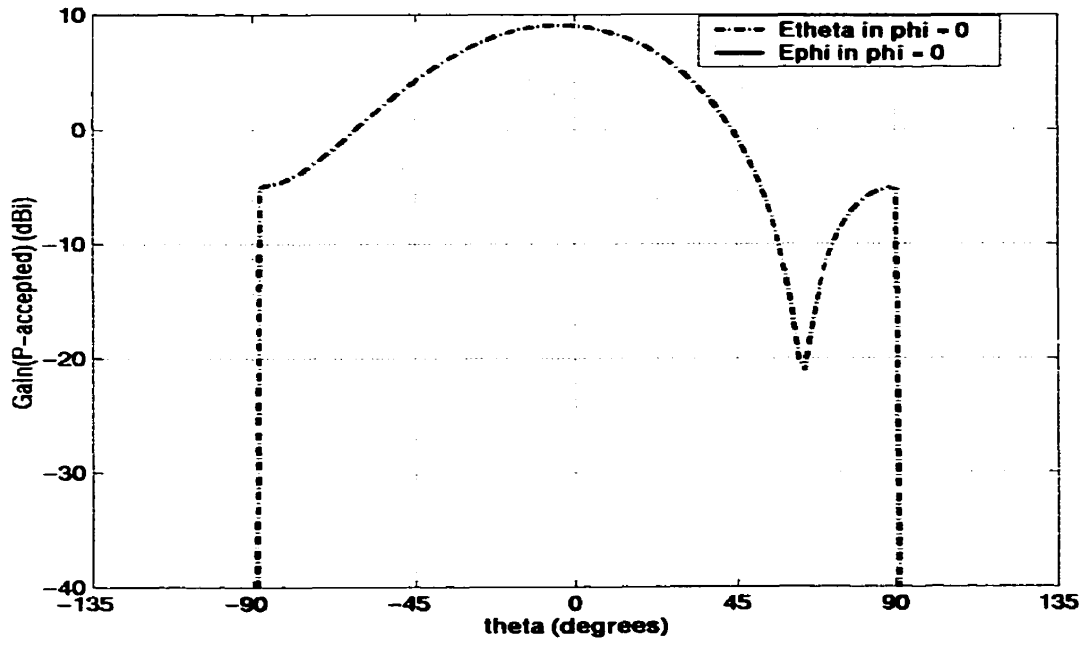

(*b*)

Figure 3.53: (a) Gain patterns in ϕ = 0 plane Antenna 3 with optimized dimensions at f_2 = 3.65 GHz. (b) Gain patterns in ϕ = 90 plane of Antenna 3 with optimized dimensions at f_2 = 3.65 GHz.

3.4.2 Parametric study of Antenna 3

In this section, a parametric study on the effects of different parameters of Antenna 3 is presented. The effect of various antenna parameters on the impedance bandwidth is investigated. To perform the parametric study, a slight change is made in the dielectric constant of a foam substrate since for fabrication purpose the available foam substrate material has ε_r = 1.03. The antenna dimensions used to perform the parametric study are taken to be the same as in Figure 3.49. Once again, these dimensions are: C_d = 41.0 mm, (x_c, y_c) = (0, −7.5 mm), (a_1, b_1) = (3.78 mm, −1.28 mm), (a_2, b_2) = (5.9 mm, 0.85 mm), t = 3.01 mm, (x_p, y_p) = (0, −3.25 mm), d = 1.40 mm, F = 23.75 mm, R_p = 0.635 mm ε_r =

1.03 and h = 5.5 mm. Figure 3.54 shows the effect of different R_p values (probe radius) on the −10 dB bandwidth as the substrate height is varied. The maximum bandwidth of 19.51% is obtained with R_p = 1.27 mm at h = 7.5 mm. Also, R_p = 1.27 mm gives the best results of −10 dB bandwidth for substrate heights more than 4.0 mm. However, R_p = 0.635 mm seems to give a little higher values of the bandwidth than R_p = 1.27 mm between h = 5.0 mm and 6.0 mm. Overall, the best bandwidth results are realized with R_p = 1.27 mm for most substrate heights. As shown in Figure 3.54, the bandwidth values are lower than 8% with R_p = 0.3 mm for most of the substrate heights.

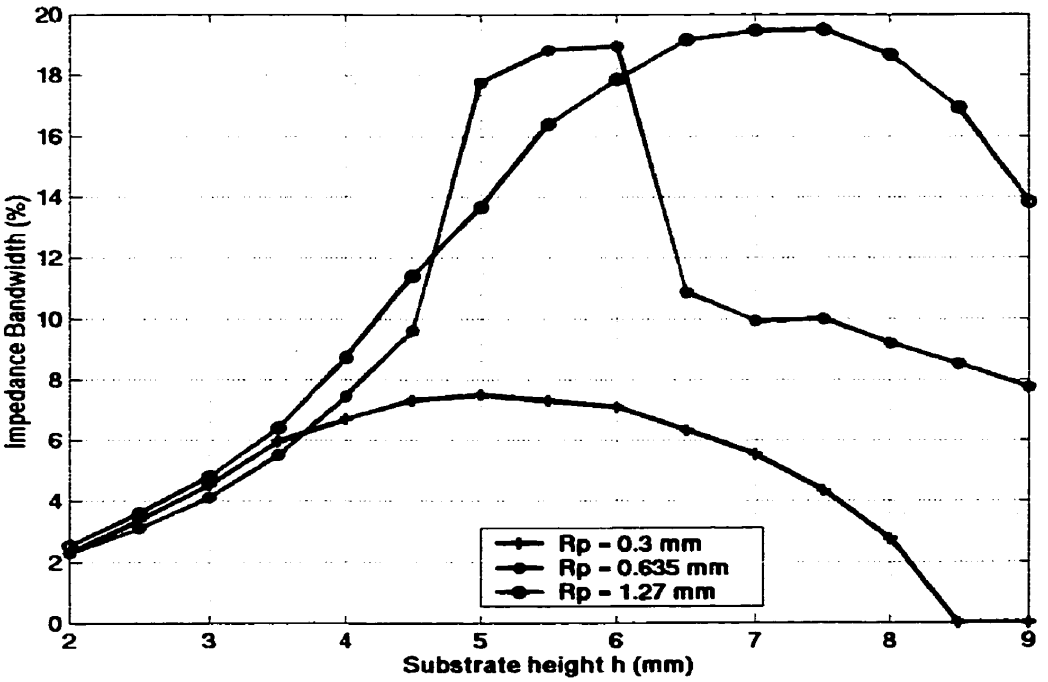

Figure 3.54: Effect of different values of R_p (probe radius) on the impedance bandwidth with C_d = 41.0, (x_c, y_c) = (0, −7.5), (a_1, b_1) = (3.78, −1.28), (a_2, b_2) = (5.9, 0.85), t = 3.01, (x_p, y_p) = (0, −3.25), d = 1.40, F = 23.75 and h = 5.5. All dimensions in mm.

Similarly, the effect of changing the probe location on the antenna bandwidth for various substrate heights is plotted in Figure 3.55. From Figure 3.55, it can be seen that

the probe location with F = 23.75 mm provides the highest bandwidths for substrate heights more than 3.0 mm, whereas the results obtained with F = 22.75 mm are slightly lower. The peak value of bandwidth occurs at h = 7.5 mm with F = 23.75 mm. On the other hand, the antenna characteristics with F = 24.75 mm become very narrowband, as depicted in Figure 3.54.

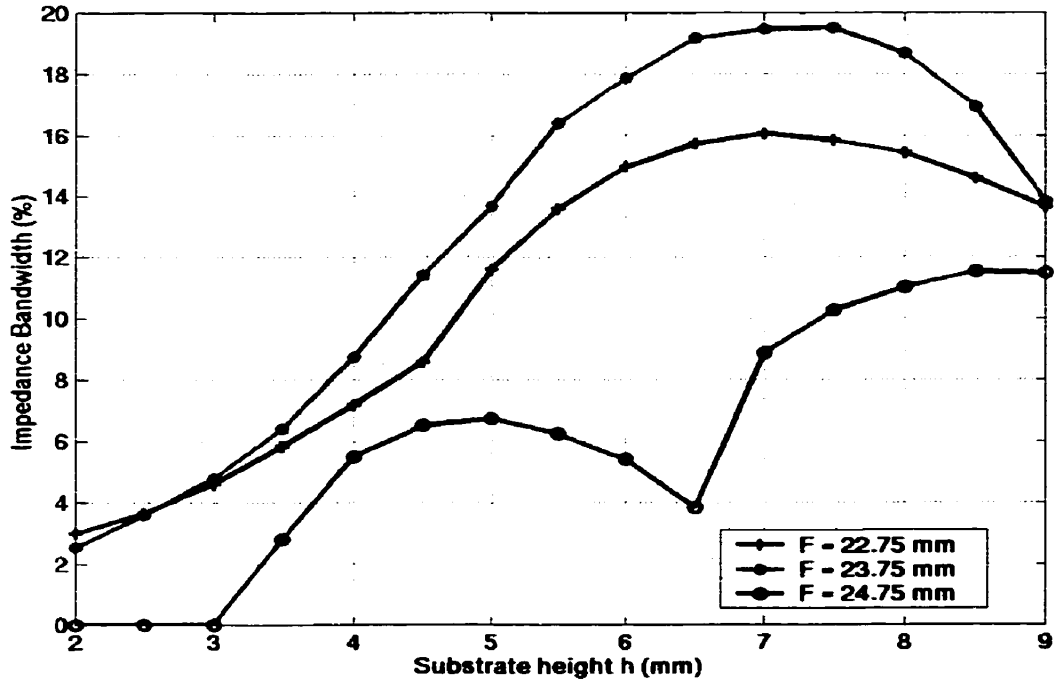

Figure 3.55: Effect of different values of F (probe location) on the impedance bandwidth with C_d = 41.0, (x_c, y_c) = (0, −7.5), (a_1, b_1) = (3.78, −1.28), (a_2, b_2) = (5.9, 0.85), t = 3.01, (x_p, y_p) = (0, −3.25), d = 1.40, R_p = 1.27 and h = 5.5. All dimensions in mm.

To observe the effect on the bandwidth, the next antenna parameter that is varied is the circular arc slot location, which is identified by the variable d. The plot of impedance bandwidth vs. substrate height h is shown in Figure 3.56 for three different values of d.

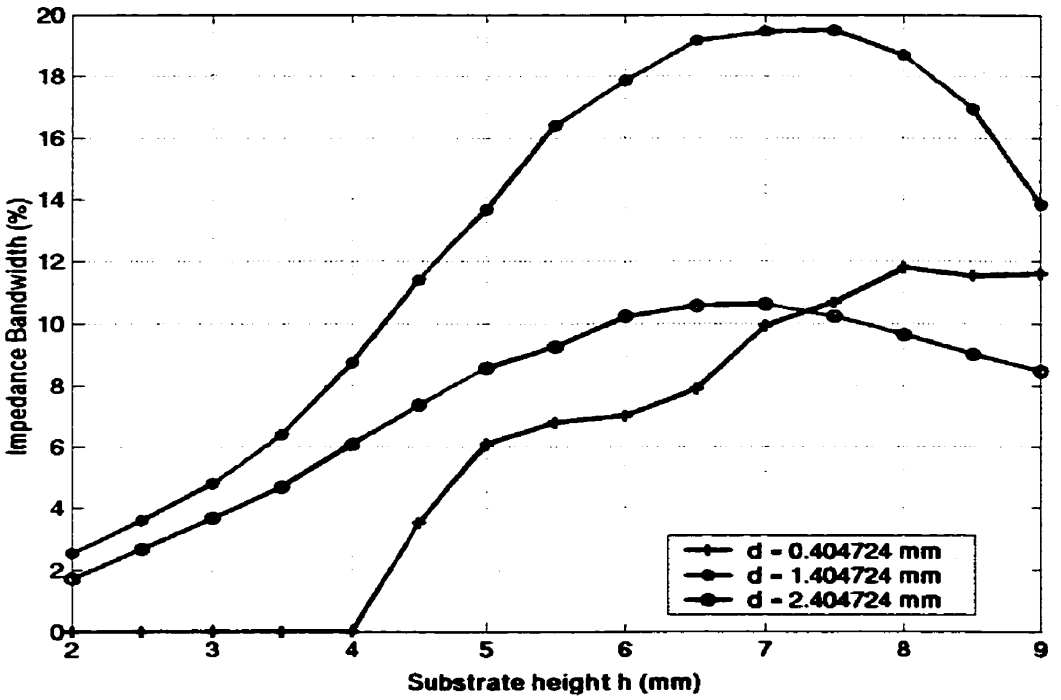

Figure 3.56: Effect of different values of d (slot location) on the impedance bandwidth with C_d = 41.0, (x_c, y_c) = (0, −7.5), (a_1, b_1) = (3.78, −1.28), (a_2, b_2) = (5.9, 0.85), t = 3.01, (x_p, y_p) = (0, −3.25), F = 23.75, R_p = 1.27 and h = 5.5. All dimensions in mm.

Clearly, Figure 3.56 shows that the best bandwidth results are realized with d = 1.40 mm where the peak bandwidth value of 19.51% occurs at h = 7.5 mm. The bandwidth results with d = 2.40 mm are a bit lower, while the slot location d = 0.40 mm gives undesirable bandwidth values. Therefore, the optimum slot location is near d = 1.40 mm. The similar study is done on the antenna bandwidth by varying the width of the circular arc slot, which is given by the variable t. Figure 3.57 shows the plot of impedance bandwidth vs. substrate height h for three different values of t. From Figure 3.57 it is very clear that slot widths t = 2.83 mm and t = 3.01 mm give very similar bandwidth results for all substrate heights.

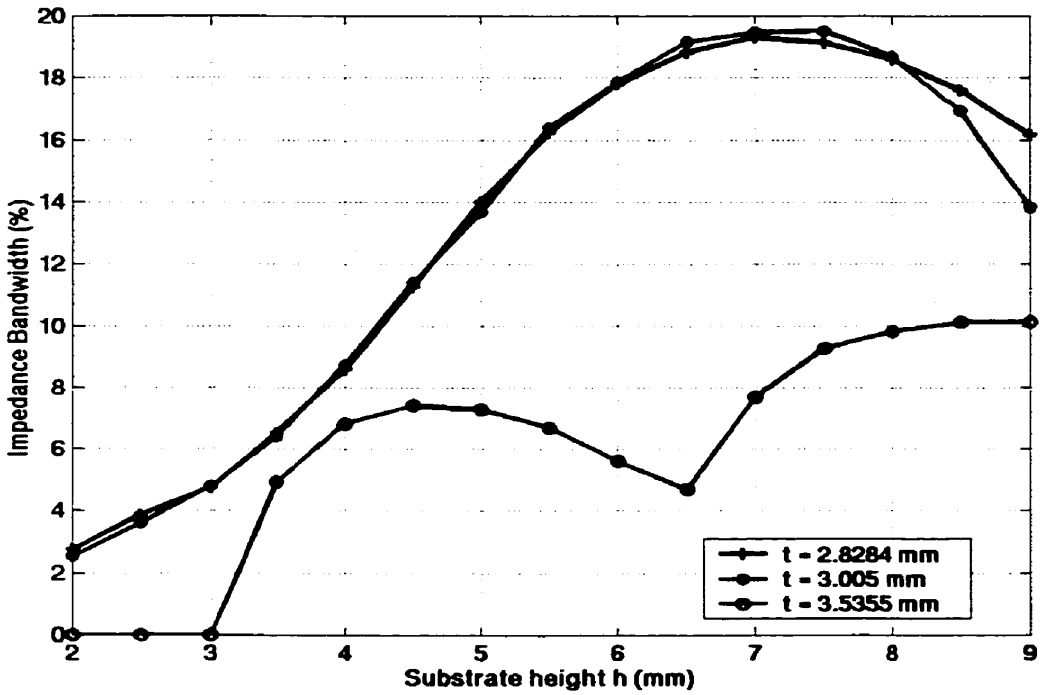

Figure 3.57: Effect of different values of t (slot width) on the impedance bandwidth with $C_d = 41.0$, $(x_c, y_c) = (0, -7.5)$, $(a_1, b_1) = (3.78, -1.28)$, $(a_2, b_2) = (5.9, 0.85)$, $d = 1.40$, $(x_p, y_p) = (0, -3.25)$, $F = 23.75$, $R_p = 1.27$ *and* $h = 5.5$. *All dimensions in mm.*

According to the results shown in Figure 3.57, the slot width of $t = 3.54$ mm does not provide very promising results of −10 dB bandwidth. The highest bandwidth value in Figure 3.57 is attained with $t = 3.01$ at $h = 7.5$ mm. Considering that the slot widths of $t =$ 2.83 mm and 3.01 mm provide good bandwidth results for all substrate heights, then the optimum slot width must be near these two values. Since the results in Figure 3.54 to Figure 3.57 have a maximum bandwidth of 19.51% at $h = 7.5$ mm, it is presumed that the optimized antenna dimensions may be: $R_p = 1.27$ mm, $F = 23.75$ mm, $d = 1.40$ mm and $t = 3.01$ mm. In order to confirm that $R_p = 1.27$ mm, $F = 23.75$ mm, $d = 1.40$ mm and $t = 3.01$ mm are the optimized antenna dimensions, the −10 dB bandwidth of the antenna is

calculated at the substrate height of h = 7.5 mm for various values of R_p , F, d and t. Figure 3.58 shows the plot of bandwidth vs. probe radius. The other antenna dimensions are shown in Figure 3.58. As the probe radius is increased, the bandwidth of the antenna also increases. The peak value is obtained when the probe radius is equal to 1.27 mm, this makes R_p = 1.27 mm the optimized probe radius value.

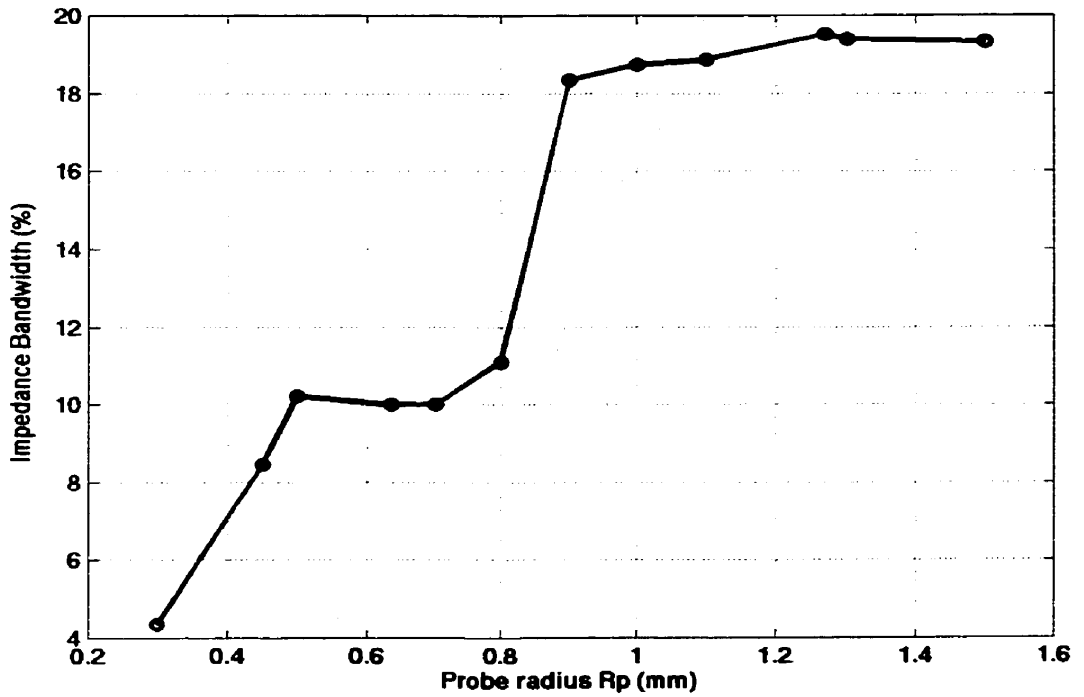

Figure 3.58: Effect of different values of R_p (probe radius) on the impedance bandwidth with C_d = 41.0, (x_c, y_c) = (0, −7.5), (a_1, b_1) = (3.78, −1.28), (a_2, b_2) = (5.9, 0.85), t = 3.01, (x_p, y_p) = (0, −3.25), d = 1.40, F = 23.75 and h = 5.5. All dimensions in mm.

In addition, Figure 3.59 shows the plot of bandwidth vs. probe location at h = 7.5 mm with the other antenna dimensions as listed in Figure 3.36. From Figure 3.59, it is clear that the maximum bandwidth occurs with F = 23.75 mm. The bandwidth increases smoothly when F is changed from 22.75 mm to 23.75 mm and then drops slightly with F = 24.0 mm. The major drop in the bandwidth occurs due to the split in the s11 curve at

the −10 dB line as F is increased from 24.0 mm to 24.25 mm. Nonetheless, F = 23.75 mm is the optimum value of the probe location, as shown in Figure 3.59.

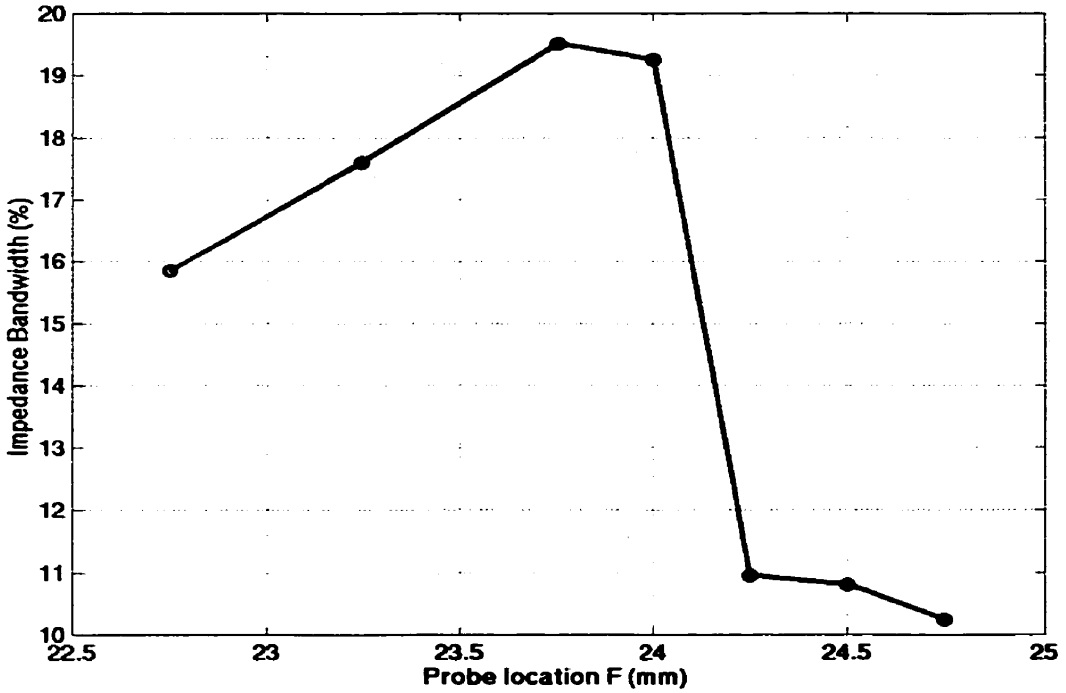

Figure 3.59: Effect of different values of F (probe location) on the impedance bandwidth with C_d = 41.0, (x_c, y_c) = (0, −7.5), (a_1, b_1) = (3.78, −1.28), (a_2, b_2) = (5.9, 0.85), t = 3.01, (x_p, y_p) = (0, −3.25), d = 1.40, R_p = 1.27 and h = 5.5. All dimensions in mm.

Similarly, the bandwidth results shown in Figure 3.60 are used to verify whether or not d = 1.40 mm is the optimum value. Obviously, Figure 3.60 shows that the highest bandwidth value does not occur when d = 1.40 mm, but instead it occurs when d = 1.65 mm. The peak value of the bandwidth with d = 1.65 mm is 21.15%. Therefore, the optimum location of the circular arc slot on the patch is with d = 1.65 mm. The split in the s11 curve at the −10 dB line causes the large drop in the bandwidth when d is increased more than 1.65 mm.

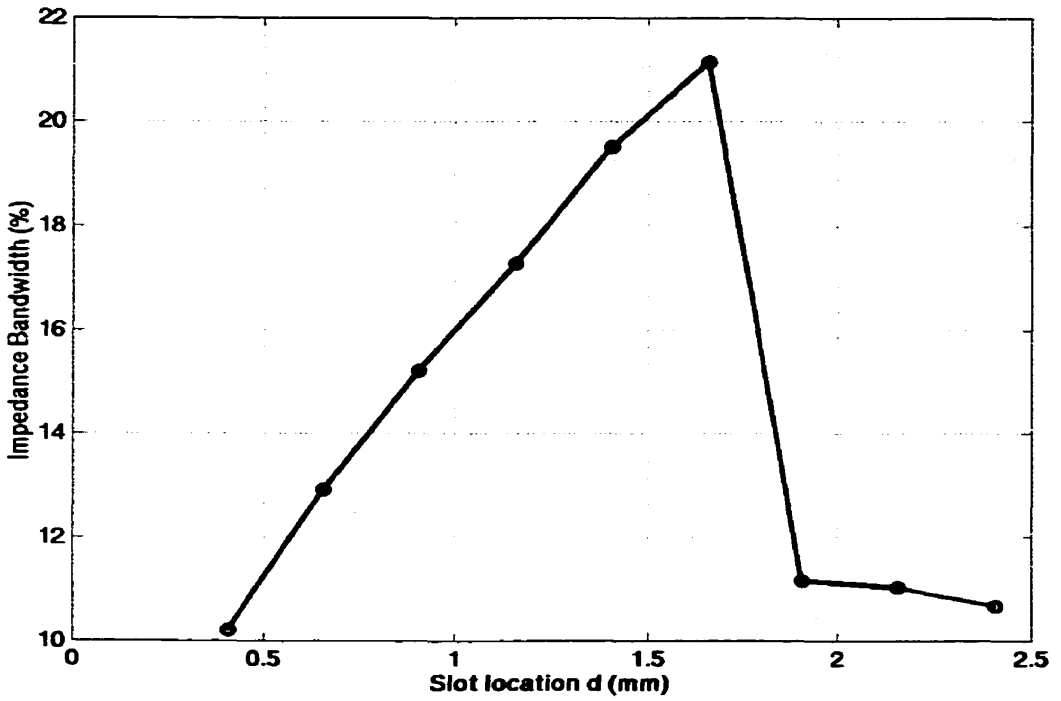

Figure 3.60: Effect of different values of d (slot location) on the impedance bandwidth with C_d = 41.0, (x_c, y_c) = (0, −7.5), (a_1, b_1) = (3.78, −1.28), (a_2, b_2) = (5.9, 0.85), t = 3.01, (x_p, y_p) = (0, −3.25), F = 23.75, R_p = 1.27 and h = 5.5. All dimensions in mm.

In a like manner, the results shown in Figure 3.61 are used to optimize the width of the circular arc slot. Figure 3.61 shows the plot of bandwidth vs. slot width at the substrate height of h = 8.0 mm. The impedance bandwidth increases smoothly when t is increased from 2.12 mm to 3.01 mm. Because of the split in the s11 curve, the sharp decline in the bandwidth happens when t is changed from 3.01 mm to 3.18 mm. From Figure 3.61, it can be seen that the maximum bandwidth value is realized with t = 3.01 mm. Hence, the optimized value of the slot width is equal to 3.01 mm.

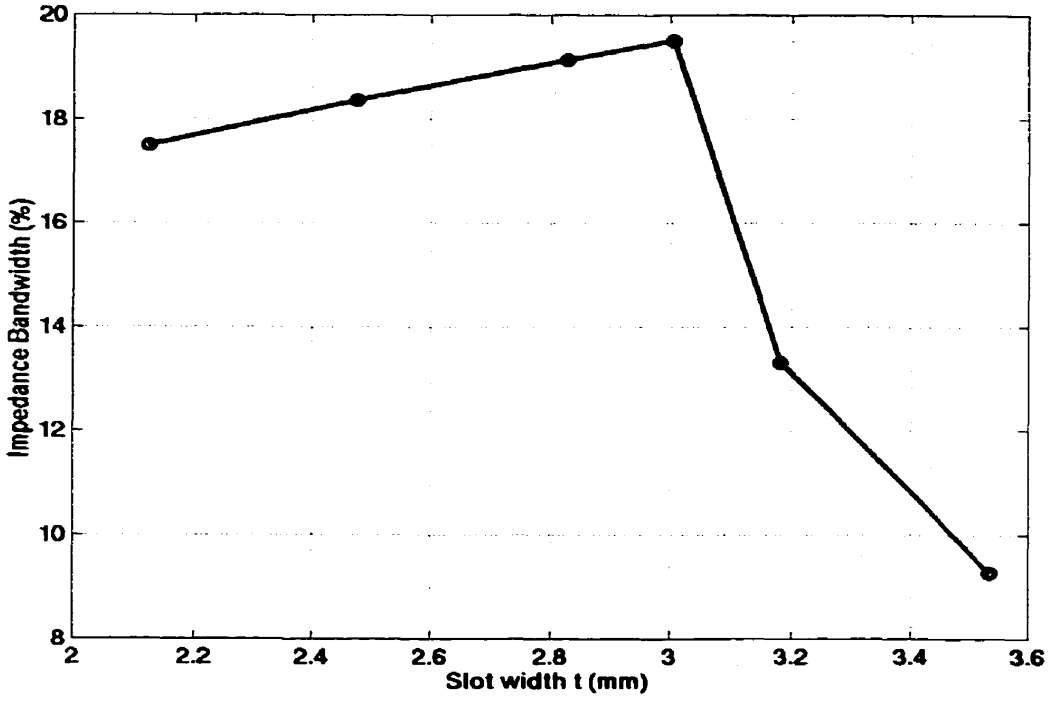

Figure 3.61: Effect of different values of t (slot width) on the impedance bandwidth with C_d *= 41.0,* (x_c, y_c) *= (0, −7.5),* (a_1, b_1) *= (3.78, −1.28),* (a_2, b_2) *= (5.9, 0.85), d= 1.40,* (x_p, y_p) *= (0, −3.25), F = 23.75,* R_p *= 1.27 and h = 5.5. All dimensions in mm.*

3.4.3 Simulation results of Antenna 3 matched with a tuning stub

Since the Antenna 3 does not have very broadband characteristics, the stub tuning matching technique is also implemented on this antenna to increase its impedance bandwidth. The return loss of Antenna 3 without the stub tuning matching network is shown in Figure 3.62 with the antenna dimensions: C_d = 31 mm, (x_c, y_c) = (0, −2 mm), (a_1, b_1) = (5 mm, 4 mm), (a_2, b_2) = (7 mm, 6 mm), t = 2.83 mm, (x_p, y_p) = (0, −2 mm), F = 17.5 mm, R_p = 0.635 mm, h = 5.5 mm. Figure 3.39 shows that the Antenna 3 resonates near two resonance frequencies at f_1 = 3.52 GHz and f_2 = 5.04 GHz. The −10 dB impedance bandwidth is calculated to be 10.28%, which is not very large. Figure 3.63

shows the Smith chart plot of the impedance of Antenna 3, which has the potential bandwidth of approximately 39.68%. To achieve this broad bandwidth, the impedance locus loop on the smith chart can be matched using 50Ω transmission lines with a stub of length L_1, which is located a distance L_2 from the 50Ω via position. The geometry of the circular patch antenna with a circular arc slot matched using the stub tuning matching method is shown in Figure 3.64.

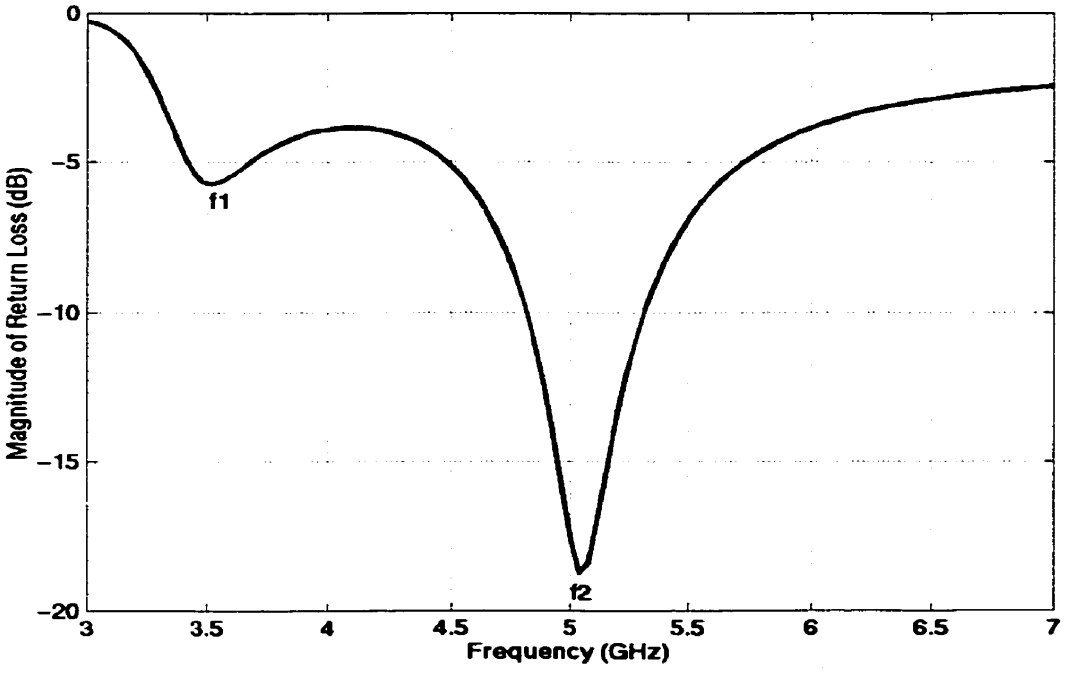

Figure 3.62: Return loss of Antenna 3 with antenna dimensions of C_d = 31, (x_c, y_c) = (0, −2), (a_1, b_1) = (5, 4), (a_2, b_2) = (7, 6), t = 2.83, (x_p, y_p) = (0, −2 mm), F = 17.5 mm, R_p = 0.635, h = 5.5 mm. All dimensions in mm.

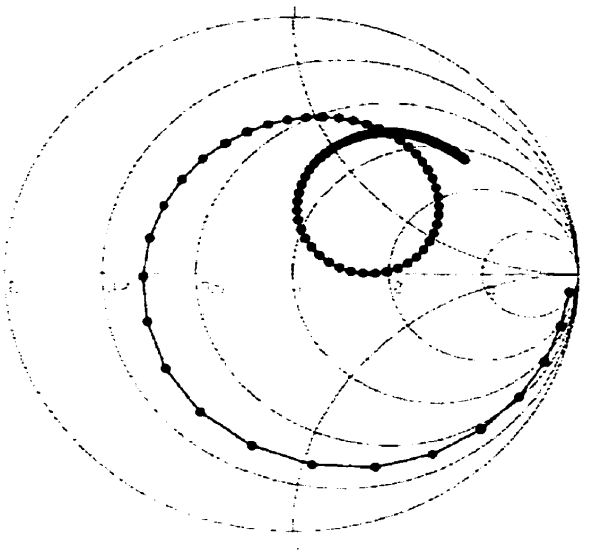

Figure 3.63: Smith chart plot of Antenna 3 with antenna dimensions of $C_d = 31$, $(x_c, y_c) = (0, -2)$, $(a_1, b_1) = (5, 4)$, $(a_2, b_2) = (7, 6)$, $t = 2.83$, $(x_p, y_p) = (0, -2\ mm)$, $F = 17.5\ mm$, $R_p = 0.635$, $h = 5.5\ mm$. All dimensions in mm.

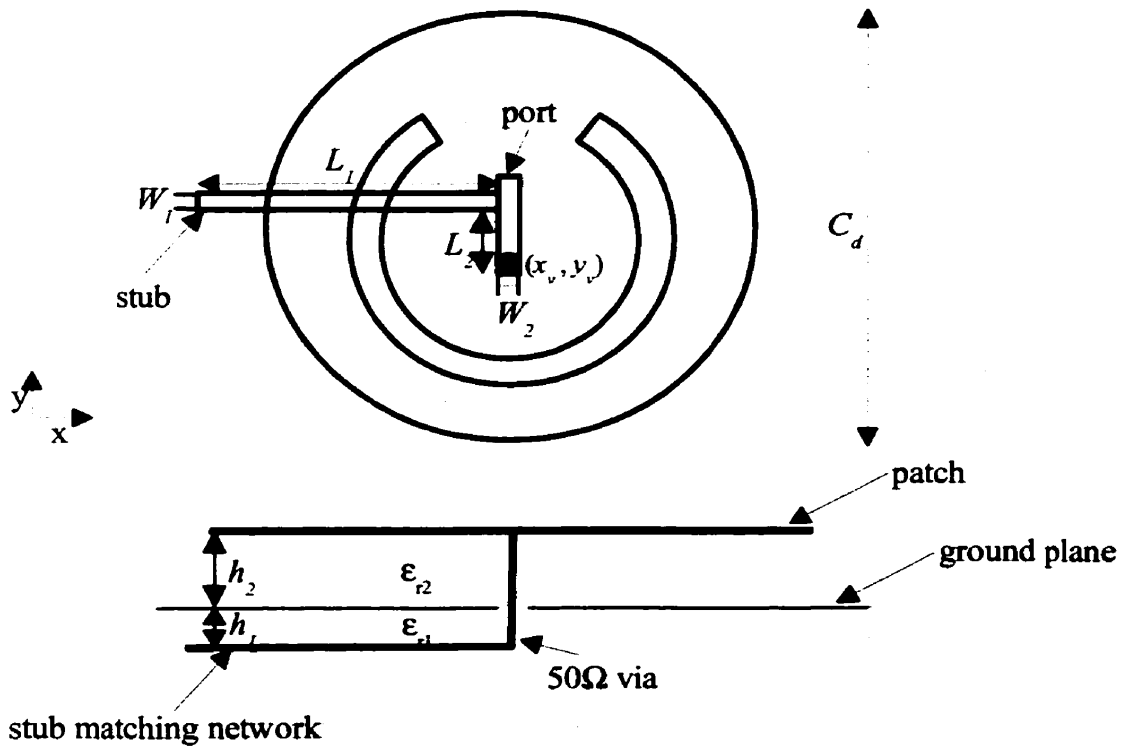

Figure 3.64: Geometry of Antenna 3 matched using the stub tuning matching method.

As shown in Figure 3.64, the Antenna 3 with dimensions $C_d = 31$ mm, $(x_c, y_c) = (0, -2$ mm), $(a_1, b_1) = (5$ mm, 4 mm), $(a_2, b_2) = (7$ mm, 6 mm) and $t = 2.828$ mm is matched with the stub tuning matching technique. The patch is situated on top of a foam substrate with height $h_2 = 5.5$ mm over the ground plane. The single stub matching network is placed on the other side of the ground plane on a substrate with $\varepsilon_{r1} = 2.5$ and $h_1 = 0.46$ mm, which is fed using a 50Ω transmission line at the position denoted as the port in Figure 3.64. The signal is sent through a 50Ω via to the circular patch from the single stub matching network. In the stub matching network, the widths of the 50Ω transmission lines are $W_1 = W_2 = 1.31$ mm and the length of the stub is $L_1 = 19.4$ mm, which is located a distance of $L_2 = 4.53$ mm from the 50Ω via.

The simulated results for the return loss of this antenna using the software Ansoft ENSEMBLE are plotted in Figure 3.65. It can be seen from Figure 3.65 that it resonates near $f_1 = 4.82$ GHz and $f_2 = 5.45$ GHz. After matching, the −10 dB impedance bandwidth is increased from 10.28% to 23.17%. This increase in the impedance bandwidth is also verified by the Smith chart plot of the impedance of the antenna, which is shown in Figure 3.66. If the two smith chart plots of the antenna impedance shown in Figure 3.63 and Figure 3.66 are compared, it can be seen that the loop on the Smith chart in Figure 3.66 is matched well to 50Ω, which increases the impedance bandwidth of the Antenna 3.

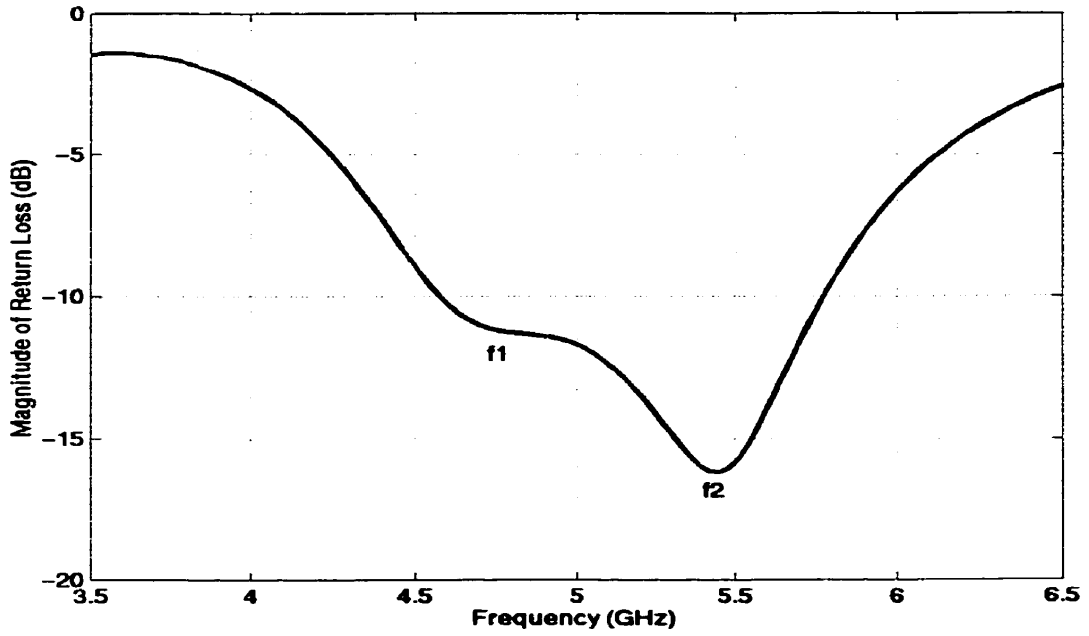

Figure 3.65: Return loss of Antenna 3 matched using the tuning stub with dimensions: $C_d = 31$, $(x_c, y_c) = (0, -2)$, $(a_1, b_1) = (5, 4)$, $(a_2, b_2) = (7, 6)$, $t = 2.83$, $(x_v, y_v) = (0, -2)$, $h_1 = 5.5$, $h_2 = 0.46$, $W_1 = W_2 = 1.31$, $L_1 = 19.4$ *and* $L_2 = 4.53$. *All dimensions in mm.*

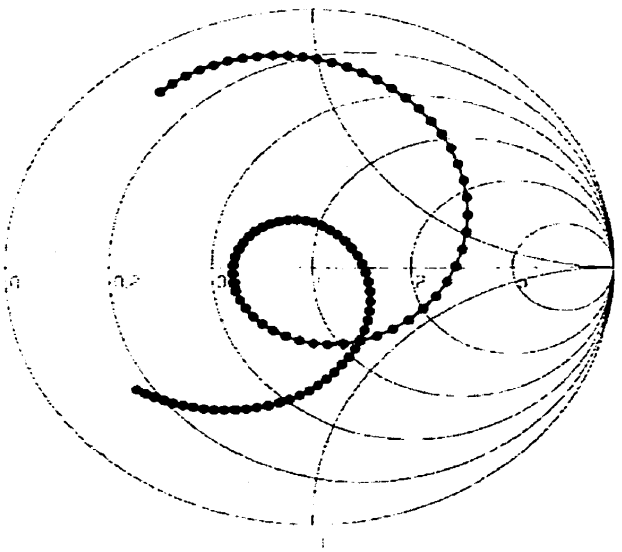

Figure 3.66: Smith chart plot of Antenna 3 matched using the tuning stub with dimensions: $C_d = 31$, $(x_c, y_c) = (0, -2)$, $(a_1, b_1) = (5, 4)$, $(a_2, b_2) = (7, 6)$, $t = 2.83$, $(x_v, y_v) = (0, -2)$, $h_1 = 5.5$, $h_2 = 0.46$, $W_1 = W_2 = 1.31$, $L_1 = 19.4$ *and* $L_2 = 4.53$. *All dimensions in mm.*

The radiation pattern plots in the $\phi = 0$ plane and $\phi = 90$ plane at $f_l = 4.82$ GHz show that the antenna has good broadside radiation and crosspolarization levels, which are shown in Figure 3.67.

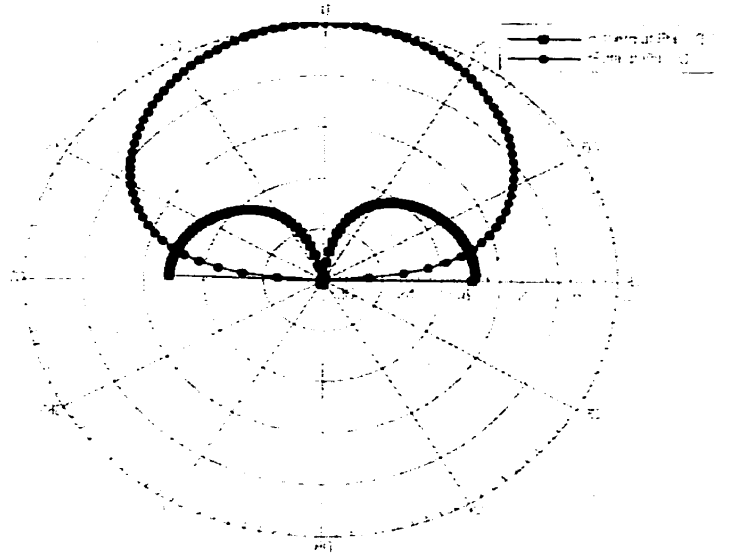

(*a*)

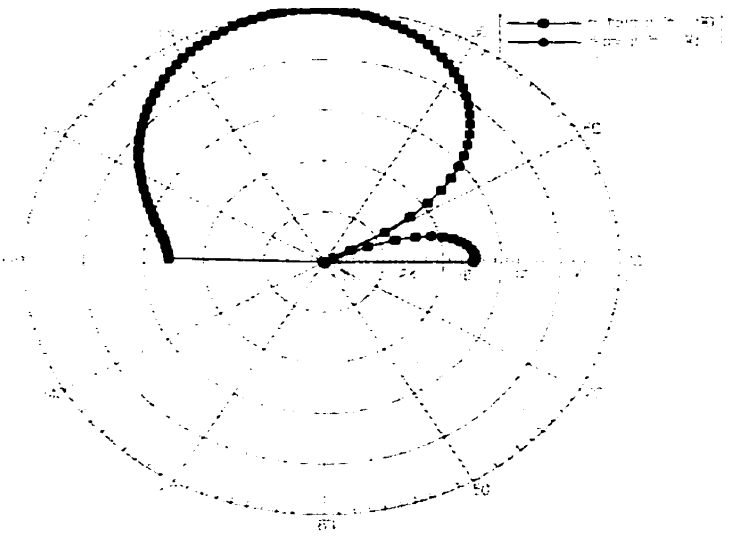

(*b*)

Figure 3.67: (a) Radiation patterns in $\phi = 0$ plane of Antenna 3 matched using the tuning stub at $f_l = 4.82$ GHz. (b) Radiation patterns in $\phi = 90$ plane of Antenna 3 matched using the tuning stub at $f_l = 4.82$ GHz.

Similarly, Figure 3.68 shows that for f_2 = 5.45 GHz the results of the radiation patterns also demonstrate good broadside radiation characteristics, however, the crosspolarization level in $\phi = 0$ plane is a bit higher.

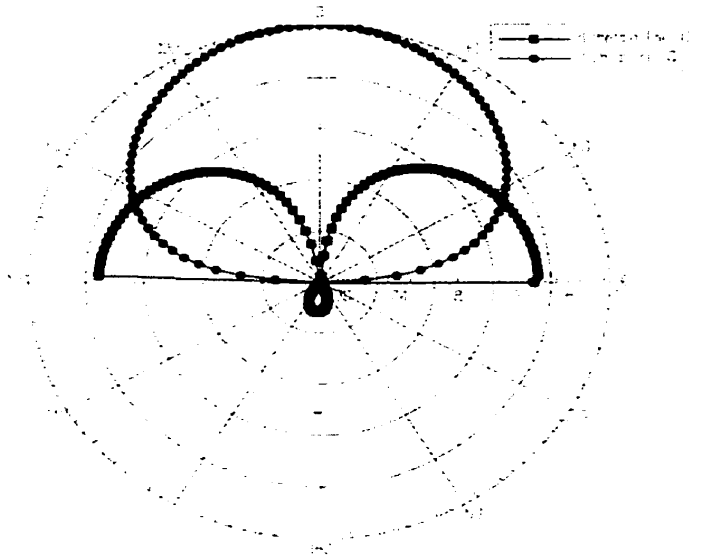

(*a*)

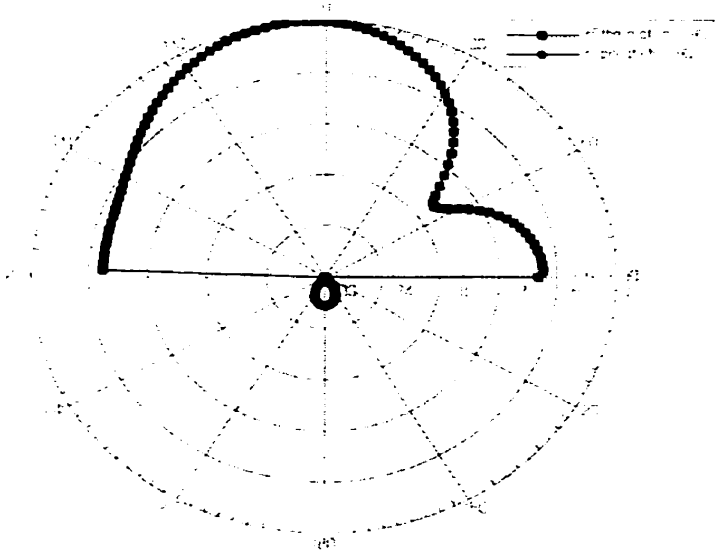

(*b*)

Figure 3.68: (a) Radiation patterns in $\phi = 0$ plane of Antenna 3 matched using the tuning stub at f_2 = 5.45 GHz. (b) Radiation patterns in $\phi = 90$ plane of Antenna 3 matched using the tuning stub at f_2 = 5.45 GHz.

It is evident from the gain patterns plots of the antenna shown in Figure 3.69 that the antenna has good broadside radiation characteristics and crosspolarization levels at the two operating frequencies. The antenna has broadside gain of 9.20 dBi at the first resonance frequency f_1 = 4.82 GHz in the ϕ = 0 plane and ϕ = 90 plane, as shown in Figure 3.69. The backward radiation shown in the gain patterns plots in Figure 3.69 is due to the stub matching network. Likewise, Figure 3.70 shows that the broadside gain of Antenna 3 matched with the stub tuning at f_2 = 5.45 GHz is equal to 8.05 dBi. Figure 3.70 demonstrates that the crosspolarization level in the ϕ = 0 plane for f_2 = 5.45 GHz is higher than f_1 = 4.82 GHz, however, it is very similar in the ϕ = 90 plane for both f_1 and f_2.

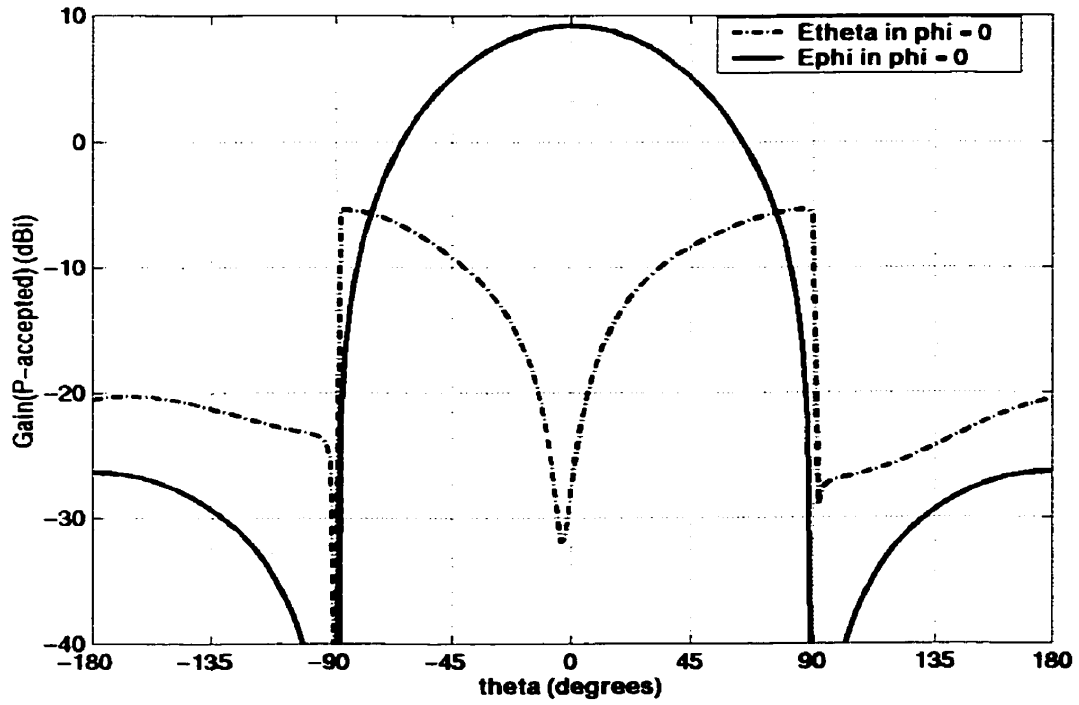

(*a*)

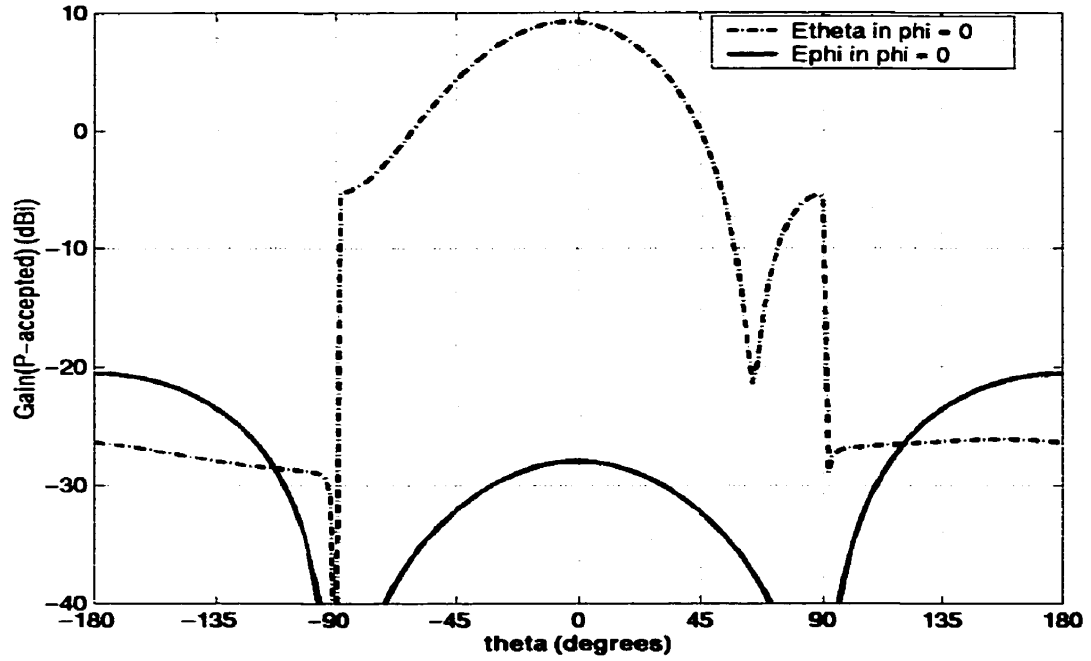

(*b*)

Figure 3.69: (a) Gain patterns in ϕ = 0 plane of Antenna 3 matched using the tuning stub at f_l = 4.82 GHz. (b) Gain patterns in ϕ = 90 plane of Antenna 3 matched using the tuning stub at f_l = 4.82 GHz.

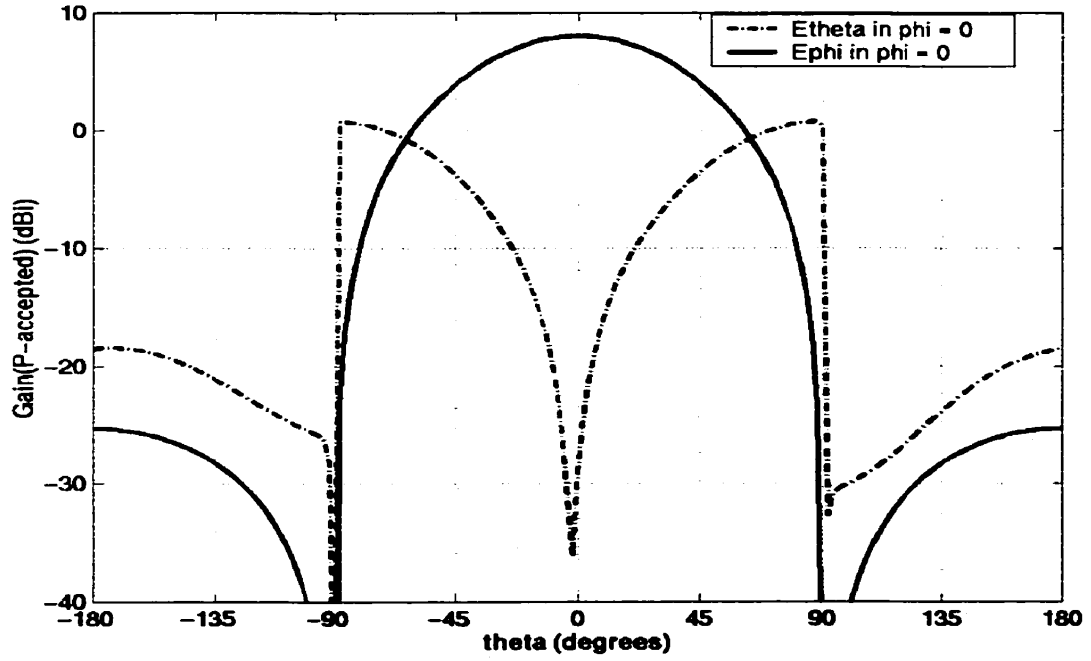

(*a*)

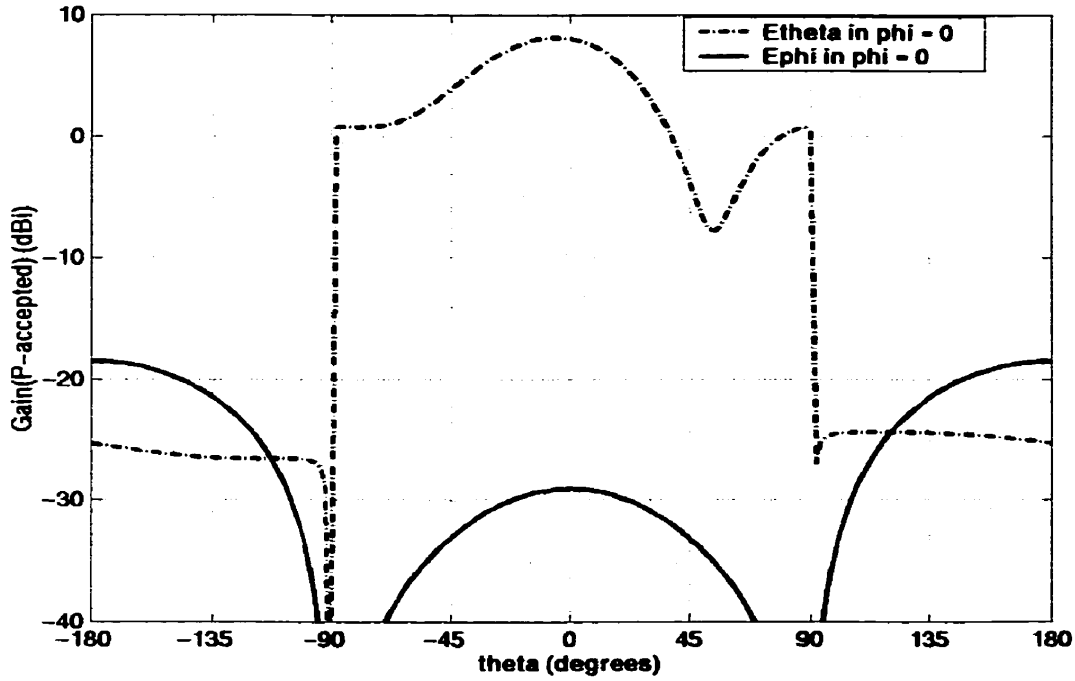

(*b*)

Figure 3.70: (a) Gain patterns in ϕ = 0 plane of Antenna 3 matched using the tuning stub at f_2 = 5.45 GHz. (b) Gain patterns in ϕ = 90 plane of Antenna 3 matched using the tuning stub at f_2 = 5.45 GHz.

3.5 Analysis of Antenna 4

Earlier it has been shown by Luk et al. that an L–shaped probe is an excellent feed for thick circular patch antennas [23]. With this antenna, an impedance bandwidth of 24% and an average gain of 7.5 dBi are achieved [23]. Later on, it was shown by Guo et al. that a single U–slot circular patch antenna with a L–probe feeding has broad bandwidth in the range of 38% and a gain of 6.8 dBi [24]. A new configuration of a broadband patch antenna is studied in this thesis using the similar idea, where the slot has been replaced with a circular arc shaped slot. This new broadband antenna gives a bandwidth of 40% and high gain value of 9.0 dBi. The parametric study of this antenna is given in this section.

Figure 3.71 shows the geometry of this antenna. The circular patch with diameter C_d is separated from the ground plane with a foam substrate of $\varepsilon_r = 1.0006$, and a circular arc shaped slot is cut in the center of the patch. The center point of the two circular arcs is given by (x_c, y_c), as shown in Figure 3.71. The parameters (a_1, b_1) and (a_2, b_2) denote the end points of the first and second arc, respectively. The width of the circular arc slot is indicated by the variable t. The patch is proximity fed by an L–shaped coaxial probe. The position of the L–shaped probe with respect to the patch is specified by the parameter D. The parameters used to designate the dimensions of the L–shaped probe are indicated on Figure 3.71. The height of the foam substrate separating the patch and the ground plane is denoted by H. The parameters L_v and L_h represent the vertical and horizontal height of the L–shaped probe respectively, as shown in Figure 3.48. The width of the L–shaped probe is given by $2R$.

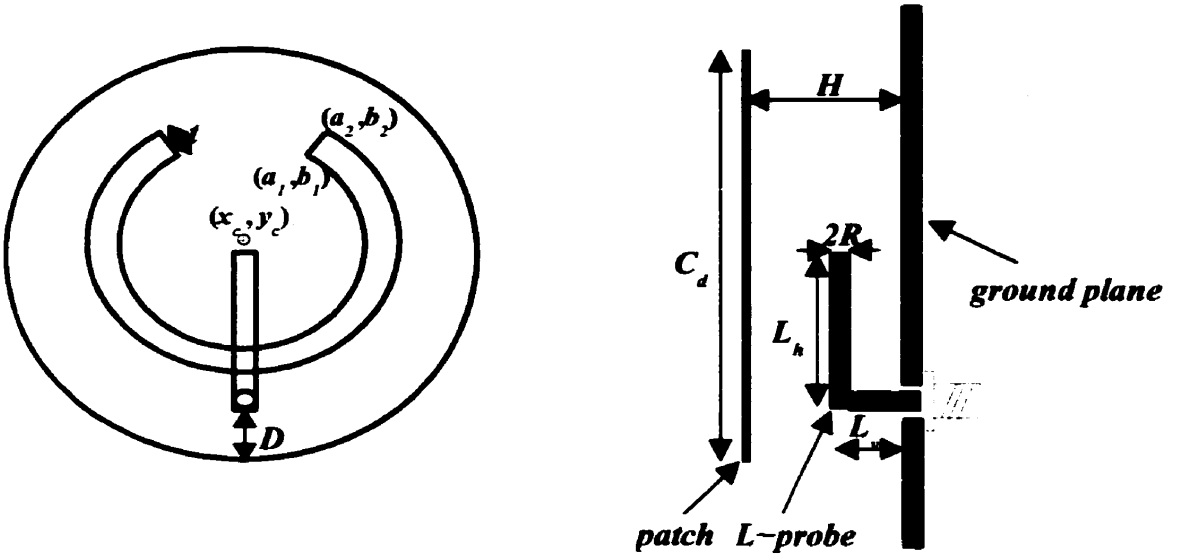

Figure 3.71: Geometry of a circular patch with a circular arc slot and L-shaped probe.

3.5.1 Resonance frequencies and impedance bandwidth

Extensive computations are performed to study the characteristics of this antenna. The effect of different parameters of the antenna on the resonance frequencies and impedance bandwidth is presented in this section. The following dimensions of the antenna are considered: C_d = 34 mm, (x_c, y_c) = (0, 1 mm), (a_1, b_1) = (5 mm, 8 mm), (a_2, b_2) = (7 mm, 10 mm), t = 2.83 mm, L_h = 14.5 mm, L_v = 5.5 mm, R = 1 mm, D = 3 mm and H = 9 mm. With these dimensions, the frequency f_1 occurs at 3.7 GHz and f_2 at 4.95 GHz, as shown in Figure 3.72. The −10 dB bandwidths in the first and second bands are 17.6% and 16.15%, respectively. Figure 3.72 also shows the effect of changing the location of the circular arc slot on the impedance bandwidth. As the circular arc slot is moved up, the frequency f_1 increases from 3.7 GHz to 3.75 GHz, while f_2 stays fixed at 4.95 GHz. The location of the arc slot has a significant effect on the −10 dB bandwidth. The two bands

merge together and the bandwidth of 39.77% is achieved with the center of the circular arc slot at (x_c, y_c) = (0, 1.75 mm), as shown in Figure 3.72. Accordingly, the optimized location of the circular arc slot has its center point at (x_c, y_c) = (0, 1.75 mm).

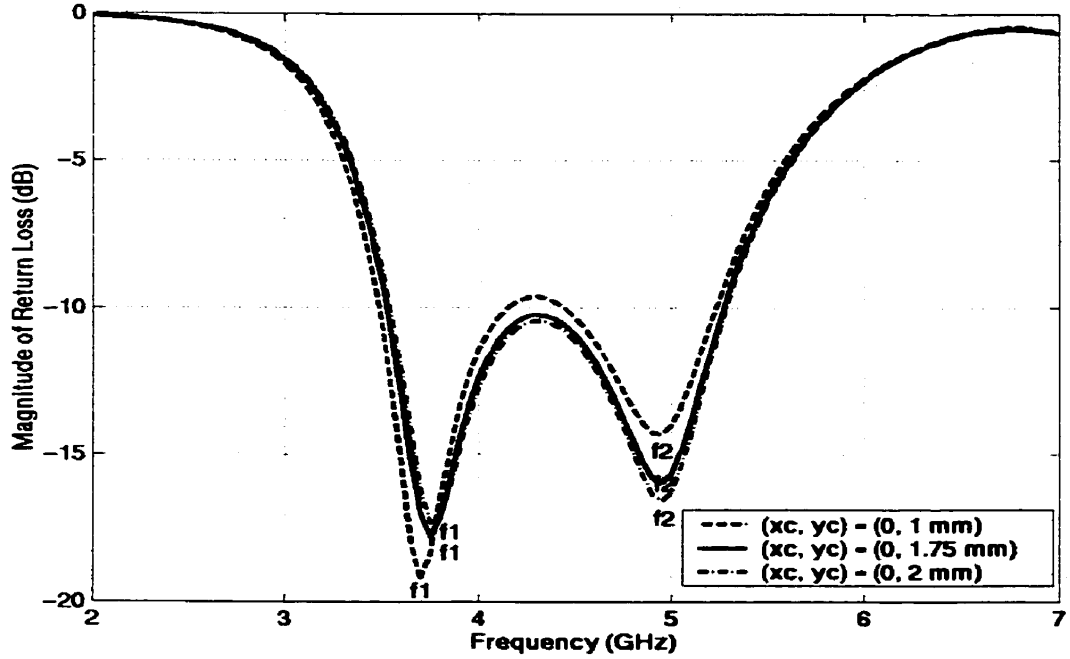

Figure 3.72: Return Loss of Antenna 4 for different (x_c, y_c) values with antenna dimensions: C_d = 34, t = 2.83, L_h = 14.5, L_v = 5.5, R = 1, D = 3, H = 9.0. All dimensions in mm.

Various values of L_v (the vertical length of the L−shaped probe) are simulated to observe the effect on the −10 dB bandwidth. The other antenna dimensions are C_d = 34 mm, (x_c, y_c) = (0, 1.75 mm), (a_1, b_1) = (5 mm, 8.75 mm), (a_2, b_2) = (7 mm, 10.75 mm), t = 2.83 mm, L_h = 14.5 mm, R = 1 mm, D = 3 mm and H = 9.0 mm. Figure 3.73 shows the computed results of the return loss of the antenna for different values of L_v. As the length L_v is increased from 5.0 mm to 5.5 mm, the frequency f_1 decreases and f_2 increases, while the −10 dB bandwidth increases from 34.76% to 39.77%. However, by increasing the

parameter L_v to 6.0 mm, the antenna loses its broadband characteristics. This is illustrated in Figure 3.73.

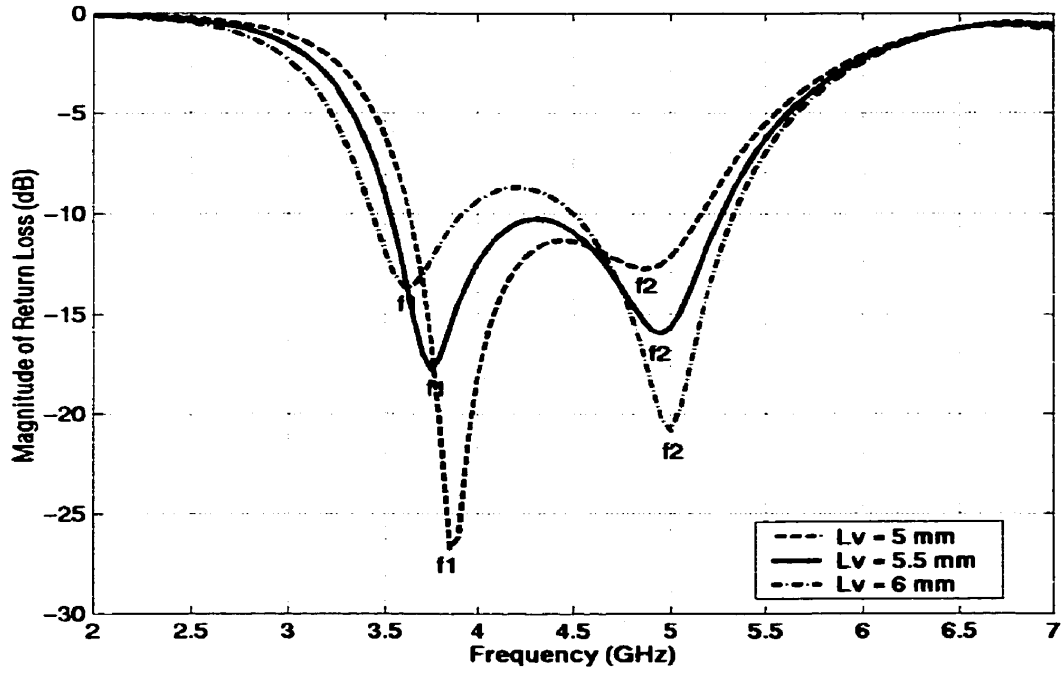

Figure 3.73: Return Loss of Antenna 4 for different L_v values with antenna dimensions: C_d = 34, (x_c, y_c) = (0, 1.75), (a_1, b_1) = (5, 8.75), (a_2, b_2) = (7, 10.75), t = 2.83, L_h = 14.5, R = 1, D = 3, H = 9.0. All dimensions in mm.

The next parameter to be studied is L_h that is the horizontal length of the L-shaped probe. The computed results for the return loss of the antenna for different values of L_h are shown in Figure 3.74. It can be seen from Figure 3.74 that as the horizontal length of the L-shaped probe L_h is increased from 14.0 mm to 15.0 mm, the frequencies f_1 and f_2 both decrease as well as the −10 dB bandwidth of the antenna. Consequently, the length L_h = 14.0 mm gives the best result of 40% for the impedance bandwidth of the antenna, where f_1 = 3.8 GHz and f_2 = 5.0 GHz. Therefore, the horizontal length of the L-shaped probe L_h = 14.0 mm is considered to be the optimized length.

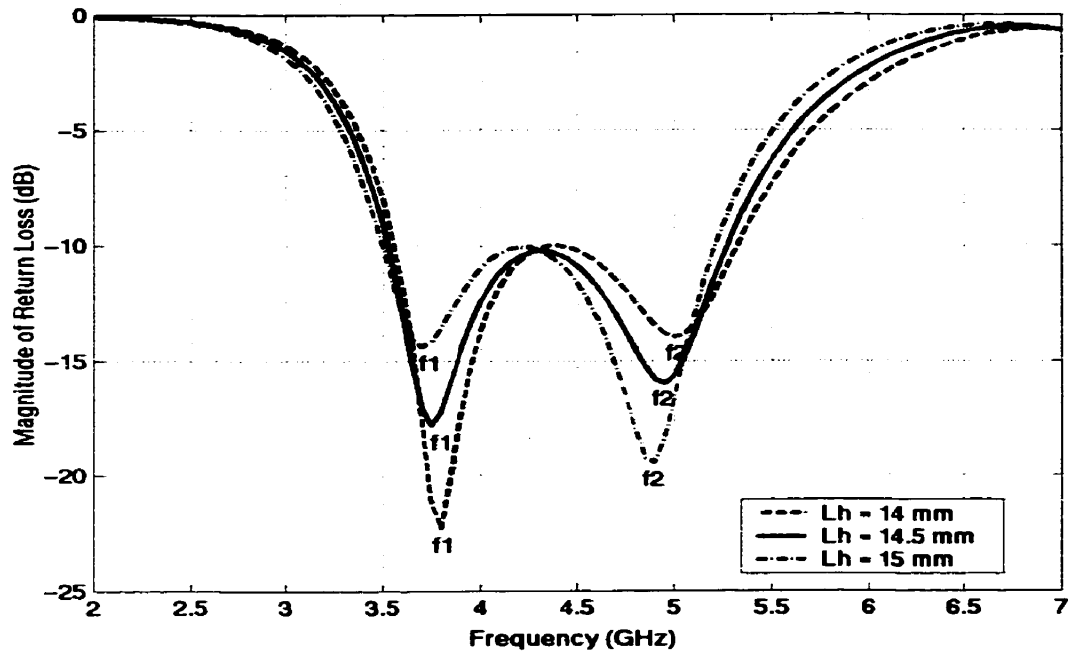

Figure 3.74: Return Loss of Antenna 4 for different L_h values with antenna dimensions: C_d = 34, (x_c, y_c) = (0, 1.75), (a_1, b_1) = (5, 8.75), (a_2, b_2) = (7, 10.75), t = 2.83, L_v = 5.5, R = 1, D = 3, H = 9.0. All dimensions in mm.

Figure 3.75 presents the simulated results of the return loss for different values of t, which is the thickness of the circular arc slot. The considered values of the slot thickness are: t = 2.48 mm, t = 2.83 mm and t = 3.18 mm. As t is increased from 2.48 mm to 2.83 mm, the frequency f_1 tends to increase from 3.75 GHz to 3.8 GHz, while f_2 stays constant. With this increase in t, the −10 dB bandwidth of the antenna increases from 39.55% to 40%. However, if t is increased from 2.83 mm to 3.18 mm, f_1 stays constant but f_2 increases from 5.0 GHz to 5.05 GHz and −10 dB bandwidth decreases from 40% to 39.78%. Therefore, t = 2.83 mm gives the best result of the impedance bandwidth.

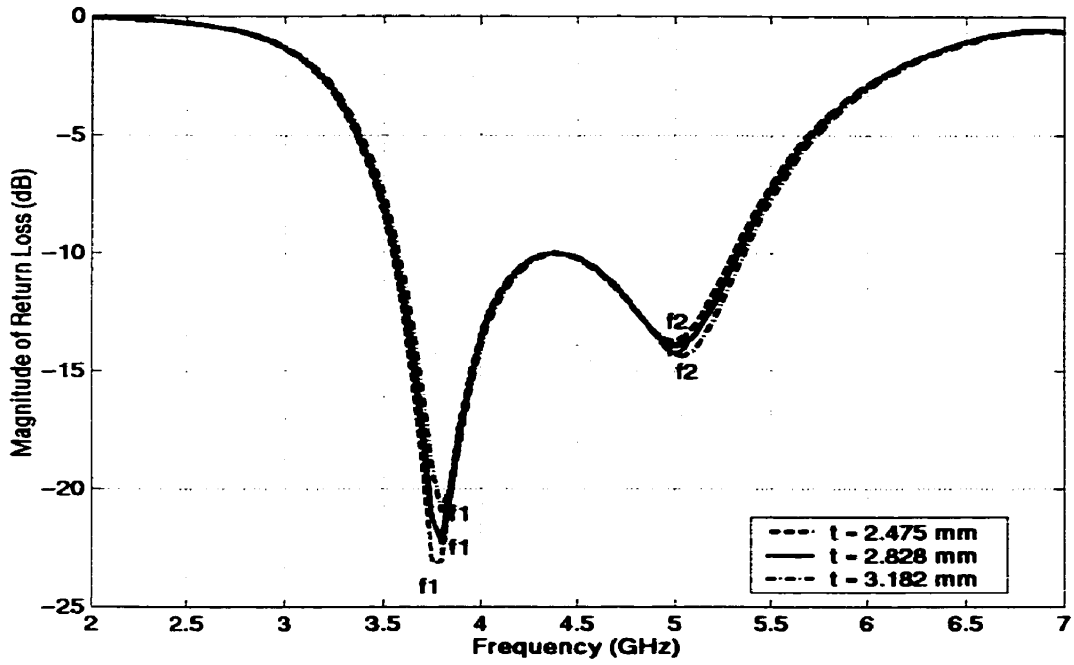

Figure 3.75: Return Loss of Antenna 4 for different t values with antenna dimensions: C_d = 34, (x_c, y_c) = (0, 1.75), (a_1, b_1) = (5, 8.75), (a_2, b_2) = (7, 10.75), L_h = 14, L_v = 5.5, R = 1, D = 3, H = 9.0. *All dimensions in mm.*

The location of the L−shaped probe which is specified by the parameter D also has a significant effect on the impedance bandwidth of the antenna. By increasing D from 2.5 mm to 3.0 mm, the frequencies f_1 and f_2 stay fixed but the −10 dB bandwidth of the antenna increases from 39.55% to 40%, as shown in Figure 3.76. If the value of D is increased from 3.0 mm to 3.5 mm, there is a considerable change in the impedance bandwidth of the antenna. The antenna becomes dual band, this is shown in Figure 3.76. The results of the return loss shown in Figure 3.76 make D = 3.0 mm the optimized value.

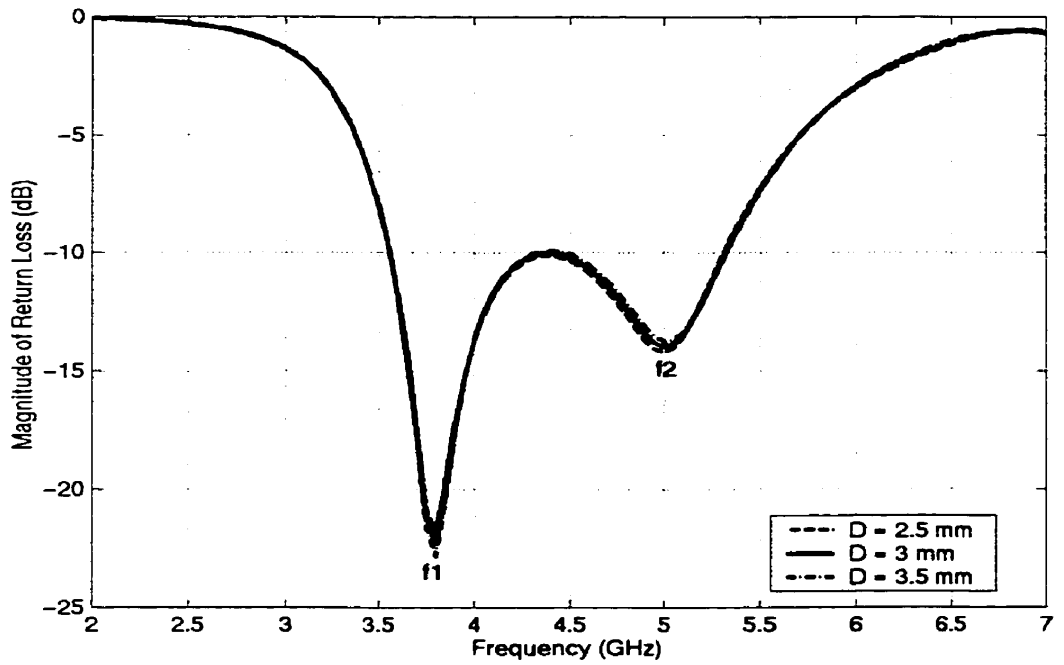

Figure 3.76: Return Loss of Antenna 4 for different values of D with antenna dimensions: $C_d = 34$, $(x_c, y_c) = (0, 1.75)$, $(a_1, b_1) = (5, 8.75)$, $(a_2, b_2) = (7, 10.75)$, $t = 2.83$, $L_h = 14$, $L_v = 5.5$, $R = 1$, $H = 9.0$. *All dimensions in mm.*

By varying the diameter of the circular patch from C_d = 34 mm to 33 mm with the other antenna dimensions of (x_c, y_c) = (0, 1.75 mm), (a_1, b_1) = (5 mm, 8.75 mm), (a_2, b_2) = (7 mm, 10.75 mm), t = 2.83 mm, L_h = 14 mm, L_v = 5.5 mm, R = 1 mm, D = 3 mm and H = 9 mm, it is observed that the impedance bandwidth does not change from 40%. However, if C_d is increased from 34 mm to 35 mm, the antenna loses its broadband properties. Therefore, C_d = 34 mm with the above mentioned antenna dimensions gives the best result of the impedance bandwidth of 40%. With these optimized dimensions, the two resonance frequencies of the antenna occur at f_1 = 3.8 GHz and f_2 = 5.0 GHz, as shown in Figure 3.77.

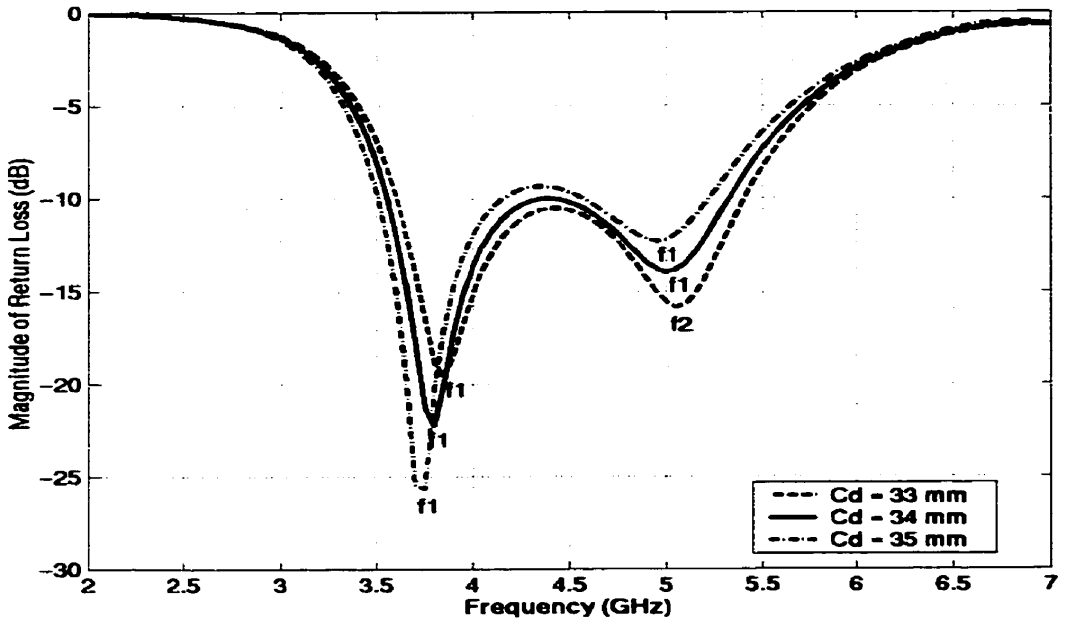

Figure 3.77: Return Loss of Antenna 4 for different values of C_d with antenna dimensions: $(x_c, y_c) = (0, 1.75)$, $(a_1, b_1) = (5, 8.75)$, $(a_2, b_2) = (7, 10.75)$, $t = 2.83$, $L_h = 14$, $L_v = 5.5$, $R = 1$, $D = 3$, $H = 9.0$. All dimensions in mm.

3.5.2 Radiation patterns and gain patterns

The results shown in Figure 3.77 show that the optimized dimensions of Antenna 4 give impedance bandwidth of 40%. The two resonance frequencies of this antenna with the optimized dimensions occur at f_1 = 3.8 GHz and f_2 = 5.0 GHz. Figure 3.78 shows the E and H plane radiation patterns computed by Ansoft Ensemble at f_1 = 3.8 GHz. According to these results, it can be seen that Antenna 4 also demonstrates broad radiation characteristics. The computed results of E_θ and E_ϕ in $\phi = 0$ plane and $\phi = 90$ plane at f_1 = 3.8 GHz are shown plotted in Figure 3.78. The crosspolarization level in $\phi =$ 0 plane at f_1 = 3.8 GHz is below −13 dB and it is negligible in $\phi = 90$ plane.

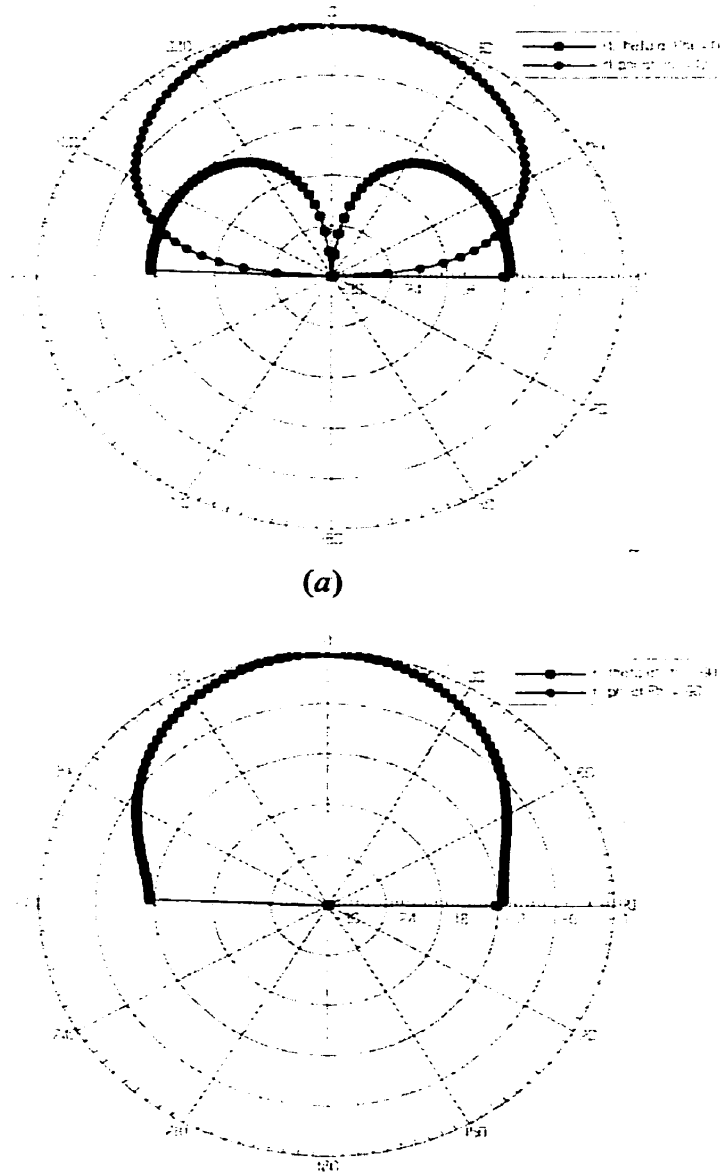

(*a*)

(*b*)

Figure 3.78: (a) Radiation patterns in ϕ *= 0 plane of Antenna 4 with optimized dimensions at* f_1 *= 3.8 GHz. (b) Radiation patterns in* ϕ *= 90 plane of Antenna 4 with optimized dimensions at* f_1 *= 3.8 GHz.*

Figure 3.79 shows the computed results of E_θ and E_ϕ in $\phi = 0$ plane and $\phi = 90$ plane at $f_2 = 5.0$ GHz. The crosspolarization level in $\phi = 0$ plane at $f_2 = 5.0$ GHz is slightly higher

than at f_1 = 3.8 GHz. The radiation pattern in $\phi = 90$ plane for f_2 = 5.0 GHz is different from f_1 = 3.8 GHz, it is more broader at f_1 = 3.8 GHz. Nonetheless, the crosspolarization in $\phi = 90$ plane for both f_1 and f_2 is extremely low.

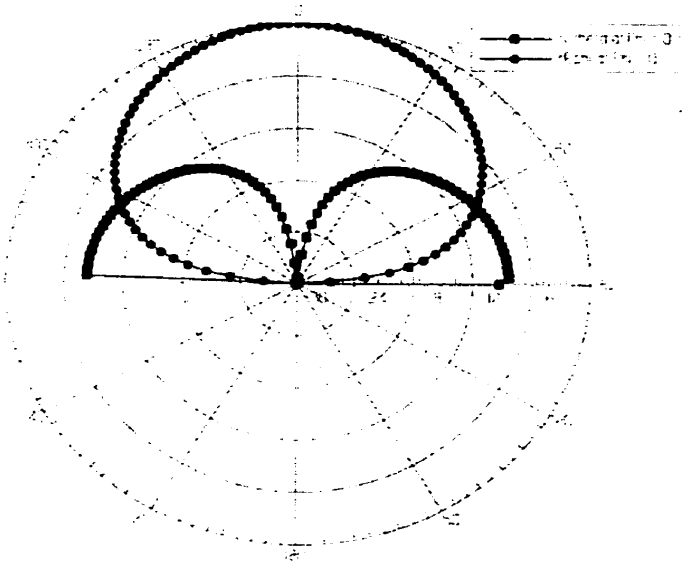

(*a*)

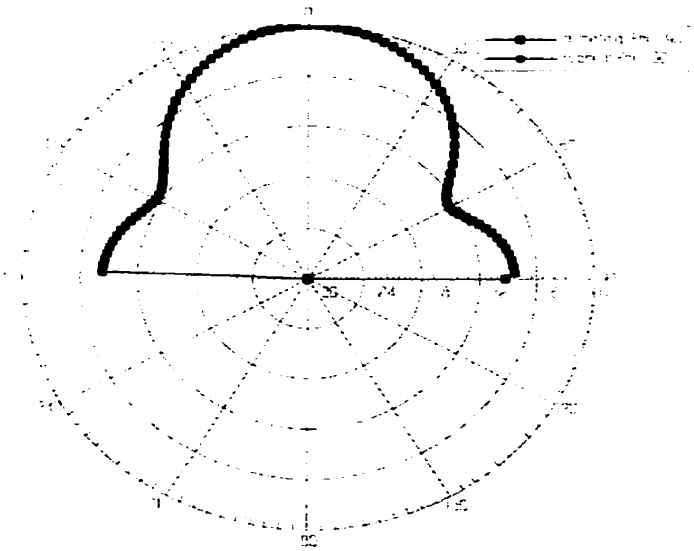

(*b*)

Figure 3.79: (a) Radiation patterns in $\phi = 0$ plane of Antenna 4 with optimized dimensions at f_2 = 5.0 GHz. (b) Radiation patterns in $\phi = 90$ plane of Antenna 4 with optimized dimensions at f_2 = 5.0 GHz.

Figure 3.80 shows the gain patterns of Antenna 4 at f_1 = 3.8 GHz in $\phi = 0$ plane and $\phi = 90$ plane. Similarly, the computed gain patterns of this antenna at f_2 = 5.0 GHz in $\phi = 0$ plane and $\phi = 90$ plane are plotted in Figure 3.81. By comparing the gain patterns of both f_1 = 3.8 GHz and f_2 = 5.0 GHz, it can be seen that both resonance frequencies have similar gain patterns in the $\phi = 0$ plane, while they are a bit different in the $\phi = 90$ plane. The polarization is the same for both resonance frequencies. The broadside gain of the antenna at f_1 = 3.8 GHz in $\phi = 0$ plane and $\phi = 90$ plane is 7.93 dBi and 8.52 dBi at f_2 = 5.0 GHz. Figure 3.80 and 3.81 show that the crosspolarization level is below −13 dB in $\phi = 0$ plane at f_1 = 3.8, but it is slightly higher at f_2 = 5.0 GHz in the same plane. In $\phi = 90$ plane, the crosspolarization level for both f_1 and f_2 is very low.

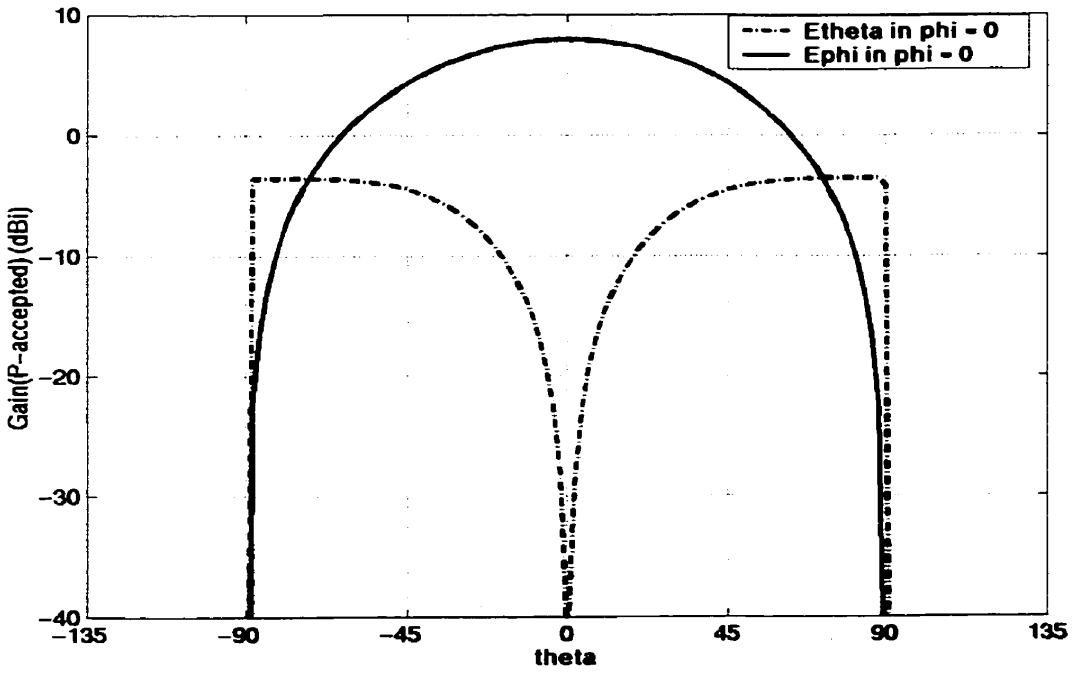

(*a*)

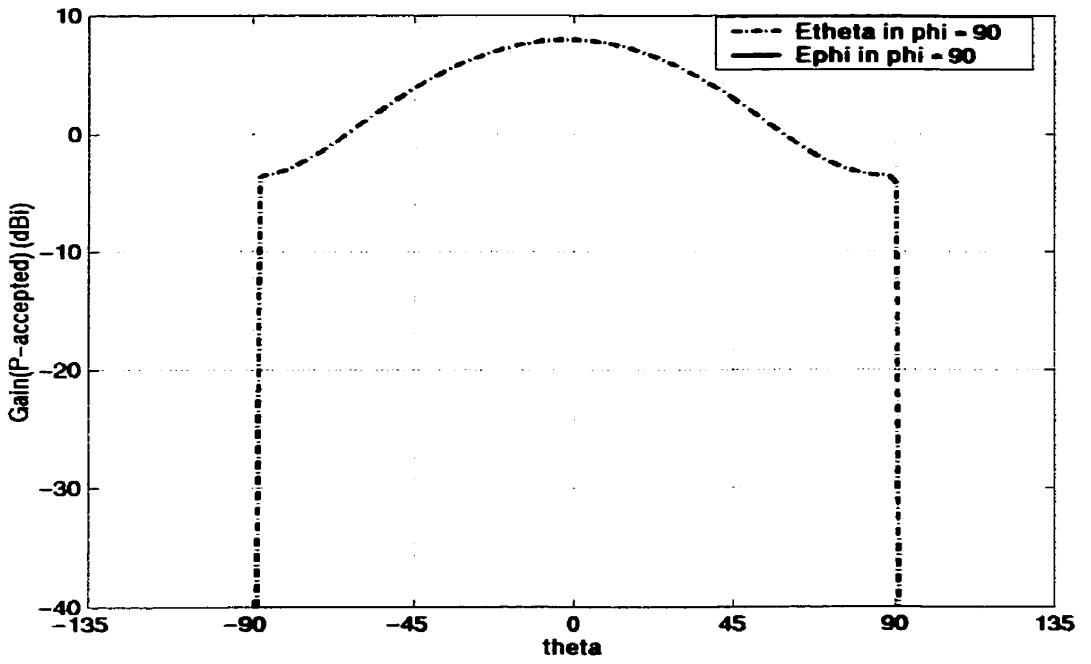

(*b*)

Figure 3.80: (a) Gain patterns in ϕ = 0 plane of Antenna 4 with optimized dimensions at f_1 = 3.8 GHz. (b) Gain patterns in ϕ = 90 plane of Antenna 4 with optimized dimensions at f_1 = 3.8 GHz.

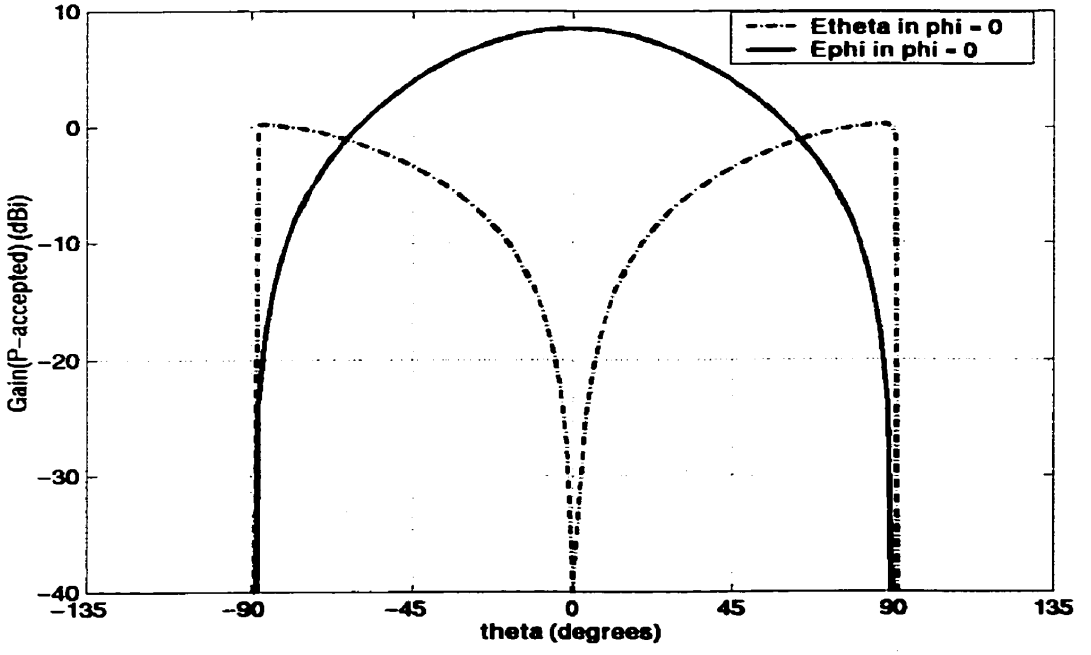

(*a*)

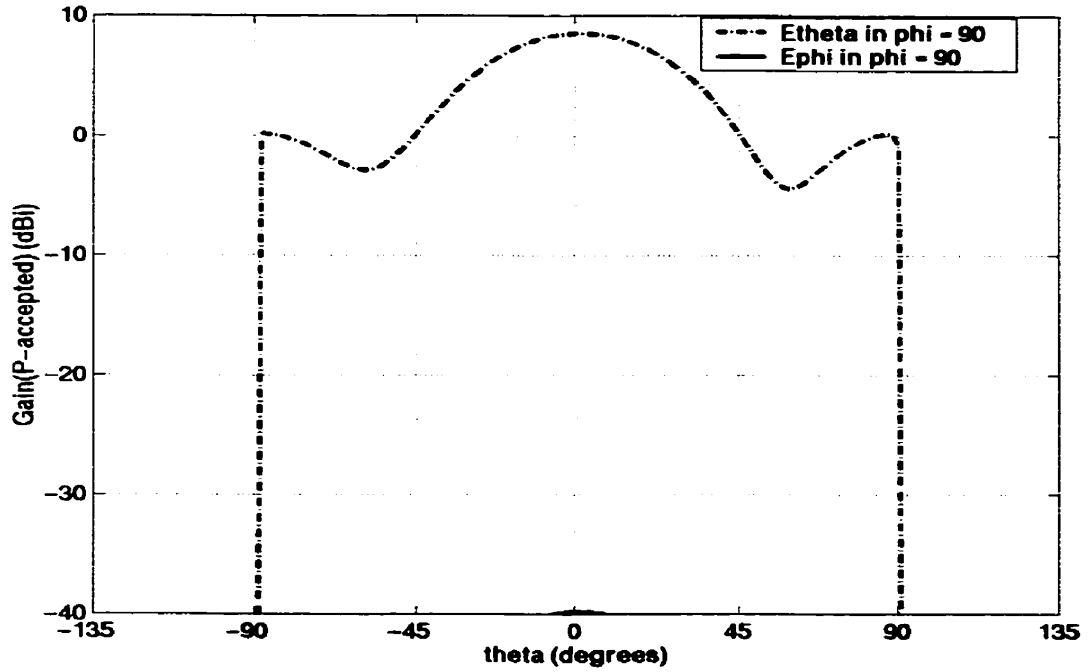

(*b*)

Figure 3.81: (a) Gain patterns in ϕ = 0 plane of Antenna 4 with optimized dimensions at f_2 = 5.0 GHz. (b) Gain patterns in ϕ = 90 plane of Antenna 4 with optimized dimensions at f_2 = 5.0 GHz.

3.5.3 Parametric study of Antenna 4

As it was done for the other broadband patch antennas, a parametric study of Antenna 4 is also presented. The effect of various antenna parameters on the impedance bandwidth is studied thoroughly. The dielectric constant of the foam substrate has been changed to ε_r = 1.03 to do the parametric study on the circular patch antenna with an arc slot and L–shaped probe. The following antenna dimensions are used to perform the parametric study: C_d = 34 mm, (x_c, y_c) = (0, 1.75 mm), (a_1, b_1) = (5 mm, 8.75 mm), (a_2, b_2) = (7 mm, 10.75 mm), t = 2.83 mm, L_h = 14 mm, L_v = 5.5 mm, R = 1 mm, D = 3 mm, H = 9.0 mm. Figure 3.82 illustrates the impact that different values of $2R$ (width of L–

shaped probe) have on the −10 dB bandwidth as the substrate height is varied. For substrates heights smaller than 8.5 mm, all three values of $2R$ give small bandwidth results. At $H = 9.0$ mm, the two resonances seem to merge together to form a wideband. It is clear from Figure 3.82 that the peak bandwidth of 40.0% is obtained with $2R = 2.0$ mm at $H = 9.0$ mm. The L−shaped probe width of $2R = 1.5$ mm also produces similar results to $2R = 2.0$ mm. As Figure 3.82 shows, $2R = 2.5$ mm does not give broad bandwidth at $H = 9.0$ mm. In general, the best bandwidth results are realized with $2R = 2.0$ mm for most substrate heights. Therefore, $2R = 2.0$ mm is considered to be the optimum value of L−shaped probe width.

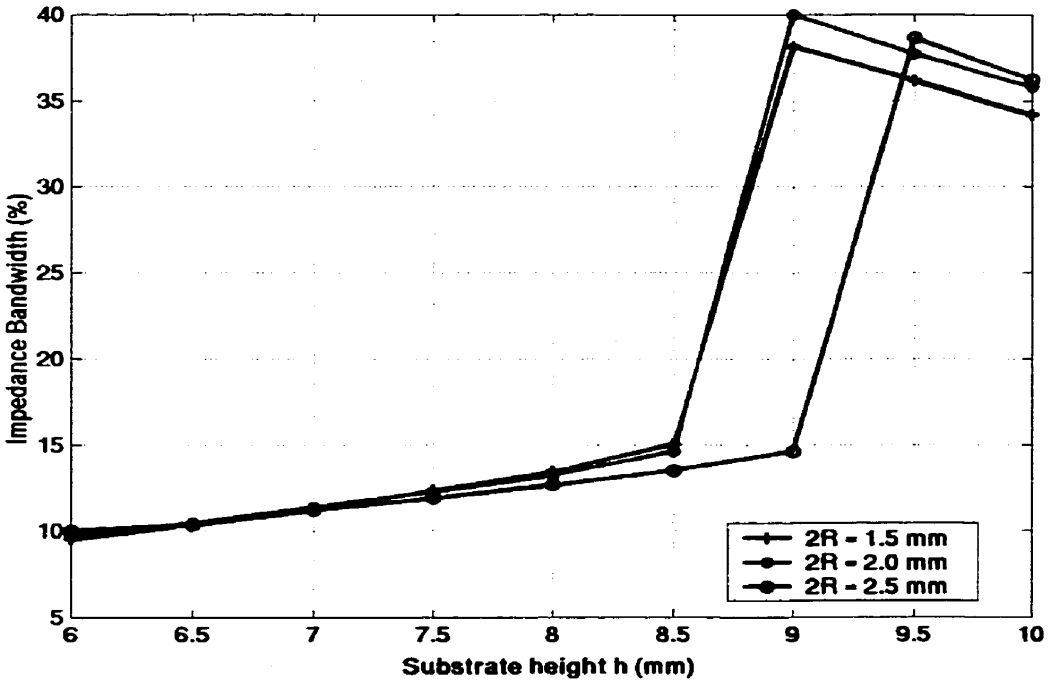

Figure 3.82: Effect of different values of 2R (width of L−shaped probe) on the impedance bandwidth with $C_d = 34$, $(x_c, y_c) = (0, 1.75)$, $(a_1, b_1) = (5, 8.75)$, $(a_2, b_2) = (7, 10.75)$, $t = 2.828$, $L_h = 14$, $L_v = 5.5$, $D = 3$, $H = 9$. All dimensions in mm.

Next, the effect of various horizontal lengths of the L–shaped probe on the antenna bandwidth is studied. The plot of impedance bandwidth vs. substrate height for three L_h (horizontal length of an L–shaped probe) values is shown in Figure 3.83. With L_h = 13 mm, the antenna does not attain its broadband characteristics. Again, the maximum bandwidth of 40% is achieved at H = 9.0 mm with L_h = 14 mm. Similar bandwidth results are obtained when L_h = 15 mm, with a slightly lower bandwidth value at H = 9.0 mm.

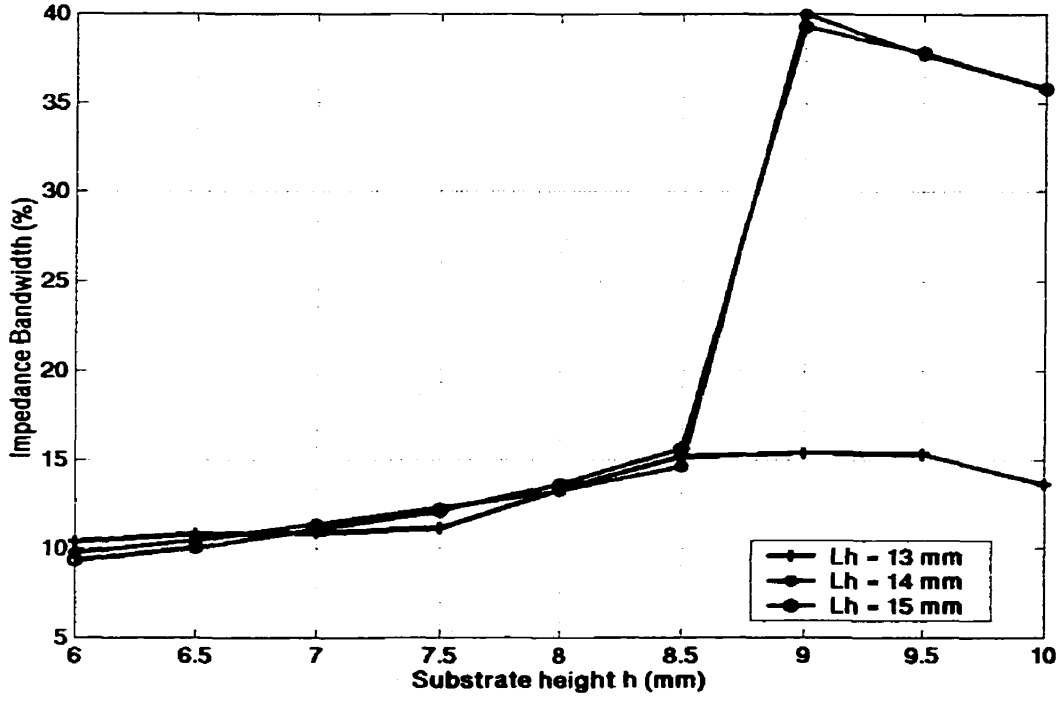

Figure 3.83: Effect of different values of L_h (horizontal length of L–shaped probe) on the impedance bandwidth with C_d = 34, (x_c, y_c) = (0, 1.75), (a_1, b_1) = (5, 8.75), (a_2, b_2) = (7, 10.75), t = 2.828, L_v = 5.5, $2R$ = 2.0, D = 3, H = 9. All dimensions in mm.

A similar parametric study is done with the vertical length of the L–shaped probe. The effectiveness of dissimilar lengths of L_v on the antenna bandwidth for different substrate

heights is shown plotted in Figure 3.84. Substrate heights from 6.0 mm to 8.5 mm, L_v = 5.5 mm and 5.75 mm, give very similar results. With L_v = 5.5 mm, the peak bandwidth of 40% takes place at H = 9.0 mm, whereas the bandwidth of 39.87% is obtained with L_v = 5.75 mm at H = 9.5 mm. From Figure 3.84 it can be seen that the L_v = 5.0 mm produces a little lower bandwidth results.

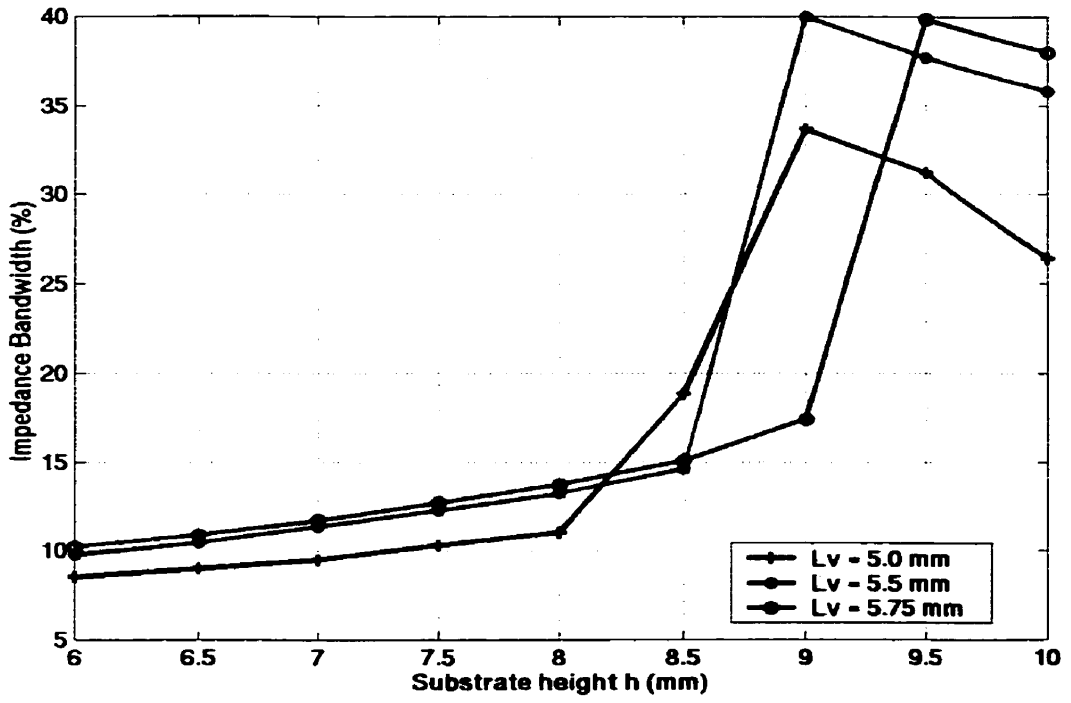

Figure 3.84: Effect of different values of L_v (vertical length of L–shaped probe) on the impedance bandwidth with C_d = 34, (x_c, y_c) = (0, 1.75), (a_1, b_1) = (5, 8.75), (a_2, b_2) = (7, 10.75), t = 2.828, L_h = 14.0, 2R = 2.0, D = 3, H = 9. All dimensions in mm.

The next antenna parameter that is studied is the L–shaped probe location, given by the variable D. According to the results in Figure 3.85, all three values of D give narrow bandwidths from H = 6.0 mm to 8.5 mm. The location of an L–shaped probe with D = 3.0 mm gives the best bandwidth result of 40.0% at H = 9.0 mm. The D = 2.0 mm also

produces good results, while the results obtained with D = 4.0 mm are not as good. Therefore, the optimum location of the L−shaped probe is realized with D = 3.0 mm.

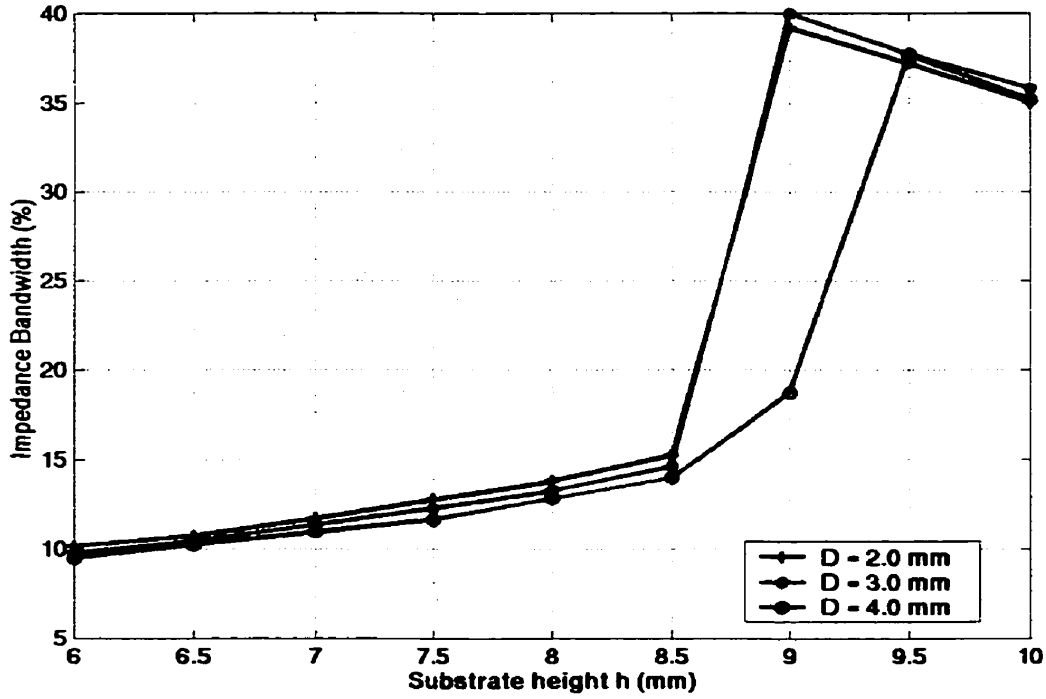

Figure 3.85: Effect of different values of D (location of L−shaped probe) on the impedance bandwidth with C_d = 34, (x_c, y_c) = (0, 1.75), (a_1, b_1) = (5, 8.75), (a_2, b_2) = (7, 10.75), t = 2.828, L_h = 14.0, L_v = 5.5, 2R = 2.0, H = 9. All dimensions in mm.

The location of the circular arc slot on the patch is also an important parameter, which is studied next. By changing its center from (x_c, y_c) = (0, 1.75 mm) to (x_c, y_c) = (0, 2.75 mm), similar bandwidth results are produced. Nonetheless, the peak bandwidth of 40.0% still occurs at H = 9.0 mm with (x_c, y_c) = (0, 1.75 mm). Clearly, Figure 3.86 shows that narrow bandwidths are achieved with (x_c, y_c) = (0, 0.75 mm) for most H values. Hence, the optimum slot location is with (x_c, y_c) = (0, 1.75 mm).

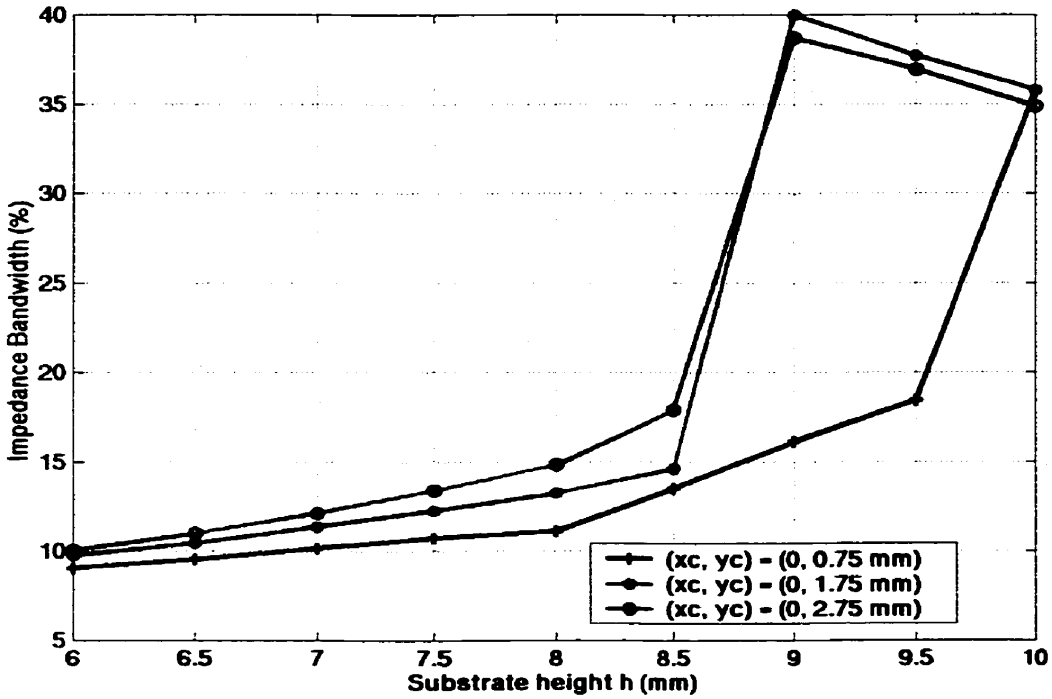

Figure 3.86: Effect of different values of (x_c, y_c) (location of arc slot) on the impedance bandwidth with C_d = 34, t = 2.828, L_h = 14.0, L_v = 5.5, D = 3.0, $2R$ = 2.0, H = 9. All dimensions in mm.

Similarly, the effect of different values of t (width of circular arc slot) on the antenna bandwidth is displayed in Figure 3.87. The plot in Figure 3.87 illustrates very clearly that all three values of t = 2.12 mm, 2.83 mm and 3.54 mm have a very similar impact on the impedance bandwidth for all substrate heights. Once again, the maximum bandwidth of 40% is achieved at H = 9.0 mm. This peak value of bandwidth is attained with t being equal to 2.83 mm. Consequently, the width of the circular arc slot is optimum when it is equal to 2.83 mm.

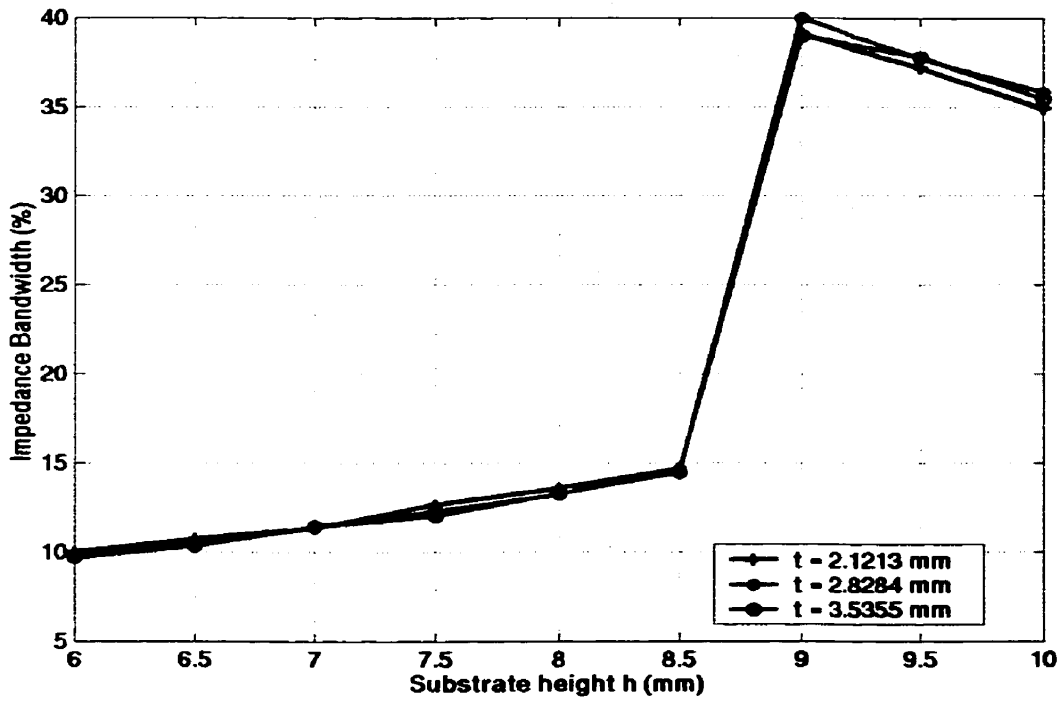

Figure 3.87: Effect of different values of t (width of circular arc slot) on the impedance bandwidth with C_d = 34, (x_c, y_c) = (0, 1.75), (a_1, b_1) = (5, 8.75), (a_2, b_2) = (7, 10.75), L_h = 14.0, L_v = 5.5, D = 3.0, 2R = 2.0, H = 9. All dimensions in mm.

3.6 Summary

This chapter discussed a conventional and three new designs of broadband microstrip patch antennas, which were

1. A rectangular microstrip patch antenna with a U–shaped slot.
2. A rectangular microstrip patch antenna with a circular arc slot.
3. A circular patch antenna with a circular arc slot.
4. A circular patch antenna with a circular arc slot and L–shaped probe.

The characteristics of these antennas were studied in terms of their resonance

frequencies and impedance bandwidth. The effect of various antenna parameters on the two resonance frequencies and bandwidths were studied extensively for each antenna. It was found that Antenna 1 and Antenna 2 have broadband characteristics. The impedance bandwidth of 30% were achievable with both of these antennas. However, Antenna 3 did not exhibit very broadband properties. The stub tuning matching technique was applied to increase the impedance bandwidth of this antenna, which increased the bandwidth from 10.28% to 23.17%. The stub tuning matching method was also implemented on the rectangular patch with a circular arc slot. The other broadband patch antenna that was studied greatly was Antenna 4. The impedance bandwidth of 40% was calculated with the optimized dimensions, which is very broad. The far field radiation patterns of these antennas had good crosspolarization levels. Approximate equations for the operating frequencies were derived by analyzing the surface current distribution on the patch for the Antenna 1 and Antenna 2. Their results were compared with Ansoft ENSEMBLE computations for different probe locations and found to be accurate within 3.63%.

Chapter 4

Dual band Microstrip Patch Antenna

4.1 Introduction

The microstrip patch antenna with a single U–shaped slot has broadband characteristic [12–22], in which two close resonant frequencies are combined to give a wideband operation. If the resonant frequencies are far apart, a dual–frequency operation can be achieved. Recently, several dual–frequency designs of single–feed slotted rectangular microstrip antennas have been reported [28–32]. The two operating frequencies of such dual–band slot–loaded rectangular patch antennas are of the similar polarization and broadside radiation patterns. In such dual–band designs, different frequency ratios for the two operating frequencies can be obtained. The frequency ratios are within 1.6–2.0 for the antennas [28, 29, 31], 1.43–1.6 for the antenna [30] and 1.12–1.27 for the antenna [32]. However, the –10 dB bandwidths of such dual–band antennas [28–32] are very narrow, in the range of 1–2% in each operating band. In this thesis, a new type of dual–band antenna has been designed, which has a frequency ratio of $f_2 / f_1 = 1.57$ and a bandwidth of 6.16% in the first band and 9.49% in the second band of operation. This makes the proposed dual–band antenna more suitable for dual frequency applications where a frequency ratio of 1.57 and wide bandwidths are required.

The new dual–band microstrip patch antenna consists of two asymmetric U–shaped slots. The results for the resonance frequencies, bandwidth and radiation patterns are discussed in this chapter. The resonance properties of this antenna are also studied.

4.2 Rectangular microstrip patch antenna with dual U slots

Figure 4.1 shows the geometry of the new dual–band microstrip patch antenna with two asymmetric U–shaped slots. Two U–shaped slots are cut on a rectangular microstrip patch of dimensions $L \times W$, which is separated from the ground plane with a foam substrate of height h and $\varepsilon_r = 1.0006$. The position of the inner and outer U slots on the rectangular patch are indicated by two parameters a_1 and b_1, and a_2 and b_2, respectively. The lengths of the horizontal arm and the vertical arms of the inner U slot are denoted by parameters W_{s1} and L_{s1}, respectively. The width of the inner U slot is indicated by the parameter t_1. Similarly, the parameters W_{s2} and L_{s2} identify the lengths of the horizontal arm and the vertical arms of the outer U slot, respectively. The parameter t_2 defines the width of the outer U slot. The rectangular microstrip patch is fed at a point (x_p, y_p) using a 50Ω coaxial probe with the inner diameter of 1.27 mm, as shown in Figure 4.1. The 50Ω coaxial probe is located slightly below the center of the patch along the y–direction. The variable F is used to define the distance between the probe location (x_p, y_p) and the top edge of the microstrip patch.

In this thesis, a parametric study of this new dual–band microstrip patch antenna is done, which is shown in the following section. The effect of various parameters on the impedance bandwidth of the antenna is shown.

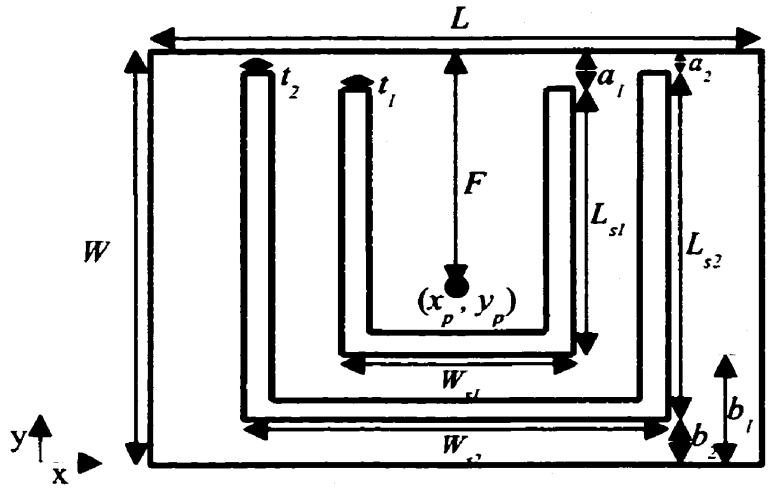

Figure 4.1: Geometry of the microstrip patch antenna with two asymmetric U slots.

4.2.1 Resonance frequencies and impedance bandwidth

To study the properties of the rectangular patch antenna with two U slots, the following dimensions are considered initially: L x W = 38.5 mm x 28 mm, L_{s1} x W_{s1} = 19.5 mm x 12 mm, L_{s2} x W_{s2} = 24 mm x 20 mm, a_1 = 1.5 mm, b_1 = 7.0 mm, t_1 = 2.1 mm, a_2 = 1.0 mm, b_2 = 3.0 mm, t_2 = 2.1 mm, F = 14 mm, foam substrate height h = 5.5 mm. Figure 4.2 shows that the two resonance frequencies of the antenna with the above mentioned dimensions occur at f_1 = 3.96 GHz and f_2 = 6.2 GHz. The computed −10 dB bandwidth of the antenna in the first band is 7.56% and 0% in the second band. Hence, the dimensions of the antenna must be optimized to realize dual band operation. The effect of various values of W_{s1} is also displayed in Figure 4.2. It can be seen from the results in Figure 4.2 that as W_{s1} is decreased f_1 increases, while f_2 stays the same. The two frequencies move close together with the decrease in W_{s1}. On the other hand, the −10 dB bandwidth decreases from 7.56% to 0% in the first band and it increases in the second

band from 0% to 6.45%. The value of W_{s1} = 12 mm gives the best result in Figure 4.2 for good matching and high bandwidth in the first band.

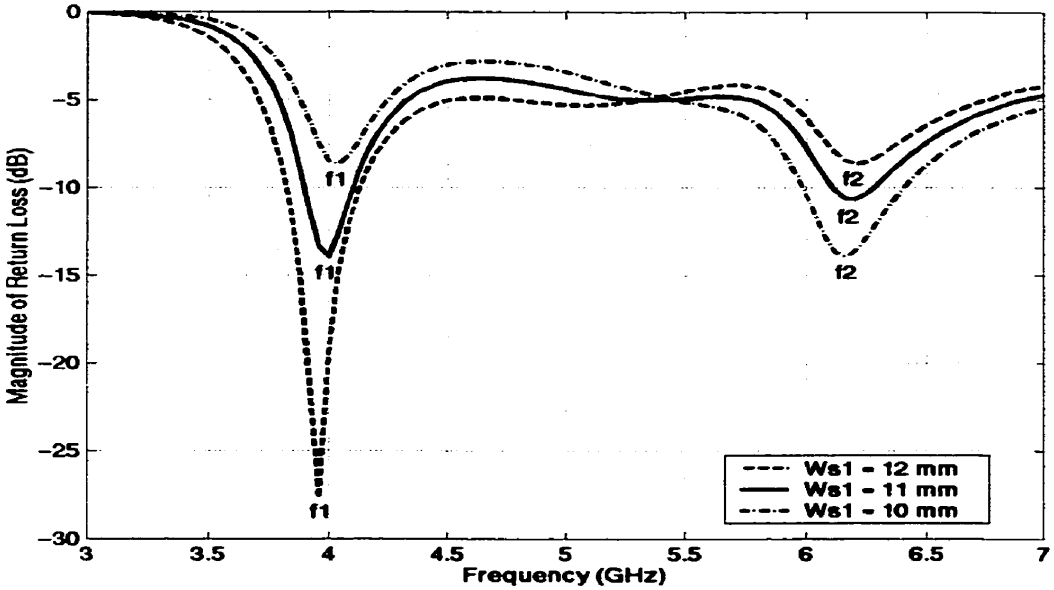

Figure 4.2: Return Loss of antenna in Figure 4.1 for different values of W_{s1} with antenna dimensions of L = 38.5, W = 28, L_{s1} = 19.5, L_{s2} = 24, W_{s2} = 20, a_1 = 1.5, b_1 = 7.0, t_1 = 2.1, a_2 = 1.0, b_2 = 3.0, t_2 = 2.1, F = 14, h = 5.5. All dimensions in mm.

Following that, the effect of various values of L_{s1} on the −10 dB bandwidth in the two bands is studied. The computed results of the return loss of the antenna with L_{s1} = 19.5 mm, 18.5 mm and 17.5 mm are shown in Figure 4.3. According to these results, as the length L_{s1} is decreased from 19.5 mm to 17.5 mm, the frequency f_1 does not change but the matching gets worse, while f_2 increases from 6.2 GHz to 6.24 GHz with better matching. By observing the −10 dB bandwidth in the two bands in Figure 4.3, it can be viewed that it decreases in the first band and seems to increase in the second band. Despite the fact that the bandwidth is increasing in the second band with the decrease in L_{s1}, the value of L_{s1} = 19.5 mm is chosen to be best value due to better matching in the first band.

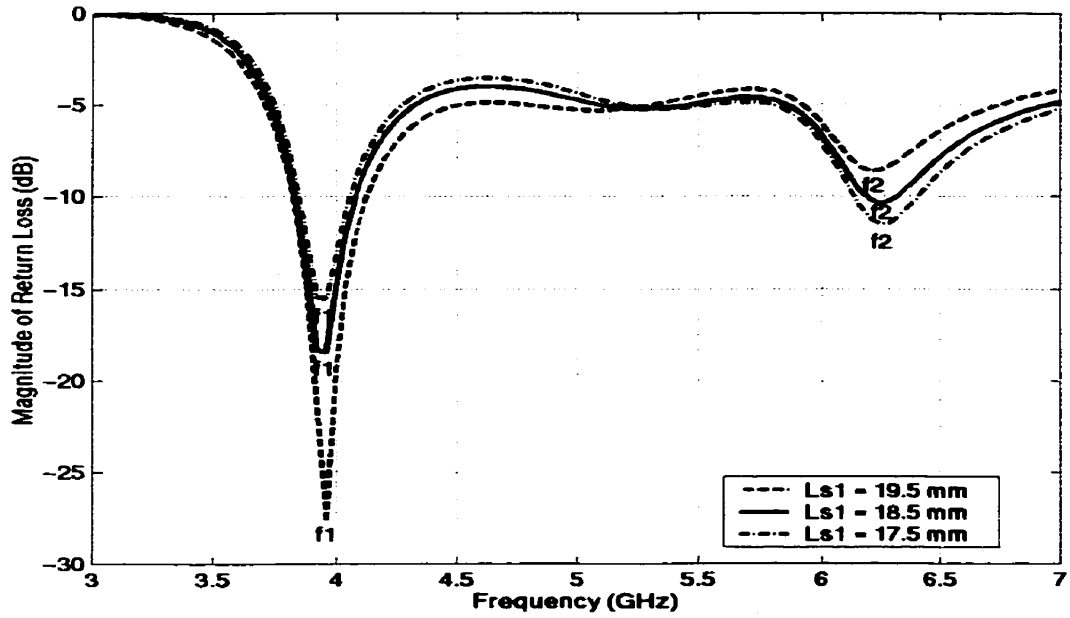

Figure 4.3: Return Loss of antenna in Figure 4.1 for different values of L_{s1} with antenna dimensions of L = 38.5, W = 28, W_{s1} = 12, L_{s2} = 24, W_{s2} = 20, a_1 = 1.5, b_1 = 7.0, t_1 = 2.1, a_2 = 1.0, b_2 = 3.0, t_2 = 2.1, F = 14, h = 5.5. All dimensions in mm.

It is observed that by lowering the inner and outer U slots so that the parameters a_1, b_1, a_2, b_2 change to a_1 = 2.5 mm, b_1 = 6.0 mm, a_2 = 2.0 mm, b_2 = 2.0 mm while keeping the rest of the antenna dimensions same as the initial dimensions, the frequency f_1 stays the same and the matching improves, however the frequency f_2 seems to disappear. Similarly, when the widths of the inner and outer U slots are changed to t = 2.0 mm with the rest of the antenna dimensions as the initial values, f_1 stays fixed and f_2 disappears. Therefore, the dual band operation of the antenna is not possible when these changes are made to the antenna dimensions. The various lengths of W_{s2} (width of the outer U slot) are also simulated with the Ansoft ENSEMBLE to examine the properties of the patch antenna with two U slots. The computed results of the return loss for various lengths of W_{s2} are shown in Figure 4.4. By inspecting the results in Figure 4.4, it is obvious that as W_{s2} is

increased from 20 mm to 24 mm while keeping everything else the same as the initial values, f_1 remains at 3.96 GHz with good matching and f_2 decreases from 6.2 GHz to 5.92 GHz with improved matching. The two resonance frequencies f_1 and f_2 move closer to each other as the width of the outer U slot is increased, hence the frequency ratio f_2 / f_1 can be controlled by varying W_{s2}.

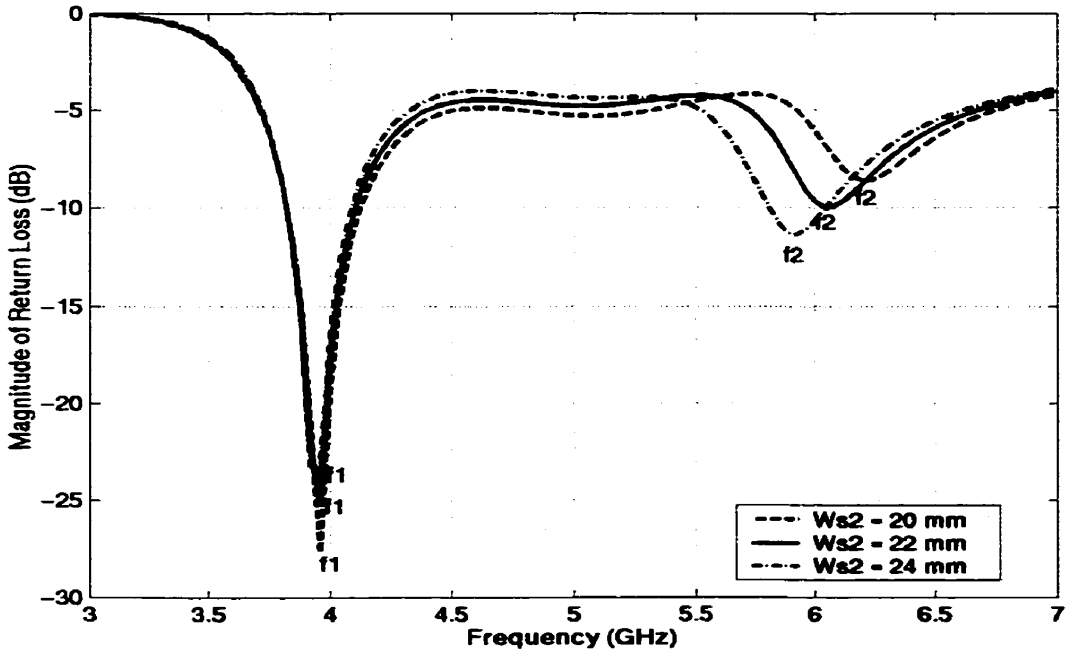

Figure 4.4: Return Loss of antenna in Figure 4.1 for different values of W_{s2} with antenna dimensions of L = 38.5, W = 28, L_{s1} = 19.5, W_{s1} = 12, L_{s2} = 24, a_1 = 1.5, b_1 = 7.0, t_1 = 2.1, a_2 = 1.0, b_2 = 3.0, t_2 = 2.1, F = 14, h = 5.5. All dimensions in mm.

Figure 4.4 shows that the −10 dB bandwidth in the first band decreases slightly but it improves in the second band of operation with W_{s2} = 24 mm. Since W_{s2} = 24 mm gives the highest value of the −10 dB bandwidth in the second band in Figure 4.4, it is chosen to be the best value of W_{s2}.

The other parameter that has a significant effect on the −10 dB bandwidths of the antenna in the two bands is the probe position. Figure 4.5 displays the simulation results

of the return loss of the antenna for three different probe locations. The antenna dimensions are shown in Figure 4.5. By lowering the coaxial probe position from (x_p, y_p) = (0, −1 mm) with F = 15 mm to (x_p, y_p) = (0, −2 mm) with F = 16 mm, f_1 decreases from 3.92 GHz to 3.88 GHz and f_2 increases from 6.0 GHz to 6.08 GHz. While −10 dB bandwidth in the first band reduces slightly from 6.65% to 6.16%, it rises from 8.64% to 9.49% in the second band.

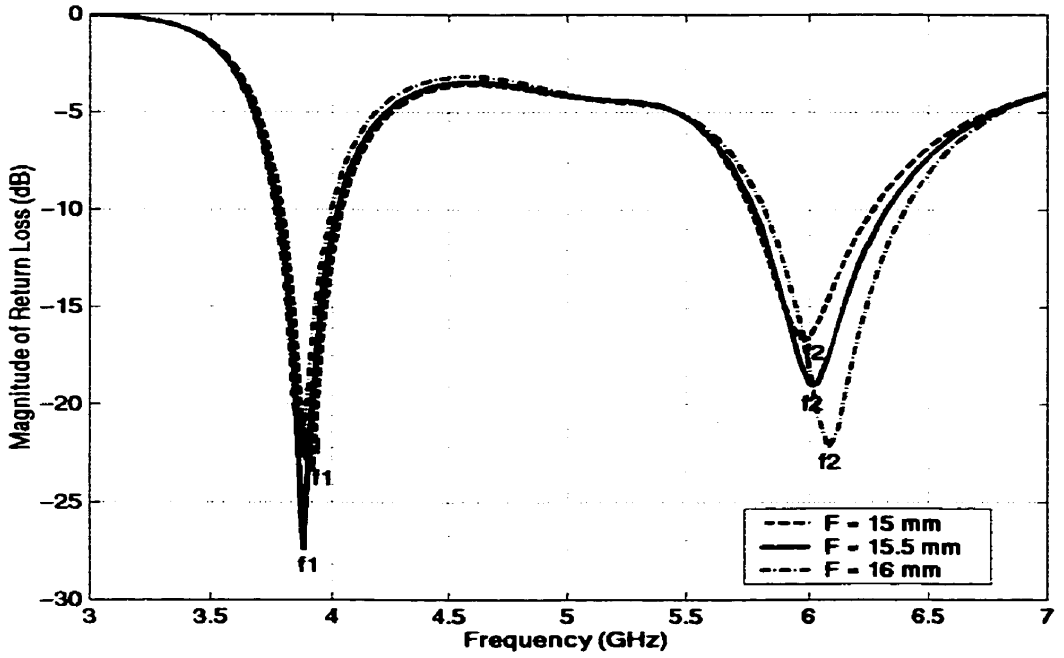

Figure 4.5: Return Loss of antenna in Figure 4.1 for different feed locations with L = 38.5, W = 28, L_{s1} = 19.5, W_{s1} = 12, L_{s2} = 24, W_{s2} = 24, a_1 = 1.5, b_1 = 7.0, t_1 = 2.1, a_2 = 1.0, b_2 = 3.0, t_2 = 2.1, Foam substrate height h = 5.5. All dimensions in mm.

The configuration with F = 16 mm and the antenna dimensions shown in Figure 4.5 gives the best results in terms of good matching and −10 dB bandwidth in the two bands. The optimum ratio of the two frequencies for this configuration is calculated to be f_2 / f_1 = 1.57. Since the bandwidth in the second band is improved with this configuration, a small reduction in the bandwidth of the first band is tolerable.

4.2.2 Radiation Patterns and Gain Patterns

The far field radiation patterns of the rectangular patch with two asymmetric U–shaped slots with the optimal dimensions are discussed in this section. According to the previous section, the two resonance frequencies of the optimized rectangular patch with dual U slots occur at f_1 = 3.88 GHz and f_2 = 6.08 GHz. Figure 4.6 shows the computed results of E_θ and E_ϕ in $\phi = 0$ plane and $\phi = 90$ plane at f_1 = 3.88 GHz. The crosspolarization level in $\phi = 0$ plane for f_1 = 3.88 GHz is lower than −13 dB and in $\phi = 90$ plane it is below −35 dB.

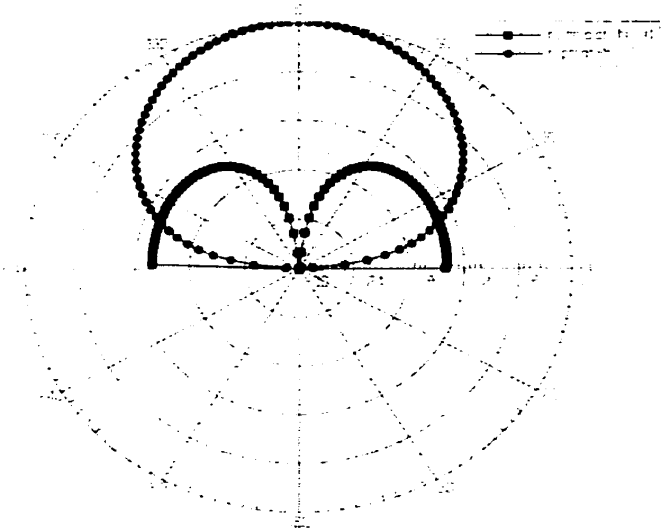

(*a*)

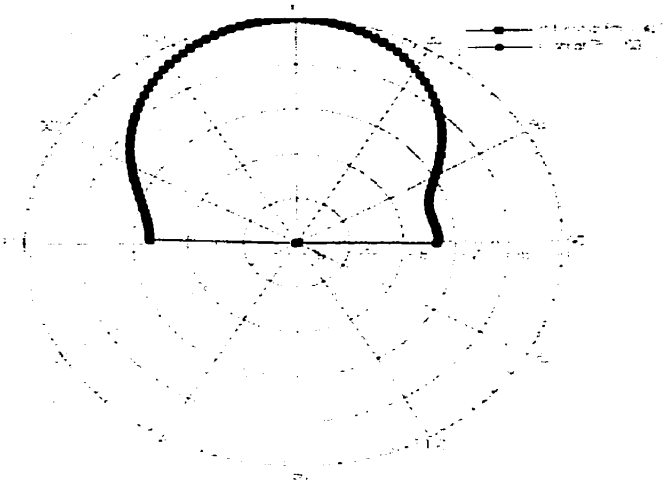

(*b*)

Figure 4.6:(a) Radiation patterns in $\phi = 0$ *plane of the antenna in Figure 4.1 with optimized dimensions at* $f_1 = 3.88$ *GHz. (b) Radiation patterns in* $\phi = 90$ *plane of the antenna in Figure 4.1 with optimized dimensions at* $f_1 = 3.88$ *GHz.*

The radiation patterns in $\phi = 0$ and $\phi = 90$ plane at $f_2 = 6.08$ GHz in Figure 4.7 show that the crosspolarization level in $\phi = 0$ plane is a lot higher compared to $f_1 = 3.88$ GHz. But in $\phi = 90$ plane the crosspolarization level for $f_2 = 6.08$ GHz is also below −35 dB, which is negligible.

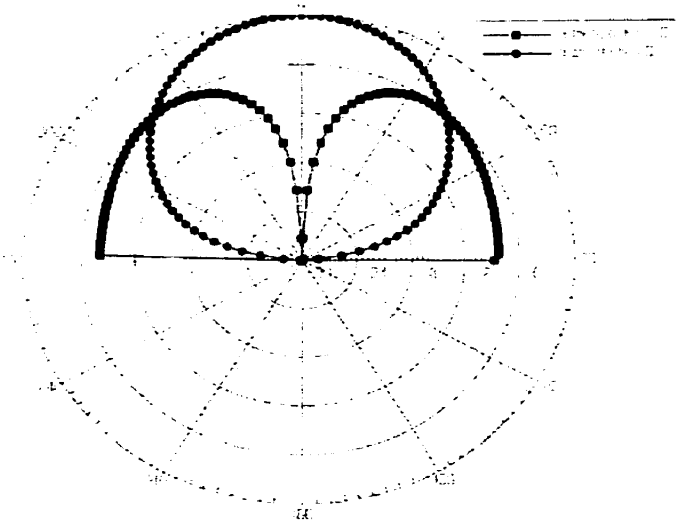

(*a*)

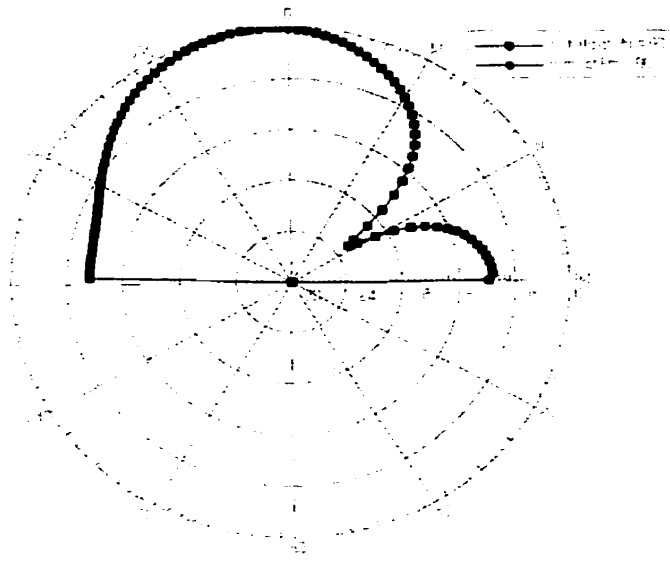

(*b*)

Figure 4.7:(a) Radiation patterns in $\phi = 0$ *plane of the antenna in Figure 4.1 with optimized dimensions at* $f_2 = 6.08$ *GHz. (b) Radiation patterns in* $\phi = 90$ *plane of the antenna in Figure 4.1 with optimized dimensions at* $f_2 = 6.08$ *GHz.*

In Figure 4.8, the gain patterns of the antenna at $f_1 = 3.88$ GHz in $\phi = 0$ plane and $\phi = 90$ plane are shown. Figure 4.9 displays the computed gain patterns in the two principle planes $\phi = 0$ and $\phi = 90$ at $f_2 = 6.08$ GHz. The results in Figure 4.8 and 4.9 demonstrate that the gain patterns are very similar at both f_1 and f_2. The polarization is also the same at both resonance frequencies. At the first resonance $f_1 = 3.88$ GHz, the broadside gain of the antenna is 9.09 dBi, while it is a bit lower at the second resonance $f_2 = 6.08$ GHz with the value of 7.7 dBi. While comparing the crosspolarization levels at two resonances f_1 and f_2 in $\phi = 0$ plane, Figure 4.8 and 4.9 show that f_2 has higher crosspolarization level than f_1. On the other hand, in $\phi = 90$ plane, the crosspolarization level for both f_1 and f_2 is very small.

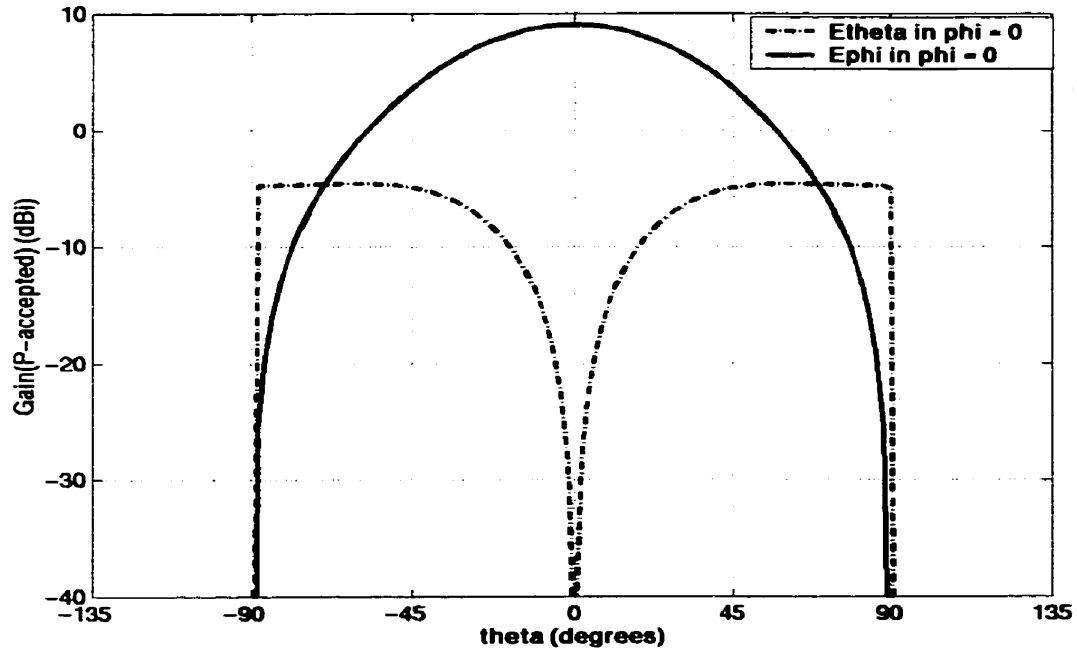

(*a*)

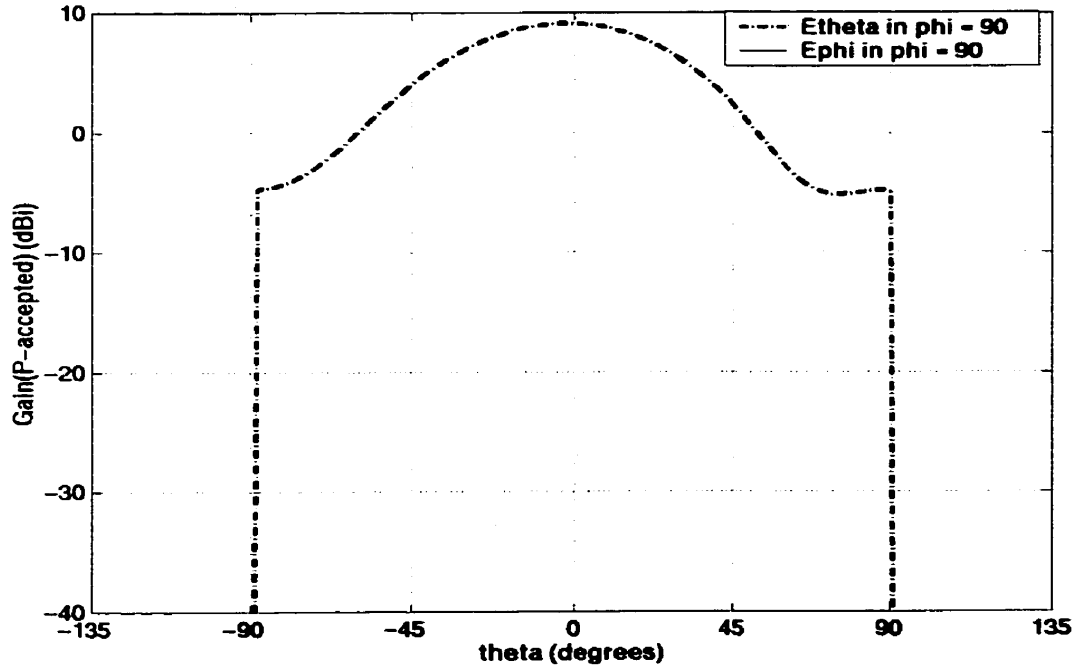

(*b*)

Figure 4.8: (a) Gain patterns in ϕ = 0 plane of the antenna in Figure 4.1 with optimized dimensions at f_l = 3.88 GHz. (b) Gain patterns in ϕ = 90 plane of the antenna in Figure 4.1 with optimized dimensions at f_l = 3.88 GHz.

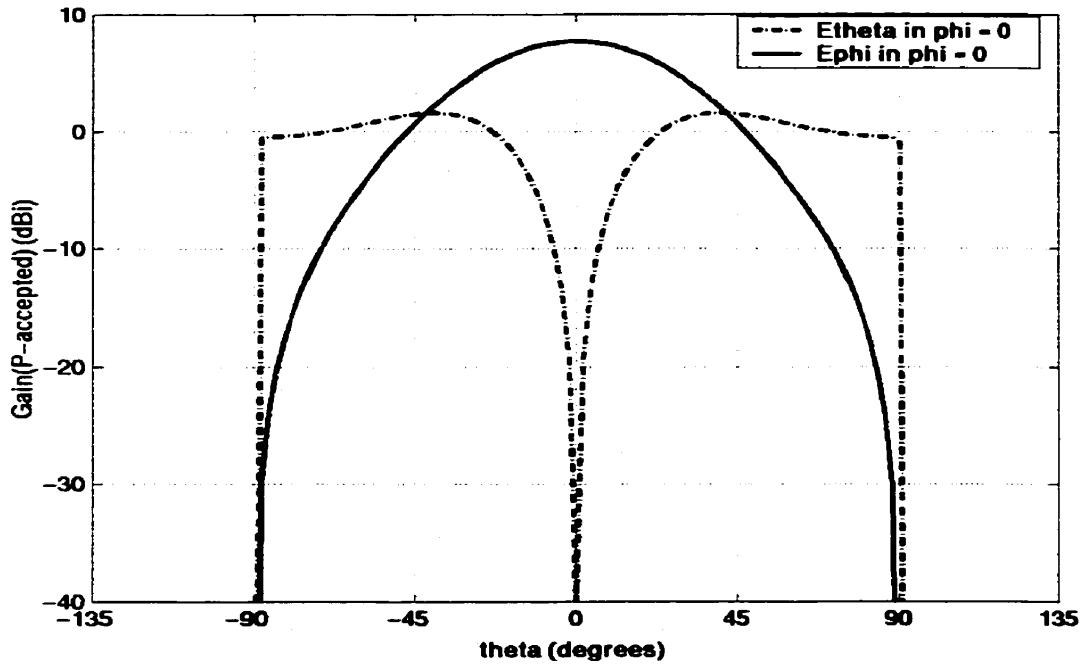

(*a*)

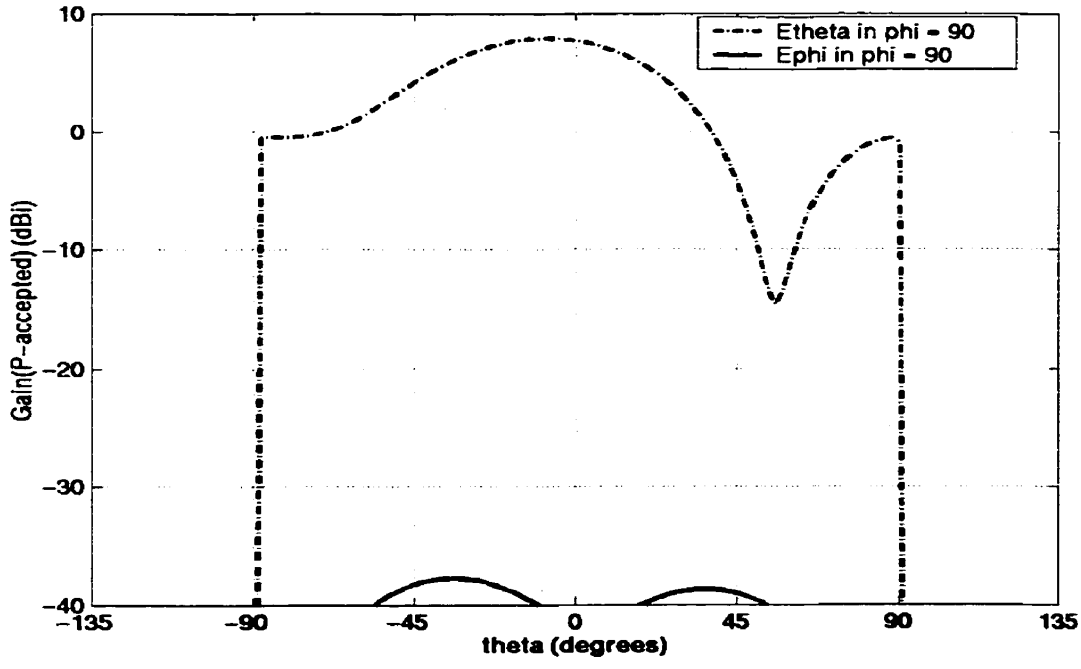

(*b*)

Figure 4.9:(a) Gain patterns in ϕ = 0 plane of the antenna in Figure 4.1 with optimized dimensions at f_2 = 6.08 GHz. (b) Gain patterns in ϕ = 90 plane of the antenna in Figure 4.1 with optimized dimensions at f_2 = 6.08 GHz.

4.2.3 Surface Current Components and current distribution analysis

The surface current distribution on the microstrip patch at $f_1 = 3.88$ GHz is displayed in Figure 4.10 (a). The two U slots have a strong affect on this current distribution of the TM_{01} mode. The surface currents originate behind the two U slots, are strong in between them and are forced to travel around them. The resonance for this mode occurs when the current path length is equal to one half wavelength. This resonant condition near f_1 is implemented on the average current–line path length consisting of two components A and B, as shown in Figure 4.10 (b). This current path length also accounts for the fringing fields on the patch. Note that the component A is equal to one half of the horizontal arm of the inner U slot and B is the average distance between the two non–radiating edges of the patch. The components A and B can be obtained from Figure 4.1, in terms of the antenna parameters as $A = W_{s1}/2$ and $B = (W + 2\Delta W) - (b_2 + \Delta W)/2$.

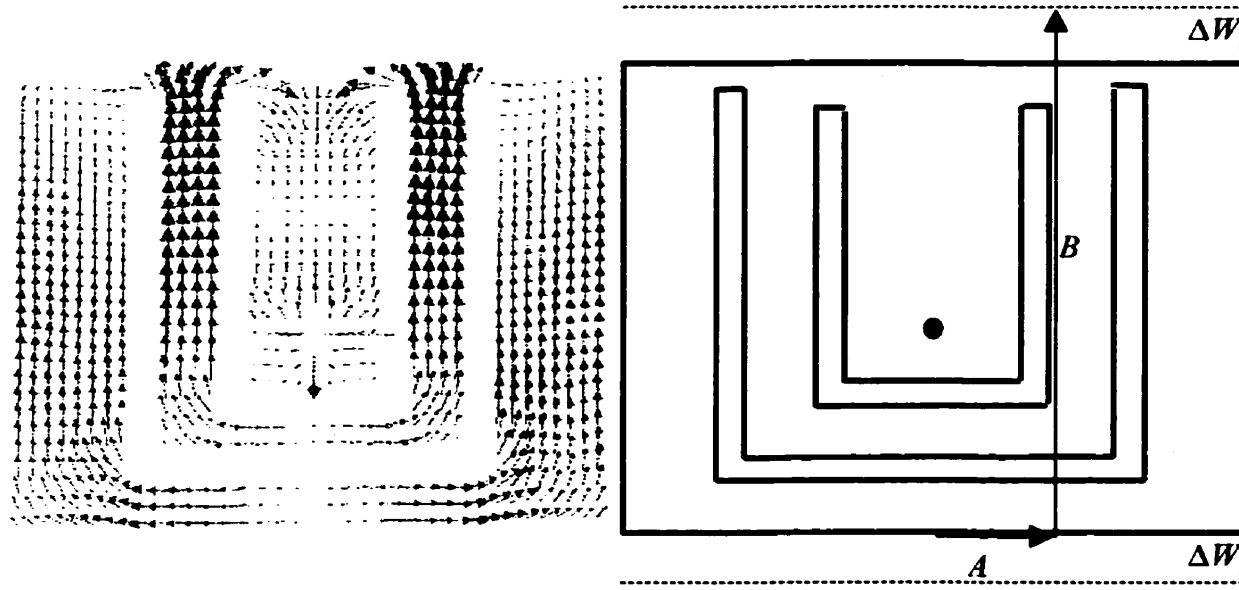

Figure 4.10: (a) Surface current distribution on microstrip patch at f_1 = 3.88 GHz. (b) Surface current–line path on the patch at f_1 = 3.88 GHz.

The sum of these components is set equal to one half wavelength as, $\lambda_1/2 = W_{s1}/2 + W + 3\Delta W/2 - b_2/2$. An approximate equation for f_1 can then be written as

$$f_1 = \frac{c}{(2(\frac{W_{s1}}{2} + W + \frac{3}{2}\Delta W - \frac{b_2}{2})\sqrt{\epsilon_e})}, \quad c = velocity\ of\ light \tag{4.1}$$

The resonant condition is very different at the second frequency $f_2 = 6.08$ GHz. The surface current distribution is strong behind the outer U slot and at the patch center, as shown in Figure 4.11 (a). However, it circulates around the arms of the inner U slot, and terminates at the probe location P. One current–line path in terms of the wavelength can be identified, as shown in Figure 4.11 (b), which also accounts for the fringing fields on the patch. This path is the average current–line path length, which consists of components M, N, O and Q. Note that the sum of these components appears to be equal to one wavelength. These components in terms of the antenna parameters can be written as $M = W_{s1}/2 + 1/2(W_{s2}/2 - t_2 - W_{s1}/2)$, $N = (L_{s1} + (b_1 - b_2 - t_2)/2 + (a_1 + \Delta W)/2)$, $O = 1/2(W_{s2}/2 - t_2 - W_{s1}/2) + t_1 + (W_{s1} - 2t_1)/4$ and $Q = F + \Delta W - (a_1 + \Delta W)/2$, where ΔW is given by equation 3.2. An approximate equation for f_2 can then be written as

$$f_2 = \frac{c}{((\frac{W_{s1}}{4} + \frac{W_{s2}}{2} + L_{s1} + F + \frac{b_1}{2} - \frac{b_2}{2} + \frac{t_1}{2} - \frac{3t_2}{2} + \Delta W)\sqrt{\epsilon_e})} \tag{4.2}$$

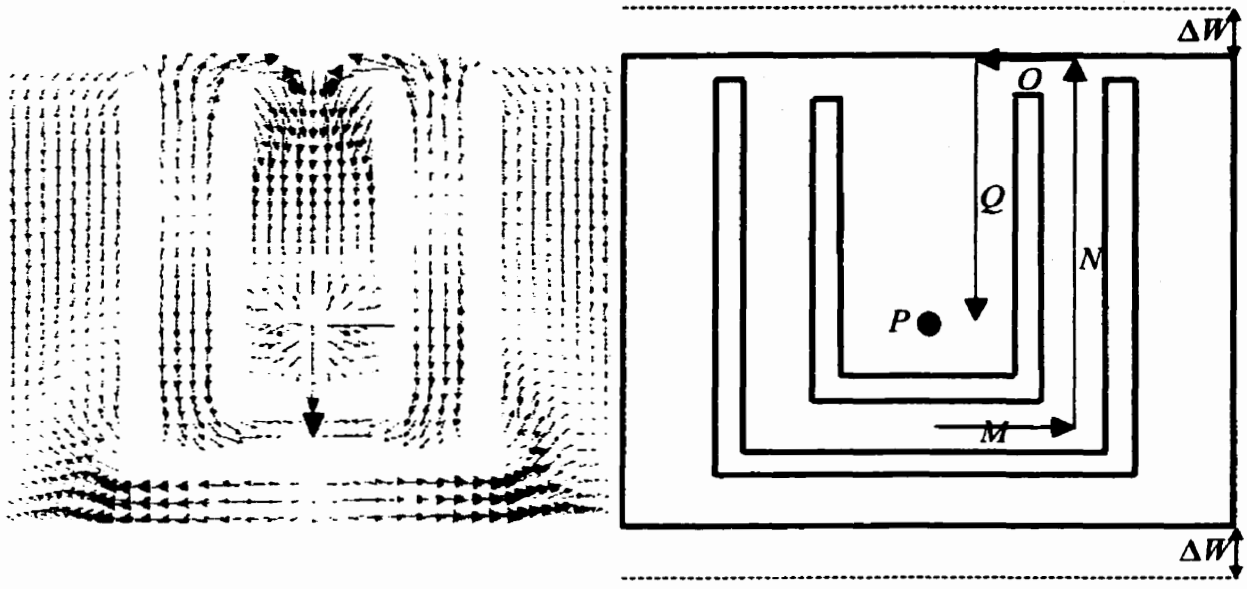

(*a*) (*b*)

Figure 4.11:(a) Surface current distribution on microstrip patch at f_1 = 6.08 GHz. (b) Surface current−line path on the patch at f_1 = 6.08 GHz.

Using equations 4.1 and 4.2, the calculated resonance frequencies of the antenna shown in Figure 4.1 are compared with the simulated resonance frequencies shown in Figure 4.2 to Figure 4.5. Table 4.1 shows the calculated results of the two resonance frequencies utilizing equations 4.1 and 4.2, together with the computed results of the software Ansoft ENSEMBLE for the different values of W_{s1} in Figure 4.2. According to the simulated results, the frequency f_1 increases as W_{s1} is decreased, which is in agreement with the computed results of equations 4.1 and 4.2. However, a small discrepancy can be observed for the results obtained for the frequency f_2 in Table 4.1. Even though, the results for the frequency f_2 in Table 4.1 demonstrate a dissimilarity, the results obtained using equations 4.1 and 4.2 are still accurate around 5%. In a similar manner, Table 4.2 compares the computed results of equations 4.1−4.2 with the simulated results from

Ansoft ENSEMBLE for the values of L_{s1} shown in Figure 4.3. The simulated and calculated values of f_1 do not change as L_{s1} is varied and the frequency f_2 increases. However, the error between the simulated and calculated values for the frequency f_2 is slightly higher.

Table 4.1: Comparison of dual U–slot microstrip patch resonance frequencies computed by ENSEMBLE software and Equations (4.1) and (4.2) for values of W_{s1} in Figure 4.2.

W_{s1} (mm)	Computed using ENSEMBLE		Calculated by Equations (4.1) and (4.2)		Error between computed and calculated values	
	f_1 (GHz)	f_2 (GHz)	f_1 (GHz)	f_2 (GHz)	Δf_1 (%)	Δf_2 (%)
12	3.96	6.2	3.9	5.96	1.52%	3.87%
11	4	6.2	3.95	5.99	1.25%	3.39%
10	4.04	6.2	4	6.02	0.99%	2.90%

Table 4.2: Comparison of dual U–slot microstrip patch resonance frequencies computed by ENSEMBLE software and Equations (4.1) and (4.2) for values of L_{s1} in Figure 4.3.

L_{s1} (mm)	Computed using ENSEMBLE		Calculated by Equations (4.1) and (4.2)		Error between computed and calculated values	
	f_1 (GHz)	f_2 (GHz)	f_1 (GHz)	f_2 (GHz)	Δf_1 (%)	Δf_2 (%)
19.5	3.96	6.2	3.9	5.96	1.52%	3.87%
18.5	3.96	6.24	3.9	6.08	1.52%	2.56%
17.5	3.96	6.24	3.9	6.2	1.52%	0.64%

Likewise, the calculated results of the resonance frequencies using equations 4.1 and

4.2 are compared with the simulated results for the different cases shown in Figure 4.4 and Figure 4.5. They are shown in Table 4.3 and 4.4, respectively.

Table 4.3: Comparison of dual U–slot microstrip patch resonance frequencies computed by ENSEMBLE software and Equations (4.1) and (4.2) for values of W_{s2} in Figure 4.4.

W_{s2} (mm)	Computed using ENSEMBLE		Calculated by Equations (4.1) and (4.2)		Error between computed and calculated values	
	f_1 (GHz)	f_2 (GHz)	f_1 (GHz)	f_2 (GHz)	Δf_1 (%)	Δf_2 (%)
20	3.96	6.2	3.9	5.96	1.52%	3.87%
22	3.96	6.04	3.9	5.84	1.52%	3.31%
24	3.96	5.92	3.9	5.73	1.52%	3.21%

Table 4.4: Comparison of dual U–slot microstrip patch resonance frequencies computed by ENSEMBLE software and Equations (4.1) and (4.2) for values of F in Figure 4.5.

F (mm)	Computed using ENSEMBLE		Calculated by Equations (4.1) and (4.2)		Error between computed and calculated values	
	f_1 (GHz)	f_2 (GHz)	f_1 (GHz)	f_2 (GHz)	Δf_1 (%)	Δf_2 (%)
15	3.92	6	3.9	5.62	0.51%	6.33%
15.5	3.88	6	3.9	5.57	0.52%	7.17%
16	3.88	6.08	3.9	5.52	0.52%	9.21%

By observing the results shown in Table 4.3, it is obvious that the simulated results of the resonance frequencies match well with the calculated results. According to the simulated results shown in Table 4.3, the various values of W_{s2} do not have any effect on

the first resonance f_1 and the similar observation is made for the calculated results. As W_{s2} is increased the values of f_2 decrease for the both cases of simulation and calculation. The errors between the simulated and calculated results are within 4% for both f_1 and f_2, as shown in Table 4.3. Table 4.4 shows that the calculated values of f_1 using equations 4.1 and 4.2 are very close to the simulated values for different probe positions. However, a small discrepancy can be seen between the computed and calculated values of f_2, which could be caused by the inductance of the probe. Small percentage errors shown in Table 4.1 to Table 4.4 justify the accuracy of the selected equations and the chosen resonant length of currents on the microstrip patch.

4.3 Summary

In this chapter, dual band operation of a microstrip patch antenna with two asymmetric U–shaped slots was studied. The characteristics of the antenna in terms of resonance frequencies and impedance bandwidth were examined. The effect of various antenna parameters on the two resonance frequencies and −10 dB bandwidth were studied extensively. The optimum ratio of the two frequencies is found to be $f_2 / f_1 = 1.57$. The far field radiation patterns for the two frequencies showed similar patterns and same polarization with good crosspolarization levels. The broadside gain of 9.09 dBi can be achieved at $f_1 = 3.88$ GHz, while the gain value was shown to be a little lower at $f_2 = 6.08$ GHz. Two equations for the operating frequencies were derived by analyzing the surface current distribution on the patch. Their results were compared with Ansoft ENSEMBLE computations and found to be fairly accurate.

Chapter 5

Antenna Fabrication Results

5.1 Introduction

In this chapter the simulation results of Antenna 1 and Antenna 2 are compared with their experimental results obtained in the Antenna Laboratory at the University of Manitoba. A foam substrate material with $\varepsilon_r = 1.03$ and height of $h = 5.91$ mm was available to build these two antennas, which is different from the dimensions discussed in Chapter 3. The size of the ground plane was taken to be 20 x 20 cm, which was large enough for the patch size. For excitation, the feed points were accurately marked and drilled through the structure.

Next the fabricated antennas were tested for the S parameters using the network analyzer and the far–field radiation patterns using the equipment in the Far Field Anechoic Chamber in the Antenna Laboratory. The experimental results for the S parameters and the far field radiation patterns of the fabricated antennas are discussed in the following sections. They are compared with their simulation results. It is found that a good agreement is achieved between them.

5.2 Results of Antenna 1

For the fabrication purpose, the following dimensions of Antenna 1 are used: $L = 40$ mm, $W = 26$ mm, $L_s = 19.5$ mm, $W_s = 12$ mm, $a = 3.7$ mm, $b = 2.8$ mm, $t = 2.1$ mm, $F =$

15 mm, a foam substrate material with ε_r = 1.03 and h = 5.91 mm. The experimental results for the return loss of this antenna with the above mentioned dimensions are shown in Figure 5.1.

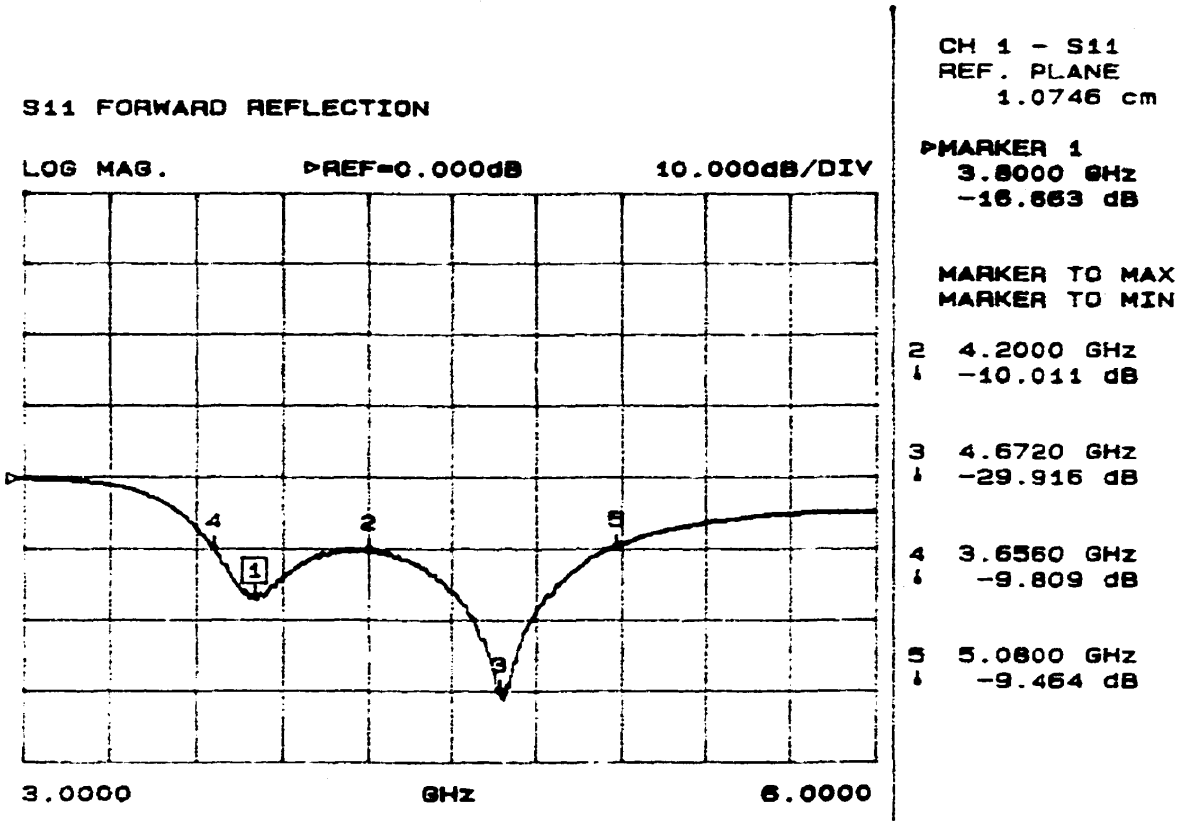

Figure 5.1: Experimental results for the Return Loss of Antenna 1 with dimensions L = 40, W = 26, L_s = 19.5, W_s = 12, a = 3.7, b = 2.8, t = 2.1, F = 15 and h = 5.91. All dimensions in mm.

Figure 5.1 shows that the first resonance occurs at f_1 = 3.8 GHz and the second resonance at f_2 = 4.67 GHz. According to the experimental results in Figure 5.1, the −10 dB bandwidth of this antenna is 32.6%. The simulation results for the return loss of Antenna 1 with the above mentioned dimensions are displayed in Figure 5.2. Figure 5.2 shows that the first resonance appears at f_1 = 4.04 GHz, while the second resonance at f_2 =

4.92 GHz, which are higher than the experimental values of f_1 = 3.8 GHz and f_2 = 4.672 GHz. This change in the resonance frequencies could be due to the change in the dielectric constant, since a foam substrate material is glued on the ground plane using a commercial glue. The −10 dB bandwidth of the antenna obtained from the simulation results is calculated to be 32.0%, which is very close to the experimental value of 32.6%.

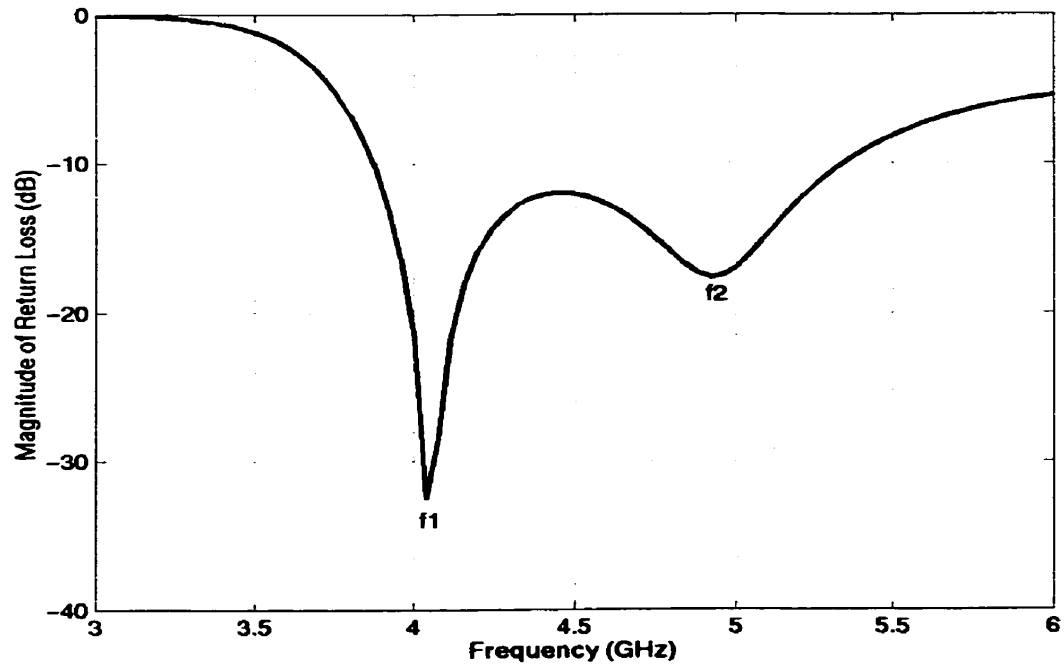

Figure 5.2: Simulation results for the Return Loss of Antenna 1 with dimensions L = 40, W = 26, L_s = 19.5, W_s = 12, a = 3.7, b = 2.8, t = 2.1, F = 15 and h = 5.91. All dimensions in mm.

The smith chart plot of Antenna 1 obtained from the experimental results is shown in Figure 5.3. Figure 5.3 shows that the loop on the smith chart is situated in the center, which demonstrates the broad bandwidth characteristics of this antenna.

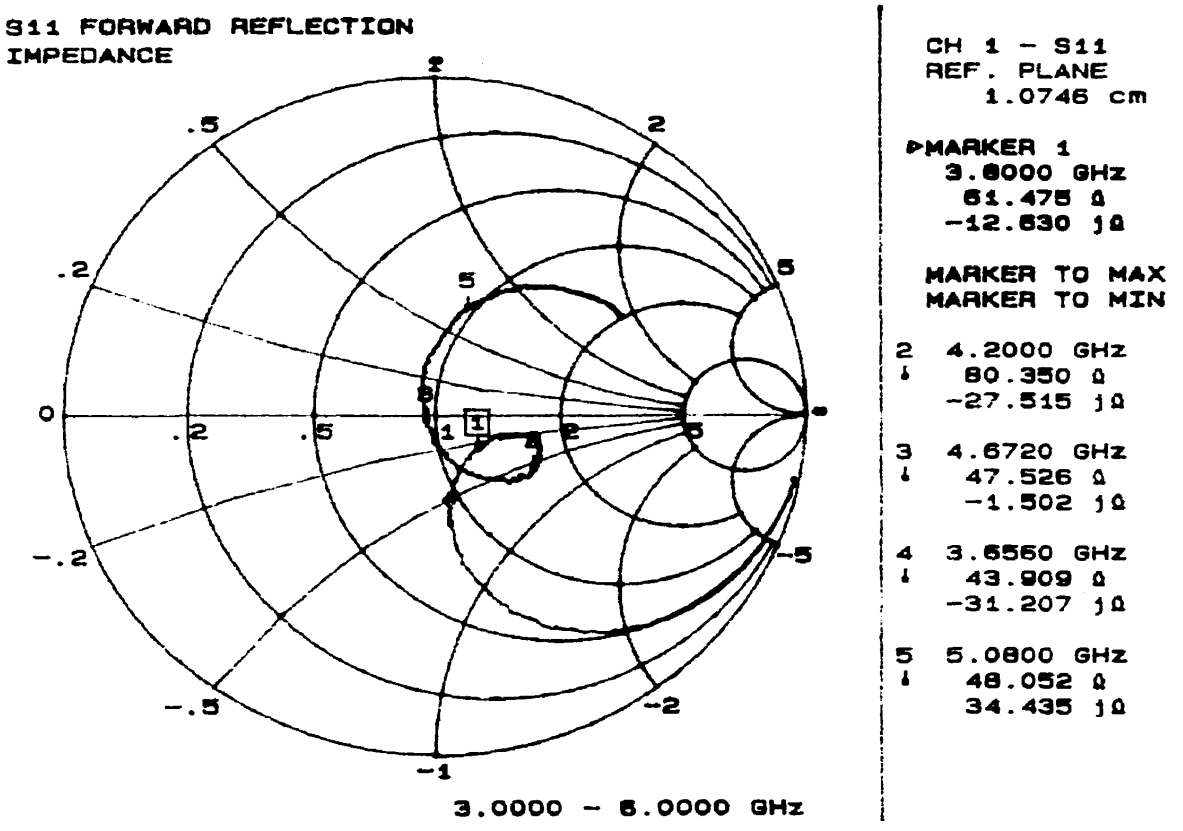

Figure 5.3: Experimental results for the Smith Chart plot of Antenna 1 with dimensions L = 40, W = 26, L_s = 19.5, W_s = 12, a = 3.7, b = 2.8, t = 2.1, F = 15 and h = 5.91. All dimensions in mm.

The smith chart plot of the single U–slot microstrip antenna obtained from the simulation is shown in Figure 5.4. By comparing the plots in Figure 5.3 and Figure 5.4, it should be noted that experimental results of the smith chart are similar to the simulation results. The results from Figure 5.1 to Figure 5.4 demonstrate that a good agreement is achieved between the experimental results and simulation results for the return loss and the smith chart plot of Antenna 1.

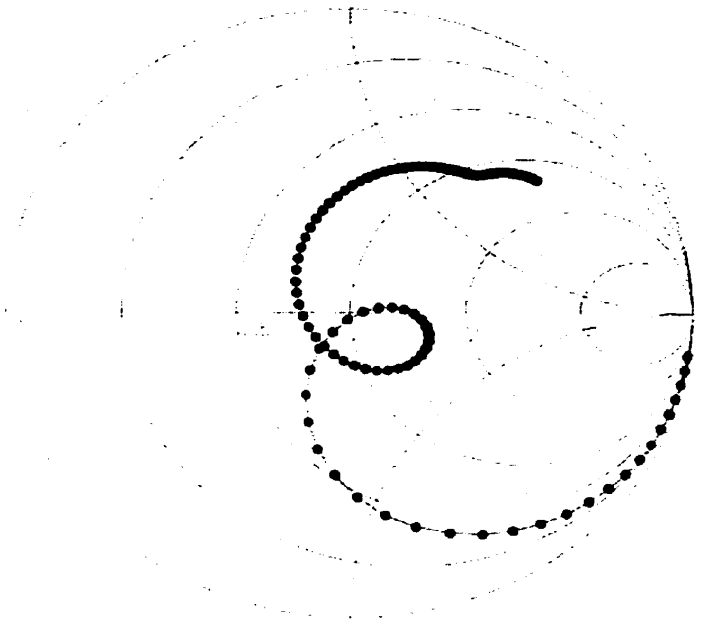

Figure 5.4: Simulation results for the Smith Chart plot of Antenna 1 with dimensions L = 40, W = 26, L_s = 19.5, W_s = 12, a = 3.7, b = 2.8, t = 2.1, F = 15 and h = 5.91. All dimensions in mm.

Next the gain patterns results of the fabricated antenna obtained from the Anechoic Chamber in the Antenna Laboratory are discussed. As shown in Figure 5.1, the experimental value of the first resonance frequency is f_1 = 3.8 GHz and the second resonance occurs at f_2 = 4.672 GHz. Figure 5.5 shows the far–field radiation patterns in the rectangular coordinates in the ϕ = 0 plane and ϕ = 90 plane at f_1 = 3.8 GHz. For comparison, the simulation results of the gain patterns at f_1 = 3.8 GHz in the ϕ = 0 plane and ϕ = 90 plane are shown plotted in Figure 5.6. The gain patterns in Figure 5.5 exhibit that the crosspolarization level in ϕ = 90 plane is very small, while it is higher in ϕ = 0 plane.

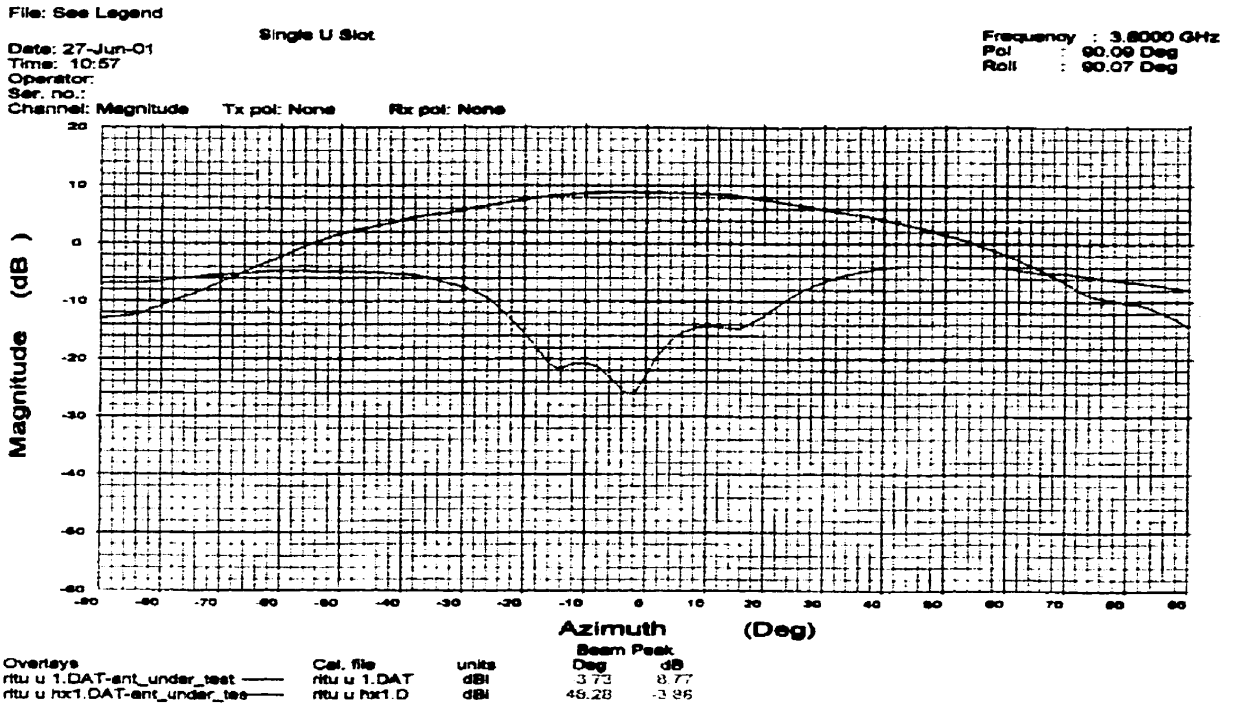

(*a*)

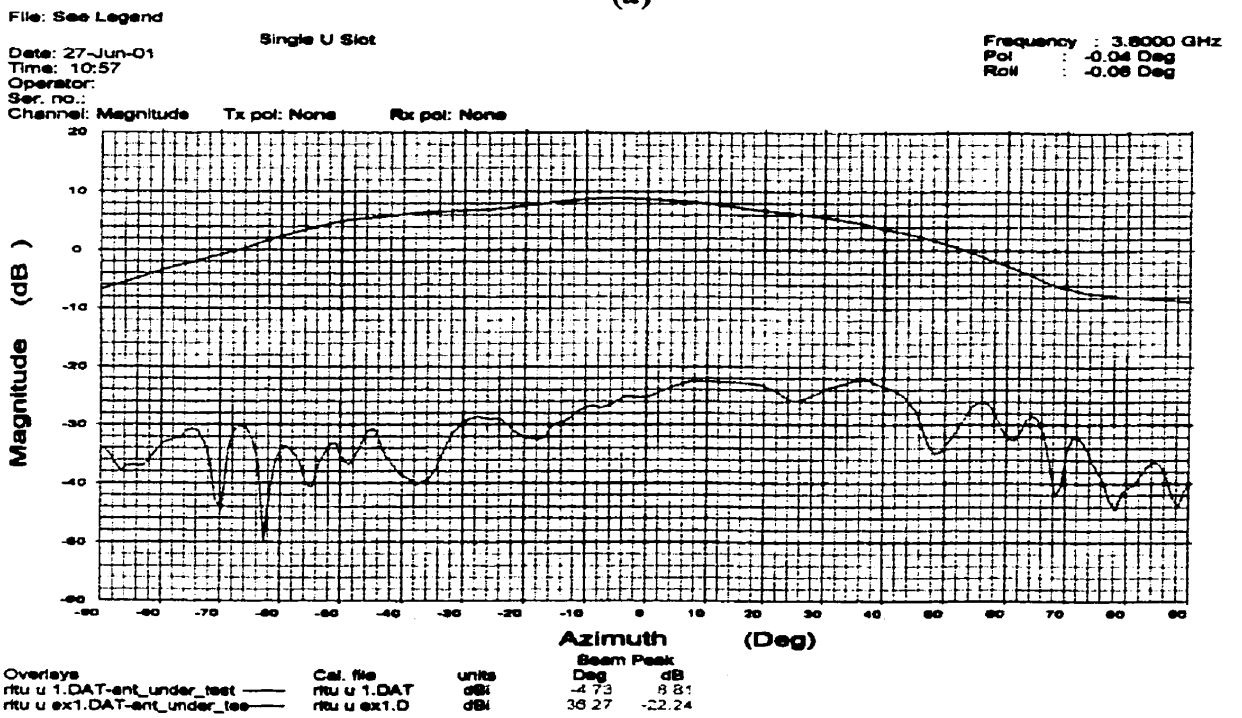

(*b*)

Figure 5.5: (a) Experimental results of Gain patterns in ϕ = 0 plane of Antenna 1 at f_l = 3.8 GHz. (b) Experimental results of Gain patterns in ϕ = 90 plane of Antenna 1 at f_l = 3.8 GHz.

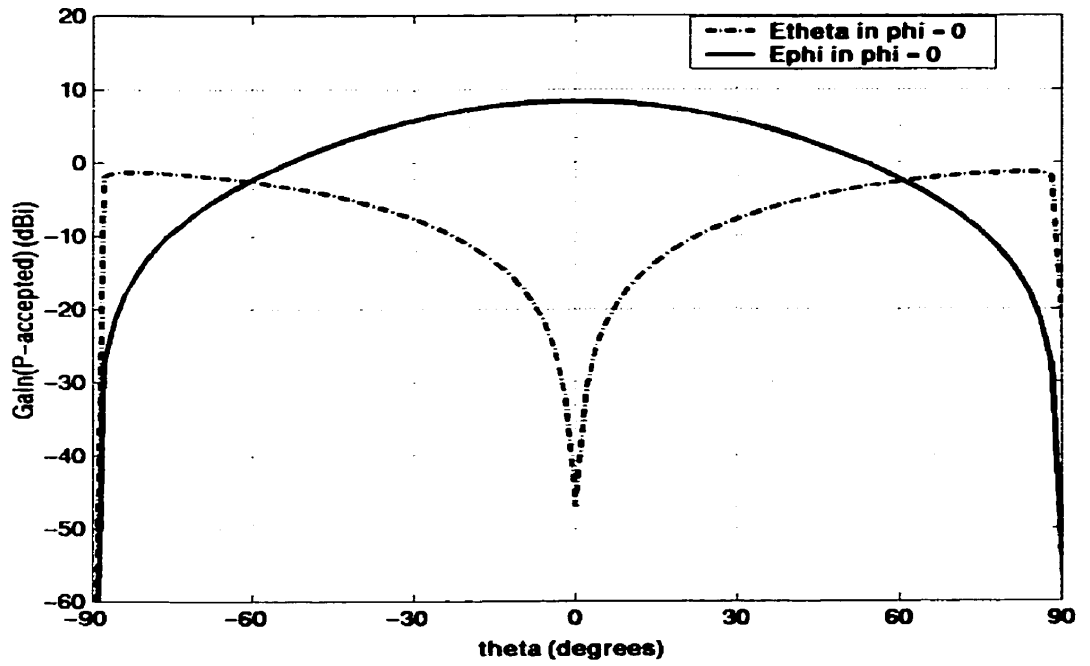

(*a*)

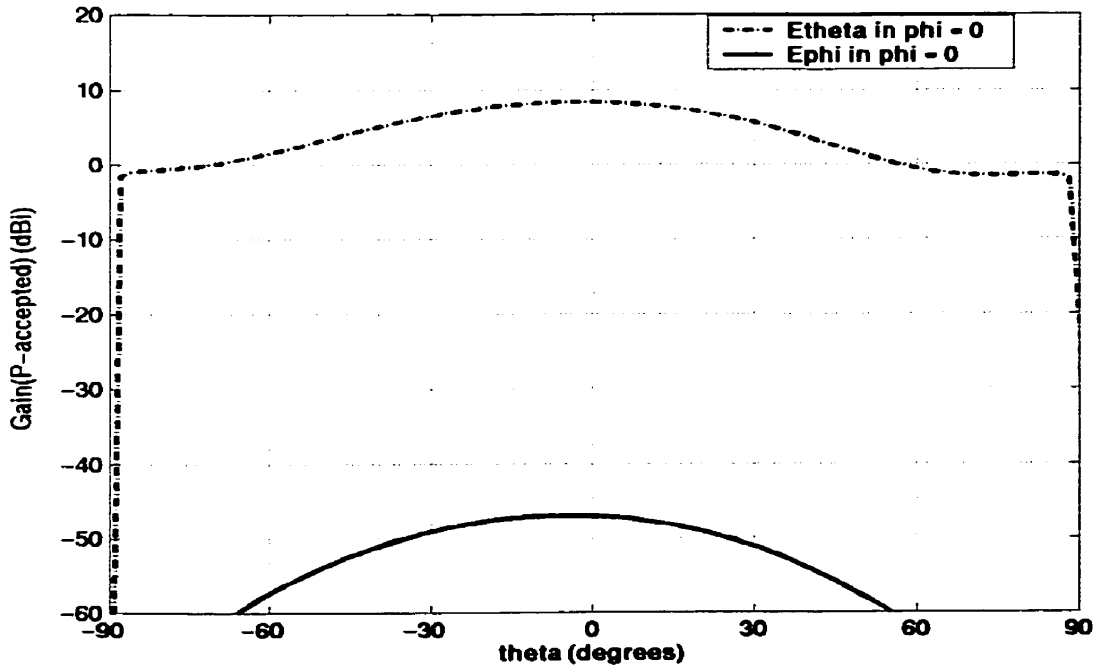

(*b*)

Figure 5.6: (a) Simulation results of Gain patterns in ϕ = 0 plane of Antenna 1 at f_1 = 3.8 GHz. (b) Simulation results of Gain patterns in ϕ = 90 plane of Antenna 1 at f_1 = 3.8 GHz.

Similarly, the simulation results of gain patterns in Figure 5.6 show that the crosspolarization level is high in $\phi = 0$ plane and it is extremely low in $\phi = 90$ plane. The maximum peak obtained from the simulation results at $f_1 = 3.8$ GHz is 8.35 dBi whereas the experimental results show a peak value of 8.77 dBi in $\phi = 0$ plane and 8.81 dBi in the $\phi = 90$ plane, which is very close to the simulated gain value.

In a similar manner, the experimental results of the gain patterns in the $\phi = 0$ plane and $\phi = 90$ plane at $f_2 = 4.65$ GHz are shown in Figure 5.7. In order to compare the experimental results with the simulation results, Figure 5.8 displays the gain patterns in $\phi = 0$ plane and $\phi = 90$ plane at $f_2 = 4.65$ GHz obtained from the software Ansoft Ensemble. At the second resonance frequency $f_2 = 4.65$ GHz, the broadside gain obtained from the simulation results has a value of 8.91 dBi while the experimental results show a peak value of 7.48 dBi in $\phi = 0$ plane and 7.63 dBi in $\phi = 90$ plane. The difference in the gain is due to the losses in the cables used to connect the antenna to the source. The experimental results in Figure 5.7 show that the crosspolarization level in $\phi = 0$ plane is higher, while it is very low in $\phi = 90$ plane. Similar observation can be made for the simulation results shown in Figure 5.8. They also show that the crosspolarization level is high in $\phi = 0$ plane and it is negligible in $\phi = 90$ plane.

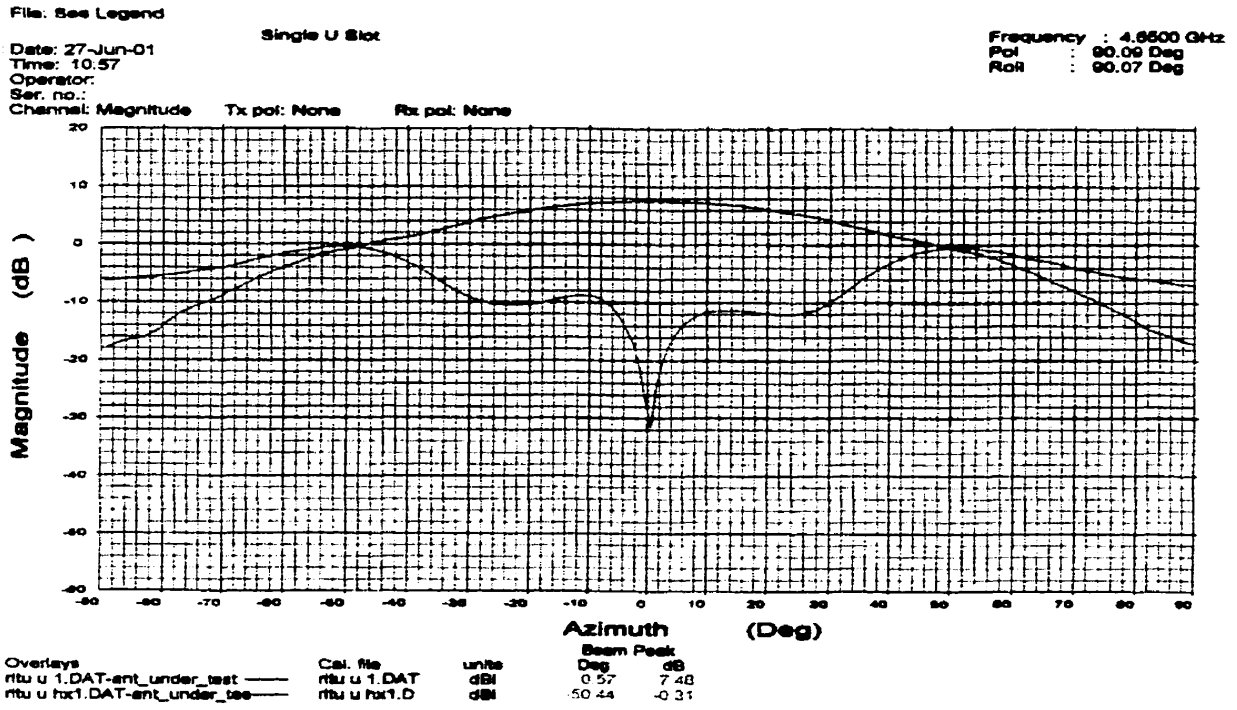

(*a*)

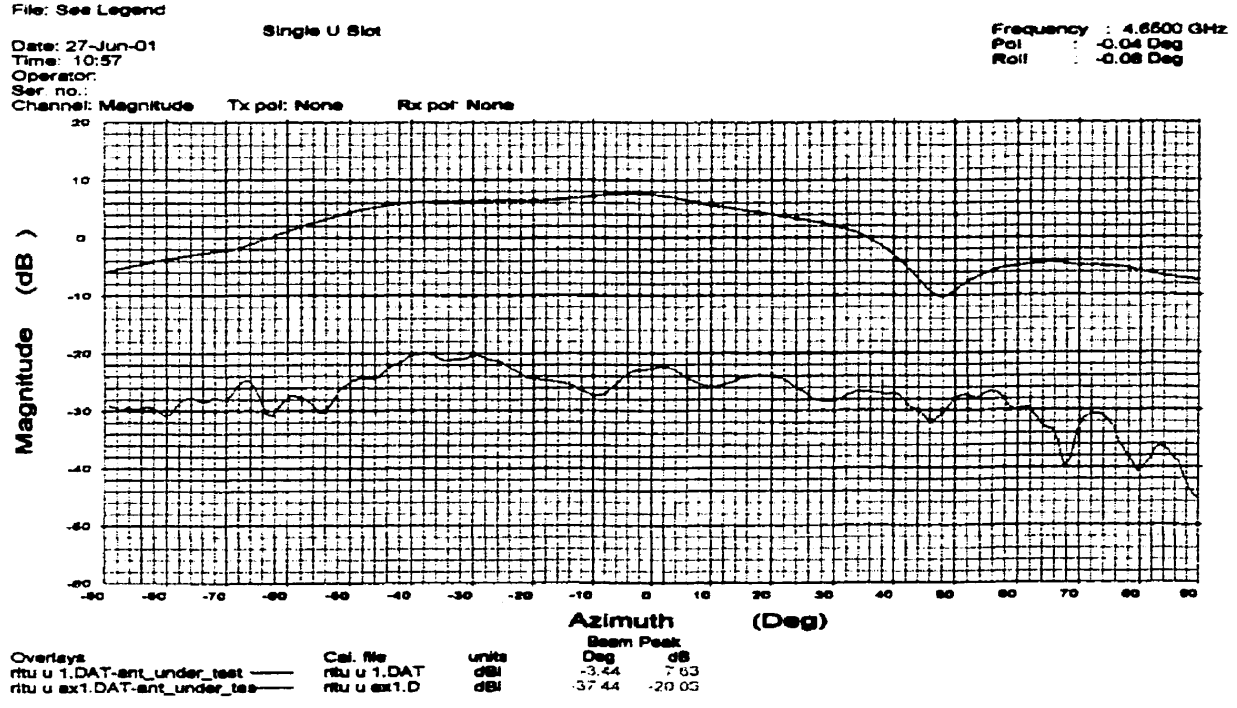

(*b*)

Figure 5.7: (a) Experimental results of Gain patterns in ϕ = 0 plane of Antenna 1 at f_2 = 4.65 GHz. (b) Experimental results of Gain patterns in ϕ = 90 plane of Antenna 1 at f_2 = 4.65 GHz.

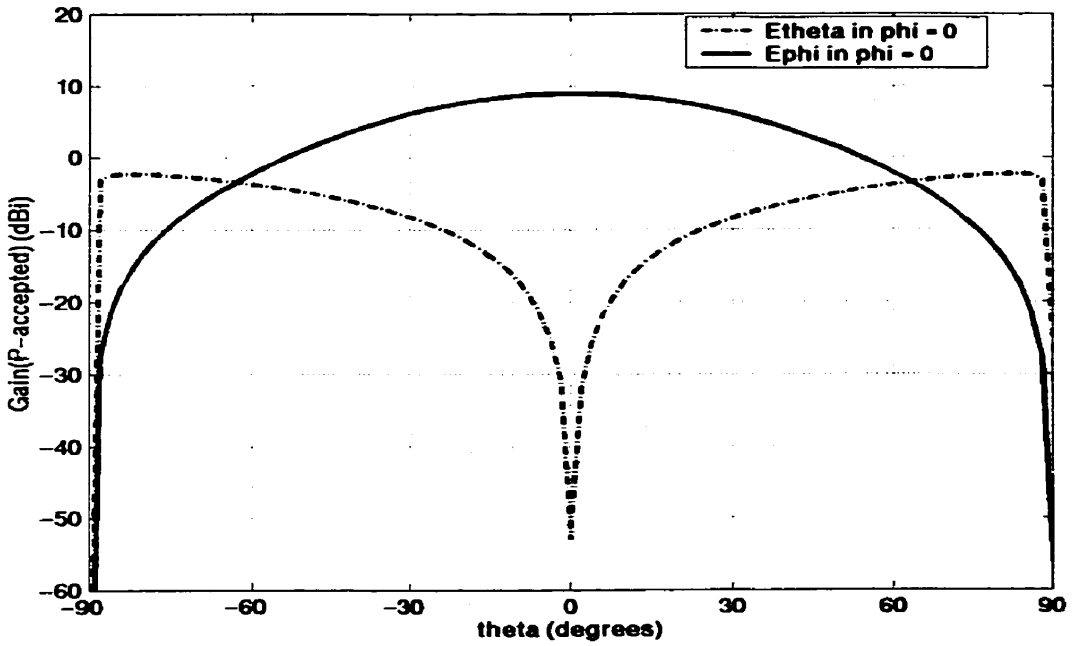

(*a*)

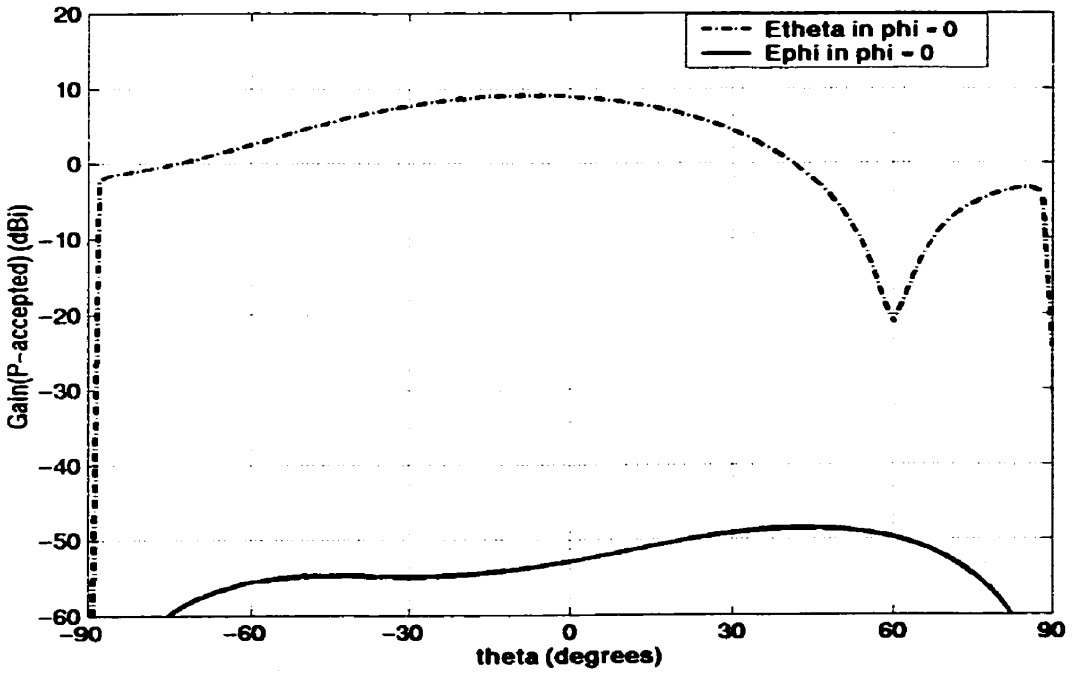

(*b*)

Figure 5.8: (a) Simulation results of Gain patterns in ϕ = 0 plane of Antenna 1 at f_2 = 4.65 GHz. (b) Simulation results of Gain patterns in ϕ = 90 plane of Antenna 1 at f_2 = 4.65 GHz.

5.3 Results of Antenna 2

The dimensions used to fabricate the circular arc slot microstrip antenna are: L = 62 mm, W = 29 mm, $(x_c, y_c) = (0, -2.5)$, $(a_1, b_1) = (5, 3.5)$, $(a_2, b_2) = (7, 5.5)$, $t = 2.83$, $d = 1.37$, $(x_p, y_p) = (0, -1.5)$, F = 16 mm, foam substrate material with $\varepsilon_r = 1.03$ and $h = 5.91$ mm. Figure 5.9 shows the results for the return loss obtained from the network analyzer of Antenna 2 with these dimensions.

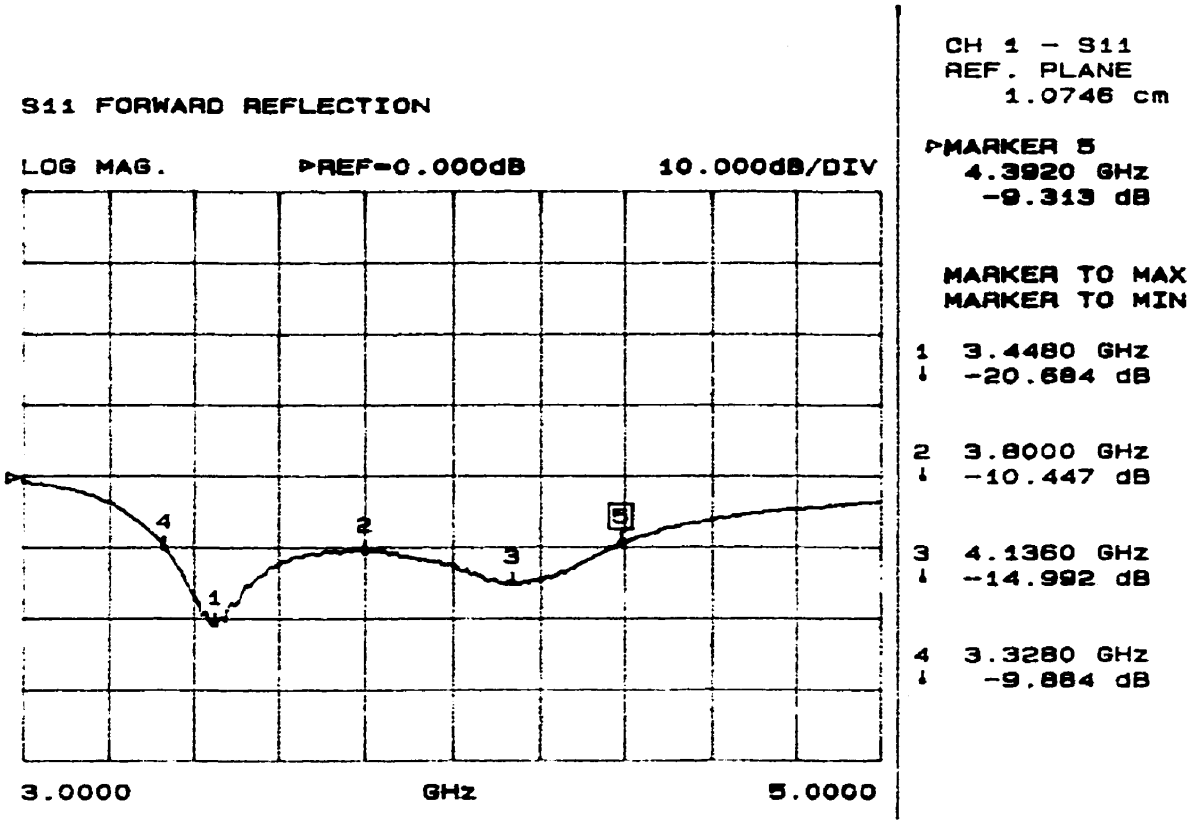

Figure 5.9: Experimental results for the Return Loss of Antenna 2 with dimensions L = 62, W = 29, $(x_c, y_c) = (0, -2.5)$, $(a_1, b_1) = (5, 3.5)$, $(a_2, b_2) = (7, 5.5)$, $t = 2.83$, $d = 1.37$, $F = 16$ and $h = 5.91$. All dimensions in mm.

As it can be seen from the experimental results in Figure 5.9, the first resonance of the antenna occurs at f_1 = 3.448 GHz and the second resonance occurs at f_2 = 4.136 GHz. The

−10 dB bandwidth of Antenna 2 is calculated to be 27.6%. For comparison, the simulation results for the return loss of Antenna 2 are shown in Figure 5.10, which shows that the first resonance appears at f_1 = 3.6 GHz and the second resonance at f_2 = 4.24 GHz. These simulated values of f_1 and f_2 are higher than the experimental values of f_1 = 3.448 GHz and f_2 = 4.136 GHz. The −10 dB bandwidth of the antenna obtained from the simulation results is calculated to be 25.69%, which is slightly lower than the experimental value of 27.6%. Overall, the experimental results are close to the simulation results.

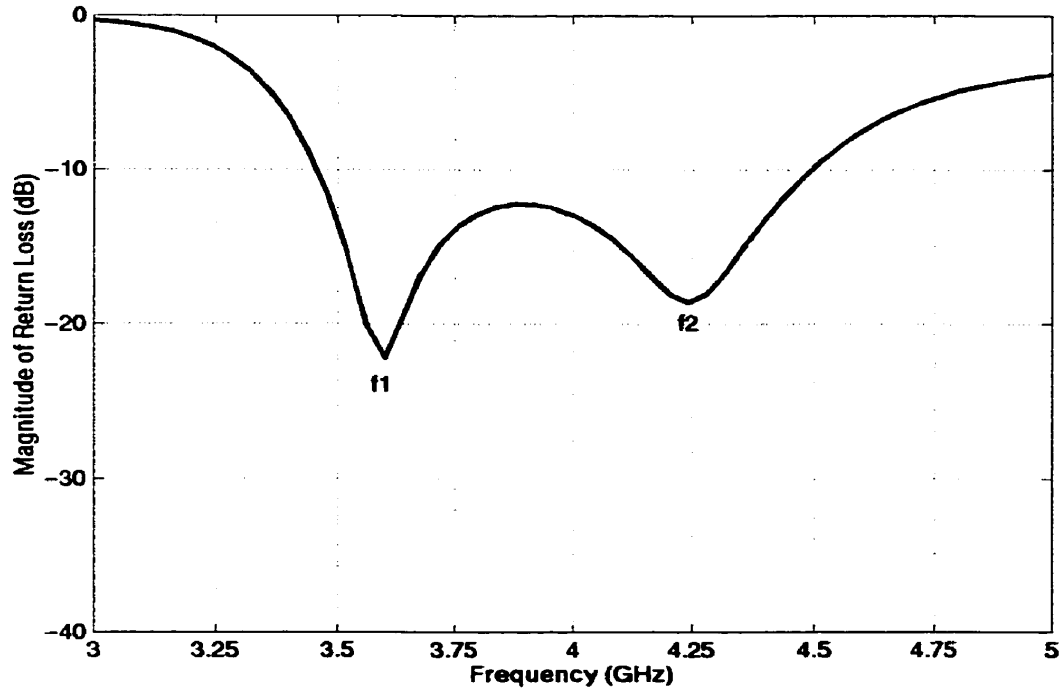

Figure 5.10: Simulation results for the Return Loss of Antenna 2 with dimensions L = 62, W = 29, (x_c, y_c) = (0, −2.5), (a_1, b_1) = (5, 3.5), (a_2, b_2) = (7, 5.5), t = 2.83, d = 1.37, F = 16 and h = 5.91. All dimensions in mm.

Figure 5.11 displays the experimental results of the smith chart plot of this antenna

obtained using the network analyzer. Since the loop on the smith chart is situated close to the center, this verifies the broad bandwidth characteristics of the antenna.

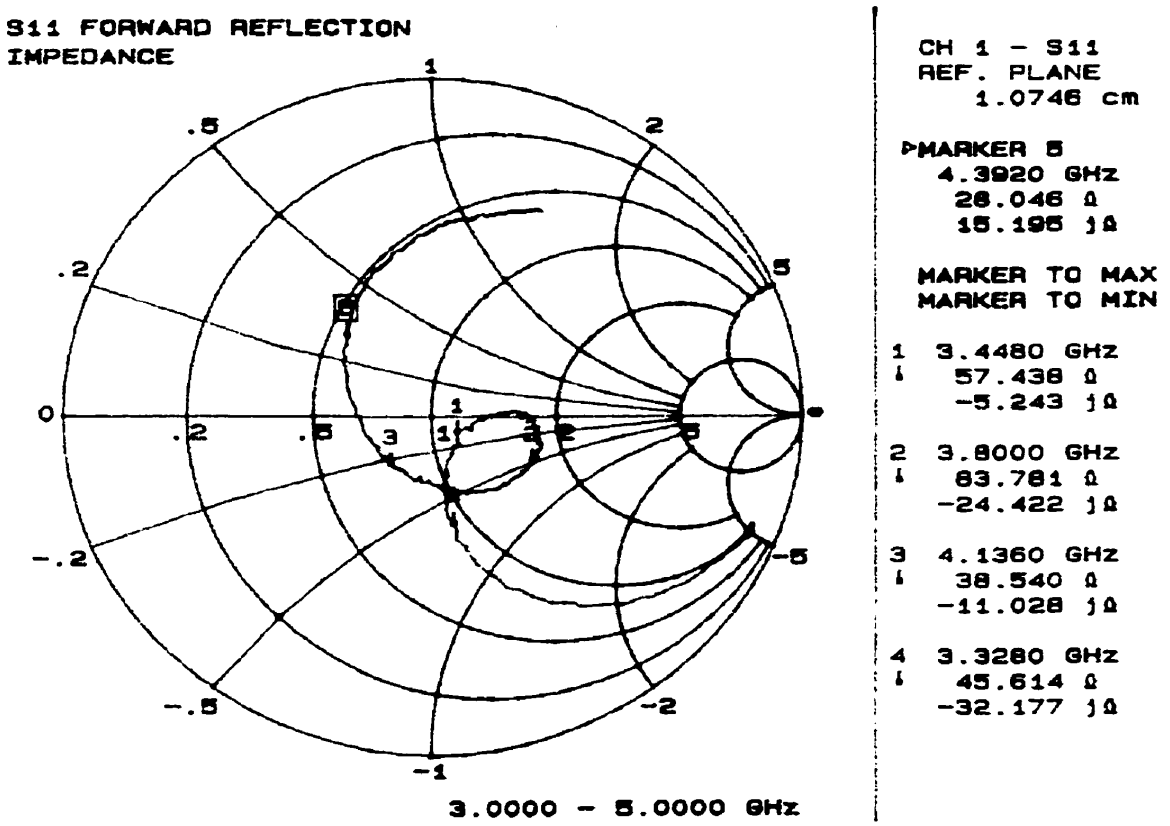

Figure 5.11: Experimental results for the Smith Chart plot of Antenna 2 with dimensions $L = 62$, $W = 29$, $(x_c, y_c) = (0, -2.5)$, $(a_1, b_1) = (5, 3.5)$, $(a_2, b_2) = (7, 5.5)$, $t = 2.83$, $d = 1.37$, $F = 16$ *and* $h = 5.91$. *All dimensions in mm.*

In a similar manner, Figure 5.12 displays the smith chart plot of Antenna 2 obtained from the simulation, which is similar to the plot obtained from the experimental results, as shown in Figure 5.11. In general, the results shown in Figure 5.9 to Figure 5.12 demonstrate that the experimental results and simulation results of Antenna 2 are in good agreement with each other.

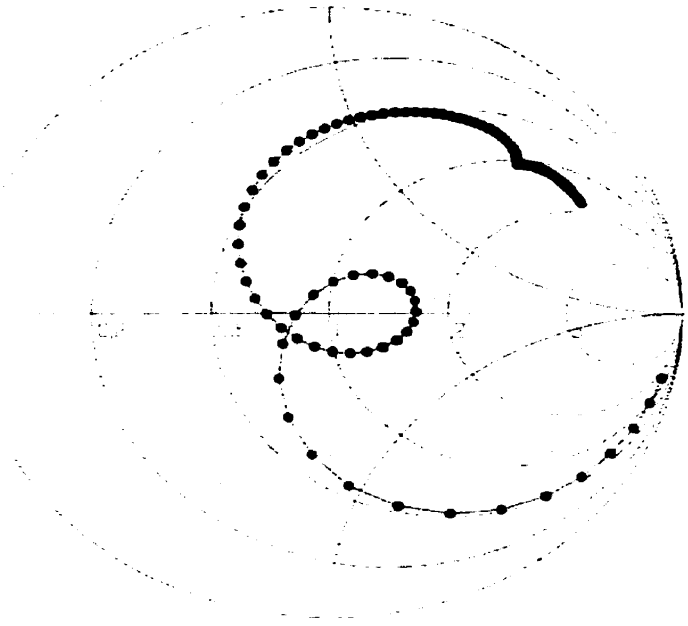

Figure 5.12: Simulations results for the Smith Chart plot of Antenna 2 with dimensions L = 62, W = 29, $(x_c, y_c) = (0, -2.5)$, $(a_1, b_1) = (5, 3.5)$, $(a_2, b_2) = (7, 5.5)$, t = 2.828, d = 1.3698, F = 16, $\varepsilon_r = 1.03$ and h = 5.91. All dimensions in mm.

Figure 5.9 shows that the experimental value of the first and second resonance frequencies are f_1 = 3.448 GHz and f_2 = 4.136 GHz, respectively. The far–field radiation patterns in the rectangular coordinates in the $\phi = 0$ plane and $\phi = 90$ plane at f_1 = 3.45 GHz are displayed in Figure 5.13. The simulation results of the gain patterns at f_1 = 3.45 GHz in the $\phi = 0$ plane and $\phi = 90$ plane are shown in Figure 5.14 for comparison. The experimental results of gain patterns show that a good crosspolarization level is achieved in $\phi = 90$ plane and it is below −13 dB in $\phi = 0$ plane. Likewise, the simulation results of the gain patterns show that the crosspolarization level in $\phi = 90$ plane is very small and it is higher in $\phi = 0$ plane.

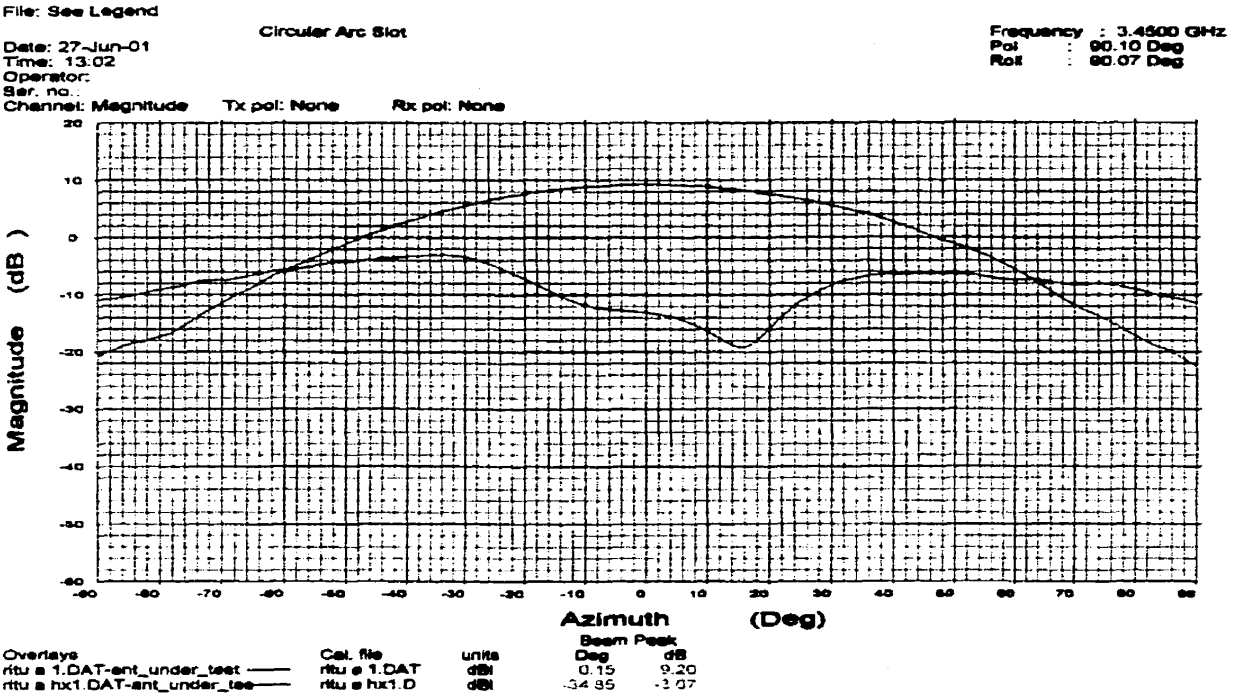

(*a*)

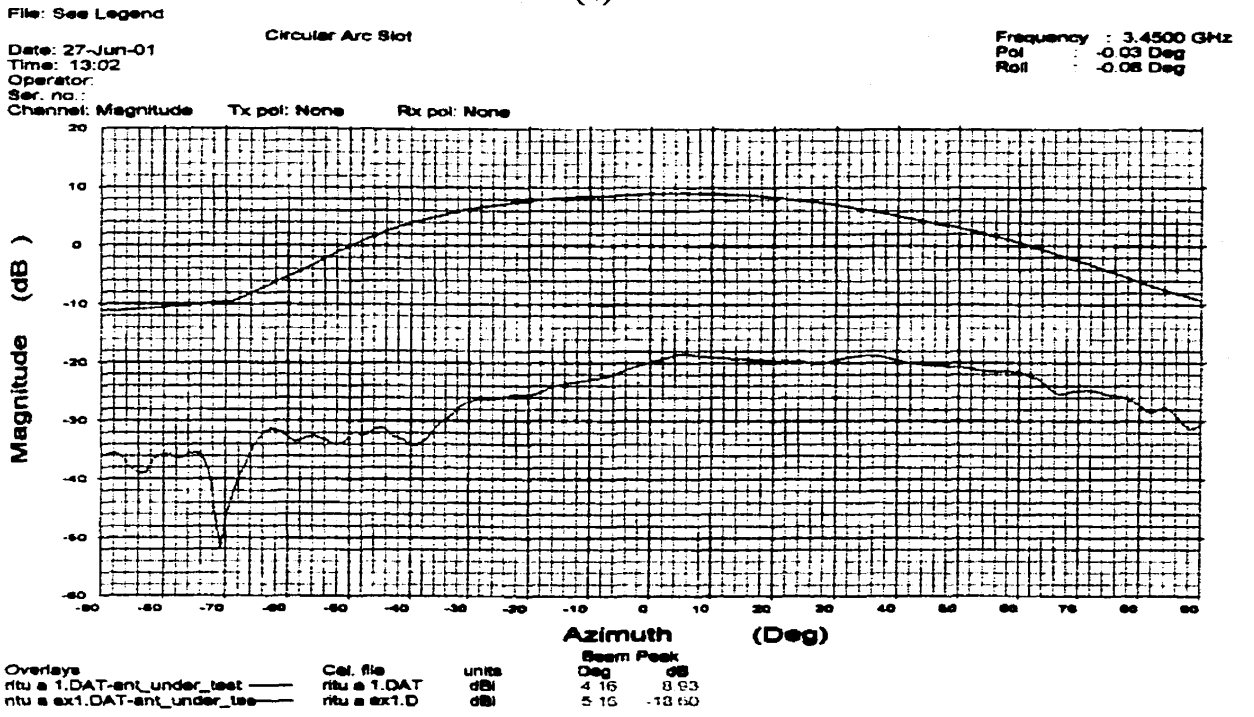

(*b*)

Figure 5.13: (a) Experimental results of Gain patterns in ϕ = 0 plane Antenna 2 at f_1 = 3.45 GHz. (b) Experimental results of Gain patterns in ϕ = 90 plane of Antenna 2 at f_1 = 3.45 GHz.

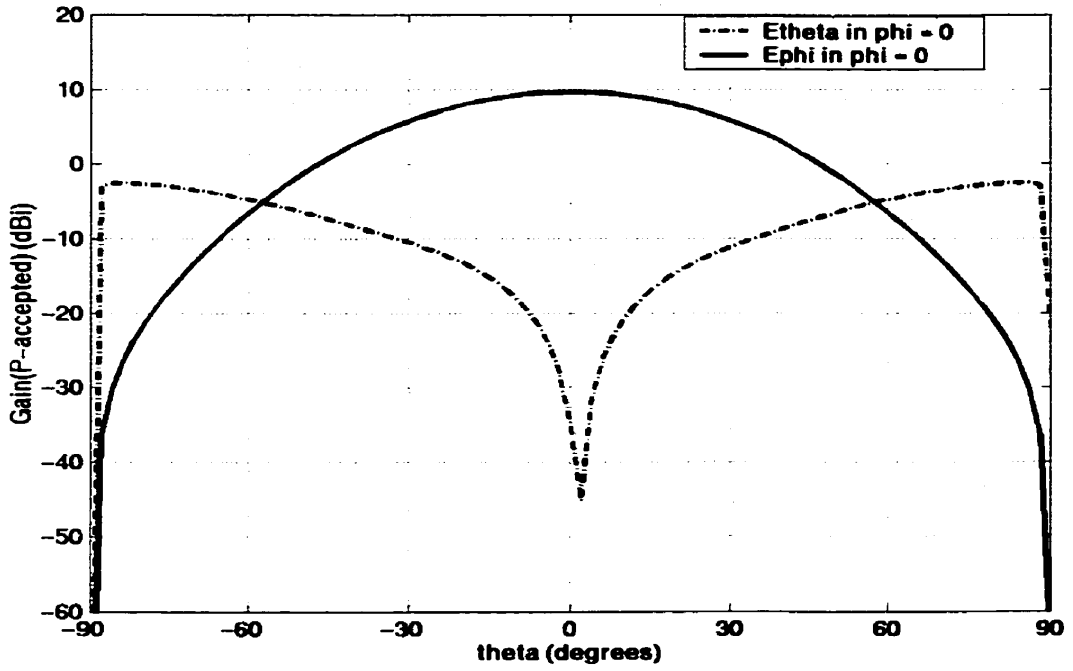

(*a*)

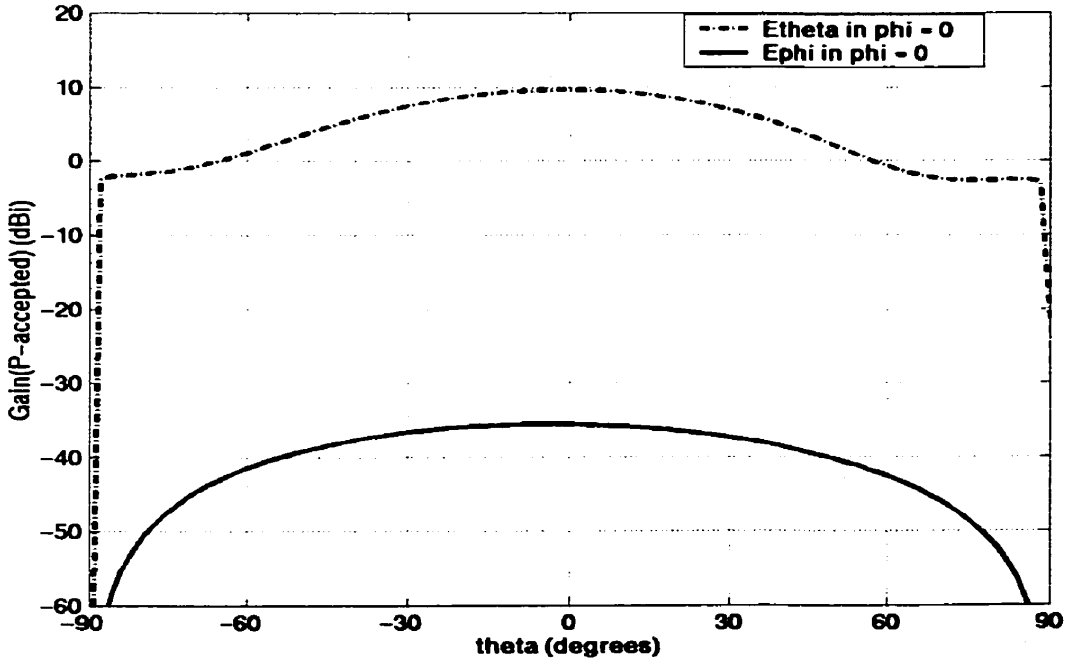

(*b*)

Figure 5.14: (a) Simulation results of Gain patterns in ϕ = 0 plane of Antenna 2 at f_l = 3.45 GHz. (b) Simulation results of Gain patterns in ϕ = 90 plane of Antenna 2 at f_l = 3.45 GHz.

At f_1 = 3.448 GHz, the maximum peak obtained from the simulation results is 9.64 dBi whereas the experimental results show a peak value of 9.2 dBi in ϕ = 0 plane and 8.93 dBi in the ϕ = 90 plane. The difference in the gain is due to the losses in the cables used to connect the antenna to the source.

Similarly, the experimental results of the far–field radiation patterns in ϕ = 0 plane and ϕ = 90 plane at f_2 = 4.15 GHz are shown in Figure 5.15. Figure 5.16 displays the corresponding simulation results of the gain patterns in ϕ = 0 plane and ϕ = 90 plane at f_2 = 4.15 GHz for comparison purposes. At the second resonance frequency f_2 = 4.15 GHz, the broadside gain obtained from the simulation results has a value of 9.6 dBi while the experimental results show a peak value of 8.77 dBi in ϕ = 0 plane and 8.68 dBi in ϕ = 90 plane. Figure 5.15 and 5.16 show that the crosspolarization level in ϕ = 0 plane is higher than f_1 = 3.448 GHz, while they are very low for both f_1 and f_2 in ϕ = 90 plane. Both experimental and simulation gain patterns results demonstrate that the crosspolarization levels are comparable in ϕ = 0 plane and ϕ = 90 plane.

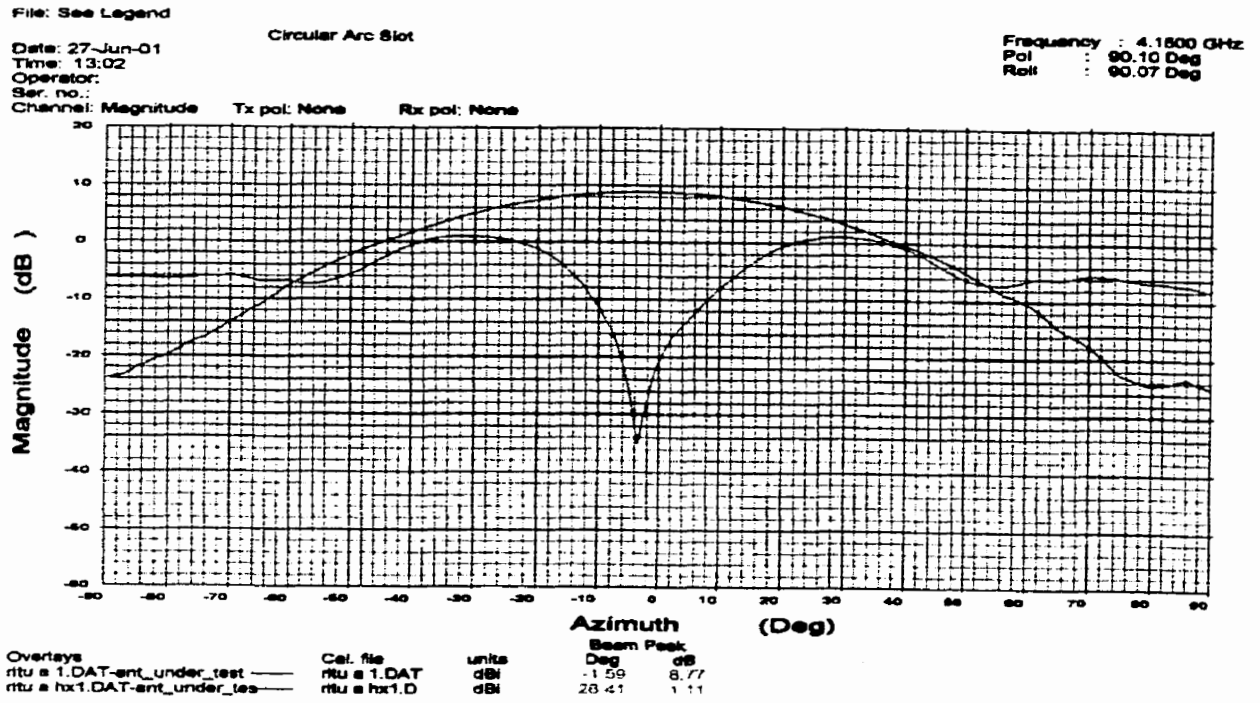

(*a*)

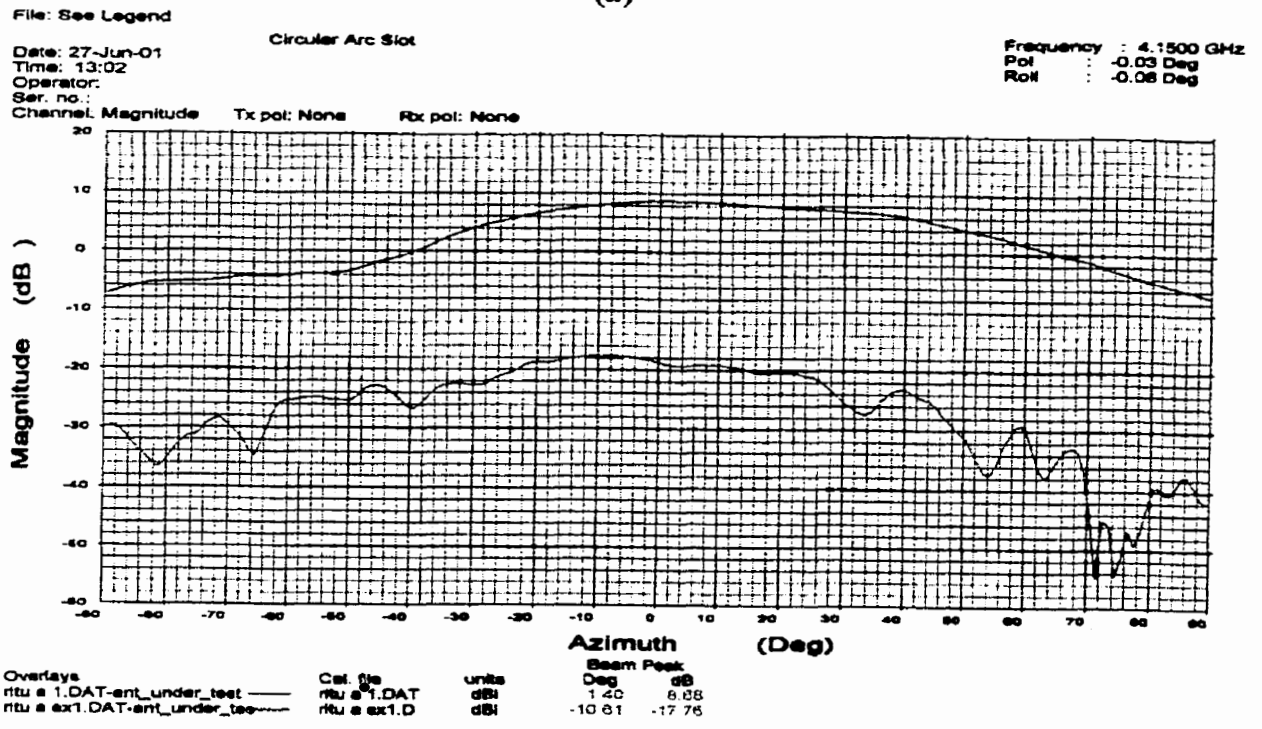

(*b*)

Figure 5.15: (a) Experimental results of Gain patterns in ϕ = 0 plane of Antenna 2 at f_2 = 4.15 GHz. (b) Experimental results of Gain patterns in ϕ = 90 plane of Antenna 2 at f_2 = 4.15 GHz.

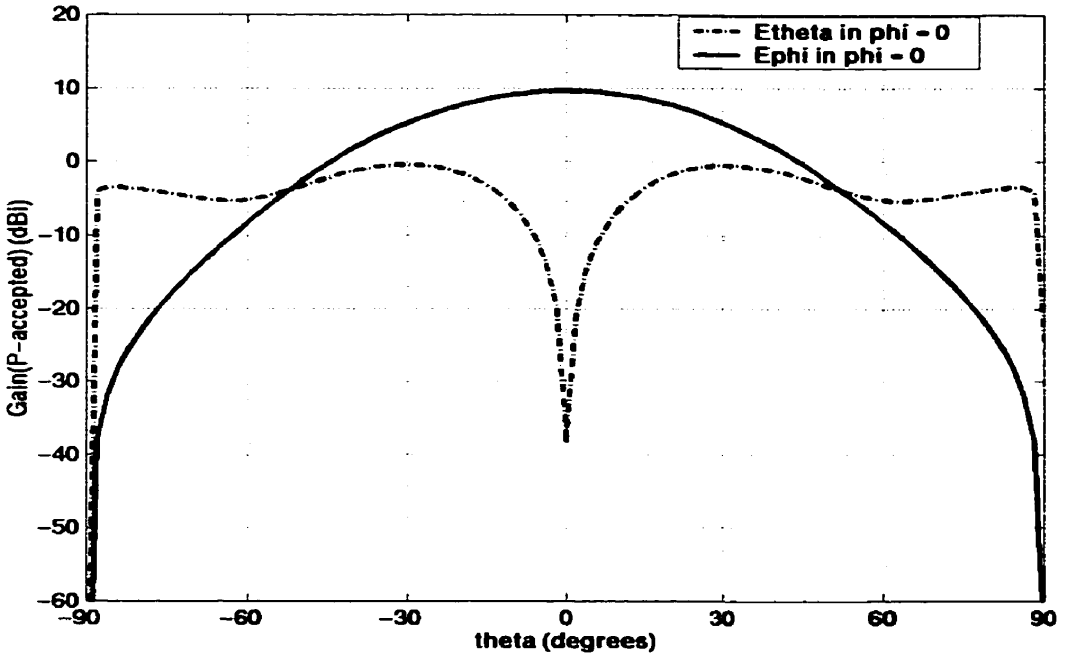

(*a*)

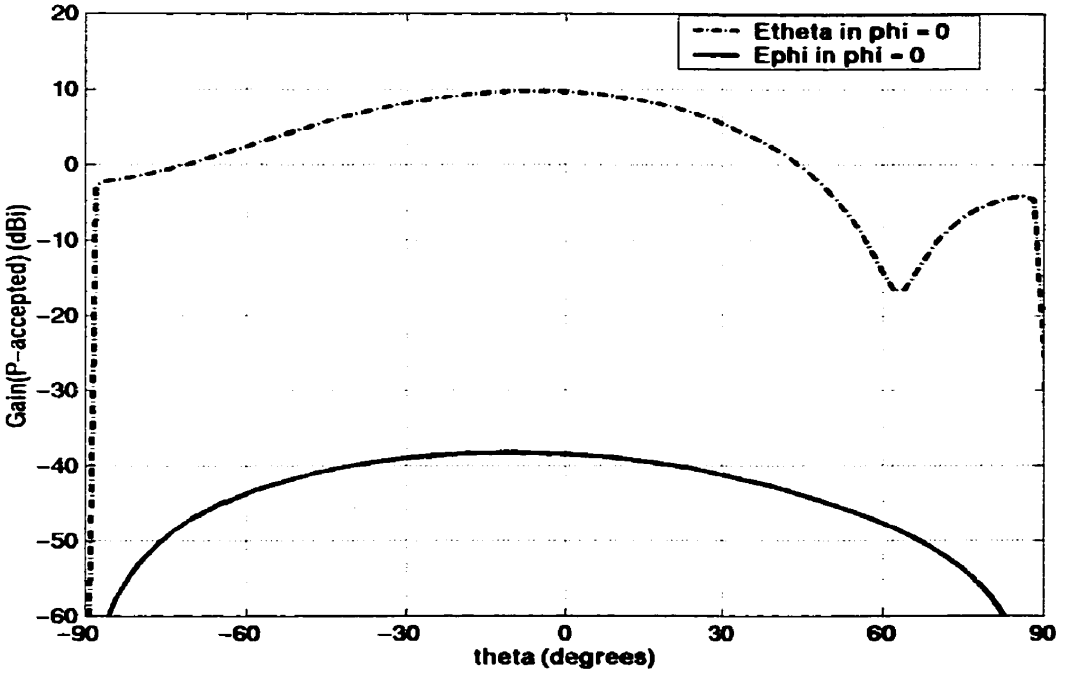

(*b*)

Figure 5.16: (a) Simulation results of Gain patterns in ϕ = 0 plane of Antenna 2 at f_2 = 4.15 GHz. (b) Simulation results of Gain patterns in ϕ = 90 plane of Antenna 2 at f_2 = 4.15 GHz.

5.4 Summary

In this chapter the experimental results of the fabricated Antenna 1 and Antenna 2 obtained from the Antenna Laboratory were presented. The fabricated antennas were tested for the S parameters using the network analyzer and the far–field radiation patterns using the equipment in the Far Field Anechoic Chamber in the Antenna Laboratory. The experimental results of the two fabricated antennas (single U slot antenna and circular arc slot antenna) were compared with their simulation results. It was found that the experimental results showed good agreement with the corresponding simulation results.

Chapter 6

Conclusion

A study was conducted on four broadband microstrip patch antennas and a dual band patch antenna. The broadband patch antennas studied exclusively in this thesis are

1. A rectangular microstrip patch antenna with a U–shaped slot
2. A rectangular microstrip patch antenna with a circular arc slot
3. A circular patch antenna with a circular arc slot
4. A circular patch antenna with a circular arc slot and L–shaped probe

The characteristics of these antennas were studied in terms of their resonance frequencies and bandwidth. The effect of various antenna parameters on the two resonance frequencies and −10 dB bandwidth were studied extensively for each antenna. Other parameters such as substrate thickness also took part in this investigation.

It was found that Antenna 1 and Antenna 2 have broadband characteristics. The bandwidth in the range of 30% were achievable with both of these antenna. Approximate equations for the operating frequencies were derived by analyzing the surface current distribution on the patch for both Antenna 1 and Antenna 2. Their results were compared with Ansoft ENSEMBLE computations and found to be accurate within 3.63%. In contrast, the circular patch antenna with a circular arc slot did not exhibit very broadband properties. The stub tuning technique was applied to increase the bandwidth of this antenna. The stub tuning method was also implemented on the rectangular patch with a circular arc slot. The other broadband patch antenna that was studied extensively was the

circular patch antenna with a circular arc slot and L–shaped probe. The impedance bandwidths in the range of 40% was obtained with this antenna, which is very broad. The far field radiation patterns of these antennas had good crosspolarization levels.

The dual band operation of a microstrip patch antenna with two asymmetric U–shaped slots was also studied. The characteristics of the antenna in terms of resonance frequencies and impedance bandwidth were examined. The optimum ratio of the two frequencies is found to be $f_2 / f_1 = 1.57$. The far field radiation patterns for the two frequencies showed similar patterns and same polarization with good crosspolarization levels. The broadside gain of 9.09 dBi can be achieved at $f_1 = 3.88$ GHz, while the gain value was shown to be slightly lower at $f_2 = 6.08$ GHz. Two equations for the operating frequencies were derived by analyzing the surface current distribution on the patch. Their results were compared with Ansoft ENSEMBLE computations and found to be fairly accurate.

The experimental results of two fabricated antennas (rectangular patch antenna with a single U–slot and rectangular patch antenna with a circular arc slot) obtained from the Antenna Laboratory were presented. The fabricated antennas were tested for the S parameters using the network analyzer and the far–field radiation patterns using the equipment in the Far Field Anechoic Chamber in the Antenna Laboratory. The experimental results of the fabricated antennas were compared with their simulation results. It was found that the experimental results showed good agreement with the corresponding simulation results.

References

[1]G.A. Deschamps, "Microstrip microwave antennas", presented at the *3rd USAF Symposium On Antennas*, 1953.

[2]J.Q. Howell, "Microstrip antennas", *IEEE APS Int. Symp. Digest*, pp. 177–180, 1972.

[3]R.E. Munson, "Conformal microstrip antennas and microstrip phased arrays", *IEEE Trans. Antennas Propag.*, Vol. AP–22, pp. 74–78, 1974.

[4]I.J. Bahl and P. Bhartia, "Microstrip antennas", *Artech House Inc.*, Dehdam, Massachusetts, 1980.

[5]Y.T. Lo, D. Solomon, and W.F. Richards, "Theory and experiment on microstrip antennas", *IEEE Trans. on Antennas and Propagation*, Vol. AP–27, pp. 137–145, 1979.

[6]W.F. Richards, Y.T. Lo and D.D. Harrison, "An improved theory for microstrip antennas and applications", *IEEE Trans. on Antennas and Propagation*, Vol. AP–29, pp. 38–46, 1981.

[7]K. Antoskiewicz and L. Shafai, "Impedance characteristics of circular microstrip patches", *IEEE Trans. on Antennas and Propagation*, Vol. AP–38, pp. 942–946, 1990.

[8]W.J. Bergman and F.V. Schultz, "The circular traveling–wave antenna", *IRE Int. Conv. Rec.*, Vol. 3, pt. 1, pp. 40–50, 1955.

[9]I.J. Bahl and S.S. Stuchly and M.A. Stuchly, "A new microstrip radiator for medical application", *IEEE Trans. on Microwave Theory and Techniques*, MTT–28, pp. 1464, 1980.

[10]R.Q. Lee, K.F. Lee and J. Bobinchak, "Characteristics of a two–layer electromagnetically coupled rectangular patch antenna", *Electronics Letters*, Vol. 23,

pp. 1070–1072, 1987.

[11]C.K. Aanandan and K.G. Nair, "Compact Broadband Microstrip Antenna", *Electronics Letters*, Vol. 22, pp. 1064–1065, 1986.

[12]T. Huynh and K.F. Lee, "Single layer single–patch wideband microstrip antenna", *Electronics Letters*, Vol. 31, pp. 1310–1312, 1995.

[13]K.F. Lee, K.M. Luk, K.F. Tong, S.M. Shum, T. Huynh and R.Q. Lee, "Experimental and simulation studies of the coaxially fed U–slot rectangular patch antenna", *IEE Proc.–Microw. Antennas Propag.*, Vol. 144, pp. 354–358, 1997.

[14]K.F. Lee, K.M. Luk, K.F. Tong, Y.L. Yung and T. Huynh, "Experimental study of the rectangular patch with a U–shaped slot", *IEEE AP–S International Symposium Digest*, pp. 10–13, 1996.

[15]Y.X. Guo, K.M. Luk, K.F. Lee and Y.L. Chow, "Double U–slot rectangular patch antenna", *Electronics Letters*, Vol. 34, pp. 1805–1806, 1998.

[16]K.M. Luk, Y.X. Guo, K.F. Lee and Y.L. Chow, "L–probe proximity fed U–slot patch antenna", *Electronics Letters*, Vol. 34, pp. 1806–1807, 1998.

[17]W.X. Zhang, C.S. Pyo, S.I. Jeon, S.P. Lee and N.H. Myung, "Aperture–coupled U–slotted patch antenna", *IEEE AP–S International Symposium Digest*, pp. 2782–2785, 1999.

[18]K.L. Wong and W.H. Hsu, "Broadband triangular microstrip antenna with U–shaped slot", *Electronics Letters*, Vol. 33, pp. 2085–2087, 1997.

[19]Y.L. Chow, Z.N. Chen, K.F. Lee and K.M. Luk, "Patch Antenna with U–slot – a design Theory" *ANTEM'98 – Symposium on Antenna Technology and Applied Electromagnetics*.

[20]M. Clenet, C.B. Ravipati and L. Shafai, "Effect of Parasitic Patch on the Band width Characteristics of U–slot Rectangular Microstrip Antenna", *ANTEM'98 – Symposium on Antenna Technology and Applied Electromagnetics*.

[21]M. Clenet and L. Shafai, "Multiple resonances and polarisation of U–slot patch antenna", *Electronics Letters*, Vol. 35, pp. 101–103, 1999.

[22]M. Clenet, C.B. Ravipati and L. Shafai, "Bandwidth enhancement of U–slot microstrip antenna using a rectangular stacked patch", *Microwave and Optical Technology Letters*, Vol. 21, pp. 393–395, 1999.

[23]K.M. Luk, L.K. Yeung, C.L. Mak and K.F. Lee, "Circular patch antenna with an L–shaped probe", *Microwave and Optical Technology Letters*, Vol. 20, pp. 256–257, 1999.

[24]Y.X. Guo, K.M. Luk and K.F. Lee, "U–slot circular patch antennas with L–probe feeding", *Electronics Letters*, Vol. 35, pp. 1694–1695, 1999.

[25]L. Shafai, "Chapter IV: Microstrip Antennas", *24.427 Antennas course notes*, University of Manitoba, Canada, pp. 43–64, 1998.

[26]C.A. Balanis, "Antenna Theory: Analysis and Design", *John Wiley & Sons, Inc.*, New York, 1997.

[27]J.F. Zurcher and F.E. Gardiol, "Broadband Patch Antennas", *Artech House Inc.*, Norwood, Massachusetts, 1995.

[28]S. Maci, G.B. Gentili and G. Avitabile, "Single–layer dual frequency patch antenna", *Electronics Letters*, Vol. 29, pp. 1441–1443, 1993.

[29]S. Maci, G.B. Gentili, P. Piazzesi and C. Salvador, "Dual–band slot–loaded patch antenna", *IEE Proc.–Microw. Antennas Propag.*, Vol. 142, pp. 225–232, 1995.

[30]Y.X. Guo, K.M. Luk and K.F. Lee, "A dual-band patch antenna with two U-shaped slot", *Microwave and Optical Technology Letters*, Vol. 26, pp. 73-75, 2000.

[31]J. Rosa, R. Nunes, A. Moleiro and C. Peixeiro, "Dual-band microstrip patch antenna element with double U slots for GSM", *IEEE AP-S International Symposium Digest*, pp. 1596-1599, 2000.

[32]H.M. Chen and Y.F. Lin, "Dual-Frequency operation of a single-feed rectangular microstrip antenna with a π-shaped slot", *Proceedings of ISAP2000, Fukuoka, Japan*, pp. 1107-1110, 2000.